# Morphologies and gas emissions from the Shamakhy-Gobustan mud volcano region, Azerbaijan

## Aliénor Labes

Master Thesis in Geosciences

Sedimentology, Paleontology, and Stratigraphy

60 credits

Department of Geosciences

Faculty of Mathematics and Natural Sciences

UNIVERSITY OF OSLO

June 2022

Morphologies and gas emission from the Shamakhy-Gobustan mud volcano region, Azerbaijan.

# Acknowledgments

First and foremost, I would like to express my sincere appreciation to my principal supervisor **Dr. Adriano Mazzini**. I owe you a considerable debt of gratitude for all your kindness, guidance, and support. Your passion for geosciences is contagious and inspiring. I am also grateful to my co-supervisors, **Dr. Alessandra Sciarra** and **Prof. Grigori Akhmanov**, for your availability and constructive feedback. Furthermore, I would like to extend an appreciation to **Dr. Alexandra Zaputlyaeva.** Thank you for taking the time to meet and share your knowledge and tips.

Secondly, I would like to thank my fellow master's students at the Department of Geosciences (UiO) for the cheerful social environment. A special thank you goes to my close friends and loved ones for the many warm and energy-boosting conversations.

Finally, a personal *merci* goes to my dear parents for always believing in me and for their unconditional love and care.

**Aliénor Labes**

*Oslo, Norway. June 7th, 2022*

IV

# Preface

This master's thesis (ECTS 60) is submitted to the Department of Geosciences, University of Oslo (UiO), in the candidacy of the Master of Science in Geosciences (ECTS 120) following the Sedimentology, Paleontology, and Stratigraphy program. The main supervisor of the thesis is Dr Adriano Mazzini (UiO, Center for Earth Evolution and Dynamics) together with co-supervisors Dr Alessandra Sciarra (National Institute of Geophysics and Volcanology) and Prof. Grigori Akhmanov (Moscow State University).

This multidisciplinary thesis investigates six mud volcanoes located in Azerbaijan. This region hosts the highest mud volcano density on Earth. The targeted structures are located in a poorly studied part of the country featuring a large variety of surface fluid degassing manifestations. The obtained results serve as a contribution to improving knowledge on mud volcano morphologies and their subsurface plumbing system, their gas composition, and quantification on their gas emissions. All data were collected in the field in the framework of the HOTMUD project (PI Adriano Mazzini).

# Abstract

Azerbaijan hosts the largest concentration of mud volcanoes on Earth. This widespread phenomenon occurs due to the combination of unique geological peculiarities. Azerbaijan is characterized by high sedimentation rates combined with the deposition of thick organic-rich series. The generation of hydrocarbons at depth resulted in petroleum basin formation. This, combined with the naturally buoyant rapidly buried sediments, created the ideal setting and conditions to generate widespread sedimentary volcanism. Some Azerbaijani mud volcano provinces have been intensively studied. Others (e.g., the Shamakhy - Gobustan region) are less explored.

Here I report a multidisciplinary study (i.e. including field mapping and observations, the study of satellite images, $CO_2$ and $CH_4$ flux measurements, and gas sampling from active seepage sites) conducted on six mud volcanoes (Maraza, Gyzmeidan, Gushchu, Melikchobanly, Madrasa, and Shikhzarli) located in the northern Shamakhy-Gobustan region. The surface morphologies feature elongated (Kichik Maraza, Melikchobanly) and pie-shaped (Gizmeydan, Gushchu, Shikhzairli) strutures. One mud volcano (Madrasa) does not display a defined edifice and is positioned on the flank of a laterally extensive fault wall. The surface degassing may occur through randomly distributed scattered pools and gryphons where gas, water, mud and oil, are released. These majority of the emissions are commonly present in the crater area (Kichik Maraza, Gizmeydan, Melikchobanly MVs). The tempo of the eruptive activity can also affect the distribution and presence of active degassing. The structures that have been recently erupting often display limited or no visual gas release features (e.g. pools or well-developed gryphons) since these have been removed during the mud breccia flows (Kichik Maraza, Gushchu, Shikhzairli). Molecular and isotopic analyses of the sampled seeps reveal that most of the gas is methane-dominated with a thermogenic origin. Gas molecular fractionation occurring during the vertical migration from the reservoirs is systematically observed. In addition in some instances it was also observed evidence of secondary microbial methane and biodegradation. An extensive campaign of flux measurements was carried out over the crater and the flanks of the mud volcanoes. Degassing was detected at all the structures, including those that did not display obvious visual seepage. Results shows that the targeted MVs release a significant amount of $CO_2$ and $CH_4$ with maximum emissions of 20.3 and 63.6 tonnes $yr^{-1}$, accordingly.

# Table of Contents

# 1 Introduction

This thesis is the result of a multidisciplinary study conducted at six selected major mud volcanoes in the Shamakhy-Gobustan region of Azerbaijan. Satellite images are coupled with field observations and in situ data acquisition (gas samples, flux measurements and seeping fluids parameters) and ultimately integrated bibliography data. The targeted structures are located in a poorly explored region of Azerbaijan where a variety of mud volcano morphologies and seeping fluids is present. The various mud volcano are investigated taking into account the influence of tectonic structures and volcanic activity. Further, the origin of the seeping fluids is discussed based on geochemical analysis of the collected samples. Ultimately, the flux measurement surveys conducted at the mud volcanoes are used to calculate $CO_2$ and $CH_4$ emission budgets.

This chapter introduces the motivation (section 1.1), previous research on Azerbaijani mud volcanoes (section 1.2), the main research objectives of this study (section 1.3), and the study outline (section 1.4).

## 1.1 Motivation

Mud volcanoes (hereafter reported as MVs) are surface piercement structures featuring the upward migration of over-pressurized fluids (gas, water, and sometimes oil) and sediments. MVs are commonly represented by a topographic elevation (from tens to hundreds of meters) with prominent mudflow (up to several kilometers in extension) and a central crater (Figure 1-1a). All MVs have a feeder channel connected to reservoirs and deeply buried source rocks. MVs are typically located at faults or anticline axis, both onshore and offshore. The primary mechanism that drives MV formation is the gravitative instability of rapidity buried and unstable sediments combined with fluid overpressure driven by the hydrocarbon (HC) generation at depth (Brown, 1990; Kopf & Deyhle, 2002; Mazzini & Etiope, 2017; Revil, 2002). Published geochemical analysis shows that MVs are a significant source of thermogenic methane with notable $CO_2$ concentrations and $C_{2+}$ organic compounds (Bonini, 2012; Dimitrov, 2002b; Mazzini & Etiope, 2017). According to Etiope et al. (2019) MVs are among the main sources of natural methane emitted on Earth together with marine seepage and oil-gas fields (Etiope et al., 2019). Investigating the composition of the gas released from MVs can contribute to a better understanding of the geochemical processes in deep sedimentary basins. Flux

measurements help improve the estimates of global emissions of methane from MVs. Such knowledge is valuable in disciplines such as meteorology, oceanography, ecology and exploration for petroleum accumulates in the subsurface (Bean et al., 2014; Deville & Guerlais, 2009; Milkov & Etiope, 2005). Mud volcanism (MV-ism), or sedimentary volcanism, is consequently a geological phenomenon that indicates fluid venting processes initiated at greater depth in petroleum bearing sedimentary basins (Dimitrov, 2002b; Etiope, 2015; Etiope & Schwietzke, 2019; Mazzini & Etiope, 2017; Milkov, 2000; Planke et al., 2003). MVs are the most significant pathway for degassing deeply buried sediments (Etiope & Schwietzke, 2019). MVs are characterized by episodic or continuous fluid release from the subsurface dominated by the rise and fall of fluid pressure. In particular, large eruptions are episodic with generally short-term (less than a few days) and powerful events (Figure 1-1b) followed by long-term dormant phases (few years or decades) (Kopf, 2002; Mazzini, Nermoen, et al., 2009). Despite their short eruption episodes, onshore MVs display an average emission of about 10-20 Tg yr$^{-1}$ (Etiope & Schwietzke, 2019). MVs have been extensively studied as the scientific community recognized their implications in exploring hydrocarbons (HCs), geo-hazards, and the global greenhouse gas budget (Mazzini & Etiope, 2017). Onshore MV structures can be studied directly in the field (Figure 1-1c) and with the use of satellite imaging (Figure 1-1e), while offshore structures can be observed with bathymetric (Figure 1-1d) or acoustic imaging (Figure 1-1f) as well as seafloor sampling.
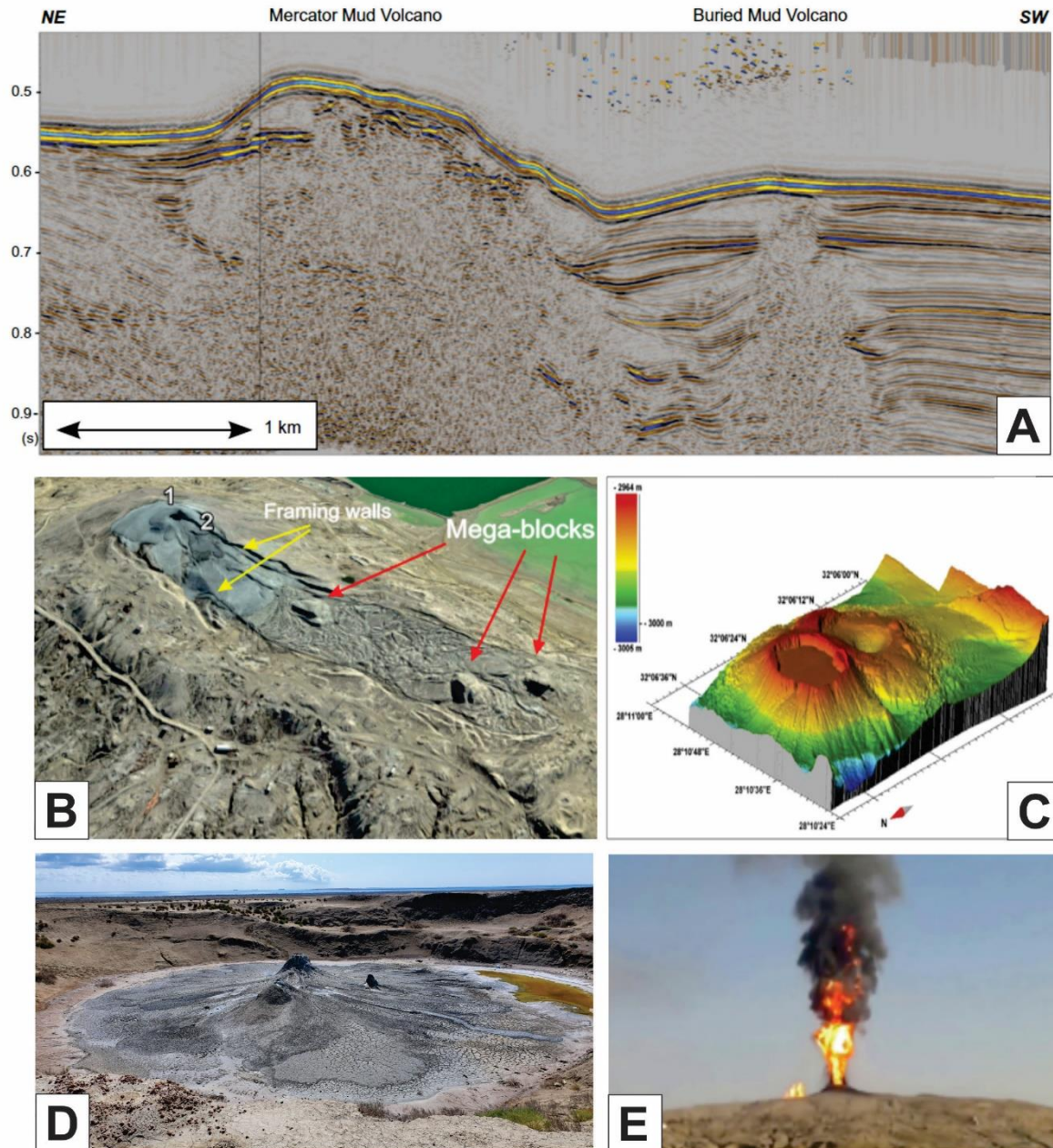
***Figure 1-1****: Images representing MVs. (A) 2D high-resolution seismic image through the offshore Mercator MV (left) and Buried MV (right) in the Gulf of Cadiz (Mazzini & Etiope, 2017). (B) Google Earth satellite picture of Lokhbatan MV in eastern Azerbaijan (Mazzini et al., 2021). (C) Multibeam through two offshore mud cones on the Egyptian continental margin (Mascle et al., 2014). (D). Group of gryphons at the center of Bahar satellite MV (Azerbaijan) (Mazzini & Etiope, 2017). (E) Flaming eruption of Lokhbatan mud volcano, Azerbaijan (Mazzini et al., 2021).*

## 1.2 Research background

Located in the South Caspian region, Azerbaijan hosts the highest density of onshore mud volcanoes on Earth (Aliyev et al., 2015; Mazzini & Etiope, 2017) (Figure 1-2). The maximum concentration of mud volcanoes is located in eastern Azerbaijan, where most of the country's petroleum fields reside (Figure 1-3a). Much research has been dedicated to Azerbaijani mud volcanoes, especially in the Absheron and the southern Shamakhy-Gobustan regions (e.g., Lokbatan, Bakhar, Dashgil, Pirekeshkyul, Garadag, and Koturdag mud volcanoes). However, few investigations are devoted to the northern Shamakhy-Gobustan region. This may be due to early reports of minimal gaseous content in these regions (Jakubov et al., 1971). The isotopic composition of methane of Shamakhy-Gobustan MVs has been reported to be heavier (-40 to -36‰) than the Absheron region (-60 to -50‰ and -50 to -40‰) or the Nizhnekurinskiy region (-50 to -40‰) (Figure 1-3b) (Aliyev et al., 2015) Hence, there is a distinct difference in the isotopic composition of methane in the different regions of eastern Azerbaijan. The Shamakhy-Gobustan has characteristics of late stage of methane generation (metagenesis) and has consequently been less investigated than the MV associated with middle stage of methane maturity (catagenesis). This is because catagenesis is the second stage of maturation of organic carbon, which generates "wet gas", and oil.

Since most MVs on Earth are located in Azerbaijan, significant $CH_4$ emissions are ongoing herein. Nevertheless, very few dedicated studies on $CH_4$ emissions have been conducted on Azerbaijani MVs (Mazzini et al., 2021 and refs therein) and there is paucity of data that could implemented the global budgets calculations. Azerbaijan also hosts the largest variety of MV morphologies on Earth. Several attempts has been done to provide a systematic classification (Dimitrov, 2002b; Ivanov et al., 1996; Kholodov, 2002; Skinner & Mazzini, 2009). However these proposals are based on local studies. More generic descriptions have been presented by few (Kopf, 2002; Mazzini & Etiope, 2017).

Overall the morphology of many MVs is controlled by large scale tectonic structures. The Shamakhy-Gobustan region is particularly relevant because it has been exposed to various tectonic phases that affected the genesis and development of sedimentary volcanoes.
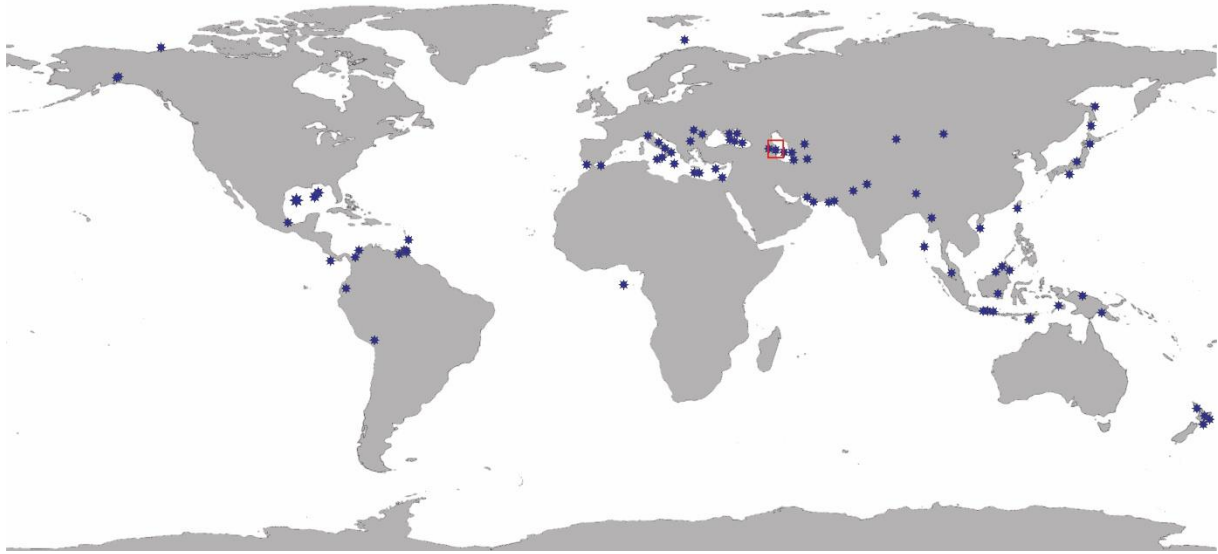
***Figure 1-2*** *Map illustrating the main clusters of (confirmed) MV distribution around the globe. Azerbaijan indicated by a small red square (Mazzini and Etiope., 2017).*
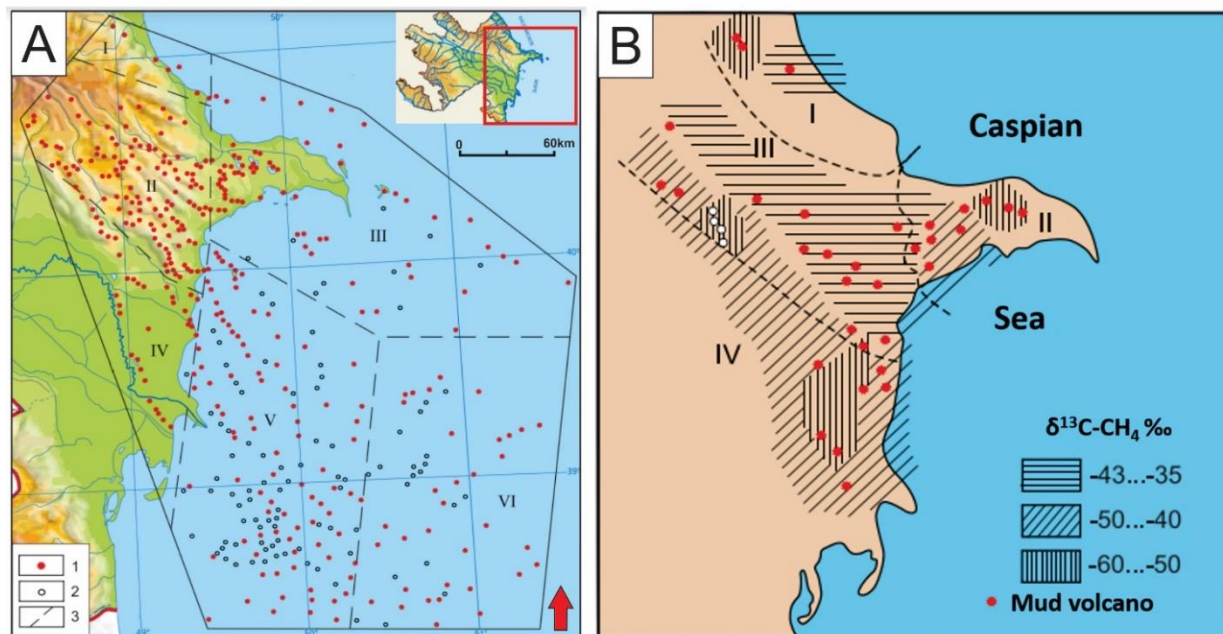


***Figure 1-3*** *Map of eastern Azerbaijan. (A) Area distribution of Mud Volcanoes in least of Azerbaijan. 1establishedd, 2-suspected, 3-boundaries of oil and gas-bearing districts and perspective zones of folding: I-Caspian –Guba, II- Shamakhy-Gobustan, III-Absheron, IV-Nizhnekurinskiy, V- Baku Archipelago, VI- zones of folding in the deepwater part of the Southern Caspian Sea (Aliyev et al., 2015). (B) Area distribution of isotopic composition of methane in mud volcanoes (Aliyev et al., 2015).*

# 1.3 HOTMUD Project

August 2019 took place the 2nd Azerbaijan Summer School on "Mud Volcanism and Petroleum Systems" organized by the University of Oslo in the framework of the HOTMUD project (PI Adriano Mazzini). The summer school began with a workshop at the Azerbaijan Nation Academy of Science (ANAS) in Baku where lectures were delivered by representatives of several institutes (Oil & Gas institute ANAS, University of Oslo, Moscow State University, CNR Bologna and Czech Academy of Sciences). Field excursions were arranged after the workshop where major outcrops and a dozen of onshore MVs were studied using multidisciplinary approaches, including field mapping and observations, the study of satellite images, $CO_2$ and $CH_4$ flux measurements, and gas sampling from active seepage sites. The targeted MVs were clustered in two major hydrocarbon-containing regions with distinct geological settings: Absheron and southern Gobustan-Shamakhy regions. Some famous outcrops were observed such as Oligocene-Miocene Maikop Group outcrops, Pirekeshkul outcrops, and the Yanar Dag ("burning mountain"), Dashgil MV, Bakhar Satellite MV, Koturdag MV and Lokbatan MV.

After the summer school, additional days were dedicated to scientific research activities focusing on the study of 6 MVs (Maraza, Gyzmeidan, Gushchu, Melikchobanly, Madrasa, and Shikhzarli) in the northern Gobustan-Shamakhy region. The Shamakhy-Gobustan region and the location of the investigated structures are shown in Figure 1-4, where the name of the targeted MVs are marked in bold in the figure text. Note that there are inconsistencies in the spelling of the names of some of the targeted mud volcanoes in past literatures. For example, some authors use the name Gushchu (Aliyev et al., 2015) while other refer to it as Gushchi (Feyzullayev, 2012; Valyaev et al., 1985). This study uses the assigned names from the *ATLAS of The World Mud Volcanoes* (Aliyev et al., 2015)
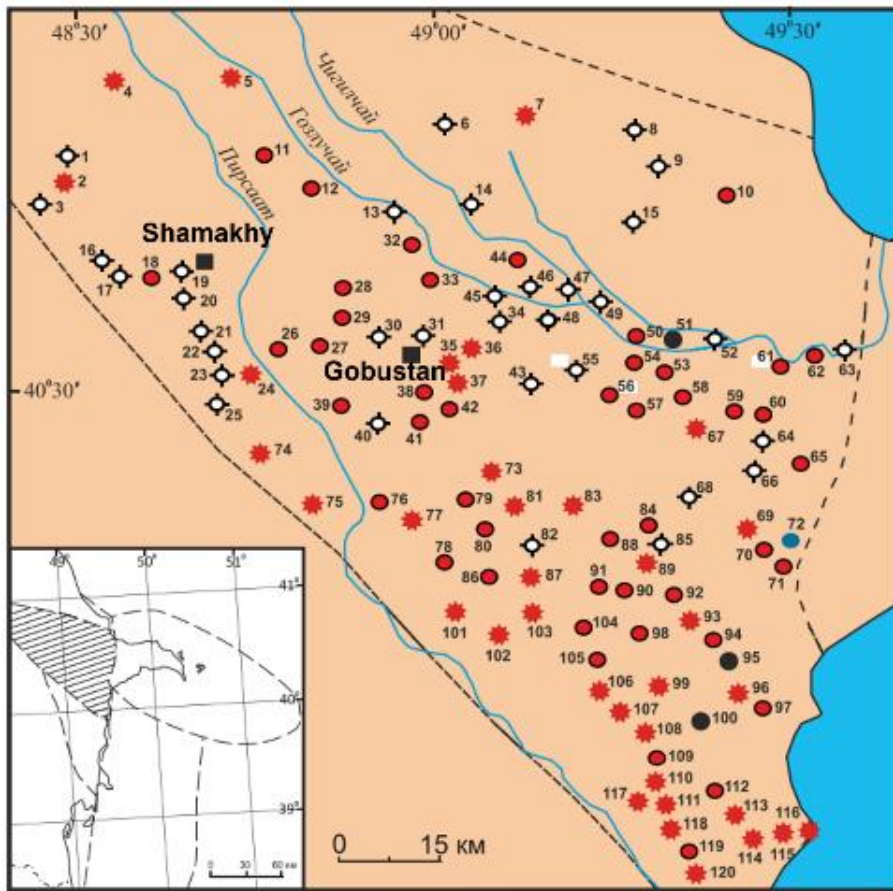
***Figure 1-4*** *Map over the location of mud volcanoes in the Shamakhy – Gobustan region. Targeted MVs of this thesis are set in bold. 1 – Sarsura; 2 – Zeiva; 3 – Bizlan; 4 – Demirchi; **5 – Gyzmeidan**; 6 – Yailag – Tudar; 7 – Gasymkend; 8 – Kekhnagyady; 9 – Kemchi; 10 – Kurkachidag; 11 – Hajyly; 12 – Khilmilli; 13 – Garayaz; 14 – Agdere; 15 – Shikhandag; 16 – Nohur; 17 – Garanohur; **18 – Madrasa**; 19 – Sarabil; 20 – Kyalakhana; 21 – Osmanbeili; 22 – Charhan; 23 – Nyuidi; **24 – Melikchobanly**; 25 – Gyrlyg – Geoglyar; 26 – Chyragly; 27 – Akhar – Bakhar; 28 – Jeirli; 29 – Chalov; 30 – Maraza; 31 – Gurbanchi; 32 – Nabur; 33 – Chaigur – banchy; 34 – Shimshadi; **35 – Kichik Maraza**; 36 – Bozaakhtarma; **37 – Shikhzarli**; 38 – Shorsulu; 39 – Ekakhana; 40 – Makhlajik; 41 – Arabgadim; 42 – Juan; 43 – Gaiblar; 44 – Yeldarasi; 45 – Garajyuzlyu; 46 – West Tuva; 47 – East Tuva; 48 – South Tuva; 49 – Siyaki; 50 – west Veis; 51 – East Veys; 52 – Neftik; 53 – Jengi; 54 – Syungur; 55 – Iyimish; 56 – Birgut; 57 – Donguzdug; 58 – Baygushlu; 59 – Sarydash – Bayanata; 60 – Gyrdag; 61 – Pirekeshkul MV group; 62 – Agdag; 63 – Arbat; 64 – Gyrgyshlag; 65 – Boransyz – Jylga; 66 – Agzygyr; 67 – Garyja; 68 – Charani; 69 – Chapilmish; 70 – Shakhgaya; 71 – Chukhuroglybozu; 72 – Gazanagyl; 73 – Sheitanud MV group; **74 – Gushchu**; 75 – Kolany; 76 – Baidar; 77 – Ayazakhtarma; 78 – Ilkhychy; 79 – Sheikh Novruz; 80 – Sundi; 81 – Nardaranakhtarma MV group; 82 – Kyurdamich; 83 – Suleymanakhtarma; 84 – Cheilakhtarma; 85 – Gadridere; 86 – Hajiveli; 87 – Agnohur; 88 – West Cheildag; 89 – East Cheildag; 90 – Galandarakhtarma; 91 – Umbaki; 92 – West Davalidag; 93 – East Davalidag; 94 – Utalgi; 95 – Agtapa; 96 – Beyuk Kyanizadag; 97 – Goturlug; 98 – Gylynch; 99 – Toragay; 100 – Kichik Kyanizadag; 101 – Hajivelieri; 102 – Dashmardan; 103 – Shekikhan; 104 – Agdam MV group; 105 – Arzani; 106 – Durandag; 107 – Gotur; 108 – Agtirme; 109 – Emjek – emjek; 110 – Solakhay; 111 – Oyoug; 112 – Gyogyarchin; 113 – Dilyangyaz; 114 – Dashgil; 115 – Bala Bahar; 116 – Bahar; 117 – Garakyura; 118 – Airanteken; 119 – Saryboga; 120 – Goturda. Edited from (Aliyev et al., 2015).*

## 1.4 Research objectives

This thesis aims to present morphological, geochemistry data, and flux measurements of the poorly studied MVs of the northern Shamakhy-Gobustan region. The key objective is to investigate whether these volcanoes will provide similar results to previously published data of the southern Shamakhy-Gobustan and the Absheron regions. An improved and more diverse overview of the geochemical subsurface will be established.

The main goals of this study are the following:

- Establish the morphology and activity of the targeted MVs by considering recent eruptive events and the distribution and types of degassing features observed on the field

- Present novel geochemical data on the targeted MVs and determine the origin of fluids released at the surface

- Quantify flux measurements of the targeted MVs to evaluate the local methane and carbon dioxide budgets released to the atmosphere from marco- and mini-seepage.

## 1.5 Study outline

The remainder of the study is outlined in the following way. Chapter two provides background information about the structural and stratigraphic framework of eastern Azerbaijan in general and the northern Shamakhy-Gobustan region in particular. The third chapter presents general concepts, data, and methods, including i) general definitions, terminology, characteristics, and processes related to mud volcanoes, ii) the methods used to collect and apply the data to create morphological, geochemical and flux analysis, and iii) limitations related to the data. The fourth chapter presents the results of this study, including i) the results related to morphology, ii) results related to geochemical (molecular and isotopic) analysis, and iii) results related to $CH_4$ and $CO_2$ flux measurements. These results are discussed in chapter five. This discussion includes i) how large scale structures (e.g. faults anticline axes) may control location, morphology and features of mud volcanoes, ii) how the origin of collected gas samples from MV seeps can be determined by analyzing their geochemical composition, and iii) the potential impact of MV seepage on the atmospheric budget of greenhouse gases. Previous studies on geochemical analysis and $CH_4$ and $CO_2$ flux measurements are used to compare and discuss the main findings. Additionally, the limitations of the study are discussed and proposals for further

work are provided at the end of the chapter five. Chapter six summarizes the main findings of this study. Lastly, a reference list and appendix are integrated at the end of this thesis.

# 2 Regional setting

The relationship between gas seepages and subsurface geology was first described in the 50s (Walter K Link, 1952). In 1993, McGregor was the first to note that seeps are often related to the intersection of permeable fractures. This has been particularly observed in MV seepages, at the junction of two or more faults and at anticlines (Bonini et al., 2013; Etiope et al., 2013; Medialdea et al., 2009). As previously mentioned, MVs are prominent in HC basins, where specific stratigraphic components (petroleum plays, buoyant shale) exist. This chapter emphasizes describing the main structural features (section 2.1) and stratigraphic framework (section 2.2) of eastern Azerbaijan. The structural and stratigraphic geology of the Shamakha – Gobustan region is discussed in more detail in section 2.3.

## 2.1 Main structural features of eastern Azerbaijan

Azerbaijan lies in the Caspian region at the junction of Europe and Western Asia. It is bordered by the Caspian Sea to the east, Armenia and Turkey to the west, Georgia to the northwest, Iran to the south, and Russia to the north. The tectonic and depositional processes ongoing in this region resulted in widespread MV-ism surface manifestations. The geological history of Azerbaijan was shaped during the last phase of the Alpine orogeny during the Pliocene-Quaternary (Gurevich & Chilingar, 1995; Panahi, 2006). It has been highly influenced by the collision of the Arabian - Eurasian lithospheric plates, where the passive continental margin of the northern Arabian plate converged with the active continental margin of the southern Eurasian plate (Allen & Armstrong, 2008). The timing of the initial collision has been a topic of discussion for many years and the most accepted period is in the Late Mesozoic (Aliev, 1960; Axen et al., 2001; Devlin & Roeder, 1999; Dewey et al., 1986; Hempton, 1987).The collision subducted the pre-existing Neo-Tethys Ocean and subsequently changed the plate boundary configuration of the area. This impacted the seismicity, structural framework and volcanism of Europe to southeast Asia (Telesca et al., 2017; Tsereteli et al., 2016). The convergence progress generated tectonic features of which several influence Azerbaijan today. The main structural features of eastern Azerbaijan are the Greater and Lesser Caucasus, the Kura (sometimes referred to as *Kur*) depression, the Talysh mountains and the South Caspian Basin (SCB)

(Figure 2-1) (Kadirov et al., 2012; Reilinger et al., 2006; Telesca et al., 2017; Tsereteli et al., 2016).
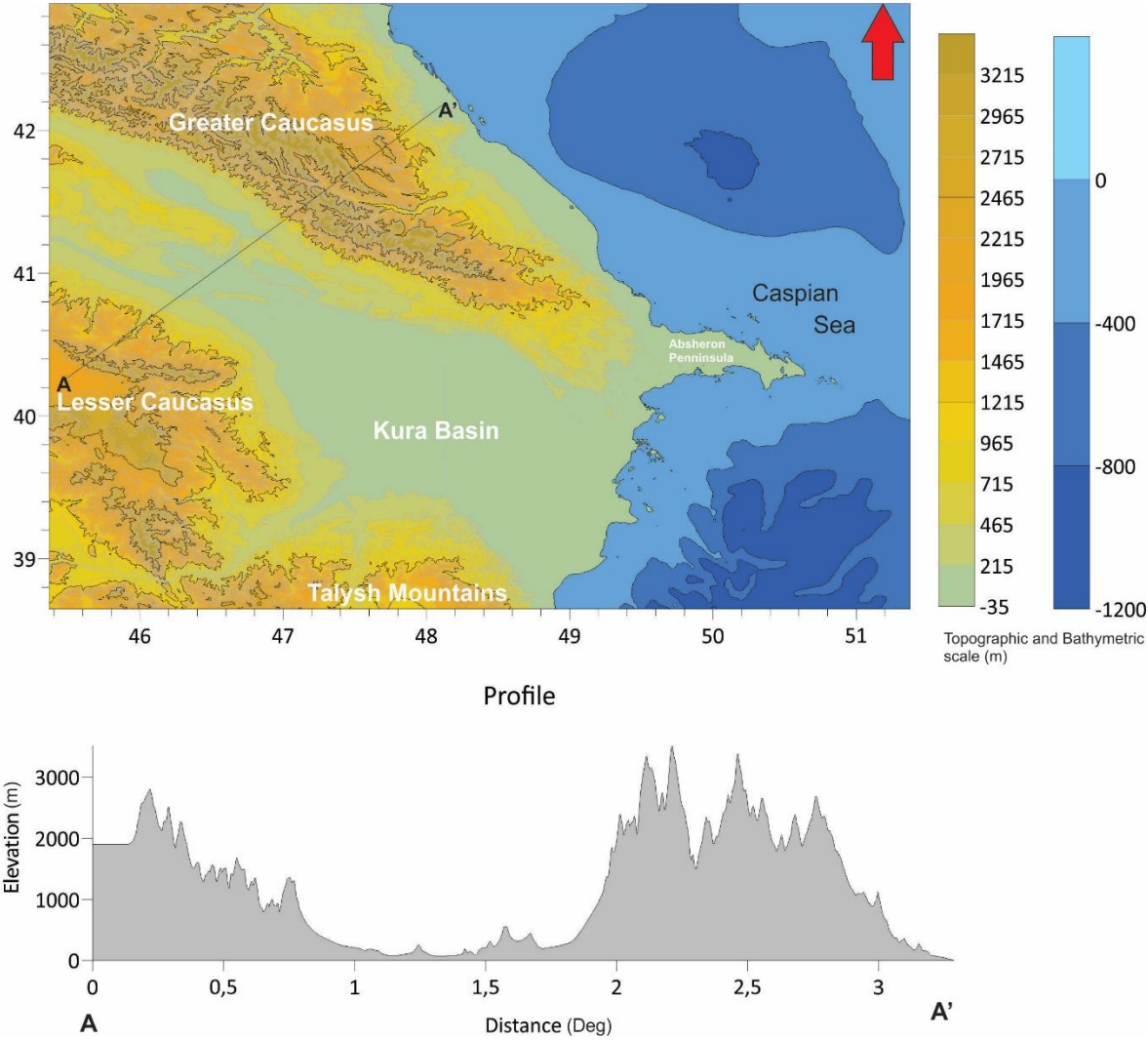


***Figure 2-1*** *Maps of Azerbaijan illustrating the main structural elements (Greater and Lesser Caucasus, Absheron Penninsula, Kura Basin and the Talysh Mountains) in Eastern Azerbaijan and a profile displaying the topographic variation along the Lesser Caucasus (A) to the Greater Caucasus (A') via the Kura Basin.*

### 2.1.1   South Caspian Basin

Various tectonic units surround Azerbaijan, but the SCB is the largest tectonic element of the area. It is a Tertiary back-arc basin and is one of the deepest basins in the world with a sedimentary package of 25-30 km. The SCB was exposed to rapid subsidence and extremely high sedimentation rates in the Quaternary (2.4 km/Ma) resulting in the deposition of 5-8 km

of sediments in the last 5 million years. Natural sediment dewatering processes were reduced by these extreme conditions resulting in overpressure units due to the lithostatic load transferred to pore water pressure. Consequently, the thick units of under-compacted shales became buoyant. The SCB also has a local low geothermal gradient (10-18 C/km) (Planke et al., 2003). With this, oil generation from immature source rocks can take place at unusually great depths. Some sources claim that oil generation in the SCB can be present up to 14 km below the surface (M.A. Abrams & A.A. Narimanov, 1997; R. S. Nadirov et al., 1997). These remarkable conditions are the main reason why mud volcanism is abundant both onshore and offshore in the SCB. More about the requirements for the formation of MVs can be found in the next chapter.

Based on volcanic sediments found in the Saatly well (Jurassic basalts, diorites and andesites rocks), the opening of the basin is estimated to originate from the Jurassic (Brunet & Cloetingh, 2003; Granath et al., 2000; Shikhalibeyli et al., 1988; Zonenshain & Pichon, 1986). Several theories regarding the age and mechanisms related to the opening to the oceanic basement of the basin have been proposed (Goodwin et al., 2020). Some authors suggests that the Caspian basin was originally part of the Paratethys Sea and it developed in the Mid Jurassic - Early Cretaceous as the Caspian and Black seas closed (Berberian, 1983; Dewey et al., 1973; Priestley et al., 1994). Others propose that the basin formation relates to the Caucasus region in times of major strike-slip movements (Şengör, 1990). A more accepted scenario is that the SCB formed as a result of the subduction of the Neo-Tethyan Ocean in the early Tertiary which was accompanied by a back-arc-rifting event (Berberian, 1983; Brunet & Cloetingh, 2003; Feyzullayev, 2012; Zonenshain & Pichon, 1986). Several studies reveal that the opening of the Caspian basin resulted in the isolation of the Caspian Sea (Abdullayev et al., 2017; Goodwin et al., 2020). This isolation along with the late Cenozoic events and the orogeny of the Greater Caucasus in the Late Eocene played an important role in the formation of the unique organic-rich stratigraphy, siliciclastic reservoirs and the onshore exposure of the Cenozoic source rocks in Azerbaijan (Goodwin et al., 2020; Saint-Germes et al., 2000). In terms of its motion, the South Caspian basement is different from the active NNE-SSW Arabian-Eurasian collision. Its westward collision results in unpredictable kinematics, which are related to on the pre-late Cenozoic framework. Many folds such as the Yasamal fold west to Baku, the Kirmaky to the north of Baku and the Malyi Kharami to the south east of the Greater Caucasus were formed in the South Caspian Basin during the late Cenozoic events.

### 2.1.2 Greater Caucasus

The Greater Caucasus mountain belt is located NW of the SCB and to the east of the Black Sea. It is a major topographic feature in Russia, Georgia and Azerbaijan, extending more than 1,100 km (Abdullayev et al., 2021). Jurassic sediments dominate the mountain range but they overly several basement units. Its formation dates from the Cenozoic when a previous Jurassic-Paleozoic back-arc basin was subjected to shortening and collisional structural inversion (Adamia et al., 2011; Adamia et al., 1981; Adamia et al., 1977; Brunet & Cloetingh, 2003; Ershov et al., 2003; Mitchell & Westaway, 1999). This fold and thrust belt opened in the early Jurassic and closed in the late Bartonian. The closure was a result of the Arabian – Eurasia collision and was followed by stages of collisions and uplift in the Langhian- Serravallian and the Zanclean-Holocene time, accordingly (Brunet & Cloetingh, 2003; Ershov et al., 2003; Zonenshain & Pichon, 1986). The Greater Caucasus is still a collisional orogen. On the western part of the Greater Caucasus is situated the highest mountain peak in Europe and Russia (Mt. Elbrus) and its maximum peak rises 5,642 m above sea level. The mountain belt has a decreasing trend in height from the east with lateral ridges that further striking towards the SE (Alizadeh et al., 2016). The continuation of the Greater Caucasus in Azerbaijan is the Absheron Ridge (more in section 2.1.5). There is an abundant number of anticlinal structures flanking the Greater Caucasus mountains, many of which are associated with oil and gas fields (Figure 2-1). These fields are part of the largest reserves in the SCB (section 2.1.4). There is an abundant amount of oil and gas fields located on the southeastern foothill of the Greater Caucasus, in eastern Azerbaijan (Alizadeh et al., 2016; Guliyev & Feizullayev, 1997; Jakubov et al., 1971). The main petroleum provinces of the Greater Caucasus region in eastern Azerbaijan include the Absheron-Pribalkhan and the Lower Kura (Figure 2-1). The Absheron-Pribalkhan ridge is dominated by anticline structures that date from the Plio-Pleistocene. The productive series are found in Pliocene sandstones with source rocks from both the Mykop Group and Diatom Formation (Tari et al., 2021). The traps are of the Absheron-Pribalkhan petroleum provinces are like the ones of the Lower Kura.

The eastern Azerbaijani play types (section 2.3) rely on the local structural and stratigraphic framework resulting from the orogeny of the Greater Caucasus. MVs are abundant in the region, especially in the Absheron and Shamakhy-Gobustan regions. They are (mostly) associated with the local petroleum fields at anticlines.

### 2.1.3    Lesser Caucasus

The Lesser Caucasus is located to the south of the Great Caucasus and runs parallel to it, measuring about 600 km (Figure 2-1). It extends in Azerbaijan, Georgia and Armenia (Allen et al., 2003; Joannin et al., 2010; Mitchell & Westaway, 1999). In Azerbaijan, the Lesser Caucasus is a volcanic belt, with general NW-SE trending oblique-slip faults, that was generated in the Neogene. The belt has repeated fault-bounded troughs that are interrupted by elevated structures and topography (Tari et al., 2021). Thick formations composed of volcanic and sedimentary formations are prominent in the southeast Lesser Caucasus. The mountain belt is cross-cut by extensional normal faults in the west. Structurally, the Lesser Caucasus is important in Azerbaijan as it has played an important role in eroding and depositing sediment in the east. It folded and thrusted deposits from the Jurassic – Miocene (Philip et al., 1989).

The Lesser Caucasus mega-anticlinorium hosts most of its MVs in Georgia but few Azerbaijani MVs are located at its southeastern foothill.

### 2.1.4    Kura Basin

The Kura basin is a sub-basin of the SCB. It is part of the Transcaucasian intermountain depression and can be divided into three depression zones: upper, middle and lower (Figure 2-1). The area within the Kura depression zone contains major oil and gas fields related to local anticlinal structures (Inan et al., 1997). These anticlinal zones are also characterized by the presence of many active MVs and mud breccia has been identified in several locations in the lower Kura depression zone (Javadova & Hauck, 2000). The depression has an unusually low temperature gradient (10 - 25 °C/km) and the oil window is therefore uncommonly deep (Michael A Abrams & Akif A Narimanov, 1997; Guliev & Feizullayev, 1996; Narimanov & Dore, 1993). Mud volcanism is not commonly associated with these depressed petroleum provinces because the of the lack of sufficiently and rapid sediment accumulation.
Both the middle and the lower zones are located in western and eastern Azerbaijan, accordingly.

This thesis is constrained to eastern Azerbaijan, the middle Kura basin is therefore excluded from this study. The lower Kura depression zone lies between the eastern Greater Caucasus to the north and the Lesser Caucasus to the south ((Kaz'min & Tikhonova, 2006; Saintot et al., 2006). Its eastern side subsides into the SCB, offshore Azerbaijan. The formation of the lower

Kura depression dates from the last deformation stage of the Alpine orogeny in the late Eocene. It was created during the mountain forming process of the Caucasus mountains where tension resulted in the formation of the block structures. In terms of structural geology, this zone is a mega synclinorium between the mega-anticlinoria of the Caucasus mountains and can be described as an abyssal structure. The depression is bordered by two deep-sited fractures: Acicay – Alet and Western Hazar. The petroleum provinces of the lower Kura basin comprise of over 15 fields with Pliocene productive series supplied by shales from the Maykop Group and by the Upper Miocene Diatom Formation in Miocene sandstones (Boote et al., 2018).

### 2.1.5 Absheron Peninsula

The Apsheron Peninsula is also an important structural element in Azerbaijan with high seismic activity and valuable petroleum production (Kroonenberg et al., 2000). It is an onshore continuation of the Apsheron - Balbhan sill, which is separated in the South by the Middle Caspian Basin (Figure 2-1). Its fold axis are curved and are different to the ones in the Greater Caucasus in terms of strike orientations. In addition, these folds are related to the formation of MVs, where overpressure from the subsurface hydrocarbons pierce the fold hinge lines or fold intersections (Allen et al., 2003; R. Nadirov et al., 1997). In fact, about one third of the world's MVs are located in the region of the Apsheron Peninsula and SCB (R. Nadirov et al., 1997).

### 2.1.6 Talysh mountains

The Talysh mountains are located in the southeast of Azerbaijan. They differ from the other tectonic structures of Azerbaijan as they were formed via the collision between the continental Iranian and Transcaucasian microplates and the suboceanic South Caspian rift. The timing of the collision dates from the Upper Cretaceous, and the subsequent subduction took place between the Paleogene-Eocene. Resulting compression, volcanism, fold and thrust belts formed during the process. Regional faults have a WNW-ESE to NNW-SSE trend and are allegedly deep-sited. Their associated folds are linked to the formation of Mud Volcanoes (Alizadeh et al., 2016; Tassi et al., 2020).

A simplified 3D illustration of the main structural features in eastern Azerbaijan is given in Figure 2-2. This provides an exaggerated overview (not to scale) of the how the features discussed in sections 2.1.1 – 2.1.6 are unified in eastern Azerbaijan.
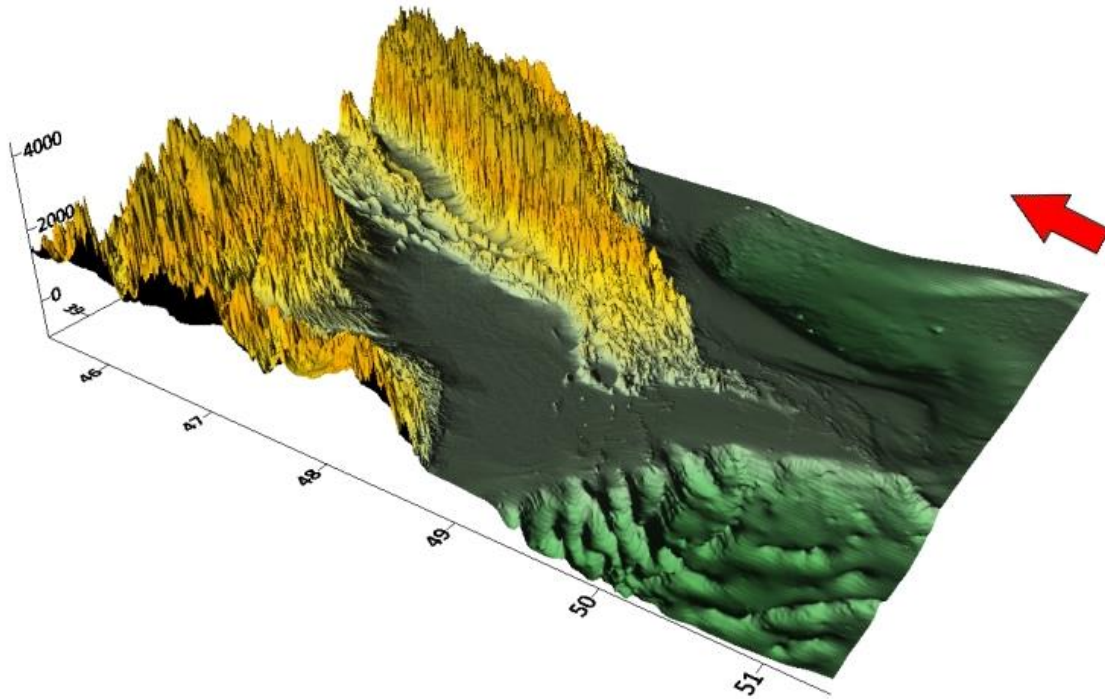
*Figure 2-2* *A simplified 3D illustration of the structural features (Greater and Lesser Caucasus, Kura depression,*
*Talysh Mountains and the SCB) of eastern Azerbaijan.*

## 2.2 Stratigraphic framework

The territory of Azerbaijan is dominated by Jurassic and Cretaceous deposits but has a
stratigraphic sequence that dates from the Cambrian to the Holocene (Figure 2-3). Structures
containing sedimentary, metamorphic and magmatic rocks are found throughout the country.
However, Azerbaijani MVs are mainly related to sediments from the Paleogene to the Miocene
epoch (O. Abbasov, 2016). This section will therefore exclude information related to the pre-
collisional stage (Late Proterozoic-Paleozoic). The stratigraphic framework is presented in two
parts: Cenozoic (sub-section 2.2.1) and source potential lithologies (sub-section 2.2.2). As the
deposits in Azerbaijan are part of major tectonic units (Greater, Lesser Caucasus, Kura
depression and Talysh mountains), this subsection will describe the stratigraphic framework
using these units as references. Information regarding micro and macro fauna is not included in
the descriptions. Note that highly detailed descriptions of the geological setting of Azerbaijan
can be found in the book written by Alizadeh et al. (2016). This section is entirely inspired by
this book (Alizadeh et al., 2016).
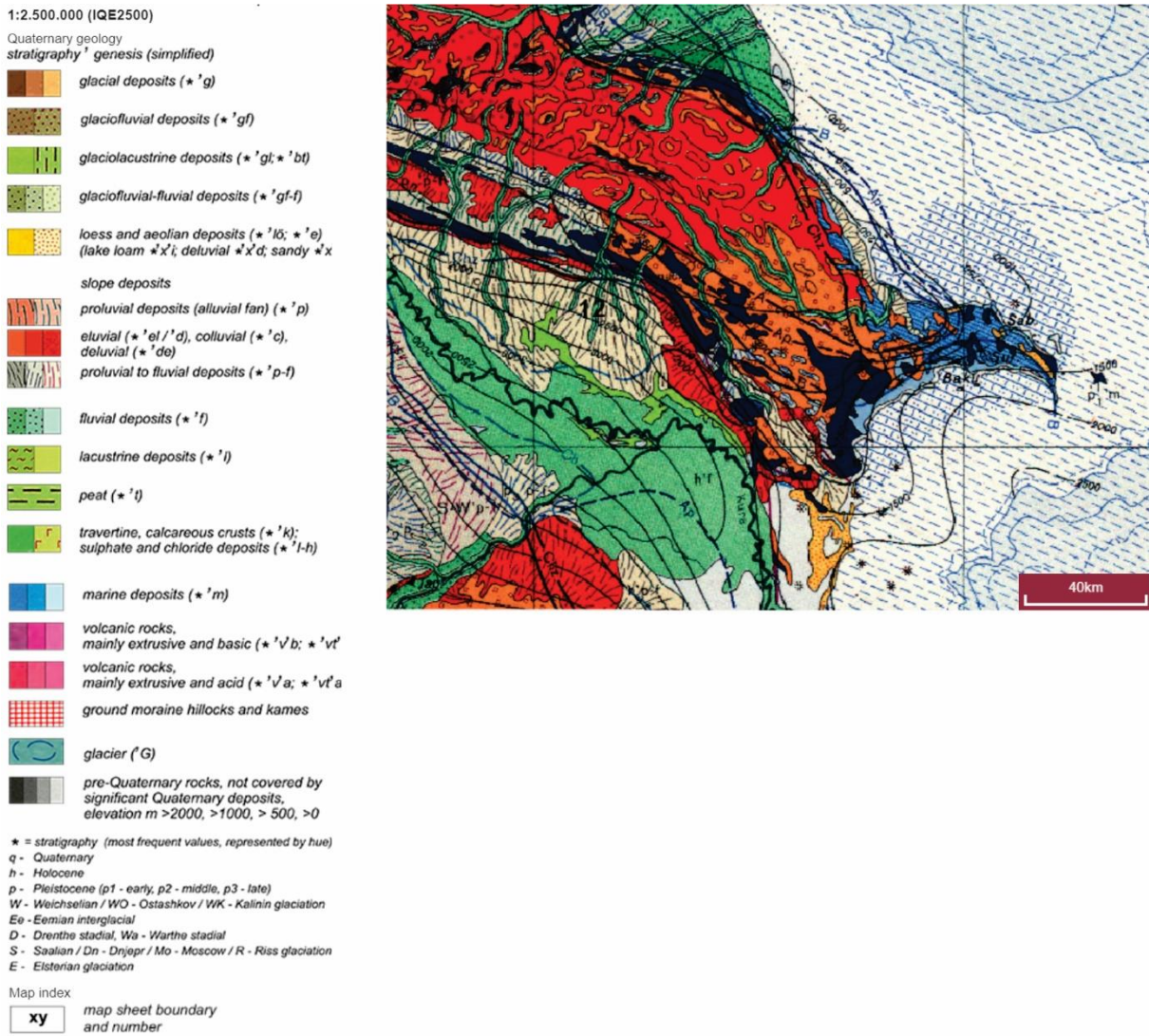
**Figure 2-3** *Regional geological map of Eastern Azerbaijan illustrating the distribution of the different deposits from a 1:5 million scale International Geological Map of Europe and Adjacent Area (GDI-BGR, 2020).*

**Paleogene** deposits are essentially composed of different types of rocks of which the majority are sedimentary, volcanogenic-sedimentary and volcanogenic. They are represented in the SE Greater Caucasus by the following zones: Sudur, Shahdagh-Khizi, Zagatala-Govdagh, Vandam and Shamakhy-Gobustan. These Paleogene rocks are mainly composed of clay, limestone, marls and sandstone. In the Kura depression, the period is reflected by sedimentary rocks found during deep drilling operations. In the Lesser Caucasus, Paleogeneic limestone, clay and marl are deposited over the Cretaceous deposits in both Lok-Garabagh and Goycha-Hakeri zones. Elsewhere, they are observed in regional throughs of Gazakh, Aghjakend, Aghdara, and Khachynchay-Khojavand troughs. In the Talysh Mountains, this period is represented through sedimentary deposits such as limestone, siltstones, marls and argillites.

**Eocene** complex overlies the formations of the Paleogene. They are largely developed in the zones of Zagatala-Govdagh and Shamakhy-Gobustan in the region of the Greater Caucasus. The Shamakhy-Gobustan region is especially significant to this study, as the investigated MVs are located in the northern part of the region. Here, the lower deposits are represented by clays, sandstones and limestones. The composition of the upper deposits are similar; they are characterized by shales and sandstones. **Young Eocene** deposits are also represented in the Kura Depression in the following areas: Tovuz-Gazakh, Khatynly, Mammadtapa, Gyragkasaman and Sajdagh. Here, the deposits resemble the ones found in the Greater Caucasus with carbonate clays, sandstone and marls interbeds. **Lower Eocene** deposits of the Kura Depression are observed in the Tovuz-Gazakh, Khatynly, Mammadtapa, Gyragkasaman and Sajdagh areas. These deposits are slightly more varied with siltstones, shales and marls in addition to alternations of limestone. In the region of the Lesser Caucasus the Eocene period is found adjacent to both the Paleocene and Upper Cretaceous formations in Lok-Garabagh and Goycha-Hakeri areas in addition to the zone of Araz. Deposits are mainly composed of volcanogenic-sedimentary rocks such as limestone, sandstone and shales. Finally, Eocene formations are represented in the Talysh zone and are dominated by sedimentary and volcanic-sedimentary deposits.

The **Oligocene** period is deposited parallel to the Eocene section. With this, they pursue the zones of Gusar-Devechi, Sudur, Shahdagh-Khizi, Zagatala-Govdagh, Vandam and Shamakhy-Gobustan. The zones of Shamakhy-Gobustan and Zagatala-Govdagh are especially notable as they include deposits from the Maykop Series. The Maykop suite are mud-dominated deposits from the **Oligo-Miocene** found 10-12 km below the surface and form the main HC source rock in Azerbaijan and in all of the SCB. These sediments are transported to the surface by the plumbing systems of mud volcanoes at anticline regimes. Both the Lower and Upper sections of the Maykop deposits are observed in the Kura Depression by sandy-argillaceous alternations, sandy shaly clays, and shaly clays with interbeds of sandstone. Oligocene deposits from the Maykop series are present in the NE piedmont of the Lesser Caucasus. Oligocene deposits are also found in the SE part of the Lesser Caucasus in the Gubatly area, and in the Araz zone. They are also present in the Talysh zones where the lower and upper sediments are composed of clay and sandstone.

**Lower Miocene** deposits are part of the Maykop Series and are present in the SE of the Greater Caucasus, Kura Depression, Lesser Caucasus and the Talysh mountains. Outcrops of the

**middle Miocene** deposits are prominent in the Shamakhy-Gbustan area of the Greater Caucasus. They are represented by marls and shales in the Tarkhanian deposits, by sandy-clayey and clayey lithofacies in Chokrakian deposits, clays with interbeds of dolomites and marls in Karaganian deposits and argillaceous facies in Konkian deposits. **Upper Miocene** deposits in Azerbaijan occupy vast areas and are mainly represented by Sarmatian and Meothic rocks occurring in the zones of Gusar-Devechi, Sudur and Shamakhy-Gobustan and zones of Gusar-Devechi, Shamakhy-Gobustan and Absheron, accordingly. The Sarmatian rocks are mainly marine or shallow-marine deposits while the Methic rocks are typically characterized by shale and clay with dolomitic and volcanic ash interbeds. Pontian deposits from the Upper Miocene are less dominant but represent important marine deposits in the Absheron peninsula and in the Shamakhy-Gobustan area.

**Pliocene** deposits are commonly found in the main structural zones of Azerbaijan such as the SE Greater Caucasus, the Kura Depression, the Lesser Caucasus, in addition to the Absheron peninsula and the areas close to the Caspian Sea. **Low Pliocene** deposits are characterized by marine deposits with large hydrocarbon diffusion and are found in the Absheron peninsula, Lower Kura and Shamakhy-Gobustan area. Drilling data from these areas show that the Absheron deposits were represented by sandy argillaceous formations and alternating sand and clay. Such deposits are found in the Gala suit in well 7, well 1 and well 900 in the Hazi Aslanov, Oguz and Neft Dashlary areas, respectively. Other suites such as the Gyrmaki, Fasila, Balakhany, Sabunchu, Surakhany suites also represent sediments of the Lower Pliocene deposits of Absheron and Kura depression. Gobustan sediments are represented by calcareous sandstone and siltstone. The **upper Pliocene** deposits in Azerbaijan are represented by the Akchagyl stage and are significant to the geology of the country. These deposits are expressed by marine, volcanogenic and continental attributes. The marine deposits are represented by sandy clays, sandstones and mud volcanic breccia. They comprise the Absheron, Gobustan and Shamakhy regions amongst other. The Absheron zone is mainly composed of clay, with laminas of ashes. The Gobustan zone is characterized by clays with lamias of ashes and mud-volcanic breccia in its lower part and sandy clays in the upper part. The Shamakhy zone is dominated by clays with some sand laminas with ashes in its lower part and sandy clay, sand and sandstones in its upper part.

**Quaternary** deposits are represented by clayey sand, limestone, conglomerates and volcanic ashes and are found throughout Azerbaijan. The **Eopleistocene** epoch is reflected in the

Absheron stage, where the deposits are dominated by marine, coastal-marine and continental facies represented by sandy clay, clay with sand lamina, marls, sandstone, limestone, ash, and gypsum. **Pleistocene** deposits in Azerbaijan are characterized by clay, silt, sand and sandstone and are represented in the Baku horizon, Mingachevir beds, Khazar horizon and the Khvalyn horizon. Here, continental sediments eventually succeed marine sediments via alluvial-proluvial and alluvial deposition. These deposits are scattered around the NE slope of the Greater Caucasus, the Less Caucasus and the Talysh mountains. They consist of pebbles and conglomerates with sand, loam and volcanic ash intrusions and are represented in the Khazar and Khvalyn horizons.

**Holocene** deposits in Azerbaijan are found throughout the country and are characterized by the horizon of **Novocaspian** and intrusions from the Khavlyn horizon. The deposits reflect typical high energy environment deposition with marine deposits in the **lower Novocaspian** presented by clays with sandy interbeds in the lower part of the Kura Depression. Towards the Caspian Sea area, however, these deposits become more rich in sand with some silt. The marine clayey deposits are then replaced by sandy and loamy alluvial marine sediments in the Holocene transition. The main continental Holocene deposits are characterized by the following formation types: lacustrine, alluvial, alluvial-proluvial, mud-volcanic and volcanogenic. The lacustrine deposits are present in both the Kura-Araz and Lenkaran areas. The alluvial-proluvial sediments have a wider range of deposition. They are observed in the plains of Shirvan and Mil, Lenkaranian Mughan, Ajinohur basin, in addition to the Mughan and Salyan lowlands. In terms of their composition, the alluvial-proluvial sediments contain silt, clay and loam. Finally, the alluvial deposits are only represented in the Kura and Araz rivers and are dominated by sand, loam and clay. Deposits of mud volcanic breccia are mainly found in the areas of the Gobustan, lower Kura Depression and Baku archipelago. The breccia has no stratigraphic units and are simply homogeneous masses of clay that were carried towards the surface via the eruptions of MVs. Note that all the Holocene deposits are present in the Absheron peninsula.

Given that no geological map of the Samakhy-Gobustan is found, the geology of the central and southern Gobustan region is illustrated in figure 2-4 in order to give an overview of the local geology near the study area.
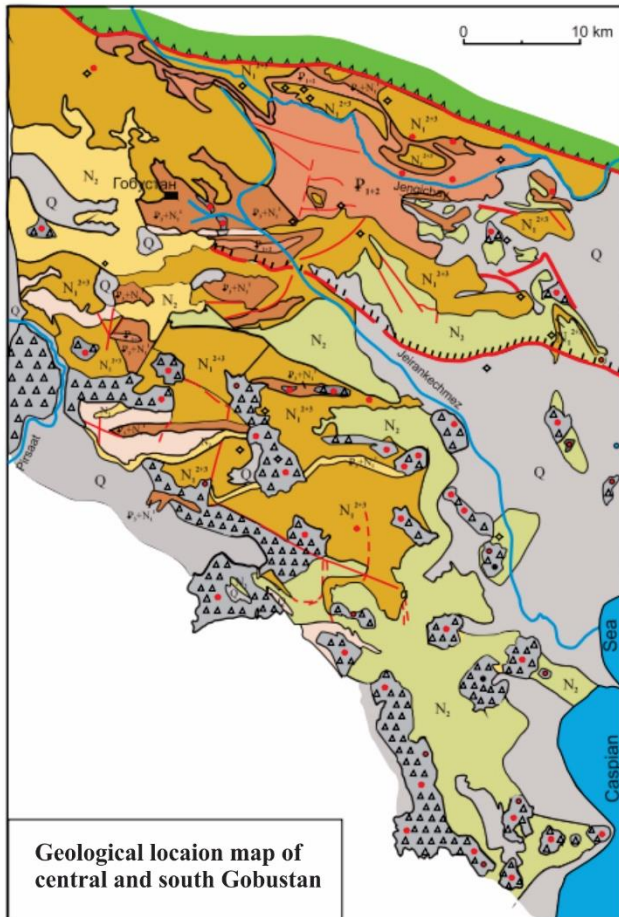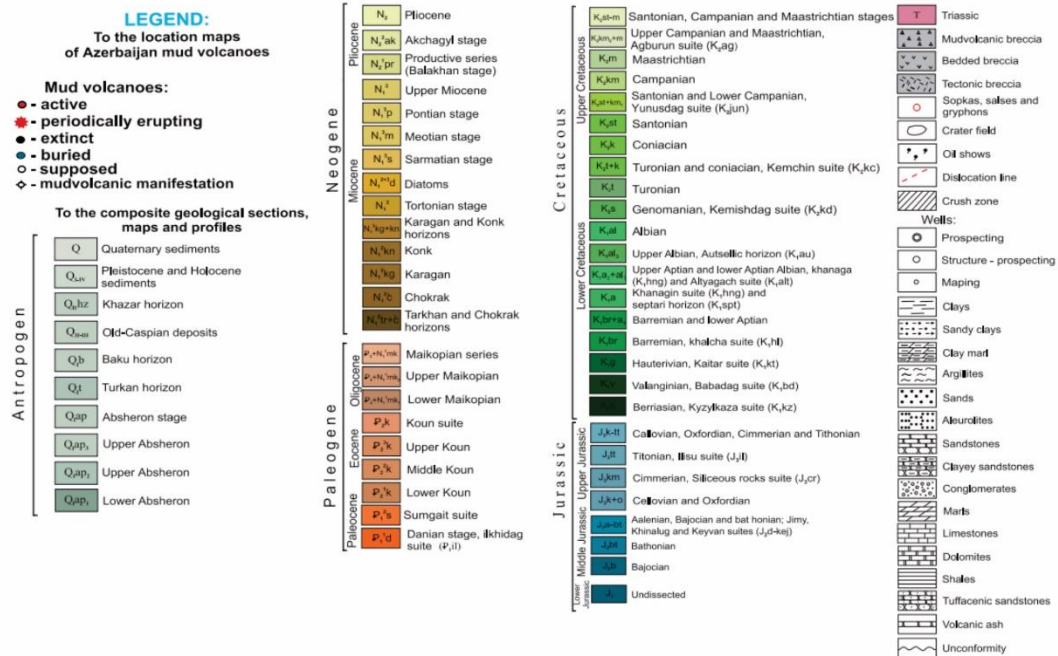
**Figure 2-4** *Geological map of central and south Gobustan including mud volcanic breccia from erupted MVs (Aliyev et al., 2015)*

## 2.3 Source potential lithologies

Every oil and gas field in the South Caspian Basin (SCB) is accompanied by mud volcanoes (Guliyev, 2006). Hydrocarbons of the SCB are present in different stratigraphic units (Upper Cretaceous to Pliocene-Anthropogene) within extremely thick sedimentary basins (>25 km). Majority of the productive series occur in Lower Pliocene reservoirs (90% of the reservoirs) (Feyzullayev et al., 2001). This section briefly discusses the two main lithologies that are key to the petroleum source rocks of the petroleum provinces in Azerbaijan: Maikop series (sub-section 2.3.1) and the Diatom suite (sub-section 2.3.1).

### 2.3.1  Maikop series

The Maikop series of the eastern Azerbaijan dates from Oligocene to the Miocene. It is composed of thick silty mudstone (up to 3 km) and is extremely rich in total organic carbon (TOC), up to 15%. The mudstone is difficult to date due to its limited assemblage of microfauna. Alternative dating methods such as chemostratigraphy and radiostratigraphy have been used to study the Maikop series (Afandiyeva). In the SCB, the Maikop series has only been analysed through MV ejecta and often use deposits from the Kura Basin as an analogue (Isaksen et al., 2007).

### 2.3.2  Diatom suite

The Miocene Diatome suite is one of the source rock with highest TOC (up to 7.8%) in the South Caspian region (Goodwin et al., 2020). Note that it has about half the TOC of the Maikop series. The Middle and Upper Miocene have espessially high source potential. The total thickness of the suite is not completely certain, but is said to smaller than the Maikop series. Studies of the Diatome suite often rely on MV ejecta.

It is essential to recognize the chronostratigraphy of these source rocks as they play a key role in most of the formation of Azerbaijani MVs.
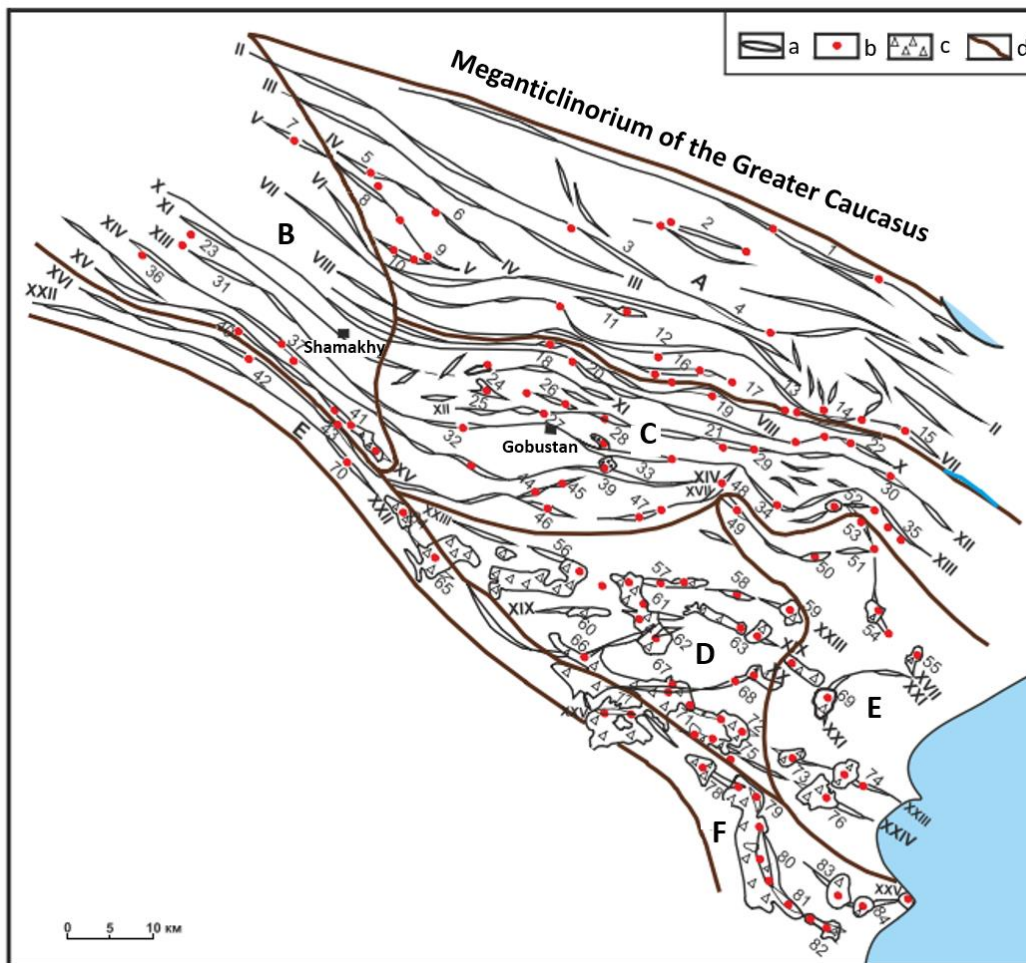
## 2.4 Shamakhy-Gobustan region

Onshore and offshore eastern Azerbaijan is divided into six regions: 1) Caspian-Guba, 2) Shamakhy-Gobustan, and 3) Absheron, 4) V-Nizhnekurinskiy, 5) Baku Archipelago, and 6) Zones of folding in the deep water part of the Southern Caspian Sea (Figure 1-3). This section will strictly focus on region 2.

The Shamakhy-Gobustan region can be decomposed into 5 tectonic zones: North Gobustan, Shamakhy, Central Gobustan, Southwestern Gobustan and South East Gobustan (Figure 2-5). Shamakhy-Gobustan region occupies a significant part of the southeastern immersion of the Greater Caucasus and is characterized by the widest distribution of mud volcanoes. There are 120 MVs in the Shamakhy-Gobustan region (Figure 1-4). Note that initially, Gobustan and Shamakhy are two separate regions, but are often reported as a single region. Gobustan is a popular area for MV exploration and is located 53.20 km south from Baku. It is not to be confused with the Gobustan district located in the middle east of Azerbaijan or the town of Gobustan located by the east coast of the Caspian Sea. The number of MVs in the Gobustan region is estimated to be 80 (Aliyev et al., 2015). Gobustan is usually subdivided into three zones: North, Central and South. According to Aliyev et al., (2015), South Gobustan hosts 43 MVs, while the Central Gobustan has 28 MVs and North Gobustan has 9 MVs. With this, one can say there is a general north to south trend in the distribution of mud volcanoes in the Gobustan area (Babayev et al., 2014). This trend can be described by the regional tectonic setting where anticline structures are prominent in the south (Jakubov et al., 1971). The Shamakhy region is located about 100 km West from Baku and is a new area of exploration for mud volcanism. The region is mostly known for its oil fields and unusually high seismic activity. According to Aliyev et al. (2015), about 6 MVs are established in this region and recent eruptions call for new investigations.

Small mud volcanoes are located in the north Gobustan region (e.g. Gyzmeydan MV) while the largest and most active volcanoes are located in the southeastern Shamakhy-Gobustan region (e.g. Toragay MV) (Figure 1-4). In eastern Gobustan, tectonic areas separated by the Zogalavachai superimposed synclinal (Figure 2-5). In the southern section, the Paleogene and Miocene deposits are thrusted over the Pliocene rocks creating good settings for MVs (e.g. Madrasa and Melikchobanly). In the western Gobustan region, sediments are dominated by Paleogene and Miocene clayey and sandy-argillaous sediment that unconformably overlie the sequence of Pontic and Akchagyl deposits. In this zone, anticlines are strongly compressed and

numerous mud volcanoes reside (Dzheyrli, Aharbahar, Shorsulu, Arabgadim, etc.) (Aliyev et al., 2015). The Central Gobustan zone is composed mainly of Paleogene-Miocene deposits that reach up to 4-4.5 km in the southern slopes of the Greater Caucasus (Aliyev et al., 2015).

***Figure 2-5*** *Structure of the structural localization of mud volcanoes in the Shamkhy-Gobustan region. Tectonic zones: A- North Gobustan, B- Shamakhy, C- Central Gobustan, D- Southwestern Gobustan, and E- South East Gobustan. Tectonic features: a-Large structures, b-mud volcanoes, c- mud volcanic breccia, d- boundaries of tectonic zones. Anticlinal zones: I-I - Altyagach-Kurkachidag (1. Kurkachidag, 2. Kemchi), I-II - Sarydashchay-Yunusdag (3. Aladash, 4. Shikhandag). III-III-Pirbeyli-Agdara, IV-IV-Gyzmeydan-Tyurfinskaya (5. **Gyzmeydan**, 6. Gurudag), V V - Demirchi-Khilmillinskaya (7. Demirchi. 8. Yeni-Gyzmeydan, 9. Khilmilli), VI-VI - Talyshnuru-Giblyadag (10. Khadzhyly, 11. Gyshgayrag), VII-VII - Nagarakhana-Islamdag (12. Geradil, 13. Sev. Neftik, 14. Neftik, 15. Islamdag), VIILVIII-Chukhuryurd-Siyakiarasy (16. Tuva , 17. Siyakiarasy), IX-X - Engekharan-Sev. Kechalyarskaya (18. Nabur. 19. East. Garajuzli). X-X - Muji-South. Kechalyar (20. North. Shimshadi, 21. Dzhengichay, 22. South. Kechalyar), XI-XI - Khankendi-South. Akhudag (23. Khankeidi, 24. Dzheyrli, 25. South. Dzheyrli, 26. Gurbanchi), XII-XII - Gozeydag-Kosmalinskaya (27. **Maraza**, 28. South. Shimshadi. 29. Jengi, 30. Gyultamin), XIII- XIII - Pyrgarachukha Boransyz-Bayanatinskaya (31. Pirgarachukha, 32. Khydyrly, 33. Gaibler-Shaiblyar, 34. Baygushlu, 35. Boransyz-Bayanata), XIV-XIV - Bizlan-Shikhzarlinskaya (36. Bizlan, 37. Garavelli, 38. Yekakhana, 39. **Shikhzarli**). XV-XV - Keyvendilee Melikchobanly (40. Zarkhi, 41. **Melikchobanly**), XVI-XVI - Beglian-Birgudskaya (42. Guneshli. 48. Birgud). XVII-XVII - Dongyzdyg-Shakhkainskaya (49. Dongyzdyg, 50. Kaftaran, 51. Agzygyr, 52. Gyrdag, 53. Gyrgyshlag, 54. Shahgaya, 55. Anart), XVIII-XVIII - Poladly-Cheilakh Tarminskaya (56. Gidzhakiakhtarma, 57. Nardaranakhtarma, 58. Suleymanakhtarma, 59. Cheilakhtarma), XIX-XIX - Sundi Cheildagskaya (60. East. Syundi, 61. Kyurdamich, 62. North. Zahardag, 63. Cheildag, XX-XX Gushchu-umbakinskaya (64. **Gushchu** , 65. Girda, 66. West Gadzhiveli, 67. East Gadzhiveli, 68. Umbaki-Ragim), XX-XXI - Utalgi-Miadzhik (69. Utalgi), XXIFXXII - Bilistan-Lengebiz (70. Lengebiz), XXIII- XXIII - Shekikhan-Kyanizadag (71. Shekikhan, 72. Agdam-Gylynch, 73. Toragai, 74. Kyanizadag), XXIV-XXIV - Arzani-Kichik-Kyanizadag-Duvanninskaya (75. Arzani, 76. K.Kyanizadag-Duvanny), XXV-XXV - tectonic zone of the Alat ridge (77. Dashmardan, 78. Baridash, 79. Northern Solakhai, 80. Southern Solakhai, 81. Airanteken, 82. Goturdag, 83. Gyrdag, 84. Dashgil). Edited from (Aliyev et al., 2015).*

# 3 Concepts and methods

The following chapter introduces relevant basic definitions and concepts (section 3.1), presents the data used (section 3.2) and describes the methods employed (section 3.3) in this study.

## 3.1 Basic concepts of Mud volcanoes

What are mud volcanoes?

There are thousands of them globally, yet their occurrence seems to remain overlooked by the general public and much of the scientific community (Aliyev et al., 2015). This section presents updated terminology and perquisites particularities of MVs, presumed necessary for the understanding of the remainder sections and chapters: definitions, terminology and general characteristics (sub-section 3.1.1), mud volcanism and petroleum systems (sub-section 3.1.2), activity mode, dimensions and morphologies (sub-section 3.1.3), MV structures (sub-section 3.1.4), main surface degassing features (sub-section 3.1.5), seepage modes (sub-section 3.1.6), general gas composition (sub-section 3.1.7), global budget gas emission (sub-section 3.1.8) and mud volcanism activity, frequency and seismicity (sub-section 3.1.9).

### 3.1.1 Definitions, terminology and general characteristics

The definition of MVs has evolved over the past centuries. Yet, they are often mistaken for other piercement structures as they share similarities with other shale intrusion expressions such as mud basins, mud mounds and piercement shale diapirs (Dimitrov, 2002b; Hovland et al., 1998; Kopf, 2002; Milkov, 2000). Updated review of MVs described by Mazzini et Etiope (2017) provides new attributes to prevent the misuse of this geological term. According to new specifications, a MV must at least fulfil all of the following characteristics:

1. Ternary system (gas, water, and sediment - and sometimes oil)
2. Diagenetic or catagenetic hydrocarbon production system
3. Sedimentary rocks with a gravitative forming mobile shales, diapirs or diatremes
4. Common discharge mud breccia (i.e., fine-grained matrix incorporating clasts) and sometimes microbial colonies

Note that the structures studied in this thesis meet these criteria. Additionally, traits and terms are essential to recognise in order to grasp a basic understanding of sedimentary volcanism. The term "MV" is often used to describe surface expressions and their discharge without considering their subsurface settings. It is essential to note that MVs are only present in sedimentary HC basins that are not affected by external thermal systems. Volcanic, geothermal, hybrid systems and any non-sedimentary settings are never affiliated with MV-ism (Etiope & Martinelli, 2009).

Environments that host MVs must also include the uprising of shales as this is necessary to initiate MVs (Revil, 2002). In a such systems, buoyant shales from low-density sediments cause gravitative instability. Overpressure caused by gas migrating from reservoirs fed by deep-sited source rocks forms below impermeable caprocks typically at anticline axis. The migration from source rocks to oil and gas traps, increases the pressure gradient. The over-pressurized gas may seep through the impermeable layer via hydro-fracturing, creating fractures in pre-existing faults. Other factors such as tectonic stresses, reactivation of faults and seismic activity may result in fracturing and leaking cap rocks. The pressurized fluids may seep to a shallower reservoir where pressure re-accumulates. This critical instability can eventually be triggered, resulting in a sudden pressure release. Large quantities of gas and saturated sediments, mudbreccia, water and sometimes oil are transported via a feeder channel to the surface during a MV eruption (Figure 3-1) (Dimitrov, 2002b).
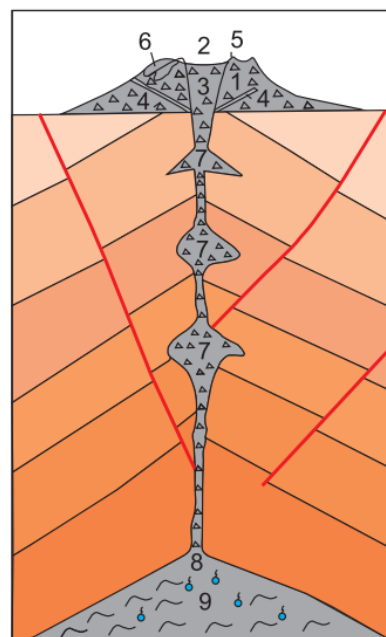


*Figure 3-1* *Conceptual drawing of the plumbing system of MVs, including the principal elements. 1-mud volcanic construction; 2-crater; 3-vent; 4-sheet deposits; 5-crateral swell; 6-mud volcanic flow; 7-mud cameras; 8-base; 9-hearth (Aliyev et al., 2015).*

### 3.1.2 Mud volcanoes and petroleum systems

MVs are commonly found in petroleum bearing sedimentary basins and are related to the "Total Petroleum System" (Magoon & Schmoker, 2000).

A petroleum system includes four essential elements: source rocks, reservoir rocks, seal rocks and overburden rocks. Additionally, some essential processes such as the generation, migration and accumulation of hydrocarbons (HCs) are necessary for conventional plays. This is also true for the initiation of (most) MVs. As previously mentioned, MVs are surface indications of migrating HCs and are generally (not always) associated with natural oil and gas reservoirs (Abrams, 2005; Etiope, 2015). In petroleum systems, hydrocarbons mature in and migrate from the source rock to shallower reservoirs of geologically younger deposits. In unstable sediments (no isostatic equilibrium) at local anticlines and/or faults, over-pressurized gas from deep sited source rocks may directly seep to the surface when related to mud volcanoes. This usually occurs in subsiding basins with high sedimentation rates (Mazzini & Etiope, 2017). Hence, MV seepage can be seen as a single primary migration mechanism. If this seepage penetrates shallower HC reservoirs, oil and gas may also migrate to the surface via MV-ism. MVs can therefore be used to assess the origin and quality of oil and gas.

The source of oil and gas in petroleum systems is from source rocks that are rich in organic material (OM). Here reaction conditions (geological time, depth of burial, and temperature) generate oil and gas molecules. Equations such as the Arrhenius equation can estimate how much OM will be converted to oil and gas molecules given a burial and temperature history (Bjorlykke, 2010).

OM can undergo four main stages to become HCs: deposition, diagenesis, catagenesis, and metagenesis. The deposition stage comprises the sedimentation of OM, in this process a small portion of organic carbon can deposited in sediments under anoxic environments. Diagenesis is where the rocks are compacted under mild pressure and temperature conditions, converting the OM into kerogen. During catagenesis, kerogen is thermally degraded, forming HC chains. Increasing burial depth and temperatures result in long HC chains (oil) to crack, forming shorter HC chains (gas). In metagenesis, HC is driven off and leaves residual carbon. This can be analysed by sampling seepage of MVs (section 1.7).

Total organic carbon (TOC) is an essential factor in generating oil and gas. A potential source rock has usually more than 1% by weight OM (> 1% TOC). Organic-rich sediments in anoxic

environments are favourable for forming high quality source rocks. This is classified by types: type I OM generates waxy crude oil, type II generates both oil and gas and type III generates gas with some oil. The Van Krevelen diagram illustrates the OM types in relation to the hydrogen to carbon ratio over the oxygen to carbon. Hence, the source rock types can also be evaluated by analyzing oil seepage from MVs.

### 3.1.3 Activity mode, dimensions and morphologies

The morphology of a MV can reflect many properties related to the composition, frequency and intensity of its previous eruption(s). MVs can be either eruptive, dormant, extinct or fossil. The eruptive phase of MVs can be dramatic. Mud breccia can be expelled tens of meters from the crater, and flames from burning (methane) gas and oil may occur. During the dormant (post-eruptive) phase, MVs are active in the subsurface as over-pressure re-accumulates under a new seal. During this stage, macro seepage can be observed in outlets called pools, gryphons and salsa lakes (section 3.1.5). New eruptive phases may occur after the dormant phase. In the extinct stage, a MV has no reported eruptions but may seep some gas within historical time. The fossil stage of a MV is reached when its structures are buried in the subsurface and can only be revealed via acoustic or drilling investigations (Mazzini & Etiope, 2017).

MVs are most active at their centre, where the radial expansion of the runoff material plays an important role in shaping the volcanoes (Perez-Garcia et al., 2009). A water-dominated eruption will result in a homogenous and flat morphology, reflecting frequent and runny outbreaks. On the other hand, a gas-dominated discharge is recognised by compacted and thick morphology with little elevation due to frequent powerful bursts rich in mud breccia (Mazzini & Etiope, 2017). Other factors such as the viscosity of the mud breccia, eruption frequency, diameter of the conduit, local topography, local subsidence and more substantial natural erosion (rain, wind, ice) impact the final morphology an MV. Note that the morphology of offshore MVs is affected by additional factors such as water depth, current direction and intensity, salinity and less affected by weathering and surficial erosions (Barber et al., 1986; Feseker et al., 2009; Kioka & Ashi, 2015).

### 3.1.4 MV structures

According to Mazzini and Etiope (2017), there are 12 different types of morphological MVs: conical, elongated, pie-shaped, multicrater, growing diapir-like, stiff neck, swamp-like,

plateau-like, impact crater-like, subsiding structure, subsiding flanks, and sink-hole type (Figure 3-1) (Mazzini & Etiope, 2017).

**Conical** shaped MVs are the most common morphology. They reflect regular low viscosity eruptions and are represented by rounded craters surrounded by multiple (conical) layers of mud and breccia representing different eruption events. Famous conical MVs are Touragay (Azerbaijan), Chandrgup (Pakistan), Sand (Iran), Texel and San Remo (Mediterranean sea). **Elongated** MVs are affected by the tectonic framework of their environment. Features such as faults and folds control their structure and seepage mechanisms. Lokbatan (Azerbaijan), Pirekeshkul (Azerbaijan) and Kazan (Eastern Mediterranean Sea) are some of the most known elongated MVs. **Pie-Shaped** MVs are flat with some relief at the centre, with a mean surface slope of < 5 deg (Kopf, 2002). According to Kopf (2002), pie-shaped MVs have larger conduits than other MVs and are characterised by the large volume of erupted material . They are represented by the Dashgil (Azerbaijan), Dvurechenskii (Black Sea) and Mercator (Gulf of Cadiz). **Multicrater** MVs are characterised by having several conduits but no main crater. Examples of such volcanoes are Bahar (Azerbaijan) and Hesperides (Gulf of Cadiz). **Growing diapir-like** MVs sit on elevated, massive, stiff mud breccia constantly extruded from the crater. The accumulated mud breccia makes such a volcano relatively tall as the material is difficult to erode. Koturdag (Azerbaijan) and Raznokol (Taman Peninsula) MVs are examples of growing diapir-like volcanoes. **Stiff neck** MVs are characterised by long and tall conduits consisting of mud breccia or carbonate sandstone. The so-called "neck" grows as the number of eruptions increases. Examples of stiff-neck MVs are the Kobek and Boya-Dagh in Turkmenian. **Swamp-like** morphology is found in MVs that erupt saturated and fine mud breccia. The flowy consistency of the extruded material prevents any buildup from happening, and the volcano is unable to accumulate material and therefore never grows vertically. Pangangson (Java), Lipad (Borne) and Tabin (Malaysia) and exampled of Swamp-like MVs. **Plateau-like** structures are flat at the top, with slight elevation. Several plateau-like MVs are found near compressional structures, and many are surrounded by deformations caused by fractures or ridges (Dupré et al., 2008). Akhtarma Pashali (Azerbaijan) and Amon (Eastern Mediterranean) are plateau-like MVs. **Impact crater-like** MVs are characterised by an indented crater caused by a powerful eruption where the crater collapses. Examples of such volcanoes are the Bakhar satellite MV (Azerbaijan) and the Morne Diablo MV (Trinidad). **Subsiding structure** and **Subsiding flanks** are two types of MV morphologies caused by local subsidence. Subsiding structure MVs are depressed at the centre, where elevation is consequently low and include seepage features.

Bleduk Kuwu (Java) and Chirag (Caspian Sea) MVs have subsiding structure morphologies. Subsiding flanks show depression around the crater and are therefore taller than the subsiding structure MVs. Subsidence around the structures are presumed to occur due to local structural features, and seismic images have proved the presence of faulted zones by the flanks of these volcanoes. The Napag (Iran) and Håkon Mosby (Norwegian Sea) MVs have subsiding flanks characteristics. **Sink-hole** structures are dominated by single salsa lakes in the centre of a depressed crater. Degassing takes place within the lake and several other areas of the volcano. These structures are not well studied but are thought to be created by the accumulation of gas resulting in over-pressure followed by an eruption. The Pink Porsykel MV (Turkmenistan) present a sink-hole morphology.
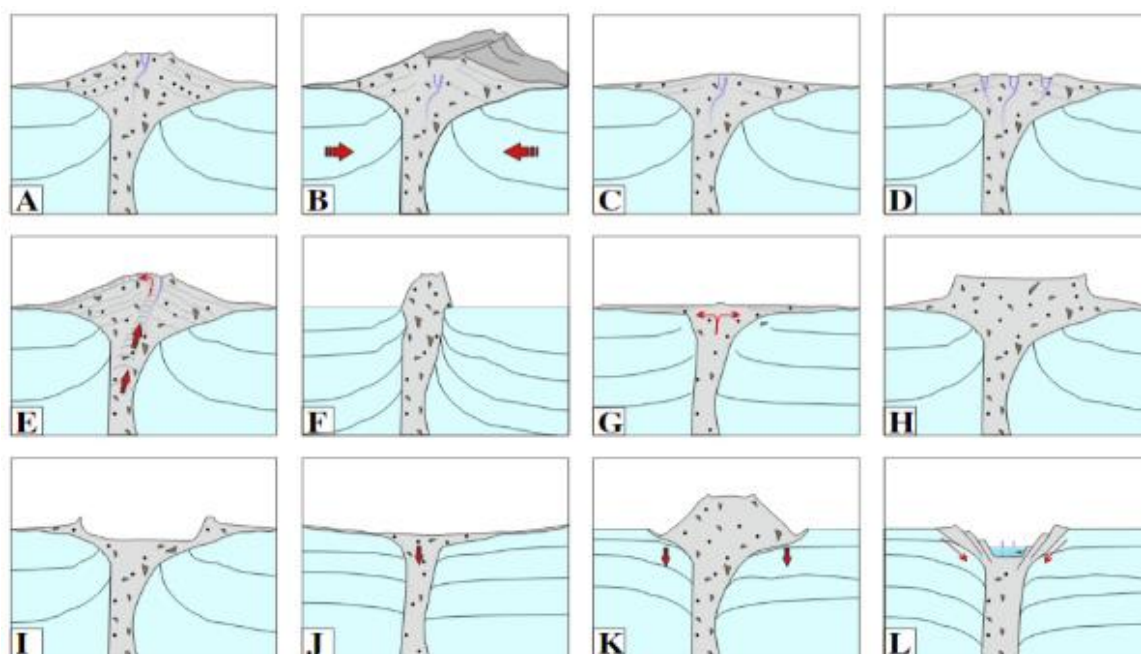


***Figure 3-1*** *Illustration of the 12 different MV morphologies: (A) conical (B) elongated (C) pie-shaped (D) multicrater (E) growing diapir-like (F) stiff neck (G) swamp-like (H) plateau-like (I) impact crater-like (J) subsiding structure (K) subsiding flanks (L) sink-hole type (Mazzini & Etiope, 2017).*

### 3.1.5 Main surface degassing features

MVs can be detected in the field by identifying degassing structures, bacterial colonies, and erupted mud breccia. Seepage structures are not to be confused with MV structures. These surface expressions result from the upward migration of gas and sediments rich in hydrocarbons due to pore-fluid overpressure. They form within dormant craters, post powerful eruptions, and seep gas, mud, water, and oil. Multiple environmental factors such as seismicity and atmospheric pressure can affect the formation of these degassing features (Etiope & Ionescu,

2015; Mellors et al., 2007). These effects are discussed below in sections 3.1.8 and 3.1.9. Onshore MVs have three main seepage structures: gryphons, salsa lakes and pools.

**Gryphons**, or mud cones, are small seized (>4 m) conical outlets that emit gas, mud, water, and oil (Figure 3-2 a,b). The morphology and eruption styles of gryphons may vary depending on the viscosity of the erupted mud and the degassing mode. If gas is dominant and the structure has a small opening, the gryphon may be called a "splatter". If the structure has a larger opening filled with mud, it is a "bubbler". A "clast-rich" gryphon intuitively seeps sediments rich in clasts and are often taller than the other two types. The bubbling activity of gryphons can be intermittent. All gryphon structures grow by superposing their own erupted mud over time. Erosion (commonly from rain) may preserve the vertical growth and even completely erode inactive structures. In the case of drought, gryphons may be sealed. Here two outcomes are possible: the seal bursts from fluid accumulation, or the fluids find a new pathway to the surface, creating a new, neighboring mud cone. Gryphons are commonly found in groups where seepage is most abundant (crater center and tectonic structures). In the case of an undefined MV crater, gryphons can be used to locate its position.

**Pools** are water-dominated, low rounded structures that emit water, gas and small amounts of sediments (Figure 3-2 c). They measure between a few centimeters to about a meter. A study by Mazzini et al. (2009b) suggests a connection between the overburden in gryphons and the formation of pools(Mazzini, Svensen, et al., 2009). According to this study, pools are (almost) always found next to gryphons because they are connected at the subsurface by the plumbing system. Over-pressure at gryphons could open and fracture local weakness areas, allowing fluids to migrate to meteoric water sites, forming pools at the surface.

**Salsa Lakes** resemble pools in shape and fluid discharge (Figure 3-2 d). However, these structures are much bigger (up to tens of meters wide). Their significant size makes them bigger emitters. In addition, they are also more resistant to local changes and are therefore stable structures.

**Sinter** structures are less common (Figure 3-2 e). They form when seeps of methane gas ignite and burn intensively with no interruptions. Over time, this process eventually "bakes" the brownish grey, structureless solid mud breccia into a brownish-red structureless molten mud breccia. This process can take place at different locations where mud breccia erupts. The structure becomes a "sinter cones" when this happens in gryphons. In the case of mud breccia

flow, the burning methane results in "sinter striations". When the burning of methane stops, seepage continues resulting in "diffused sintering".

Additional associated products from MVs are **bacterial colonies** (Figure 3-2 f). These colonies thrive on the mud and are fed by the seeping methane that both onshore and offshore MVs frequently release. Methanogenic carbonates are common bio-products found at offshore MVs. These authigenic deposits result from the anaerobic methane oxidation and sulfate reduction operated by archea and sulfate-reducing bacteria colonies (Akhmetzhanov et al., 2008; Gontharet et al., 2007; Greinert et al., 2001; Greinert et al., 2010; Hovland et al., 1987; Kocherla et al., 2015; Naehr et al., 2000). Onshore, the colonies are usually found in pool or gryphon structures that are calm and rich in water. The bacteria type present in the colonies may vary at each site as they develop according to the gas composition released. This also affects their colour, which can vary between greenish, brownish, and even pinkish.

**The Mud-breccia** is defined as the mixture of clay, silt, sand and clasts that have been brecciated throughout all the sedimentary units intersected by the feeder channel (Figure 3-2 g). This mélange is therefore very useful to reconstruct subsurface rock characteristics and stratigraphic successions. Some of the clasts can reach more than 1 m$^3$ in size.
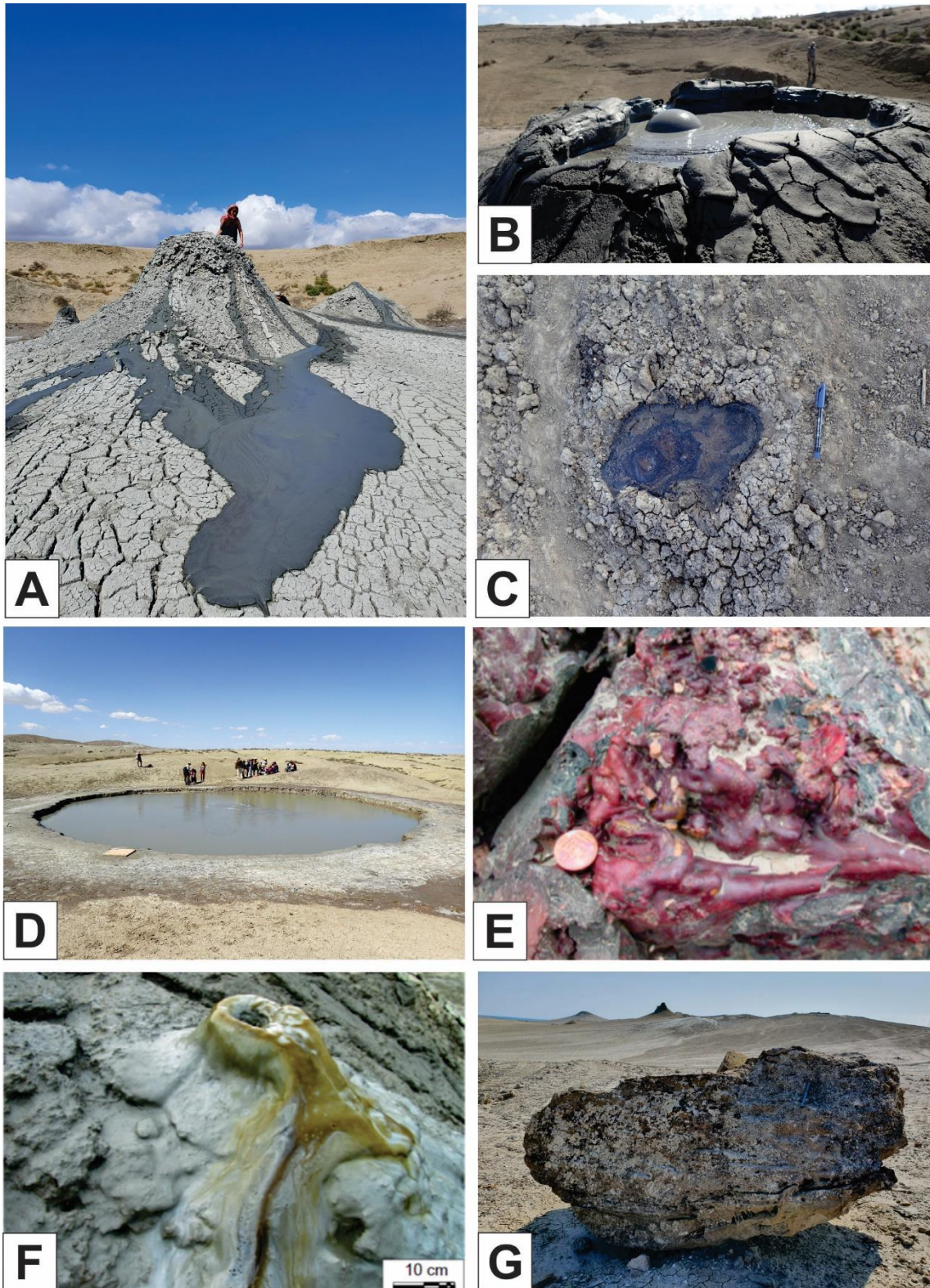
***Figure 3-2*** *Degassing features and material from MVs. (A) A group of gryphons. (B) Gryphon crater with bubbling activity. (C) Small oil-rich pool. (D) Salsa lake. (E) Sinter clast (Mazzini & Etiope, 2017). (F) Bacterial colonies on a small gryphon. (G) large MV breccia clast.*

### 3.1.6 Seepage modes

Seepage is a general term for the visible and non-visible migration of gas. Seepage flow can either be continuous or episodic, and the rate at which it streams is also variable. Specific names are used to define particular seepage types.
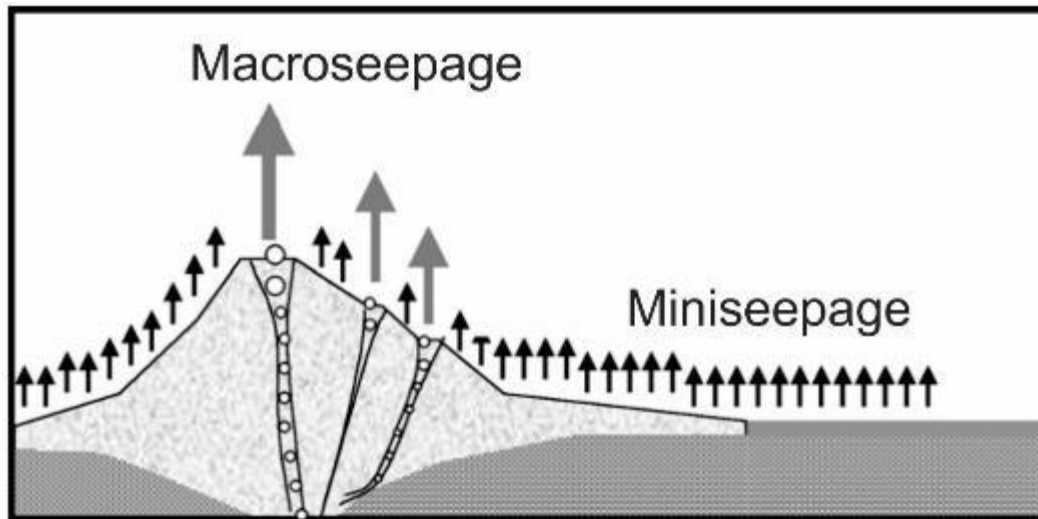


***Figure 3-3*** *Sketch illustrating gas seepage from MVs. Macro-seepage (grey arrows) is released from degassing structures (gryphons, bubbling pools) and miniseepage (black arrows) is released through soil pores. Edited from (Milkov, 2005).*

**Seeps** or **Marcoseeps** are two interchangeable terms used to describe visible and invisible concentrated manifestations. There are two types of macro-seeps flows: focused and diffused. Focused flow includes visible gas seeps, oil seeps, gas-bearing springs often present at MVs crater sites. Here, focused flow can be "channeled" or "vented". Diffused flow is defined as the invisible, often associated with **miniseepage.** Miniseepage is a term used to describe invisible seepage that occurs at regions characterized by macro-seepage. Miniseepage flows from the subsurface to the surface via soil pores (Figure 3-3). Miniseepage can spread over hundreds of square meters, and measuring miniseepage flux can significantly increase the understanding of how much gas is released to the atmosphere from natural systems. **Microseepage** is different from macro-seeps and miniseepage. This term describes invisible, diffused flow which is far and not related to MV occurrence (Etiope, 2015; Spulber et al., 2010). Given that this thesis focuses on MV-ism, microseepage will therefore not be discussed further.

Macro-seeps can be dictated by two different fluid migration mechanisms: advection (Darcy's law) and diffusion (Fick's law), accordingly. Diffusion relates to the concentration gradient where the movement of gas changes from a volume of high concentration to a volume of lower concentration. Fick's law dictates this mechanism by the following equation:

$$F = -D_m \nabla C \qquad\qquad (\nabla = \delta/\delta_x + \delta/\delta_y + \delta/\delta_z)$$

Where $F$ units is the gas flux, $D_m$ is the molecular diffusion coefficient ($m^2/s$) and $C$ is the gas concentration ($kg/m^3$).

Gas seeps are typically ruled by advection, where the gas flux is determined by pressure gradient and rock permeability. Theoretically, Darcy's law can express the advection, where gas in a dry, porous media, flows following the equation:

$$v = -k \nabla P / \mu \qquad\qquad (\nabla = \delta/\delta_x + \delta/\delta_y + \delta/\delta_z)$$

where $v$ is the velocity (m/s) of the gas, $k$ is the intrinsic permeability ($m^2$), $\mu$ is the dynamic gas viscosity ($kg\ m^{-1}s^{-1}$) and $\nabla P$ is the pressure difference ($kg\ m^{-1}s^{-2}$) between two defined ends.

Natural gas seepage from MVs is usually measured by determining the total flux of gas, where both advection and diffusion mechanisms are considered. Combining Darcy's law with Fick's law gives the following equation for the total flux of gas:

$$F = [-n\ D_m (dC/dz)] + [v\ C]$$

where diffusion is $[-n\ D_m (dC/dz)]$ and advection is $[v\ C]$.

Unfortunately, this equation requires the acquisition of complex data. Measuring variables such as gas velocity or the molecular diffusion coefficient is complicated, especially in the field. Direct flux measurements are commonly done using the closed-chamber method, where the gas flux is calculated by the following equation (Hong et al., 2013):

$$F = (V_c/A_c) \times (c_2 - c_1)/(t_2 - t_1)$$

Where $V_c$ ($m^3$) is the volume of the chamber, $A_c$ ($m^2$) its area, $c_1$ and $c_2$ ($mg\ m^{-3}$) are $CH_4$ and/or $CO_2$ concentrations at times $t_1$ and $t_2$.

Note that the equations above do not account for any changes in the nature of the fluid or the permeability of the rock through which the fluid flows. The nature of the fluid affects pressure gradient but not rock permeability (Muskat & Wyckoff, 1946). The migration of fluids from the source rock or secondary accumulations to the surface is prone to many geodynamic and

secondary chemical processes. The relation between the stratigraphic and structural setting with the seepage is essential to consider. In 1952, Link proposed different types of hydrocarbon seeps in relation to the stratigraphic and structural setting (W.K. Link, 1952). According to his classification, MVs belonged to the intrusion/fault seep category (a sub-category of standard fault/fracture seep). These seeps are less impacted by the stratigraphic setting and are more "tectonically" controlled (Ciotoli et al., 2020).

### 3.1.7 General gas composition and origin

The gas from the MVs is typically rich in hydrocarbons (HC) from petroleum bearing sediments. Previous studies show that the gas released from MVs is mainly thermogenic (around 76%) and is dominated by methane (often more than 80 vol%) and includes high $CO_2$ concentrations (mostly between 1-10%) as well as minor amounts of nitrogen and alkanes (ethane and butane) (Mazzini & Etiope, 2017; Milkov et al., 2003; Saroni et al., 2020). Thermogenic gas is produced in deep sediment at temperatures typically up to 190-200°C by the thermal degradation of organic matter or oil cracking (catagenesis) (Hunt, 1996). The production of such gas is often associated with substantial hydrocarbon deposits (Mazzini & Etiope, 2017). It is worth mentioning that the MV gas can also have microbial (sometimes referred to as biotic) origins, if the gas is produced in shallower and cooler sediments (diagenesis) by microbes that rely on the $CO_2$ reduction or acetate fermentation pathways (Hunt, 1996; M.J. Whiticar, 1999). The study of HC-rich gas is achieved by the analysis of major-element, trace element, and the $C_1/(C_2+C_3)$ ratios to quantify the amount of methane ($C_1$) in relation to the sum of ethane ($C_2$) and propane ($C_3$). This ratio is used to differentiate biotic gases from thermogenic gases. Biotic systems generally entirely produce methane (>99%), while thermogenic gases comprise methane with significant quantities of alkanes (up to 10%). Generally, gas dryness ratio $C_1/(C_2+C_3)$ follows a general reversed trend, decreasing with the reservoir depth..Carbon isotope variation is denoted by $\delta^{13}C$, and uses the Vienna Pee Dee Belemnite standard (VPDB) and its unit is in permil. Hydrogen isotope variation is denoted by $\delta D$ and uses Vienna Standard Mean Ocean Water (VSMOW) (Zaputlyaeva et al., 2020). Binary genetic diagrams proposed by Bernard et al. (1977), Schoell (1983) and Whiticar et al. (1986) as well as Gutsalo and Plotnikov (1981) have been used in the past to help determining the origin of methane, ethane, propane and carbon dioxide (Bernard et al., 1977; Gutsalo & Plotnikov, 1981; Martin Schoell, 1983; Whiticar & Faber, 1986) . The proposed diagrams use

the following ratios respectively: $d^{13}C$-$C_1$ versus $C_1/(C_2 + C_3)$, $d^{13}C$-$C_1$ versus $dD$-$C_1$ and $d^{13}C$-$C_1$ versus $d^{13}C$-$CO_2$. These graphs exclude genetic fields such as abiotic and secondary microbial origins resulting in offsets and empirical plotting. In 2011, Milkov introduced genetic fields that could be used to recognise gas with a secondary microbial origin (Milkov, 2011). In 2014 and 2017 Etiope and Schoell and Etiope genetic fields for abiotic gas were added (Etiope, 2017; Etiope & Schoell, 2014).

Finally, in 2018, Milkov and Etiope proposed new diagrams with additional genetic fields, allowing more accurate plotting of geochemical data (Milkov & Etiope, 2018). These new plots also consider the molecular and isotopic changes following the generation of natural gas.

As the complexity of the genetic diagrams has increased, so has the amount of published geochemistry data as our knowledge about MV systems have evolved.

### 3.1.8 Global budget gas emissions

Methane is a greenhouse gas that is 28 times more powerful than carbon dioxide over a 100-year and its atmospheric concentration reached 1.892 ppm at the end of 2020 (NOAA, 2021). Accurate estimations of the global methane budget (anthropogenic and natural) is increasingly important yet seem to be difficult to deliver. These estimations are based on the bottom-up or top-down approaches using inverse models and atmospheric measurements, but their reliability have been debated (Bergamaschi et al., 2010; Etiope & Schwietzke, 2019; Saunois et al., 2016; Turner et al., 2015). In fact, bottom-up and top-down estimations may be contradictive when investigating natural sources (Etiope et al., 2019). Isotopic ($\delta^{13}C$) base models such as the global box model and atmosphere combined with 3D forward modelling have helped improving the understanding of dominant sources (anthropogenic and natural) and their distributions (spatial and temporal).

The measurement of geological methane flux to the atmosphere started in Europe in the 2000s (Etiope et al. 2006; Tang et al. 2010). Geological $CH_4$ emissions are the third most dominant natural source of $CH_4$ (40-60 Tg yr$^{-1}$) after freshwater (115-125 Tg yr$^{-1}$) and wetlands (160-170 Tg yr$^{-1}$) ((Ciais et al., 2013; Etiope & Ionescu, 2015; Etiope et al., 2008; Saunois et al., 2016; Schwietzke et al., 2016). Sources of geological $CH_4$ can be fossil and recent (Pleistocene and Holocene), and their differences should be distinguished when dealing with atmospheric methane estimates. Fossil geological $CH_4$ sources are deep sited, radiocarbon free and emitted through natural seepage such as hydrothermal systems, cold seeps, $CO_2$ rich manifestations,

hyperalkaline springs and MVs. Recent geological CH$_4$ sources are shallow and emitted by estuaries, deltas, bays and permafrost.

MVs are the largest natural geological sources of methane, releasing up to 8.1Tg CH$_4$ Yr$^-$ (Etiope et al., 2019). The total MV methane emissions is estimated by adding all the macro-seepage and miniseepage divided by the seepage area (Mazzini and Etipoe, 2017). This accounts for about 25-30% of the total geological CH$_4$ emissions (Etiope, 2015). Despite this, MV values are often ignored when accounting for the global top-down CH$_4$ budget but should be considered when dealing with atmospheric methane (Etiope & Klusman, 2002; Hmiel et al., 2020). This is mostly due to the uncertainty related to measuring MV emissions and direct flux measurements from active MVs are yet to be completed. In the dormant stage, however, MVs allow the unique chance to measure seepage directly (Etiope & Schwietzke, 2019).

### 3.1.9   Mud volcanism activity, frequency and seismicity

Earthquakes are phenomenon that generate strain and stress perturbations. They can cause major alterations impacting features such as aquifers, geothermal systems and MVs. The relationship between the occurrence of large earthquakes and the methane eruptions at MVs is well known. Multiple studies around the world have documented this correlation, particularly in Azerbaijan, Caspian sea, Andaman, Makran, Mexico, Italy and Japan (Abikh, 1863; Aliyev, 2004; Babayev et al., 2014; Manga et al., 2009; Mellors et al., 2007; Rudolph & Manga, 2010). Notably, a study by Maestrelli et al. (2017) aimed at quantifying the relationship to constrain the generating factors (Maestrelli et al., 2017). They analyzed physically derived quantities such as dynamic stress and ground velocities to evaluate the potential triggering effects of earthquakes on MV eruption. Results showed a clear and dominant impact of seismic shaking. Most studies observe that eruptions can take place on the same day, a few days, or months after earthquake events. Delayed eruptions are not well understood, and more studies are needed to truly understand the processes generated by seismic waves. Associations between the magnitude and distance of earthquakes with MV eruptions have been proposed by Manga et al. (2009) and Mazzini and Etiope (2017), and their correlations can be plotted. Some remarkable earthquakes causalities on MV located tens of kilometers away from the epicenter have been observed in the Napag MV eruption after the earthquake (M 6.6) located about 430 km away, the Pingtung MV eruption after the Taiwan (M 5.5) located about 250 km away or also the

eruptions of Kalang Anyar, Gunung Anyar, and Polungan MVs after the Yogyakarta earthquake (M 6.3) located 270 km away (Mazzini and Etiope, 2017).

# 3.2 Methods

This chapter presents the workflow for the methods applied in this study to meet the main objectives described in chapter 1. The workflow (Figure 3-4) is divided into four main stages: stage 1 (satellite images), stage 2 (fieldwork), stage 3 (laboratory work) and stage 4 (data processing). These stages are further divided into sub-stages to establish the results. More specifically, the satellite and field morphological observations results are derived from sub-stage 1 (mapping and elevation profiles, crater and mudflow outline, potential degassing area) and parts of sub-stage 2 (field observations). The geochemical data results are derived from parts of sub-stage 2 (in situ measurements) and sub-stage 3 (molecular composition analysis, isotopic composition analysis and air contamination calculations) and parts of sub-stage 4 (plotting). Finally, the flux maps with seepage area are obtained from parts of sub-stage 1 (in situ measurements) and sub-stage 4 (flux data processing).

The following sections present the methods used in Satellite-based investigations (section 4.1), fieldwork (section 4.2), laboratory work (section 4.3) and data processing (section 4.4).
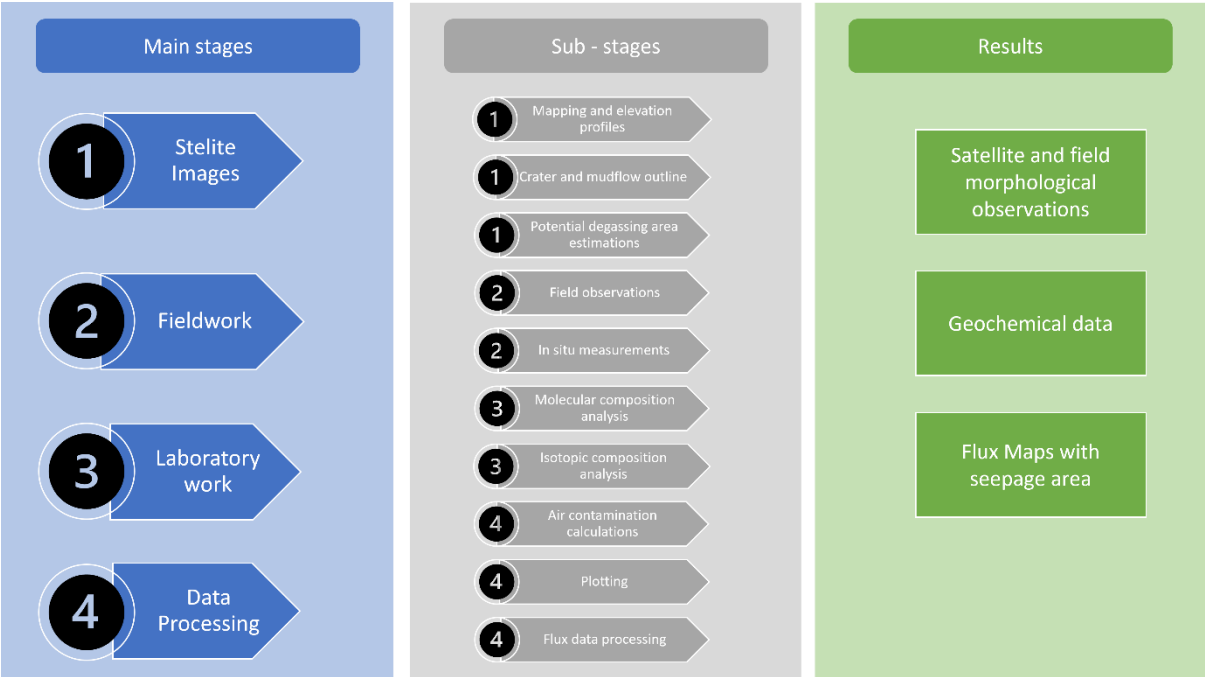


***Figure 3-4*** *Flowchart illustrating the main stages (blue) and sub-stages (grey) used in this thesis to obtain the desired results (green).*

### 3.2.1    Satellite-based investigations

Investigations using Google Earth satellite images of the targeted MVs were conducted prior to the Azerbaijan Summer School fieldwork to i) distinguish and to observe large scale structures (e.g faults anticline axes) and understand how they may control location, morphology and features of MVs, ii) appreciate the scale of the MV structures comparing satellite images and field observations,  iii) extract degassing features from satellite images and compare them with those observed on the field, and iv) distinguish various MV morphologies from satellite images comparing with direct field observations. The combined effect of external factors such as tectonic control and large scale geological structures are also considered during these analyses.

The satellite-based investigation began by creating a new project in Google Earth. The targeted MV structures were pinned using coordinates and names provided by the HOTMUD project. Most MVs have several names variants but this study uses the English variants, commonly accepted by the organizers of the HOTMUD project.

The location of large-scale structures can be observed on satellite images by turning on the "terrain" option to show topography and elevation. The distance and orientation of large scale structures can help determine their influence on MVs. Here it is assumed that the greater the distance from MVs, the less influential the large-scale structures will be on MV morphology and features. Large scale structures that are orientated normal to MVs are believed to have more impact on the formation of those MVs.

Morphometric parameters and feature descriptions such as calderas, visible mudflow and potential degassing area were measured using the "measure distance and area" tool by clicking on the ⌨ icon in Google Earth. The latest is of crucial importance to calculate flux estimates for structures were measured using the fluxmeter on site. Observing the various types of seepages modes (gryphons vs pools), their dimensions, and seepage activity is also done using the satellite images. Main concentrations and clusters of seepages are estimated by roughly counting them. Identifying seepage types is not done on satellite images due to the limitations of image resolution.

Morphometric parameters and feature descriptions were noted based on images from 2019-2022. Estimating the error percentage of such a procedure is difficult. Based on the quality of

the images (features measuring less than 0.5 m in diameter are hard to distinguish) it is appropriate to assume there is a least a 10% error in these satellite-based investigations (Oppo et al., 2020).

Elevation profiles of each targeted MV were made in Google Earth using the following steps:

1. Select the "add path" tool
2. Give the profile a name (structure name)
3. Use mouse point and click to create the profile
4. Click "ok" to save the path
5. Select a new path under "places"
6. Right clock on the pathname and select "Show Elevation Profile"

The profiles and screenshots of MVs from satellite images were then exported for further editing and interpretation in Photoshop and CorelDraw software. Crater zones were defined using the elevation profiles along with satellite images.

Interpreted mud flows corresponding to previous eruptions was done using the historical imagery tool in Google Earth and using contrasting colors to highlight the mud in Photoshop. Assemblages of the satellite images used for mud flow interpretations at each MV structure of this study can be found in Appendix 2-7.

### 3.2.2 Fieldwork

Additional days in the field were organized after the Azerbaijan Summer School to i) locate and define crater zones and various types of seepages concentrations and clusters in the field, ii) describe the activity of seepages with possible quantitative characteristics, iii) collect in-situ measurements to obtain immediate reading on the properties of the seeping water, iv) collect gas samples for further laboratory analysis and, v) measure soil $CH_4$ and $CO_2$ exhalation fluxes for further geostatistical analyses at the targeted MVs.

### 3.2.2.1   Field observations

The MV site name, sample ID, date, coordinates and general comments were recorded directly in field notes. Several sampling stations were assigned to each MV site. The nomenclature of the sample ID was as followed:

<p style="text-align:center"><strong>AZ19-XX</strong></p>

where **AZ** stands for Azerbaijan, **19** stands for 2019 and **XX** is the sample number (start with 14 due to the preceding data collection during the Azerbaijan Summer School).

Detailed interpretation of the nearby large scale structures, crater, structure type and degassing features were noted at each MV. Morphological remarks specifically included seepage structure type, size, seepage activity and dominating fluids. Additional remarks such as concentrations and clusters of degassing features at each MV was noted. Pictures were taken with the camera of an iPhone XS and a digital Olympus Tough F200. Videos of some of the locations were also recorded for future remarks. The coordinates were recorded via global positioning systems (GPS) provided by the App "HandyGPSlite" and a digital compass used on an iPhone XS.

Complex landscape sometimes limited observations, and identifying the structure type, crater rim and mudflow was challenging. For more accurate observations and evaluations of the seepage activity, a few days should be spent at each volcano. Estimating the degassing activity at the seepage sites was therefore difficult as only a few hours were spent at each volcano.

### 3.2.2.2   In-situ measurements

Reading on the properties of the seeping water at the targeted seepage localities were done using a VWR pHenomenal (MU 6100 H model). This instrument is with robust IP 67 rated housing making it a very suitable tool to measure pH, mV, conductivity and oxygen in field applications (Figure 3-5).
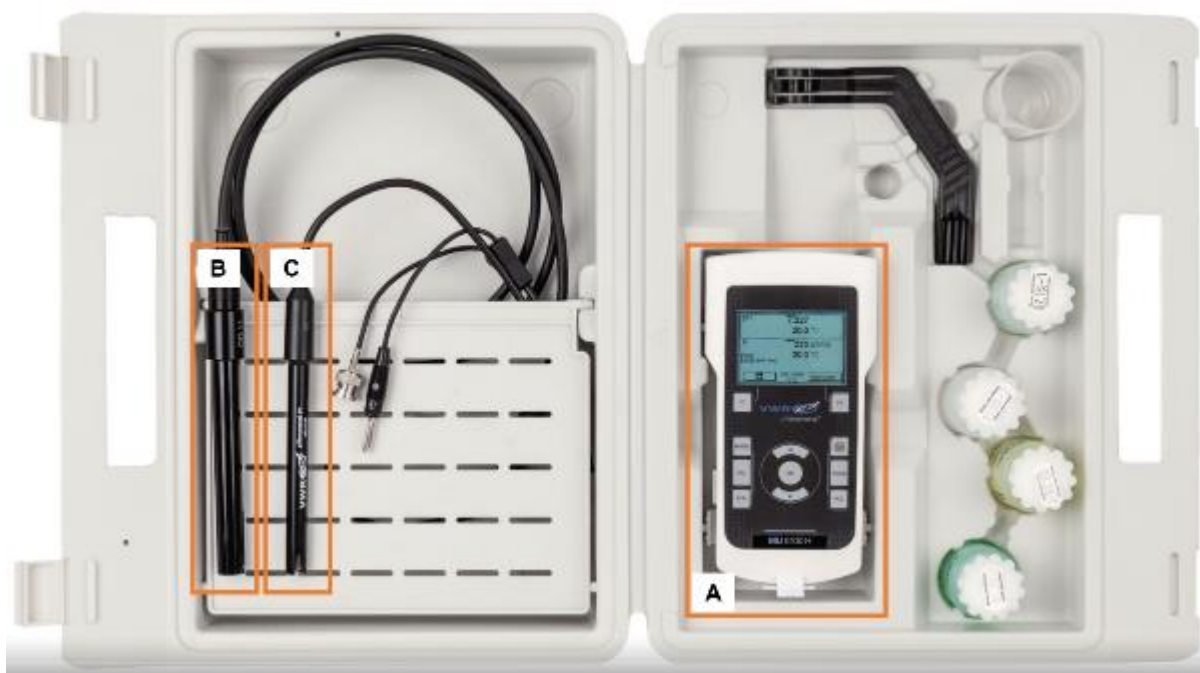
**Figure 3-5** *Photo of a VWR pH enomenal (MU 6100 H model) showing the instrument and its cables in a robust plastic carrying case. A) pHenomenal® MU 6100. B) Conductivity probe CO 11 with built-in temperature sensor (1,5 m cable). C) pH electrode 111 with built-in temperature sensor (1 m cable). (Avantor, 2022).*

Note that only two of these at the same time. USB output is waterproof) and a VWR Thermocouple Traceable Digital thermometer (with a range between -200°C to +1370°C, this thermometer is also water resistant and resists dirt, dust, fumes and water. WxDxH: 83×38×178 mm. Resolution: 0,1; 1,0 °C). With these tools, temperature (unit: °C; accuracy: ±1,0; ±2,0 (>+740) °C), Eh (unit: mV; accuracy: ±0,3/±1), conductivity (unit: µS/cm; accuracy: ±0,5% of measured value) and pH (unit: none; accuracy: ±0,005 + 1 digit) inside mud volcanoes were measured by placing the connected BNC (for pH) and 8-pin (for conductivity and DO) cable directly in the mud or water of the structures. A separate Brannan Immersion Glass Thermometer (filling type with blue Kerosene, maximum temperature measurement of +110 °C, and a length of 305 mm) was used to record the external temperature (unit: °C; accuracy: +/-1.0°C) with aim to provide data which can display the temperature contrast between the inside and outside of MVs.

### 3.2.2.3 Gas sampling

To assess the geochemical (molecular and isotopic) composition of the gas seepage at each studied MV, dry gas sampling at active seepage sites (gryphons and pools) was done using the inverted-funnel method. This method entails placing an inverted plastic funnel above the

active bubbling spots (Figure 3-6). The equipment needed for this method are as follows: 15 cm diameter funnel connected to a 50 cm rubber tube, a large bucket filled (over 20 cm in diameter) with brine solution, glass vials (15 mL), rubber septums, aluminium caps crimper, marker and a field notebook.
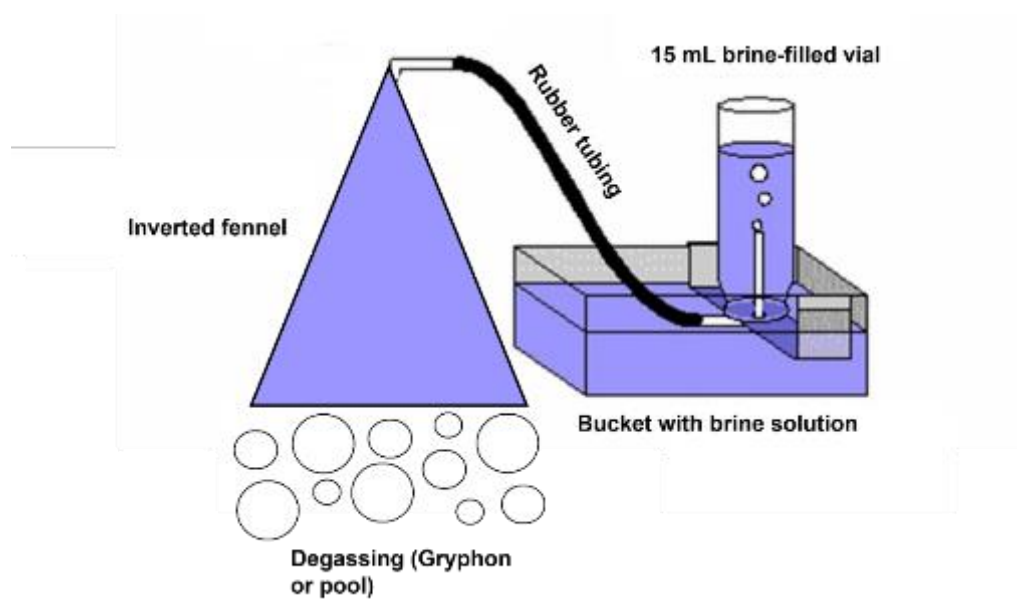


***Figure 3-6*** *Simplified and conseptual illustration of the inverted fennel method used to collect gas samples from degassing features in the field. Edited from (Senese, 2010).*

The cylindric end of the funnel was attached to a rubber tubing with a thorion valve. The end of that rubber tubing was placed in 15 mL glass vials filled with brine. The vials are placed upside down in a bucket, covered by brine solution. As the vials get filled with gas, the brine from within the vial is extruded in the bucket. This procedure makes it possible to observe the otherwise invisible gas progressively filling the vials. When the vials were filled, a metallic cap is placed under water (to avoid air contamination) and sealed using a crimper. Four duplicate gas samples were taken at each sampling station. In total, 88 gas samples were collected in the field.

Assessing whether a degassing structure was a good candidate for gas sampling or not was done by observing at their position in relation to the MV crater and by examining their bubbling activity over time (about a minute). Degassing features located at or near the crater were often chosen over the ones away from the crater. It is assumed that these structures seep more gas as they are located above the feeder channel. Degassing features that are located away from the

MV crater are more likely to be formed due to branching from the feeder channel in the subsurface. These structures are assumed to release less gas and are more likely to be prone to secondary reactions with shallow clays or water sources.

The bubbling rate of the degassing structures was not noted. Instead, the bubbling activity was rated by the following: small, intermediate, or vigorous. In some cases, selecting the degassing feature was challenging due to poor bubbling activity. It is important to note that not all the degassing features of a MV are active at the same time, meaning that this selection was random and depended solely on the timing of the field observations.

### 3.2.2.4    Gas flux measurements

$CO_2$ and $CH_4$ flux measurements were carried out throughout the surface of mud volcanoes to estimate the amount of gas released. Such measurements were done using the "accumulation-chamber" (sometimes called the closed chamber) method, using a West Systems™ portable fluxmeter (Figure 3-7) equipped with a connecting 20 cm-diameter metallic box, a $CH_4$ laser (a TLD Tunable Laser Diode spectrometer with a range from 0.01 up to 750 mol m$^{-2}$d$^{-1}$ or 0.16–12000 g m$^{-2}$d$^{-1}$) and an infrared $CO_2$ detector (LICOR–LI820 with a range from 0 up to 600 mol m$^{-2}$d$^{-1}$ or 0–26400 g m$^{-2}$d$^{-1}$; (Sciarra et al., 2020). This method measures flux by assessing the accumulation of gas in the metallic box over time. A total of 27 $CH_4$ and $CO_2$ flux measurements were made throughout the surface of each mud volcano, both inside and outside the mud volcano calderas. Note that flux measurements were only taken at Kichik Marazaand little Maraza, Gyzmeidan, Gushcu and Melikchobanly MV. Oil and mud flow dominated the terrain at Madrasa MV. Field conditions made it difficult to use the accumulation-chamber method as it could potentially damage the West Systems™ portable fluxmeter. It was therefore established that no measurements would be taken at Medres MV. No flux measurements were taken at Shikhzarli MV due to time restrictions. Shikhzarli MV was the last stop of the fieldwork and issues with the bus engine affected the time at this locality. Other field procedures such as gas sampling and field notes/photos were prioritized.

***Figure 3-7*** *Photo of the West Systems™ portable fluxmeter with the logo printed on the accumulation chamber(WestSystems, 2020).*

### 3.2.3   Laboratory measurements

The gas samples were analysed in the laboratories of INGV (Istituto Nazionale di Geofisica e Vulcanologia) of Rome and Palermo (Italy) for the determination of the molecular and isotopic composition of $CO_2$ and $CH_4$, respectively. Molecular composition was analyzed using a MicroGC Varian 4900 CP (Figure 3-8), equipped with two Thermal Conductivity Detectors (capillary columns: 10m PoraPLOT U and 20m Molsieve 5A), with an error of ±3%.



**Figure 3-8** CP 4900 Gaschromatograph used to carry out laboratory analyses of soil gas samples, free gas and dissolved gas in the groundwater.

Carbon and hydrogen isotopes of methane and carbon dioxide were carried out on a Delta Plus XP CF-IRMS instrument (ThermoFinnigan Continuous Flow Isotope Ratio Mass

Spectrometers (Delta Plus XP; Figure 3-9) coupled with a TRACE GC equipped with a Poraplot-Q capillary column (30 m x 0.32 mm i.d.) and using a flux of 0.8 cc min$^{-1}$ of pure helium (5.6 grade) as gas carrier. Gas chromatografer (GC) III combustion interface was used to produce carbon dioxide from methane. GC-Thermal couples (TC) interface provides on-line high-temperature methane conversion into hydrogen suitable for isotope analyses. Typical reproducibility for $\delta^{13}C$ (1s=0.1‰) and dD-CH$_4$ (1$\sigma$=1‰) measurements is better than 0.2‰ and 2.5‰ respectively.



***Figure 3-9*** *Image of stable isotope laboratory of INGV Palermo focussed on isotopic composition of hydrogen, carbon and oxygen ($\delta D$, $\delta^{13}C$, $\delta^{18}O$) on a variety of samples (soil, sediment, water, and atmospheric gas), by means GC-IRMS (Isotope Ratio Mass Spectrometry).*

Carbon and hydrogen stable isotopes are useful tools determine the origin of the sampled gases (Bernard et al., 1977; Etiope, 2015; Milkov & Etiope, 2018; White, 2015).

The unit to express the data is $\delta^{13}C$ defined as the relative difference (‰) between the $^{13}C/^{12}C$ ratio of the sample and a reference standard. As international reference standard has been selected a Cretaceous marine fossil, Belemnitella americana, from the PeeDee formation in South Carolina with $^{13}C/^{12}C$ ratio of 0.011237:

$$\delta^{13}C = \left( \frac{^{13}C/_{12C\ (sample)}}{^{13}C/_{12C\ (standard)}} - 1 \right) \times 1000$$

### 3.2.4  Data processing

To properly apply and illustrate the data, various processes must be applied to i) account for air contamination in the gas samples, ii) create genetic diagrams iii) quantify $CH_4$ and $CO_2$ data from flux measurements.

#### 3.2.4.1  Air contamination

Air contamination in the gas samples must be identified and accounted for before the geochemical data is interpreted. Hence, the raw geochemical data must be normalized as it is a mixture of the "deep" endogenous and atmospheric gas (Canadell et al., 2021).

Knowing that oxygen present in the gas samples can only originate from the atmosphere, oxygen can be used as a reference gas to calculate a known average air composition and extract the gas in excess present in the gas samples. Air composition is 78% nitrogen, 21% oxygen, and 0.036% carbon dioxide, atmospheric nitrogen and carbon dioxide can be removed from the samples collected. This procedure is done in excel and is completed by the following steps:

1. First, the samples are checked for oxygen. Then an average air composition (with contamination) is estimated by re-writing the geochemical composition of the gas from ppm to percentage (Vol.%). Secondly, the gas components (in Vol.%) were summed $(He + Ne + H_2 + O_2 + CH_4 + CO_2 + C_2H_2 + C_2H_4 + C_2H_6)$. This total did not add up to 100, indicating the presence of atmospheric $N_2$, Ar and/or $CO_2$. Hence, the gas needed to be normalized.

2. The atmospheric (atm) and excess (exc) $N_2$, Ar and $CO_2$ were calculated: Here the excess gas is the deep" endogenous from the MV seeps. Note, $CO_2$ does not have to be considered while normalizing for air, as in the air it is just 400ppm which is 0,036 Vol.%. However, $CO_2$ needs to be corrected from the air when working with $\delta^{13}C\text{-}CO_2$ concentrations. $CO_2$ correction were therefor completed along with the rest as follow:

   $N_2$ **(atm)** = $O_2$ Vol%. (measured) * 3.728. If somehow $N_2$ values are negative, the excess gas has most probably escaped from the sample ($N_2$ is more volatile than $O_2$) and there is no atmospheric $N_2$.

**N₂ (exc)** = N₂ (measured) - N₂ (atm)

**Ar (atm)** = C₂H₂ (measured) /22.43

**Ar (exc)** = C₂H₄ (measured) - Ar (atm)

**CO₂ (atm)** ₌ O% (measured) * 0.00181

**CO₂ (exc)** ₌ CO₂ (measured) - CO₂ (atm)

3. A new total is calculated (He + Ne + H₂ + N₂ (exc) + CH₄ + CO₂ (exc) + C₂H₂ + C₂H₄+ C₂H₆). Note that O₂ can be considered to have only atmospheric origin due to its limited endogenous source. This sum does not add up to 100 either as the values for N₂ (atm) and the CO₂ (exc) have been removed. The molecules need to be normalized again

4. Each molecular value in each sample need to be divided by the new sum and multiplied by 100 to get the final normalized molecular composition in vol.%. This new total should add up to 100% and is only deep" endogenous gas from the MV seeps.

Finally, $\delta^{13}$C-CO₂ values must also be corrected. The following equation was applied:

$$\delta^{13}\text{C-CO}_2 \text{ (Corrected)} = (100* \text{ CO}_2 \text{ (measured))} - (\text{O}_2 * \text{CO}_2 \text{ (air)}/100 - \text{O}_2)$$

### 3.2.4.2 Data analysis

Once the values of the molecular geochemical data is normalized, they are analysed using descriptive statistics (mean and standard deviation) to draw conclusions. Note that because the dataset represents a sample of gas values from MV seepage, sample standard deviation is used. This function uses the following formula:

$$\text{Sample standard deviation} = \sqrt{\Sigma(\text{xi–x})2 / (n - 1)}$$

Where $\Sigma$ is the sum, $x_i$ is the $i^{th}$ value in the dataset, x is the sample mean and N is the total number of observations.

### 3.2.4.3 Determining the gas origin

Three genetic plots reproduced from the publication by Milkov and Etiope (2018) are used to determine the origin of gas from MV seepage. The plots are produced in Excel using the following correlations: $\delta^{13}C\text{-}CH_4$ versus $C_1/(C_2+C_3)$, $\delta^{13}C\text{-}CO_2$ versus $\delta^2H\text{-}CH_4$, and $\delta^{13}C\text{-}CH_4$ versus $\delta^{13}C\text{-}CO_2$. Note that the $C_1/(C_2+C_3)$ ratios quantify the amount of methane ($C_1$) in relation to the sum of ethane ($C_2$) and propane ($C_3$). This ratio is used to differentiate biotic gases from thermogenic gases. Biotic systems generally entirely produce methane (>99%), while thermogenic gases comprise methane with significant quantities of alkanes (up to 10%). Generally, gas dryness ratio $C_1/(C_2+C_3)$ follows a general reversed trend, decreasing with the reservoir depth.

The plots comprise of three distinct genetic fields: primary microbial, secondary microbial (SM), thermogenic and abiotic (Figure 3-7). Additional sub-fields are present in the thermogenic and primary microbial fields. The gas data plotted in the thermogenic field can be classified as Early Mature Thermogenic gas (EMT), Oil Associated gas (OA), or Late Mature Thermogenic gas (LMT). The gas data plotted in the primary microbial field can be associated with reduction or fermentation if the data are concentrated in these sub-fields.
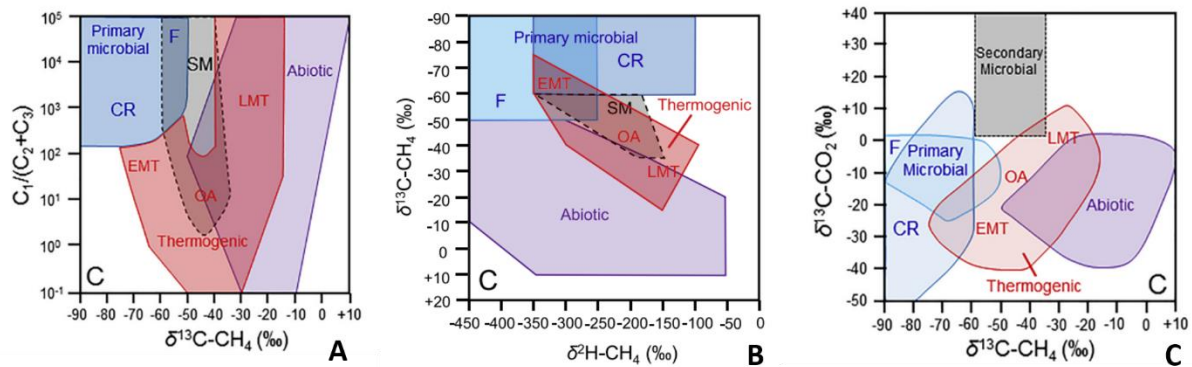


***Figure 3-7*** *Genetic diagrams of $\delta^{13}C\text{-}CH_4$ versus $C_1/(C_2+C_3)$ (A), $\delta^{13}C\text{-}CO_2$ versus $\delta^2H\text{-}CH_4$ (B), and $\delta^{13}C\text{-}CH_4$ versus $\delta^{13}C\text{-}CO_2$ (C) with revised genetic feilds from Milkov and Etiope (2018).*

If the data plot in the same fields in all three or two of the plots, it can be assumed that the field in which the data point are located are true for the origin of the gas. If clusters of data points are concentrated in different fields, the empirical plots can also indicated the types of processes that affect molecular and isotopic composition of the gases such as biodegradation (biod), thermochemical sulphate reduction (TSR) or mixing (Figure 3-8). Note that mixing of gases with different origin is commonly observed in nature, but, for simplicity, only mixing of primary microbial and thermogenic gases is shown in diagram A and C (Figure 3-8AC).
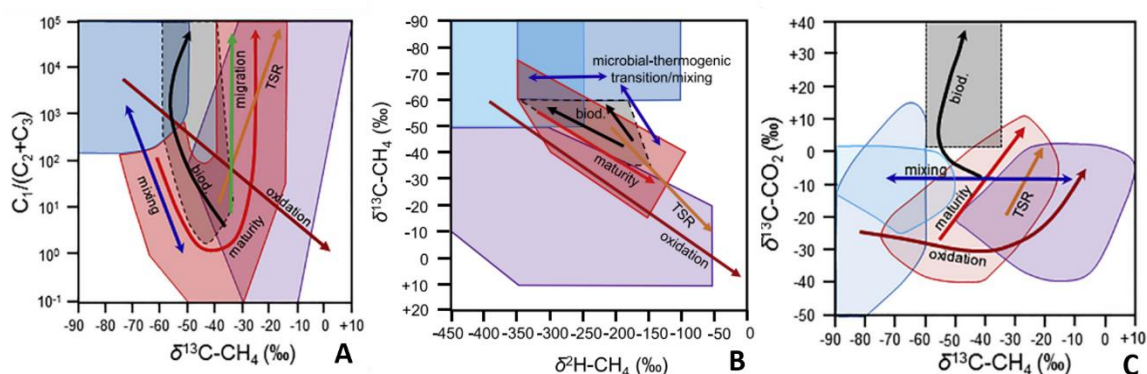


***Figure 3-8*** *Genetic diagrams of $\delta^{13}C$-$CH_4$ versus $C_1/(C_2+C_3)$ (A), $\delta^{13}C$-$CO_2$ versus $\delta^2H$-$CH_4$ (B), and $\delta^{13}C$-$CH_4$ versus $\delta^{13}C$-$CO_2$ (C) with arrows indicating processes that can affect the molecular and isotopic composition of the gas from Milkov and Etiope (2018).*

### 3.2.4.4   Mapping and Quantifying $CH_4$ and $CO_2$ Flux data

The total $CH_4$ and $CO_2$ miniseepage was estimated from the measured flux values following the approach described by Chiodini and Frondini (2001). This approach (Chiodini & Frondini, 2001) consists of summing the product of the average of each population class and its area of competence, after deduction of the background values (Sciarra et al., 2021), as follows:

$$QCO_2, CH_4 = \Sigma\ \Phi CO_{2,i} \Phi CH_{4,j} \times A_{ij}$$

where $\Phi CO_{2,i}$ and $\Phi CH_{4,j}$ are the average flux of the i-th and j-th population respectively, and $A_{i,j}$ is the pertaining area to each population (Sciarra et al., 2021).

The combination of macro- and mini-seepage values were then spatially distributed around the mud volcanoes, and graphically elaborated with Surfer 22 software. The area used for the spatial distribution was the degassing areas estimated during satellite image investigation (summarized

in Table 4-2). The $CH_4$ and $CO_2$ flux measurements of the Maraza/ Kichik Maraza, Gushchu, Melikchobanly and Gyzmeidan MV structures are given in tonnes/day (t/day).

Maps showing this data were produced in Surfer using and are colored based on flux concentration ($g/m^2$ day). The mapping procedure is the same for each MV structure. A geostatistical image processing method was applied in order to identify anomalies, heterogeneity and spatial patterns of the measured gases. This processing was used for data interpretation, for a more reliable reconstruction of the estimate maps, as well as for a preliminary quantification of the $CO_2$ and $CH_4$ fluxes. Data were elaborated using variogram modeling and an ordinary kriging algorithm. In particular, kriging technique was used to construct maps of $CO_2$ and $CH_4$ flux measurements that take into account the different population classes of data distribution. Each population class is displayed in a different color.

This range is different for every map. The flux range is characterized by three colors: blue (low), green (moderate) and yellow (high). Note that the green range is the largest and is represented by slightly different shades of green on the different maps. The blue zones represent areas of potential degassing around the mud volcanoes and are based on its area estimated from satellite observations. The potential seepage zones were estimated looking at the topographic variations around the volcanoes and analyzing the total parameter of the volcanoes using Google Earth. Note that these are simply estimations and the potential seepage area may be larger or smaller than the demarked areas of the maps below.

# 4 Results

The ensemble of collected data supporting the research objectives (section 1.4) are presented in this chapter. It comprises general field data collected at each targeted MVs (section 4.1), morphological descriptions from satellite images and field observations (section 4.2), gas molecular and isotopic composition from macro-seepage (section 4.3), and $CH_4$ and $CO_2$ and flux measurements from macro-seepage and mini-seepage (section 4.4) collected at targeted MVs.

## 4.1 General data

The studied database includes measurements from the following mud volcanoes: Maraza, Gyzmeidan, Gushchu, Malikchobanli, Madrasa, and Shikhzqgirzi. Kichik Maraza (meaning *little* in Azeri), the satellite volcano of Maraza MV, is incorporated in the database as it is an extension of Maraza MV.

Table 4-1 summarizes the field observations directly collected at the targeted MV structures during the fieldwork. A total of 23 sampling stations were recorded over 6 days. Some data (Eh, Conductivity, and pH) are only reported in table 4-1 for supporting further work in determining the properties of the degassing features located at the targeted MV structures. The internal temperatures (from 13.6 to 22.7 °C) of the MVs are lower than the external temperatures (from 24.1 to 30.6°C). On average, the pools have an internal temperature of 18.3°C, while gryphons have an internal temperature of 20.2°C. The internal temperature was not taken at all stations. Out of 23 stations, the internal temperature of 11 pools and only 7 gryphons were measured.

*Table 4-1* *Data collected at different localities during fieldwork in the Shamakhy-Gobustan region, Azerbaijan in September 2019.*

| Station number | Date | MV structure | Longitude (N) | Latitude (E) | MV Area (approx. value km$^2$) | Seepage perimeter (km) | T-int (°C) | T-ext (°C) | Eh (mV) | Conductivity (μS/cm) | pH | Comments |
|---|---|---|---|---|---|---|---|---|---|---|---|---|
| AZ19-14 | 17.9.2019 | Kichik Maraza | 40°30′35′′N | 049°01′55′′ | | | 19.4 | 30.5 | -27.8 | 7.23 | 7.80 | **Pool**, about 20 cm in diameterl. With high bubbling activity. Located on the flank of a gryphon. |
| AZ19-15 | 17.9.2019 | Kichik Maraza | 40°30′34′′N | 049°01′59′′ | | | 22.5 | 30.5 | -57.6 | 11.9 | 8.28 | **Gryphon,** 10 cm wide located aside of tall cue. Small signs of bubbles in water-dominated system |
| AZ19-16 | 17.9.2019 | Kichik Maraza | 40°30′37′′ | 049°01′53′′ | | | 19.0 | 30.5 | | | | **Gryphon**, about 15 cm in diameter. Splattering with intermediate activiy. Low amount of water is observed. |
| AZ19-17 | 17.9.2019 | Kichik Maraza | 40°30′41′′ | 049°01′49′′ | | | 18.9 | 30.5 | .37,0 | 7.94 | 7.89 | **Pool**, about 50 cm wide located at the westernmost edge of the outer rim on the outer part. Microbial colonies growing on the edge of the pool (brownish - green). |
| AZ19-18 | 17.9.2019 | Kichik Maraza | 40°30′46′′ | 049°01′58′′ | 1.59 | 6.36 | 18.5 | 30.5 | -19.4 | 7.94 | 7.55 | **Gryphon** on the eastern ridge side of gryphone. 10 cm bubbles. Moderetaly muddy bubbling. |
| AZ19-19 | 17.9.2019 | Maraza | 40°31′10′′ | 049°01′07′′ | | | | 30.5 | | | | **Gryphon** (pie-shaped) with a flat top due to recent eruption occured 29 August 2019. Very flat central surface mud flow diffused radially forming a circular shape. |
| AZ19-20 | 17.9.2019 | Maraza | 40°31′10′′ | 049°01′07′′ | | | | 30.5 | | | | **Gryphon**, second degassing feature in the center of the MV. Measures about 1m in diameter. There are several scattered circular (similar) structures representing the large bubling point. They are about 30 cm-1 m in diameter. |
| AZ19-21 | 18.9.2019 | Gyzmeidan | 40°48′39′′ | 048°42′19′′ | | | 21.1 | | -56.6 | 7.10 | 8.25 | **Pool**, about 60 cm wide with clear water. Some microbial colonies (greenish growing on the outskirts). |
| AZ19-22 | 18.9.2019 | Gyzmeidan | 40°48′39′′ | 048°42′15′′ | | | 18.2 | | -41.1 | 6.77 | 8.09 | **Pool**, about 1x1.5 m. Active in the western part of the MV. |
| AZ19-23 | 18.9.2019 | Gyzmeidan | 40°48′36′′ | 048°42′20′′ | | | 13.6 | | -37.6 | 6.85 | 7.96 | **Pool**, about 2 cm wide subelongated with mixed mud/water intermediated bubbling. Oil is observed inside. Located on the southern part of MV. Large 10 cm bubbles |
| AZ19-24 | 18.9.2019 | Gyzmeidan | 40°48′36′′ | 048°42′18′′ | | | 17.6 | | -62.2 | 7.38 | 8.41 | **Pool** measuring 70 cm diameter located at the foot of a gryphon. Intermediate bubbling is observed. High water content, with some mud. Located on SW side of the MV crater |
| AZ19-25 | 18.9.2019 | Gyzmeidan | 40°48′37′′ | 048°42′18′′ | 0.18 | 1.58 | 13.9 | | -62.9 | 6.56 | 8.41 | **Pool** measuring about 2 cm in width |
| AZ19-26 | 18.9.2019 | Gyzmeidan | 40°48′30′′ | 048°42′24′′ | | | 22.2 | | -78.1 | 8.55 | 8.65 | **Pool** measuring about 50-60 cm in diameter. Located on the flank of the valley to the south of the maim MV. Active bubbling in the pool. Low amount of mud. Microbial colonies on the outskirts. |
| AZ19-27 | 18.9.2019 | Gyzmeidan | 40°48′42′′ | 048°42′24′′ | | | 14.5 | | -49.3 | 4.05 | 8.17 | **Pool** measuring about 1 m in diameter located on the NE side of MV. Lies on the outskirts of MV crater. External flank alonjg dip. In the surrounding are presen 3 more similar sized/active pools. |
| AZ19-28 | 19.9.2019 | Gushchu | 40°26′07′′ | 048°42′24′′ | | | 22.7 | | -10.9 | 15.4 | 7.45 | **Gryphon**, about 20 cm tall with intermediate gas seepage. Mud and some oil seeping is observed. |
| AZ19-29 | 19.9.2019 | Gushchu | 40°26′06′′ | 048°42′24′′ | 0.32 | 2.10 | 21.6 | | -11.8 | 23.1 | 7.47 | **Gryphon**, about 20 cm tall. Very similar to AZ19-28, the structure is dominated by oil and mud. |
| AZ19-30 | 19.9.2019 | Gushchu | 40°26′06′′ | 048°42′24′′ | | | 20.9 | | -9.8 | 15.8 | 7.44 | **Gryphon** smaller than AZ19-28 and AZ19-29 |
| AZ19-31 | 19.9.2019 | Melikchobanly | 40°31′37′′ | 048°40′55′′ | 0.12 | 1.48 | 21.7 | 30.6 | -21.8 | 9.38 | 7.53 | **Pool**, about 20 cm wide located in the central part of the crater. Watery with oil. |
| AZ19-32 | 19.9.2019 | Melikchobanly | 40°31′37′′ | 048°40′54′′ | | | 20.2 | 30.6 | -40.9 | 9.55 | 8.00 | **Pool** similar to AZ19-31 positioned 8 m towards NW. Oil present. |
| AZ19-33 | 19.9.2019 | Madrasa | 40°31′32′′ | 048°33′57′′ | 0.04 | 0.83 | | 30.6 | | | | **Gryphon** about 50 cm tall. Moderate bubbling activity. Water dominated with significant amount of oil. Very thick oil film inside the gryohon. Samples taken keeping vial upside down. Oil inside the vial. |
| AZ19-34 | 19.9.2019 | Madrasa | 40°36′32′′ | 048°33′56′′ | | | | 30.6 | | | | **Gryphon** with vacume cleaner. Similar to AZ19-33. Samples taken with funnel. Clean samples. |
| AZ19-35 | 20.9.2019 | Shikhzarli | 40°29′12′′ | 049°02′03′′ | 4.44 | 8.25 | 20.6 | 24.1 | 7.5 | 7.95 | 7.35 | **Gyphon** located on the top of very last mud flow. High bubbling activity is observed. |
| AZ19-36 | 20.9.2019 | Shikhzarli | 40°28′49′′ | 049°01′54′′ | | | 18.2 | 24.1 | -55.7 | 7.84 | 7.28 | **Gryphon** similar to AZ19-35. |

# 4.2 Morphological descriptions

Individual morphological reviews of Maraza and Kichik Maraza (section 4.1.1), Gyzmeidan (section 4.1.2), Gushchu (section 4.1.3), Malikchobanli (section 4.1.4), Madrasa (section 4.1.5) and Shikhzarli (section 4.1.6) are reported in this section to i) present observations from satellite image and the field, ii) to interpret past eruptive events, iii) study the distribution and types of degassing features at each MV, and iv) describe the morphology of each MV. The location of each MV is shown in Figure 4-1. Note that sampling stations were selected at each structure based on locality interest and type of seepage activity. Assemblages of satellite images used for this section can be found in Appendix 2-7.
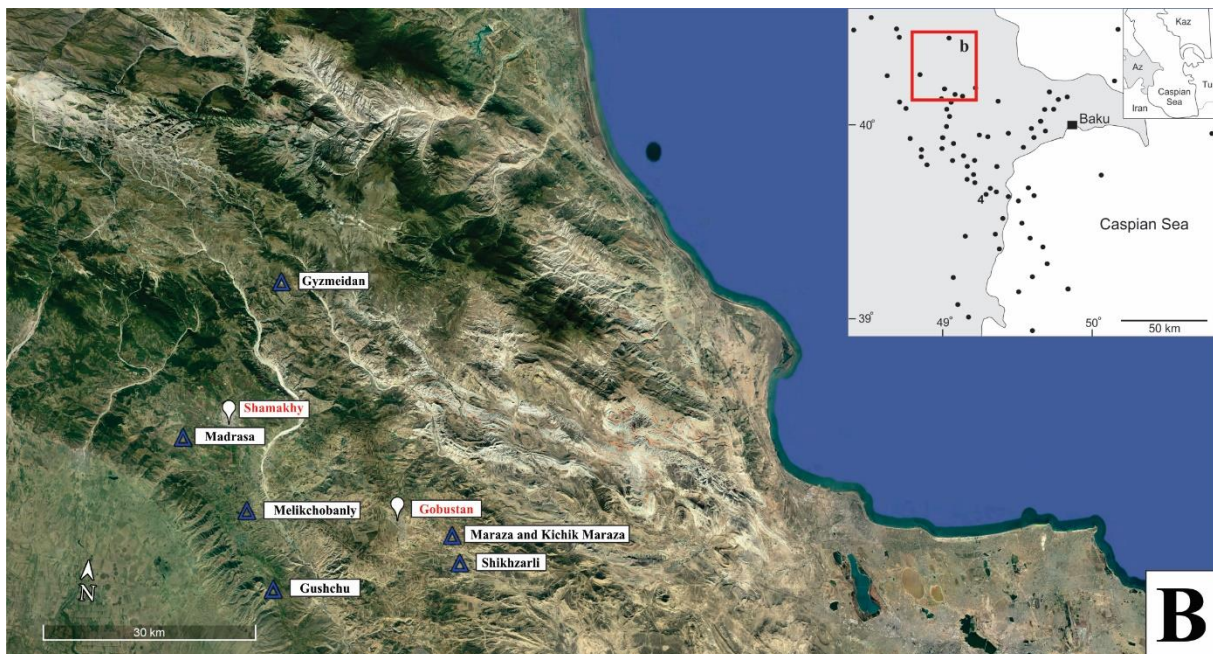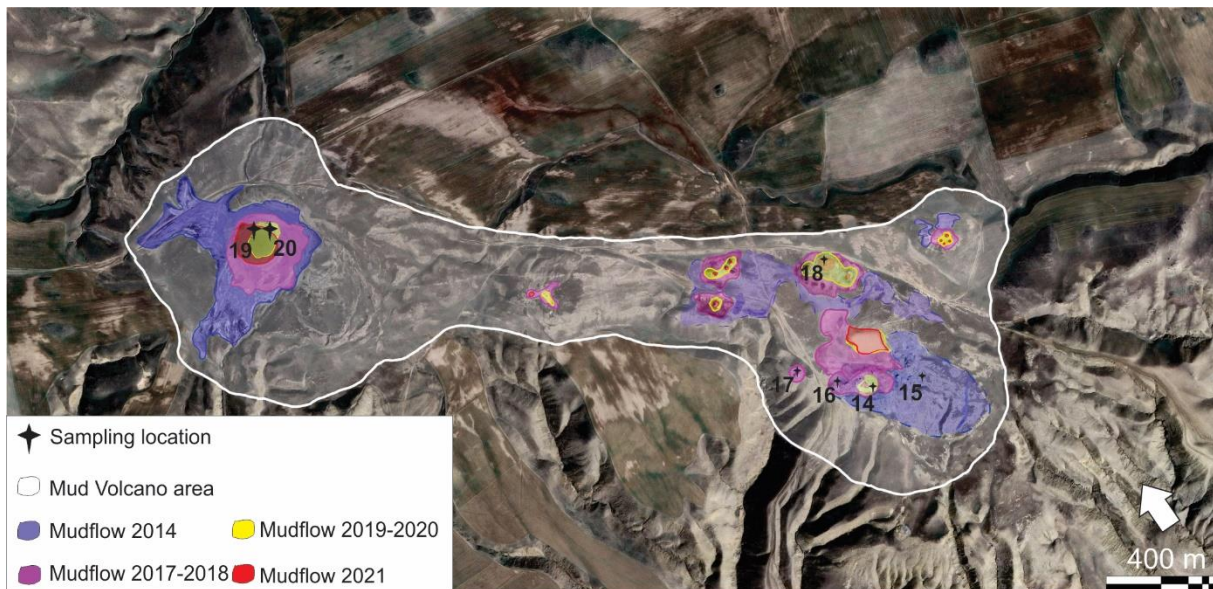


**Figure 4-1** *Satellite image (Google Earth) of the region with the investigated MVs (blue triangles) and nearby cities (white pin).*

## 4.2.1   Maraza and Kichik Mazara MV

Maraza MV and its satellite crater Kichik Maraza are located at the Central Gobustan zone (CGZ), in the south-eastern part of the Great Caucasus mega-anticlinorium. Figure 4-2 shows interpretation from satellite images from 6 distinct years: 2009, 2014, 2017, 2019, 2020 and 2021. Visual observation of the mudflow between 2009 and 2021 (total of 13 years) reveals that the volcano activity is rather constant, with some increased activity in 2014, 2017 and 2021; i.e. at about 3 years interval. Interpreted mudflows around both craters corresponding to

previous eruptions represent at least four possible eruption events between 2009 and 2021. The amount of mudflow resulting from the eruptions varies with the years, but the locations from which mud seeps is consistent. Based on satellite image investigations, the mud volcano area, including both Maraza and Kichik Maraza, is 1.38 km$^2$.



**Figure 4-2** *Satellite image (Google Earth) of Maraza and Kichik Maraza MV with sampling stations and interpreted mudflow between 2014-2021.*

The main crater (Maraza) is about 8.541 m$^2$ and the MV structure is pie-shaped. The rims are well defined and show signs of multiple eruptions during the past 13 years. The most recent mudflow covers an area of 0.1 km$^2$ (Figure 4-3a, c). Several scattered and circular degassing structures (measuring about 30 cm to 1 m in diameter) are observed around the carter (Figure 4-3e). These are only visible in the field, not on satellite images and reveal little to no degassing activity. Two gas sampling stations were placed on Maraza MV: AZ19-19 and AZ19-20 (Figure 4-2). The gas sampling station AZ19-19 is a pie-shaped gryphon (about 20 cm in diameter) with a flat top developed after the recent eruption (29th of August 2019). The gryphon at station AZ19-19 has a very flat central surface with mudflow that diffused radially forming a circular shape. AZ19-20 sampling station is also a circular and small gryphon measuring about 1 m in diameter, located in the center of Maraza MV structure.

About 1.52 km Northeast from the main crater, Kichik Maraza represents the satellite crater of Maraza MV (Figure 4-3d). Between Maraza and Kichik Maraza MV is a long strand of propagated mudflow with some degassing features. From the profile in Figure 4-3b, it is clear that the Maraza MV lies at lower elevation (675 m above mean sea level (asl)) than the Kichik

Maraza MV (737 m asl). The crater rims of Kichik Maraza MV are hard to observe both on satellite images and in the field. However, the eroded crater rims can be inferred by the distribution of several degassing structures on the outskirts of a depressed center (Figure 4-3d). The central part of the inferred crater hosts a salsa lake (measuring about 10,000 m$^2$). Gryphons and associated pools are distributed around the salsa lake. The shape of Kichik Maraza is hard to characterize and describe as it appears to have no distinct symmetry and eroded crater rims. The scattering of differently colored mud around the different degassing features (gryphons and pools) suggests active degassing at Kichik Maraza MV. There are clusters of degassing features (gryphons, pools) dispersed around the Kichik Maraza MV (Figure 4-3d, e). The size of the pools varies between 10 to 50 cm in diameter. The degassing structures are water dominated and some contain microbial colonies. The bubbling activity of the pools is low to moderate on average. A total of 6 sampling stations were placed on Kichik Maraza MV: AZ19-14, AZ19-15, AZ19-16, AZ19-17, and AZ19-18 (Figure 4-2).

Overall, Maraza MV is multi-crater mud volcano with a pie-shaped structure and exhibits little variation and spreading of poorly active degassing features. All the samples are therefore taken from gryphons located at the center of the crater. Kichik Maraza is also pie-shaped but displays a wide variety and distribution of active degassing features. The samples are mostly collected from gryphons with different localities around the crater rim. Together, Maraza and Kichik Maraza have an elongated structure and exhibit different degassing activities.
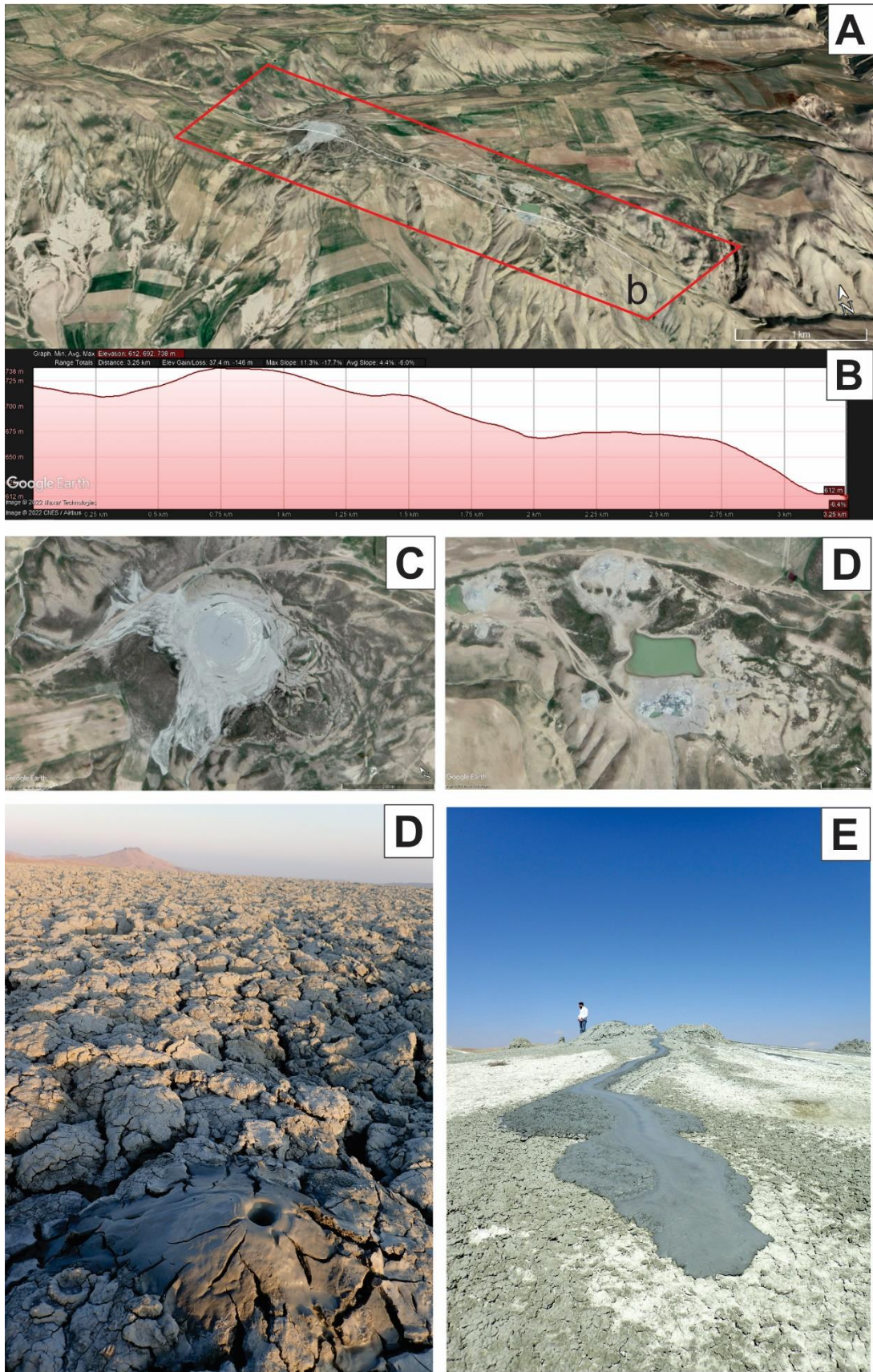
*Figure 4-3* Assemblage of satellite and field pictures of Kichik Marazaand Kichik Maraza MV. (A) Satellite image with indicated profile (B) of Kichik Marazaand little MV. (C) Areal view of Kichik Maraza MV. (D) and Kichik Maraza MV. (E) Small degassing feature (gryphon) surrounded by dried mud at Kichik Maraza MV. (F)Elongated mudflow from a gryphon at Kichik Maraza MV.

### 4.2.2   Gyzmeidan Mud Volcano

Gyzmeidan mud volcano is located on the North Gobustan zone (NGZ), about 20.5 km north from the town of Shamakhy. It is the most isolated and northernmost MV studied in this thesis. Its maximum elevation is about 1385 m asl. Figure 4-4 illustrates satellite image of Gyzmeidan MV with interpreted mudflow from years 2019, 2020 and 2021. At least three possible eruption events are indicated between 2019 and 2021.
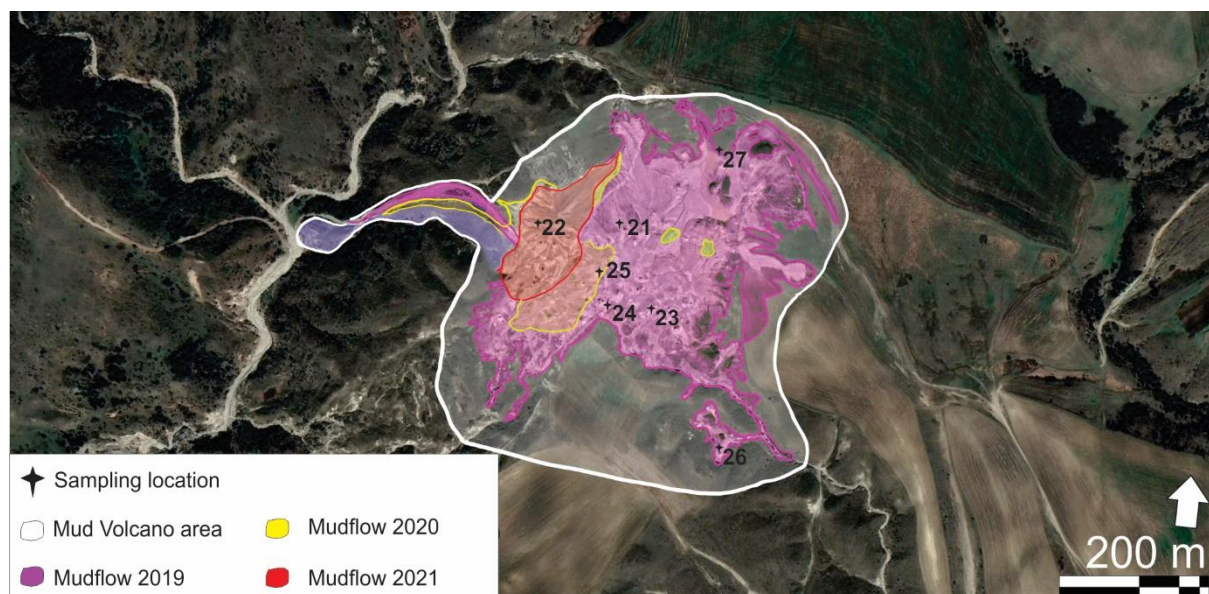


***Figure 4-4***  *Satellite image (Google Earth) of Gyzmeidan MV with sampling stations marked and interpreted mudflow between 2019-2021.*

The rims of Gyzmeidan crater are not visible on either satellite images nor in the field. Recent eruptions have most likely destroyed the crater rims and the remainder is covered by mud. The exact size and location of the crater is therefore challenging to estimate. Gyzmeidan MV has an irregular morphology characterized by broadly distributed pools and gryphons with different sizes and activity (Figure 4-5c, d, e). Mudflow from past eruptions and degassing activity is light grey, cracked and is spread unevenly. Recognizing the structure type of this MV is difficult and recalls some of the pie-shaped MVs observed elsewhere (Figure 4-5a, b). Based on satellite image investigations, the area of Gyzmeidan MV is $0.15 km^2$.

Many large (from 40 cm to 1 m in diameter) gryphons are distributed through the MV area but reveal no degassing activity. In fact, bubbling was only observed at pools. Wet (fresh) mud on the flank of several gryphons, however, indicate that the structures are indeed active. Unfortunately, without bubbling, gas sampling at gryphons was not possible. Therefore, all 7

sampling stations at Gyzmeidan MV (AZ19-21 to AZ19-27) are completed at pools (Figure 4-4). These pools have different shapes and sizes and are scattered throughout the MV (Table 4-1).

Overall, Gyzmeidan is pie-shaped with a wide variety and distribution of degassing features. The crater rims are not defined, which is likely due to erosion in addition to mudflow covering the entire MV area.
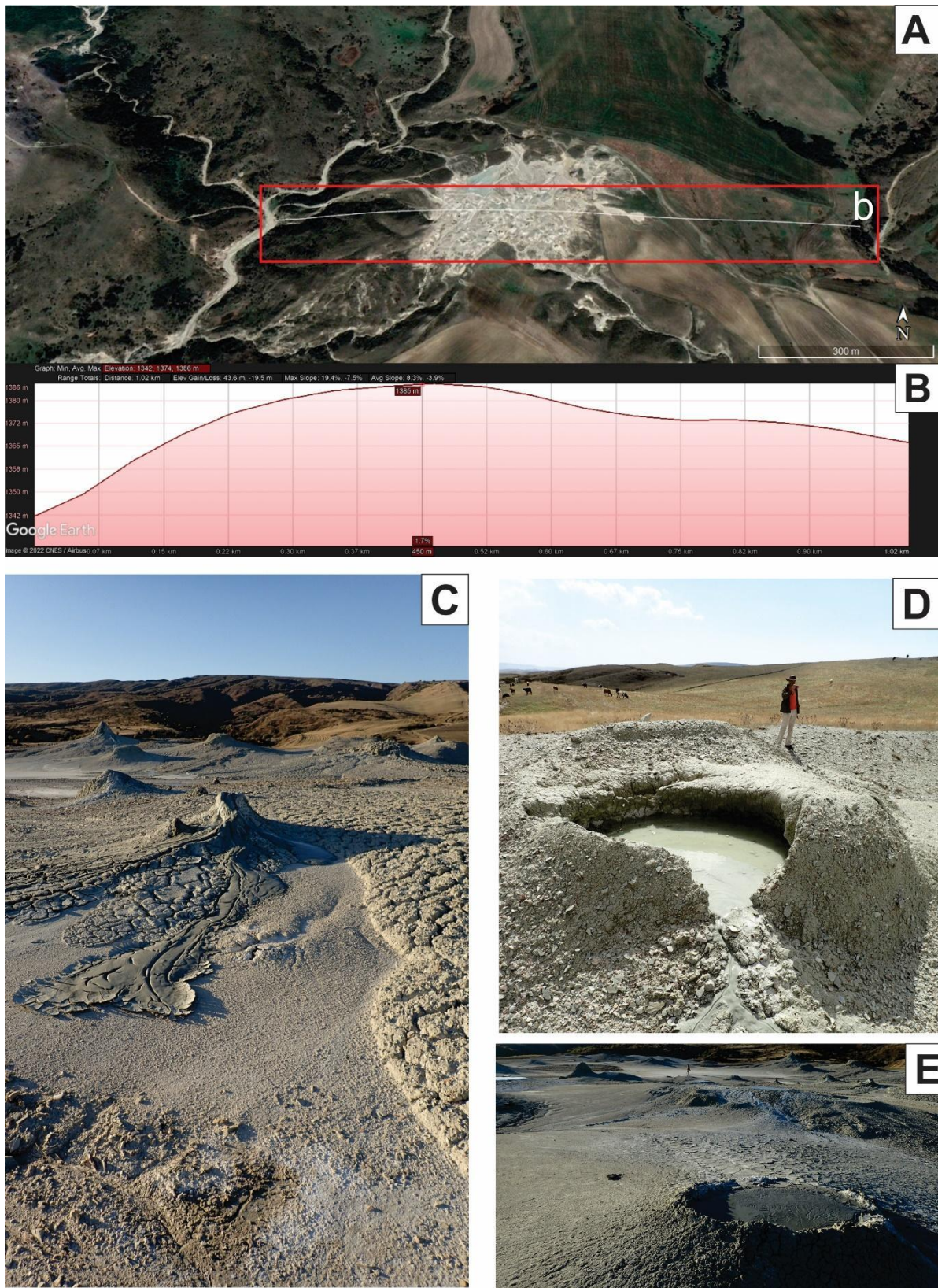
***Figure 4-5*** *Assemblage of satellite and field pictures of Gyzmeidan MV. (A) Satellite image with indicated profile (B) of Gyzmeidan MV. (C) Cluster of gryphons with visible mudflow. (D) Large gryphon with breached rim and water-dominated mud. (E) Field view of Gyzmeidan MV with several degassing structures of different seizes and morphologies.*

### 4.2.3 Gushchu MV

The Gushchu MV is located in the town of Gushchu, 22.97 km southwest from the town of Shamakhy. Its maximum elevation is about 767 m asl. In spite of the fact that the quality of satellite images of this structure are quite poor, the extend of the mud around the crater has increased by about a factor 5 between 2012 and 2021. Interpreted mudflows around the crater represents at least three possible eruption events occurring between 2012 and 2021 (Figure 4-6).
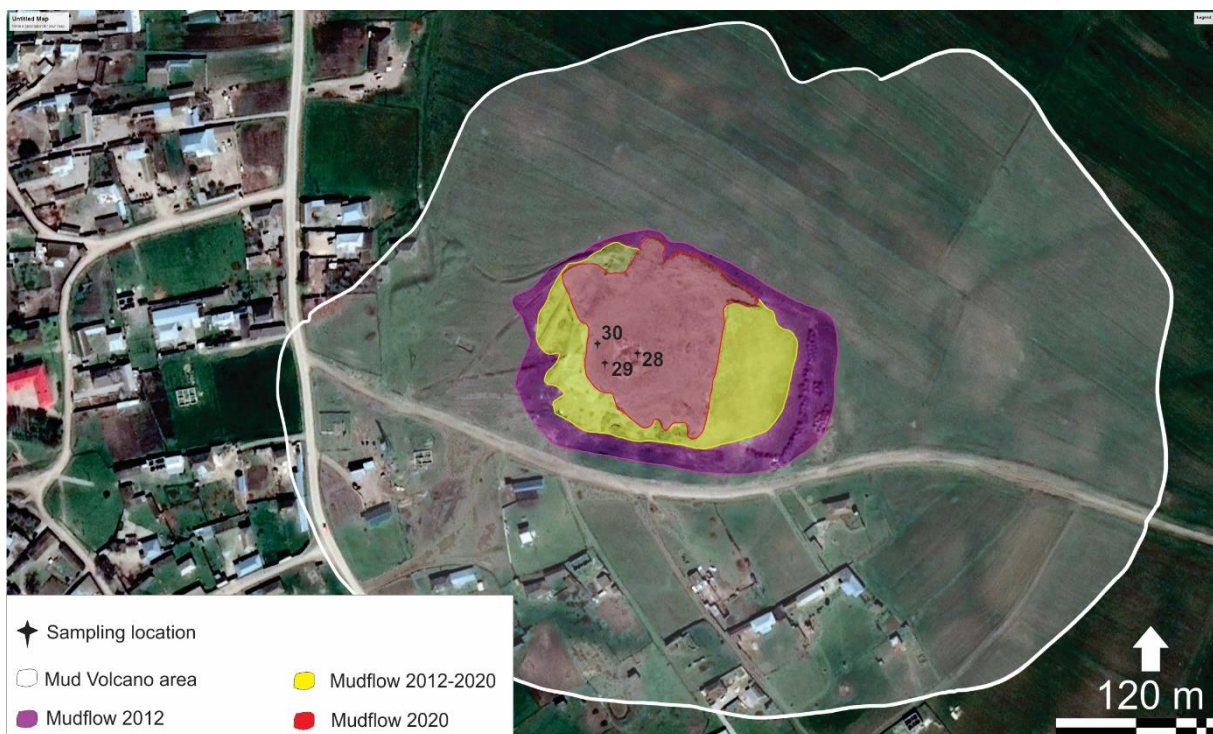


*Figure 4-6* *Satellite image (Google Earth) of Gushchu MV with indicated sampling stations and interpreted mudflow between 2012-2021.*

At first, only the main crater is observed due to its light-colored mudflow. However, when zooming out from the satellite image, two patches of mudflow are also observed to the North East (Figure 4-7a). The profile in figure 4-7b shows the presence of two smaller elevations, indicating the possible presence of satellite craters (Figure 4-7b). The satellite craters were not observed in the field, and no gas samples were collected there. Hence, the estimated area of Gushchu MV is 0.32 km$^2$.

The main crater measures about 292 m$^2$ and the MV structure is pie-shaped. Gushchu MV is situated in the middle of a farm field on a shallow dome (Figure 4-7ac). The MV has a very smooth morphology with sub-circular mudflow, distributed radially from a central point (Figure 4.20c). The mudflow covers an area less than 0.1 km$^2$ with distinct light grey color. Large variety of clasts from different lithologies are observed around the volcano. Dry mud breccia with diffused fracturing is observed throughout the entire MV surface. The central part of the crater has a gentle caldera depression (about 30 m) with a faint ring structure (4-7e). Gryphons, averaging 15 cm in height, are distributed in this central depression (Figure 4-7d). Very little degassing activity is observed on the MV structure and only three sampling stations were collected: AZ19-28, AZ19-29 and AZ19-30 (Figure 4-6).

The nearest house is no more than 100 m from the center of the volcano, meaning that seeping gas and associated potential eruptions can easily reach and become a threat for the local habitants. Based on satellite imaging, there is a 375 m$^2$ coverage of potentially endangered.
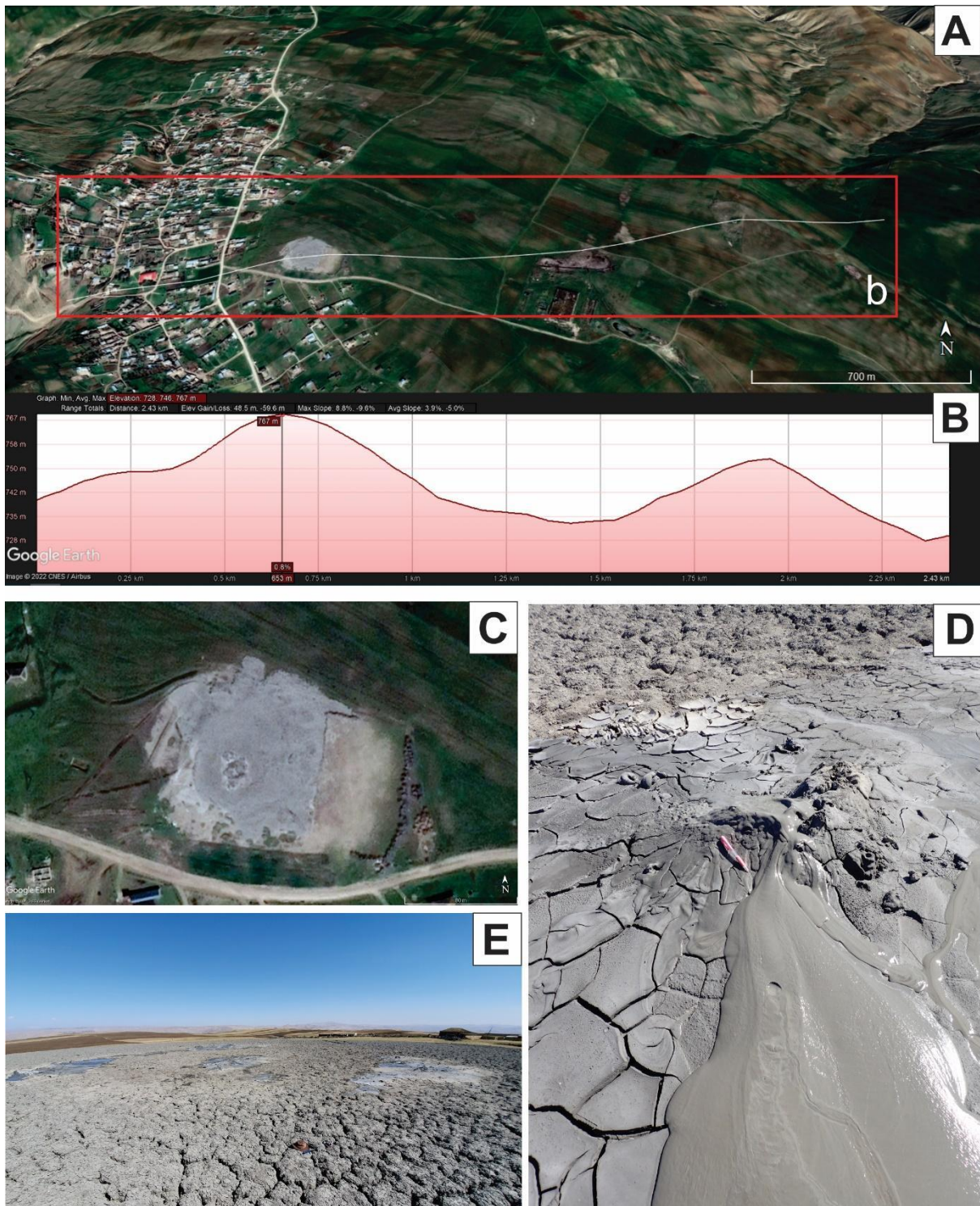
***Figure 4-7*** *Assemblage of satellite and field pictures of Gushchu MB. (A) Satellite image with indicated profile of (B) Gishchu MV.(C) Areal view of Gushchu MV. (D) Small gryphon with clear mudflow active in central depression, (E) Field picture of Gushchu MV crater with central active seeps.*

### 4.2.4 Melikchobanly MV

The Melikchobanly MV is located about 12.28 km southwest from the town of Shamakhy. Its maximum elevation is about 643 m asl. Interpreted mudflows around the crater corresponding to previous eruptions represent at least three possible eruption events between 2091 and 2021 (Figure 4-8).
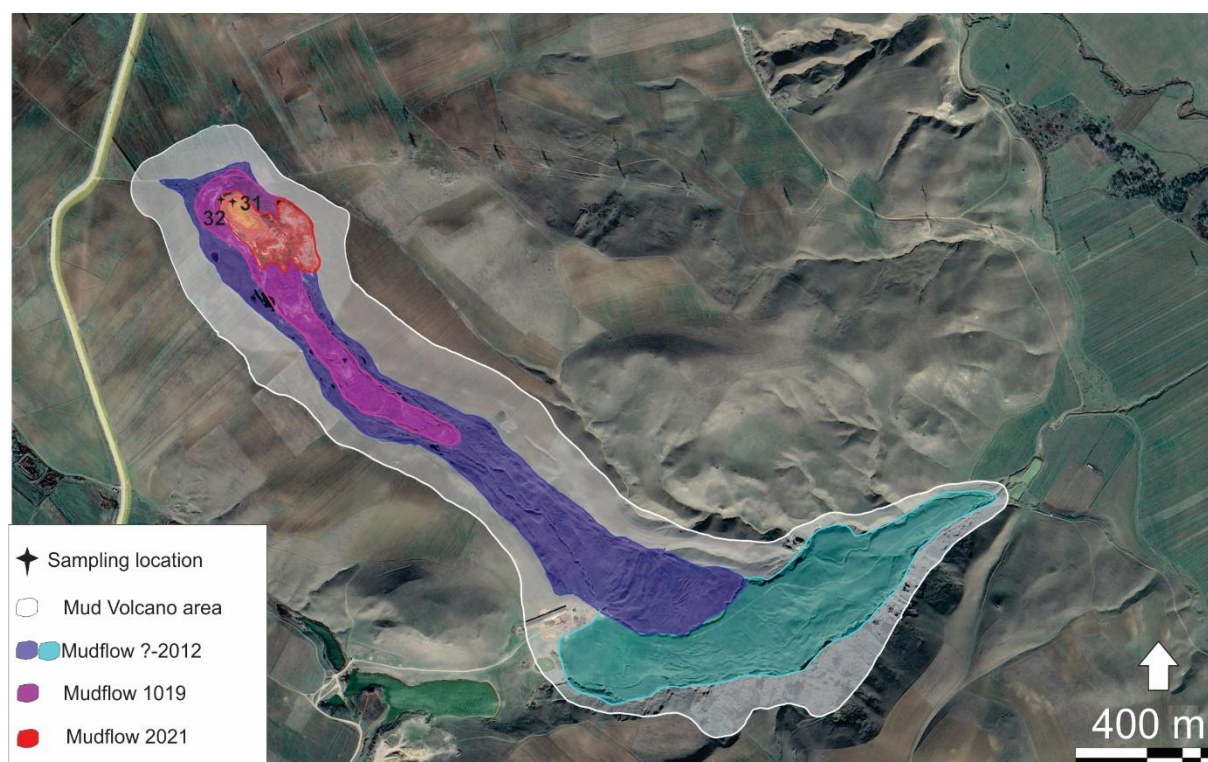


***Figure 4-8** Satellite image (Google Earth) of Melikchobanly MV with sampling stations marked and interpreted mudflow between 2012-2021.*

Based on satellite image investigations, the area of Melikchobanly MV is 0.12 km$^2$ and the main crater is estimated to measure about 112 m$^2$. Similarly, to Maraza MV, the rims of the volcano are well defined and show signs of multiple eruptions by visibly different color in the mudflow surrounding the crater. The MV recently erupted in 2019 and has a clearly visible flow, forming an SE elongated tongue that extends for about 2 km (Figure 4-9 a, b, c). The mud breccia contains large amount of clasts ranging in size (0.5 - 1 cm). In the field, several pools bubbling watery mud and oil are observed in the central part of the crater (Figure 4-9d, e, f). Some small (about 20 cm) gryphons are also present (Figure 4-9d). In the center of Melikchobanly MV the mud is soft and not walkable. Two sampling stations were collected: AZ19-31 and AZ19-32 (Figure 4-8). AZ19-31 is stationed on a 20 cm wide pool in the central

part of the crater. The pool is watery with some oil. AZ19-32 is also a 20 cm wide pool similar to AZ19-31 positioned 8 m towards NW. Oil seepage is present at this station.

Melikchobanly MV show sign of some minor seepage activity. The degassing features are small in size. The significant extension of the mudflow, indicates that copious mud eruptions produced mud breccia tongues that superposed along the South East gently dipping slope. This elongated mudflow forms a scar on the flank of the depression. This suggests that high viscosity of the mud breccia was able to erode and excavate during the flow. A similar scenario has been proposed for the Lokbatan MV close to Bahar (Mazzini et al., 2021).
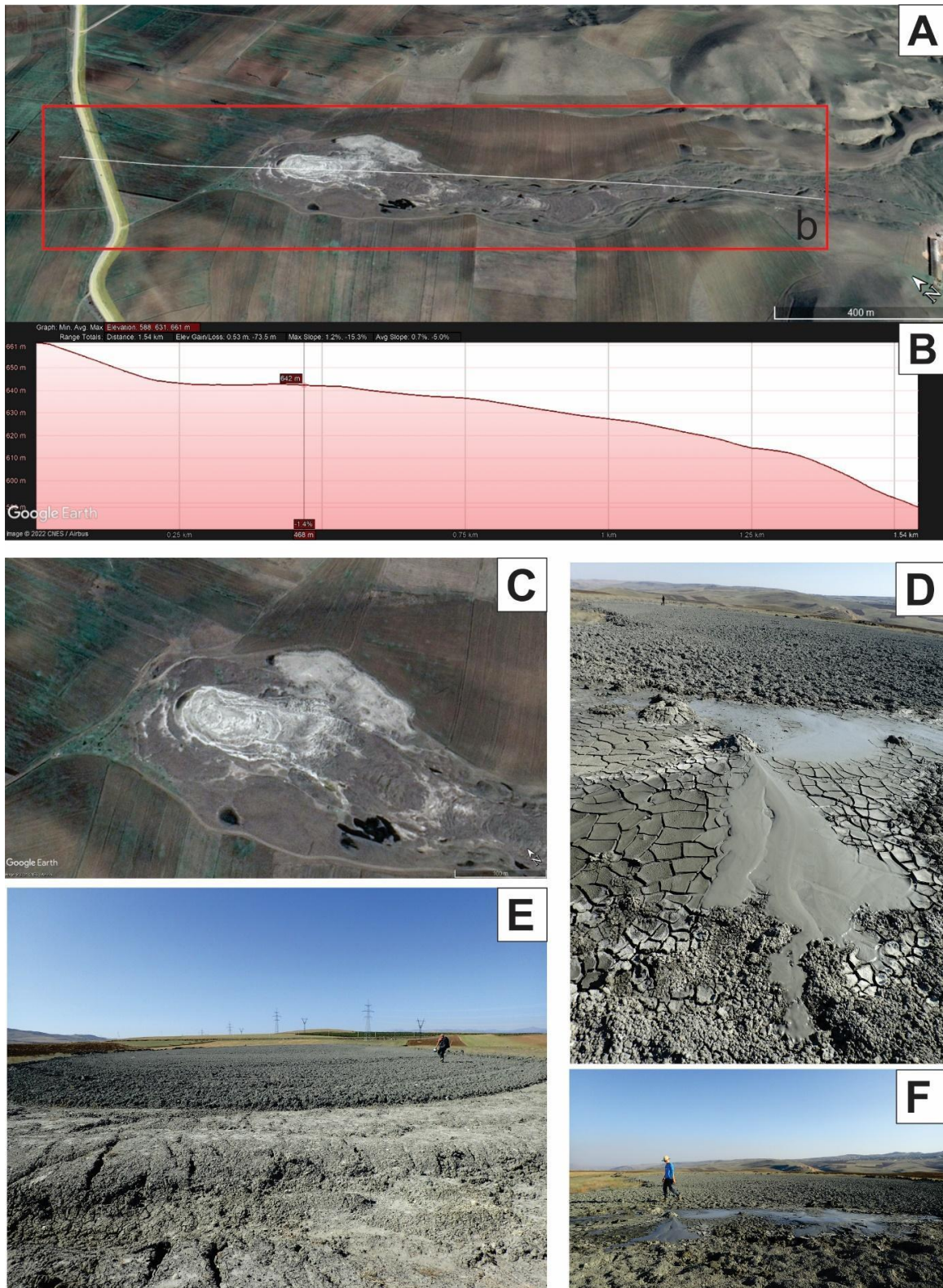
**Figure 4-9** *Assemblage of satellite and fied pictures of Melikchobanly MV. (A) Satellite image with indicated profile of (B) Melikchobanly MV. (C) Areal view from a satellite image of Melikchobanly. (D) Cluster of small gryphons with mudflow surrounded by dried and cracked mud. (F) Field view of Melikchobanly MV where the main seepage sites are located.*

### 4.2.5 Madrasa MV

Madrasa (sometimes referred to as Madrasa) MV is located in a field by the town of Madrasa, about 6.47 km southwest of the town of Shamakhy. Its maximum elevation is about 681 m asl. Interpreted mudflows around the crater corresponding to previous eruptions represents at least four possible eruption events between 2001 and 2021 (Figure 4-10).
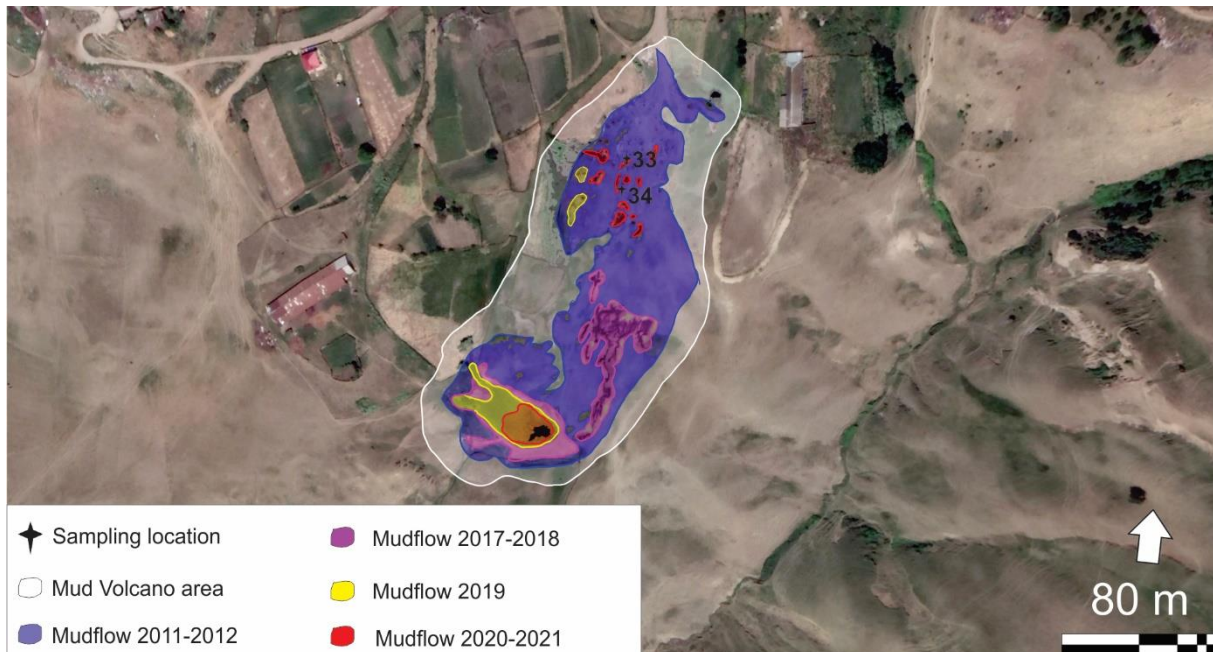


*Figure 4-10* Satellite image (Google Earth) of Madrasa MV with sampling stations marked and interpreted mudflow between 2011-2021.

The rims of the original crater are not visible on neither satellite images nor in the field. Degassing structures are dominated by water and mud with black oil resulting in spectacular oil flows that are distributed throughout the entire area (Figure 4-11 c, d, e, f). The location and size of the crater is therefore challenging to estimate. Recognizing the structure type of this MV is also a challenge at this locality. The profile made from satellite images gives no information about the morphology of the volcano (Figure 4.16a, b). Based on satellite image observation, the area of Madrasa MV is estimated to be around 39.080 $m^2$.

The volcano is situated on the flank of a laterally extensive fault structure. Seepage of thick black oil is dispersed throughout the field and runs to the southwest, perpendicular to the fault structure. Clusters of clearly oil-dominated pools and gryphons make it difficult to access and investigate the area thoroughly (Figure 4-11f). Three sampling stations were established on Madrasa MV: AZ19-33 and AZ19-34 (Figure 4-10). Overall, Madrasa MV is spectacular but

difficult to investigate. It is the only targeted structure with oil-dominated flows. The direct seepage of oil through MV degassing structures is an extraordinary phenomenon to observe.
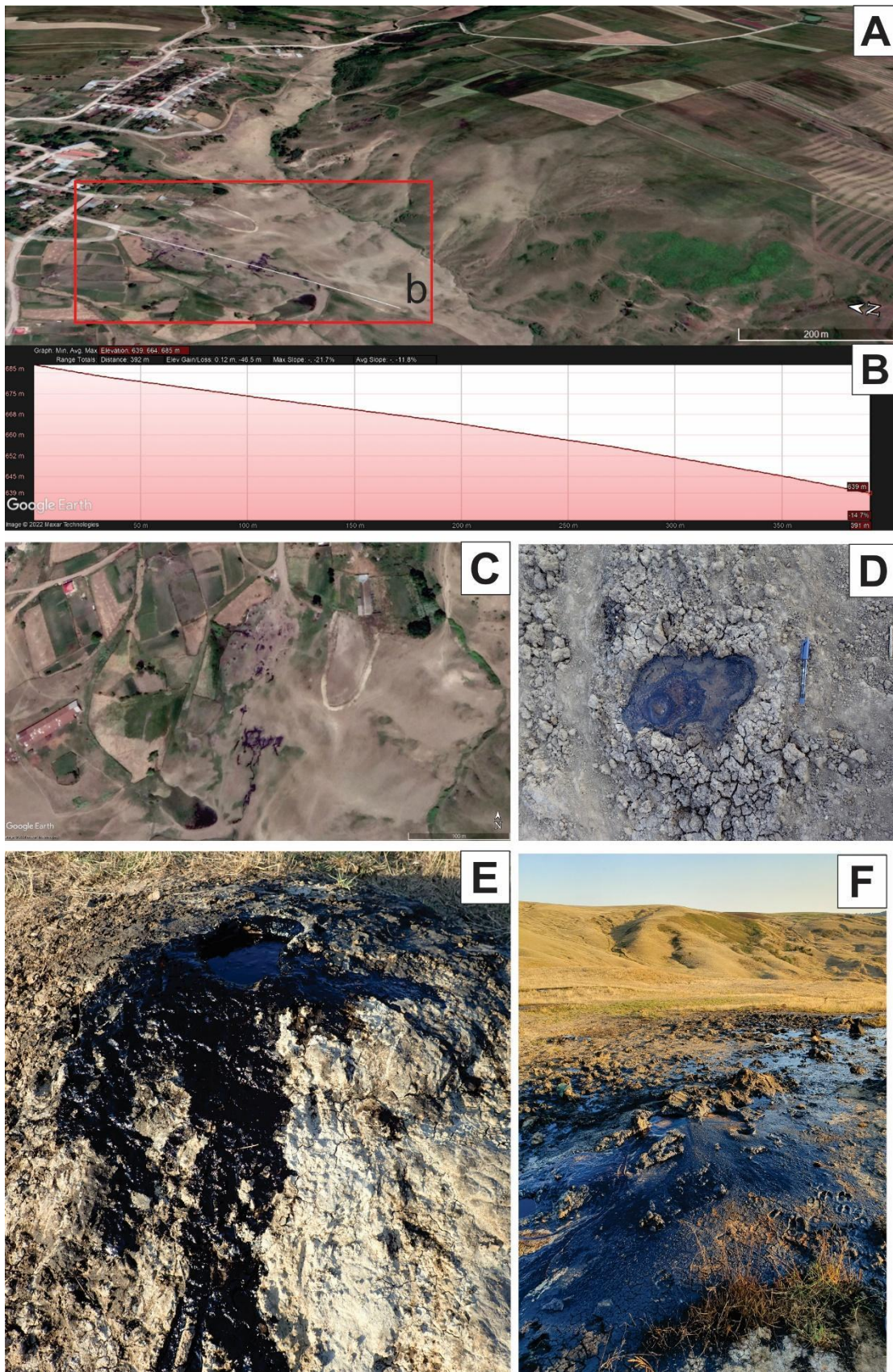
*Figure 4-11* Assemblage of satellite and field pictures of Madrasa MV. (A) Satellite image with indicated profile of (B) of Madrasa MV structure. (C) Areal view of Madrasa MV. (D) Close-up view of a oil-dominated pool. (E) Oil-dominated gryphon with oil flow over dried mud. (F) Field picture of clustered seepage features and their resulting oily-mud covering a large surface.

### 4.2.6 Shikhzarli and little Shikhzarli Mud Volcano

Shikhzarli (sometimes referred to as Shikhzarli) MV is located 1.66 km northeast from the town of Shikhzarli in Gobustan. It lies 3.94 km from Kichik Maraza MV and has a plateau structure with little elevation. Its maximum elevation is about 643 m asl. The mudflow around the crater corresponding to previous eruptions represents at least three possible eruption events between 2009 and 2021 (Figure 4-12).
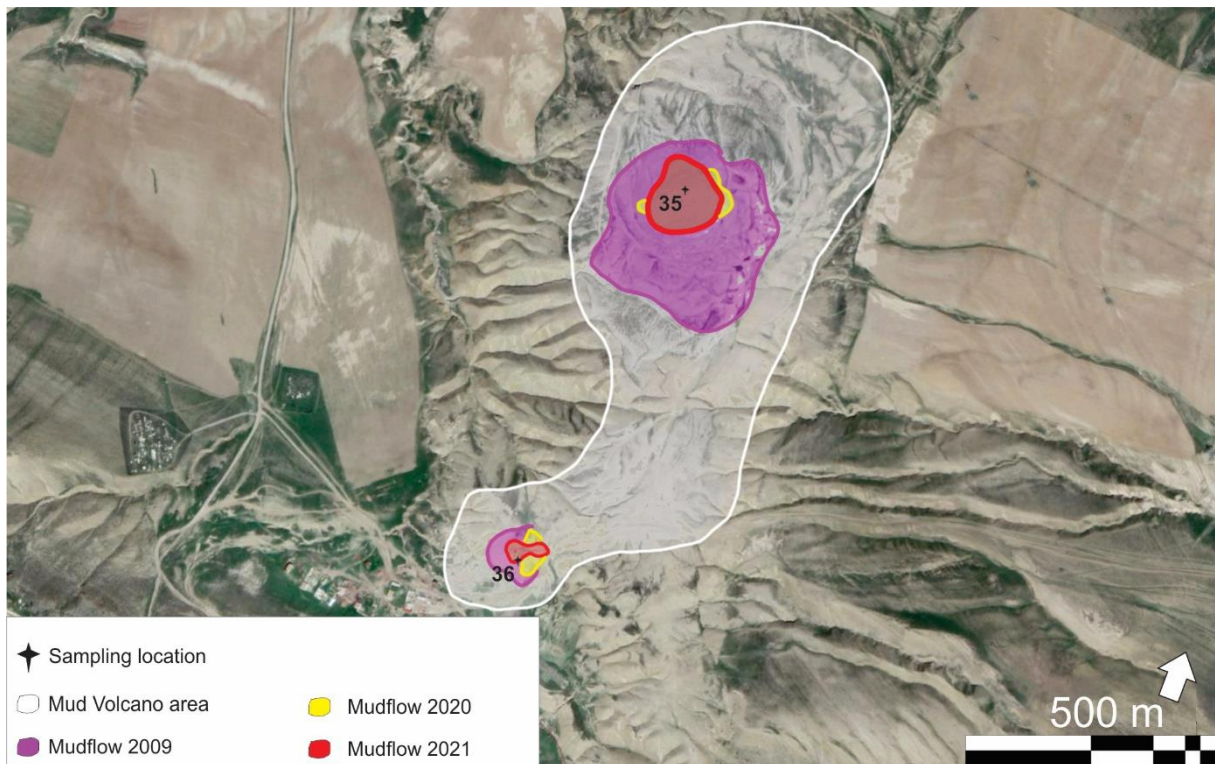


***Figure 4-12*** *Satellite image of Shikhzarli MV with sampling stations AZ19-35 (marked as 35)* and *AZ19-36 (marked as* 36) and interpreted mudflow between 2009-2021.

The rims of the crater are well defined and show signs of multiple eruptions by visibly different color in the mudflow surrounding the crater. The most recent mudflow around the crater covers an area of 0.1 km$^2$.

No obvious signs of seepage were observed in the field. Little bubbling was observed at the at and around the crater, limiting the gas sampling process. Only one sample was taken at the main crater: AZ19-35 (Figure 4-12). About 0.73 km northeast form the Shikhzarli MV is a satellite crater, little Shikhzarli MV. Between Shikhzarli and little Shikhzarli MV is a long strand of propagated mudflow with no degassing features observed. From the profile in figure 4.13b, it

is clear that the little Shikhzarli MV lies at lower elevation (608 m asl) than the Shikhzarli MV (643 m asl). Its crater rims are difficult to distinguish, especially in the eastern side. It has a pie-shaped structure with some degassing structures (gryphons) in the center. Finding bubbling sites at the satellite crater was difficult, thus only one sampling station was established: AZ19-36 (Figure 4-12).

Based on satellite image investigations, the total area of Shikhzarli MV is estimated to be ~ 0.90 km$^2$. Overall, Shikhzarli and little Shikhzarli MV does not show strong signs of degassing activity. The structures that are present have little to no bubbles. There are few degassing features and only two gryphons were sampled.
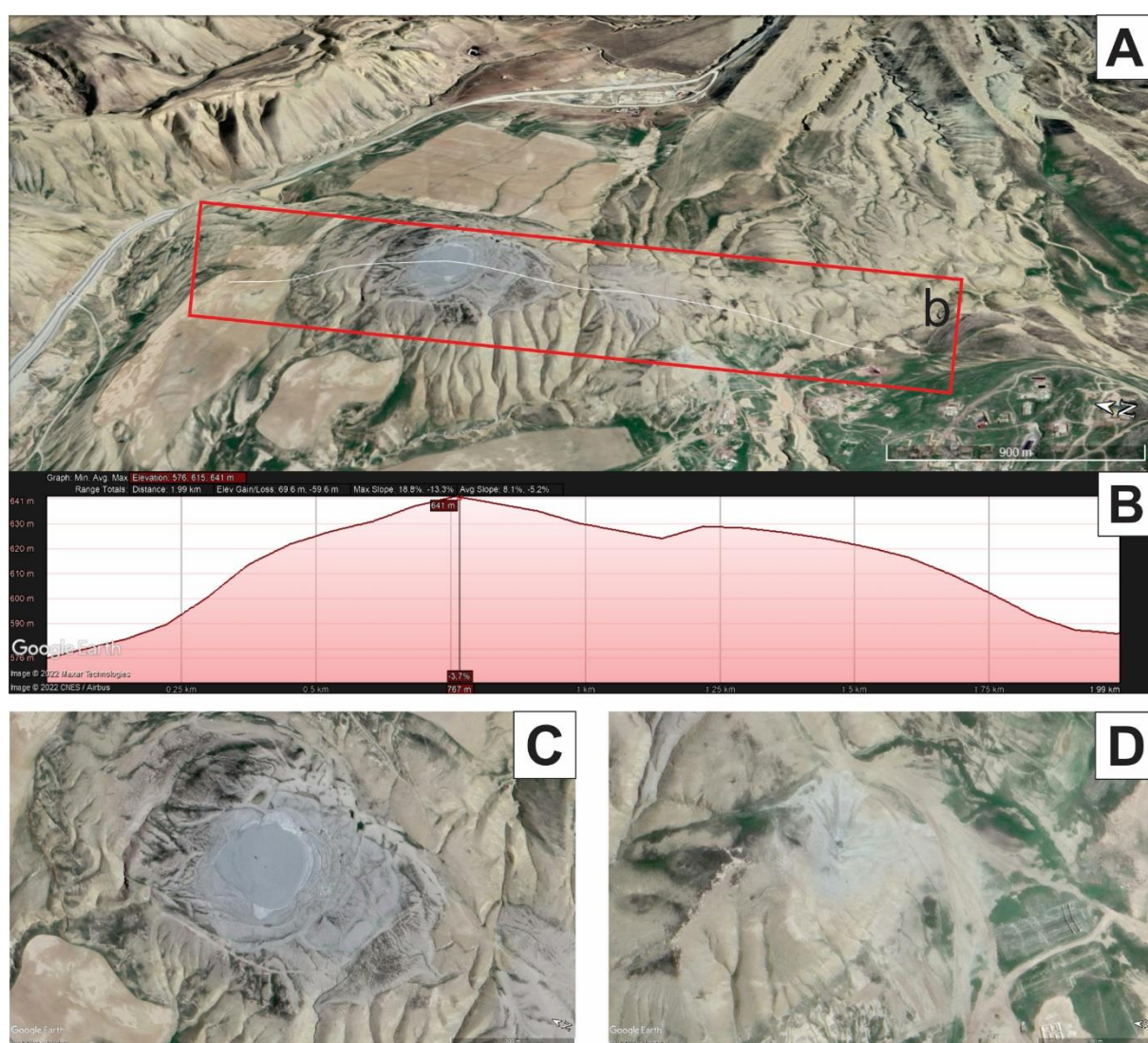


***Figure 4-13*** *Assemblage of satellite images of Shikhzarli MV. (A) Satellite image with indicated profile of (B) of Shikhzarli MV structure was taken. (C) Areal view of the main Shikhzarli crater MV. (D) Areal view of the satellite Shikhzarli crater MV*

**Table 4-2** *Summary of the observations made at each MV structure based on observations from satellite images and the field.* *Events inferred from available images in historic database of Google Earth.*

| Observation based on satellite image and field observations | MV structure | | | | | |
| --- | --- | --- | --- | --- | --- | --- |
| | **Maraza and Kichik Maraza** | **Gyzmeidan** | **Gushchu** | **Melikchobanly** | **Madrasa** | **Shikhzarli** |
| Shamakhy-Gobustan Tectonic zone | Central Gobustan | North Gobustan | Southwestern Gobustan | Shamakhy | Shamakhy | Central Gobustan |
| Nearby large scale structures | Longitudinal tectonic ruptures | Zogalavachai superimposed synclinal | Anticlines strongly broken by longitudinal and transverse faults | Normal faults | Normal faults | Longitudinal tectonic ruptures |
| MV morphology | Elongated | Pie-shaped | Pie-shaped | Elongated | N/A | Pie-shaped |
| Mud Volcano area ($km^2$) | 1.38 | 0.15 | 0.32 | 0.12 | 0.039 | 0.9 |
| Number of possible eruption events* | 4 | 3 | 3 | 3 | 4 | 3 |
| Number of sampling stations | 7 | 7 | 3 | 2 | 2 | 2 |
| Number of sampled gryphons | 6 | 0 | 0 | 0 | 2 | 2 |
| Numbre of sampled pools | 1 | 7 | 3 | 2 | 0 | 0 |

# 4.3 Gas geochemistry

This section reports novel geochemical data collected from the targeted MVs. The molecular and isotopic composition of the gas samples collected from the MV structures is presented in Table 4-3 (section 4.3.1) and plotted in figure 4-14 a, b and c (section 4.3.2) to further suggest the origin of seeping gas at each MV structure in the next chapter.

**Table 4-3** *Molecular and isotopic gas composition (normalized) at all the sampling stations in vol. %. Isotopic data: $\delta^{13}C$: ‰, VPDB; $\delta D$: ‰, VSMOW;*

| MV structure | Sample ID | Degassing structure | He | Ne | H₂ | N₂ | CH₄ | CO₂ | C₂H₆ | δ¹³C-CH₄ | δD-CH₄ | δ¹³C-CO₂ | C₁/C₂+C₃ |
|---|---|---|---|---|---|---|---|---|---|---|---|---|---|
| Kichik Maraza | AZ19-14 | Gryphon | 0.0047 | 0.0089 | 0.0121 | 0.0 | 97.9 | 1.99 | 0.06 | -43 | -183 | -5.9 | 1703 |
| | AZ19-15 | Gryphon | 0.0047 | 0.0087 | 0.0060 | 0.0 | 98.5 | 1.48 | 0.01 | -41 | -178 | -8.4 | 12400 |
| | AZ19-16 | Gryphon | 0.0039 | 0.0039 | 0.0028 | 0.0 | 98.8 | 1.16 | 0.01 | -31.6 | -183 | -5.1 | 8726 |
| | AZ19-17 | Pool | 0.0231 | 0.0619 | 0.0056 | 4.6 | 93.5 | 1.80 | 0.02 | -36 | -190 | -17.5 | 6068 |
| Maraza | AZ19-18 | Gryphon | 0.0031 | 0.0000 | 0.0113 | 0.0 | 97.9 | 2.05 | 0.06 | -39 | -178 | 5.6 | 1670 |
| | AZ19-19 | Gryphon | 0.0389 | 0.1391 | 0.0092 | 82.0 | 16.2 | 1.62 | 0.01 | -39.7 | -176 | -10.1 | 1958 |
| | AZ19-20 | Gryphon | 0.0035 | 0.0118 | 0.0011 | 84.3 | 15.4 | 0.27 | 0.02 | | | | 796 |
| Gyzmeidan | AZ19-21 | Pool | 0.0168 | 0.0263 | 0.0061 | 0.0 | 98.1 | 1.88 | 0.02 | -47.3 | -164 | -13.8 | 6331 |
| | AZ19-22 | Pool | 0.0215 | 0.0000 | 0.0089 | 0.4 | 97.4 | 2.16 | 0.01 | -45.8 | -161 | -12.6 | 10530 |
| | AZ19-23 | Pool | 0.1348 | 0.3694 | 0.0231 | 0.0 | 93.4 | 5.88 | 0.19 | -43.4 | -165 | -11.4 | 496 |
| | AZ19-24 | Pool | 0.0190 | 0.0062 | 0.0095 | 0.0 | 98.5 | 1.44 | 0.02 | -46 | -167 | -13.0 | 4112 |
| | AZ19-25 | Pool | 0.0463 | 0.1288 | 0.0085 | 69.4 | 28.8 | 1.54 | 0.02 | -45.5 | -162 | -22.4 | 1182 |
| | AZ19-26 | Pool | 0.0129 | 0.0000 | 0.0058 | 2.4 | 95.8 | 1.68 | 0.08 | -39.8 | -148 | -18.9 | 1200 |
| | AZ19-27 | Pool | 0.0211 | 0.0061 | 0.0519 | 0.0 | 98.9 | 1.02 | 0.02 | | | | 4622 |
| Gushchu | AZ19-28 | Gryphon | 0.0063 | 0.0109 | 0.0035 | 0.0 | 99.1 | 0.85 | 0.03 | -60.3 | -202 | -8.8 | 3560 |
| | AZ19-29 | Gryphon | 0.0029 | 0.0004 | 0.0003 | 1.5 | 93.9 | 4.55 | 0.11 | -59.2 | -198 | 6.8 | 854 |
| | AZ19-30 | Gryphon | 0.0048 | 0.0083 | 0.0055 | 17.4 | 75.9 | 6.56 | 0.13 | -60.4 | | -12.7 | 584 |
| Melikchobanly | AZ19-31 | Pool | 0.0342 | 0.0005 | 0.0023 | 2.3 | 96.2 | 0.93 | 0.51 | -49.9 | -181 | -19.8 | 190 |
| | AZ19-32 | Pool | 0.0290 | 0.0060 | 0.0058 | 0.0 | 98.1 | 1.34 | 0.52 | -49.1 | -187 | -11.8 | 190 |
| Madrasa | AZ19-33 | Gryphon | 0.0015 | 0.0035 | 0.0008 | 9.2 | 83.3 | 7.42 | 0.10 | -48.7 | -191 | 21.6 | 824 |
| | AZ19-34 | Gryphon | 0.0025 | 0.0065 | 0.0021 | 0.0 | 94.4 | 5.44 | 0.15 | -48 | -192 | 5.9 | 644 |
| Shikhzarli | AZ19-35 | Gryphon | 0.0175 | 0.0538 | 0.0249 | 1.7 | 90.0 | 7.93 | 0.30 | | -232 | 9.5 | 300 |
| | AZ19-36 | Gryphon | 0.0034 | 0.0000 | 0.0382 | 0.1 | 99.2 | 0.65 | 0.01 | -40.9 | -181 | -13.3 | 12437 |

### 4.3.1  Gas molecular and isotopic composition

The 3 major gas components of all sampled gas are $CH_4$, $N_2$ and $CO_2$. $CH_4$ concentrations are present in all samples (from 15.35 vol.% to 99.20 vol.%) and is the dominant gas in majority (87%) of the samples. $N_2$ is present in about half the samples with variable concentrations (from 0.1 vol.% to 84.3 vol.%). $CO_2$ concentrations are low (from 0.27 vol.% to 7.93 vol.%) but present in all samples. $C_2H_6$ is the only methane homolog detected in the sampled free gas and is present in all samples with variable concentrations (from 0.01 to 0.52 vol.%). The remaining gas components (He, Ne, $H_2$) are present in significantly less quantities and vary by two to three orders of magnitude. He and $H_2$ concentrations are present in all samples (from 0.00151 to 0.135 vol.% and 0.0519 to 0.0003 vol.%, respectively). Ne is present in most samples (from 0.0004 to 0.3694 vol.%). There is a large variation in the gas dryness ratio $C_1/(C_2+C_3)$ at the different sampling stations (from 190 to 12437).

The measured carbon isotope of $CH_4$ and $CO_2$ along with the measured deuterium isotope of $CH_4$ are reported at most of the sampling stations. Samples AZ19-20 and AZ19-27 have no isotopic measurements, while AZ19-30 only misses $\delta^{13}C\text{-}CH_4$ measurements. All the $\delta^{13}C\text{-}CH_4$ and $\delta D\text{-}CH_4$ are negative while most the $\delta^{13}C\text{-}CO_2$ are negative (5 recordings are positive). Overall, $\delta^{13}C\text{-}CH_4$ ranges from -60.40‰ to -31.60 ‰. The corresponding $\delta D\text{-}CH_4$ range from -232‰ to -148‰. The $\delta^{13}C\text{-}CO_2$ vary with a much wider range from -22.39‰ to 21.58‰. The following 5 samples have positive $\delta^{13}C\text{-}CO_2$: AZ19-18 (5.6‰), AZ19-29 (6.8‰), AZ19-33 (21.6‰), AZ19-34 (65.9‰), and AZ19-35 (9.5‰).

More specifically, gas samples from Kichik Maraza (2 count) have unusually low $CH_4$ values ranging from 15.4 to 16.2 vol.% with unusually high $N_2$ values ranging from 82.0 to 84.3 vol.%. The ethane concentrations in the samples are low (from 0.01 to 0.02 vol.%), and the gas dryness ratio varies from 796 to 1958. $CO_2$ concentrations are low (from 0.27 to 1.62 vol.%). All samples are taken from gryphons. Gas samples from Kichik Maraza MV (count 5) contain methane ranging from 93.5 to 98.8 vol.% and but has lower concentrations of methane homolog (ethane from 0.01 to 0.06 vol.%). The gas dryness ratio varies from 1670 to 12400 and $CO_2$ concentrations are low (from 1.16 to 2.05 vol.%). $\delta^{13}C\text{-}CH_4$ at Kichik Maraza MV is always negative and ranges from -31.6‰ to -43‰ and average -38.1‰. The $\delta D\text{-}CH_4$ range from -178‰ to -190‰ and average -182‰. The $\delta^{13}C\text{-}CO_2$ range from -17.5‰ to 5.6‰. Sample AZ19-18, collected on the rims of Kichik Maraza MV, has unusually high $\delta^{13}C\text{-}CO_2$ reading compared to the other stations. Only sample (AZ19-19) has isotopic measurements at Maraza

MV. The $\delta^{13}C$-$CH_4$ is -39.7‰, the $\delta D$-$CH_4$ is -176‰ and the $\delta^{13}C$-$CO_2$ is -10.1‰. Out of 5 samples from Kichik Maraza MV, 4 are from gryphons and 1 is from a pool.

All but one sample (AZ19-25) collected at Gyzmeidan MV (count 6) show methane concentrations ranging from 93.4 to 98.9 vol.%, coinciding low or zero $N_2$ concentrations (from either 0.4 to 2.4) and varying $CO_2$ concentrations (from 5.88 to 1.02 vol.%). Sample AZ19-25 is $N_2$ dominated (69.4 vol.%) with unusually low $CH_4$ concentration (28.8 vol.%). The low content of ethane (0.02 vol.%) results in gas dryness ratio of 1182. The $\delta^{13}C$-$CH_4$ at Gyzmeidan MV vary from -47.3‰ to -39.8‰ and average -44.6‰. The $\delta D$-$CH_4$ measurements are stable and range from -167‰ to -143‰ and average -161‰. The $\delta^{13}C$-$CO_2$ ranges from -22.4‰ to -11.4‰ and average -15.4‰. All samples at Gyzmeidan MV (7 count) are taken from pools.

Components of the sampled gas at Gushchu MV (count 3) include methane ranging from 99.1 to 75.9 vol.% and low content of ethane (from 0.03 to 0.13 vol.%). The gas dryness ratio varies from 584 to 3560 and the $CO_2$ concentrations are higher than the previous MV structures (from 0.85 to 6.56 vol.%). Sample AZ19-30 has a high N2 concentration (17.4 vol.%) which concurs with the lowest $CH_4$ recording (75.9 vol.%) at Gushchu MV. Isotopic measurements are generally lower at Gushchu MV. The $\delta^{13}C$-$CH_4$ ranges from -60.4‰ to -59.2‰ and average at -60.0‰. The $\delta D$-$CH_4$ range from -202‰ to -198‰ and average -200‰. The $\delta^{13}C$-$CO_2$ range from -12.7 to 6.8‰. Sample AZ19-29 (collected on the southeast part of the crater) has unusually high $\delta^{13}C$-$CO_2$ reading compared to the other samples (collected northeast and center of the crater). All samples from Gushchu MV are taken from gryphons.

Gas samples from Melikchobanly MV (2 count) contains methane ranging from 96.2 to 98.1 vol.% with the highest content of methane homolog (ethane from 0.51 to 0.52 vol.%). The gas dryness ratio has no variation at Melikchobanly MV and the $CO_2$ concentrations are low (from 0.93 to 1.34 vol.%). The $\delta^{13}C$-$CH_4$ measurements at Melikchobanly MV are constant, ranging from -49.9‰ to -49.1‰ and average -49.5‰. The $\delta D$-$CH_4$ are equally stable varying from -187‰ to -181‰ and average -184‰. The $\delta^{13}C$-$CO_2$ range from -19.9 to -11.8‰ and average -15.8‰. All samples from Melikchobanly MV are taken from pools.

The sampled gas from Madrasa MV (4 counts) have slightly more varying methane concentrations than the previous MVs (from 83.3 to 94.4 vol.%). $N_2$ concentrations are also inconsistent (from 1.7 to 9.2 vol.%) and the $CO_2$ values are higher than in all the other sampled

MVs (from 5.44 to 7.93 vol.%). Ethane measurements are moderate (from 0.10 to 0.15 vol.%) and the gas dryness ratios vary from 300 to 824. Similarly, to $\delta^{13}$C-CH$_4$ measurements at Melikchobanly MV, the $\delta^{13}$C-CH$_4$ values at Madrasa MV are persistent and range from -48.7‰ to -48‰, and average -48.4‰. The $\delta$D-CH$_4$ vary from -192‰ to -191‰ and average -192‰. The $\delta^{13}$C-CO$_2$ readings at Madrasa MV are all positive ranging from 5.9‰ to 21.6‰, and average 13.7 ‰. All samples from Madrasa are taken from gryphons.

Only two samples are taken at Shikhzarli MV. The sample is taken from a gryphon and is dominated by methane (99.2 vol.%), CO$_2$ (0.65 vol.%) and N$_2$ (0.1 vol.%). Low C$_2$H$_6$ concentrations lead to a high gas dryness ratio of 12437. Measurements at Shikhzarli MV show that the $\delta^{13}$C-CH$_4$ varies -48‰ to -40.9‰, and the corresponding $\delta$D-CH$_4$ ranges from -232‰ to -181‰. There is a large variation in the $\delta^{13}$C-CO$_2$ from -13.3‰ to 9.5‰. This is not unexpected given that one sample (AZ19-35) is taken at the center of the main crater, while the other (AZ19-36) is collected at the satellite crater, located about 0.73 km NE form the Shikhzarli.

Overall, the composition of the gas collected at the targeted MV structures is CH$_4$-dominated typical for most MVs in petroleum-bearing sedimentary basins (Babadi et al., 2021; Bonini et al., 2013; Dia et al., 1999; Dimitrov, 2002a). Whether the CH$_4$ gas is primary microbial, secondary microbial or thermogenic is further discussed in section 5.1. Table 4-4 summarizes the main results that will be used to determine the origin of the gas collected at each MV of this study.

**Table 4-4**: Summary of the dominated molecular gas type and δ13C-CH4, δD-CH4, δ13C-CO2 and C1/(C2+C3) ratio ranges at the targeted MV.

| MV structure | Sample ID | Dominant gas | RANGES | | | | Additional discharge | Sampling location | |
|---|---|---|---|---|---|---|---|---|---|
| | | | $\delta^{13}C\text{-}CH_4$ (‰) | $\delta D\text{-}CH_4$ (‰) | $\delta^{13}C\text{-}CO_2$ (‰) | $C_1/(C_2+C_3)$ | | | |
| Kichik Maraza | AZ19-14 | $CH_4$ | | | | | | Rim (North) | |
| | AZ19-15 | $CH_4$ | | | | | | Rim (Northeast) | |
| | AZ19-16 | $CH_4$ | -31.6‰ to -43‰ | -178‰ to -190‰ | -17.5‰ to 5.6‰ | 796-12400 | Microbial mats | Rim (Northwest) | |
| | AZ19-17 | $CH_4$ | | | | | | Rim (Northwest) | |
| | AZ19-18 | $CH_4$ | | | | | | Rim (Southwest) | |
| Maraza | AZ19-19 | $N_2$ | -39.7‰ | -176‰ | -10.1‰ | | | Crater (North) | |
| | AZ19-20 | $N_2$ | | | | | | Crater (North) | |
| Gizmeydan | AZ19-21 | $CH_4$ | | | | | Microbial mats | Center | |
| | AZ19-22 | $CH_4$ | | | | | | West | |
| | AZ19-23 | $CH_4$ | | | | | Oil | South | No crater |
| | AZ19-24 | $CH_4$ | -47.3‰ to -39.8‰ | -167‰ to -143‰ | -22.4‰ to -11.4‰ | 496-10530 | | South | |
| | AZ19-25 | $N_2$ | | | | | | Center | |
| | AZ19-26 | $CH_4$ | | | | | Microbial mats | Southeast | |
| | AZ19-27 | $CH_4$ | | | | | | Northeast | |
| Gushchu | AZ19-28 | $CH_4$ | | | | | Oil | Crater (Center) | |
| | AZ19-29 | $CH_4$ | -60.4‰ to -59.2‰ | -202‰ to -198‰ | -12.7 to 6.8‰ | 584-3560 | Oil | Crater (Center) | |
| | AZ19-30 | $CH_4$ | | | | | | Crater (Center) | |
| Melikchobanly | AZ19-31 | $CH_4$ | -49.9‰ to -49.1‰ | -187‰ to -181‰ | -19.9 to -11.8‰ | 190 | | Crater (North) | |
| | AZ19-32 | $CH_4$ | | | | | | Crater (North) | |
| Madrasa | AZ19-33 | $CH_4$ | -48.7‰ to -48‰ | -192‰ to -191‰ | 5.9‰ to 21.6‰ | 644-824 | Oil | North | |
| | AZ19-34 | $CH_4$ | | | | | Oil | North | No crater |
| Shikhzarli | AZ19-35 | $CH_4$ | -48‰ to -40.9‰ | -232‰ to -181‰ | -13.3‰ to 9.5‰ | 300-12437 | | Crater (Center) | |
| | AZ19-36 | CH4 | | | | | | Satellite crater (Center) | |

### 4.3.2 Empirical Plots

The origin of natural gases described in section 4.3.2 are characterized using $\delta^{13}C$-$CH_4$ versus $C_1/(C_2+C_3)$, $\delta^{13}C$-$CO_2$ versus $\delta D$-$CH_4$, and $\delta^{13}C$-$CH_4$ versus $\delta^{13}C$-$CO_2$ binary genetic diagrams proposed by Milkov and Etiope (2018) in Figure 4-14 a, b and c. The diagrams define of overlapping gas genetic fields, and possible alternation and mixing processes may affect the $\delta D$ -$CH_4$, $\delta^{13}C$-$CH_4$, $\delta^{13}C$-$CO_2$ and $C_1/(C_2+C_3)$ values of the gas samples. An integrated use of these diagrams is usefull to define the origin of the sampled gases.

Methane isotope composition of the gas (from -60.40‰ to -31.60 ‰) coupled to the ratio $C_1/(C_2+C_3)$ (from 190 to 12437) (figure 4-14a) indicates that the sampled gases have predominantly secondary microbial origin. Secondary microbial gas is the product of petroleum anaerobic biodegradation, which commonly occurs during the uprising of thermogenic gases. Note that majority of this field overlaps with the primary microbial, thermogenic and the abiotic field. More specifically, all the data from Gushchu MV plots at the border between primary microbial (i.e.,formed from decomposition of sedimentary organic matter) and secondary microbial because of its lower $\delta^{13}C$-$CH_4$ range (-60.4‰ to -59.2‰). Two data points from Kichik Maraza MV plot outside the secondary microbial gas field, in the late mature thermogenic gas field. All the data points from Melikchobanly (2 count) plot in both the early mature thermogenic gas field and the secondary microbial gas field.

The deuterium isotope composition for methane (from -232‰ to -148‰) coupled to the carbon isotope composition of methane (from -60.40‰ to -31.60 ‰) (figure 4-14b) indicates that the natural gases samples at the targeted MVs may have thermogenic origin. However, the secondary microbial gas field overlaps almost entirely the thermogenic gas field. Only one data point from Kichik Maraza (AZ19-16) plots outside the secondary microbial gas field. AZ19-16 plots in the thermogenic gas field, which overlaps with the abiotic field. Additionally, data from Gushchu MV are isolated from the rest, and plots at the border between primary microbial and secondary microbial field.

Finally, methane isotope composition of the gas (from -60.40‰ to -31.60 ‰) coupled to the carbon isotope composition of $CO_2$ (from -22.39‰ to 21.58‰) (figure 4-14c) indicates that the natural gases samples at the targeted MVs have mainly thermogenic origin (i.e., generated within organic-rich sediments due to thermal cracking of the kerogen). Parts of the termogenic gas field overlaps with the abiotic gas field. Two data from Gushchu MV plots at the border

between primary microbial. Five data points from four different MVs (Kichik Maraza, Gushchu, and Madrasa) plot in the secondary microbial field.
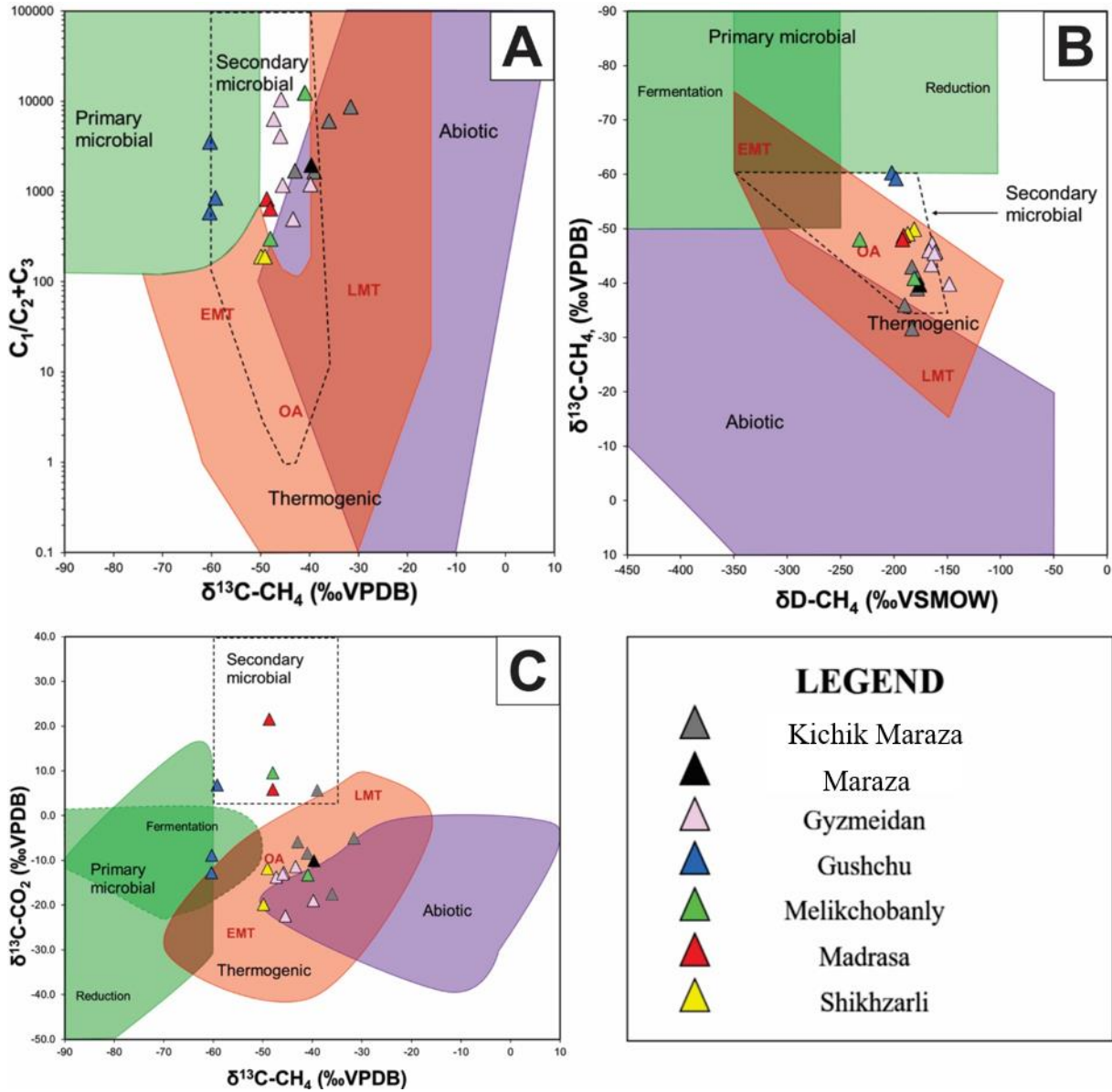


***Figure 4-14*** *Genetic diagrams after Milkov and Etipoe (2018) with the following distinct fields: Abiotic, Thermogenic, Primary Microbial, Secondary Microbial gas (SM), CO₂ Reduction (CR), Methyl Type Fermentation (F), Early Mature Thermogenic gas (EMT), Oil Associated gas (OA), and Late Mature Thermogenic gas (LMT). (A) δ¹³C-CH₄ versus C₁/(C₂+C₃) (B )δ¹³C-CH₄ versus δD-CH₄ and (C) δ¹³C-CH₄ versus δ¹³C -CO₂*

# 4.4 Flux measurements

Flux measurements were carried on four MVs: Maraza, Gyzmeidan, Gushchu, Melikchobanly. No measurements were done on either Madrasa or Shikhzqgirzi MVs due to challenging field conditions described in sub-sub section 3.2.2.4. This section presents maps indicating the localities of the flux measurements (i.e. macro- and mini-seepage) (section 4.4.1), a table summarizing the results from the $CO_2$ and $CH_4$ flux measurements in tonnes per day (t/day), tonnes per year (t/yr) and tonnes per $km^2$ year (t/$km^2$yr) (section 4.4.2) and flux maps illustrating both $CH_4$ and $CO_2$ flux from the targeted MV structures (section 4.4.3).

### 4.4.1 Locality of macro- and mini-seepage

Figures 4-15, 4-16, 4-17 and 4-18 display maps illustrating the location at which $CH_4$ and $CO_2$ flux measurements were taken at Kichik Maraza, Gyzmeidan, Gushchu and Mealikchobanli MVs accordingly. In total, 111 measurement points were completed. Flux measurements were taken above and around seeps with prominent signs of degassing activity. All maps display the location of macro-seeps (red square) and mini-seeps (blue circle).

In total, 36 $CH_4$ and $CO_2$ flux stations were completed throughout Melikchobanly and Kichik Maraza MV (Figure 4-15). More specifically, there are 21 macro-seepage stations and 21 mini-seepage stations. No macro-seeps were measured on the main northern Maraza crater but mini-seepage measurements were made at the center, west, north, and south side of the crater. One flux measurement was made between the Maraza crater and Kichik Maraza MV. Macro- and mini-flux measurements were made around the most prominent degassing structures, in both the north, center and south of Kichik Maraza MV. At Gyzmeidan MV, 30 $CH_4$ and $CO_2$ flux stations were completed of which 14 were from macro-seepage stations and 17 from mini-seepage stations (Figure 4-16). The surface of the volcano is pitted by many degassing structures with irregular distributions. The majority of the data on Gyzmeidan MV is collected at the center and on the western side of the MV structure. With only 15 station, Gushchu MV represent the structure with the least amount of $CH_4$ and $CO_2$ flux measurements (Figure 4-17). There is a total of 11 macro-seepage stations and 9 mini-seepage stations. Several degassing structures located at the center of the crater and on the south-eastern where some measurements were taken. A total of 30 $CH_4$ and $CO_2$ flux stations were completed throughout Melikchobanly

MV. There is a total of 8 macro- and 22 mini-seepage stations (Figure 4-18). Most of the active seeps are located at the crater, where most of the macro- and mini-seepage were measured.
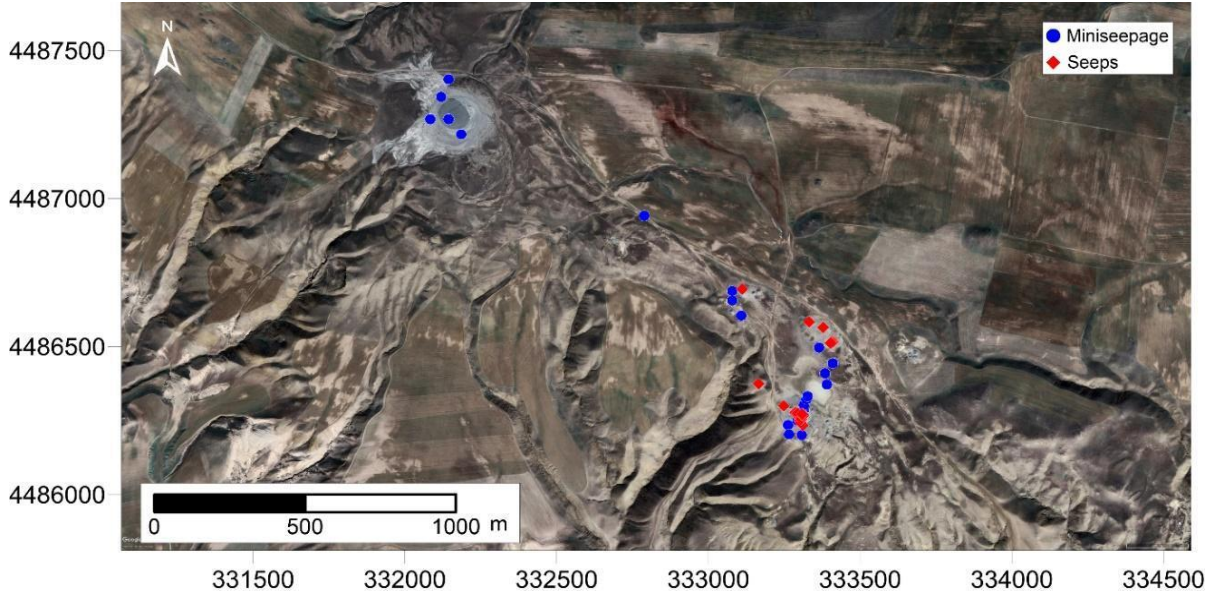


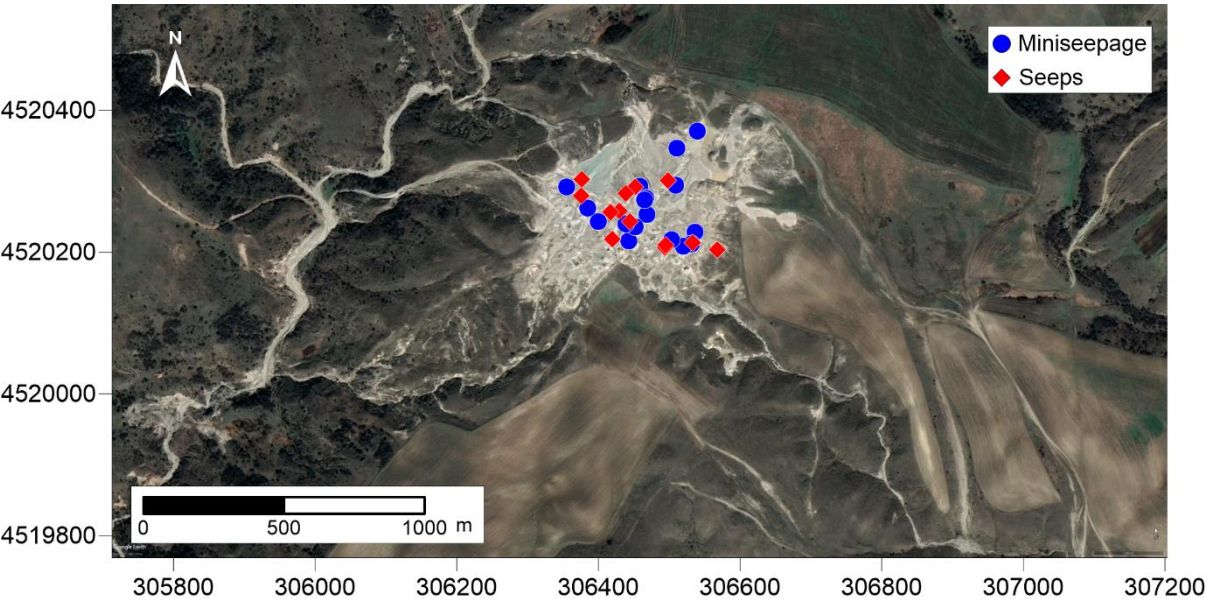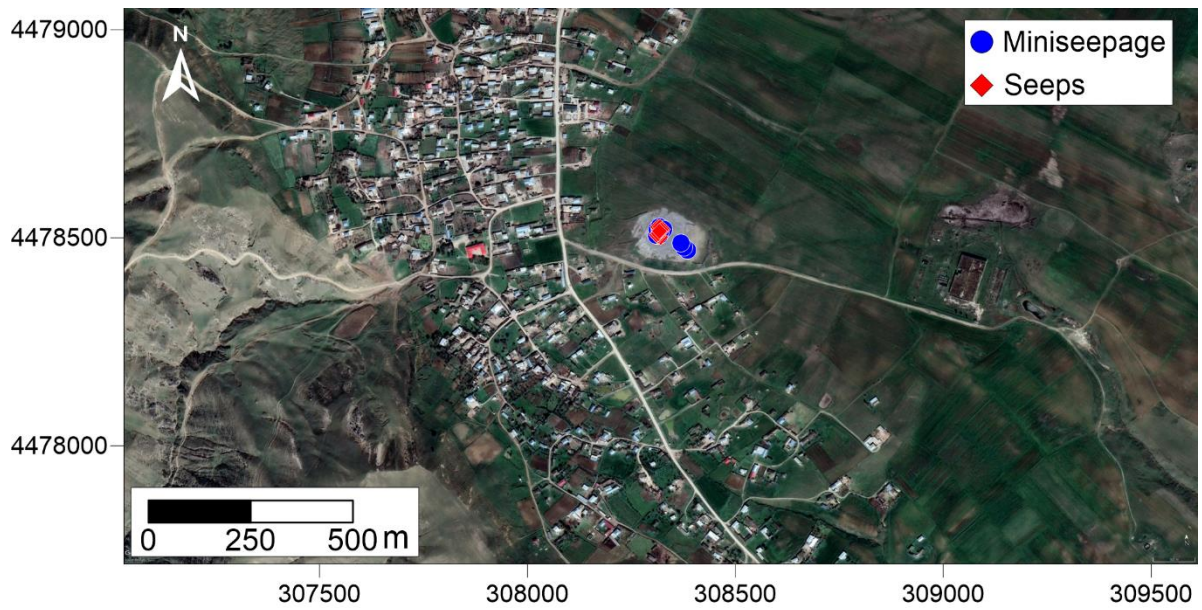***Figure 4-15*** *Measurement stations for macro- and mini-seepage over Maraza and Kichik Maraza MV.*



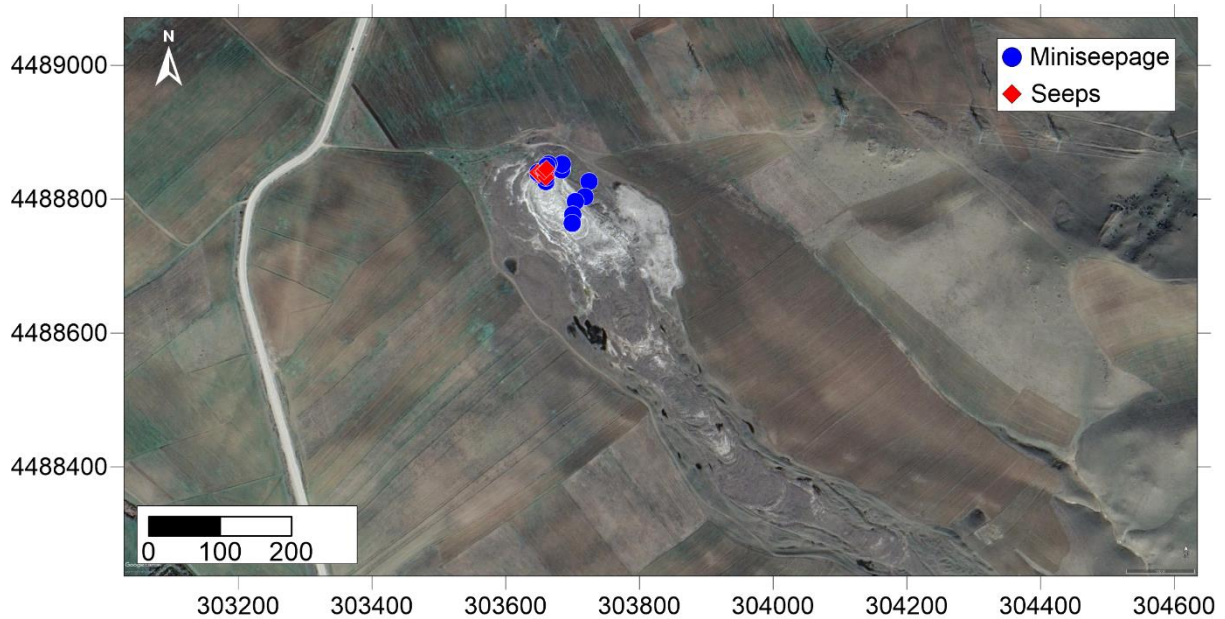***Figure 4-16*** *Measurement stations for macro- and mini-seepage over Gyzmeidan MV.*

***Figure 4-17****: Measurement stations for macro- and mini-seepage over Gushchu MV.*



***Figure 4-18****: Measurement stations for macro- and mini-seepage over Melikchobanly MV.*

## 4.4.2   Flux measurements

To provide a visual overview of the flux measurements, eight individual flux maps illustrating both $CH_4$ and $CO_2$ flux in the targeted MV structures are presented in sections 4.4.2.1. The flux maps display flux variation (g/m$^2$ day) across each MV structure using a color bar range.

The annual emissions (t/day and t/yr) and the MV area (approx. value km$^2$) of each structure are summarized in table 4-5. The data show the presence of both $CH_4$ and $CO_2$ emissions at all measured MVs. $CH_4$ flux measurements are significantly higher than $CO_2$ flux measurements at 3 structures: Maraza, Gushchu, and Melikchobanly.

The total, $CH_4$ and $CO_2$ flux measurements from macro- and mini-seepages at Maraza and Kichik Maraza MV is 63.63 t/yr and 13.75 t/yr, accordingly. These high values account for emissions over an area of 0.53 km$^2$. Measurements at Gushuch MV are significantly lower with total $CH_4$ and $CO_2$ emissions of 0.83 t/yr and 0.20 t/yr respectively. These values are estimated based an area of 0.32 km$^2$. The total $CH_4$ flux measurements at Melikchobanly MV is 2.85 t/yr, which are much higher than the total $CO_2$ flux measurements of 0.14 t/yr. area of 0.12 km$^2$. The total $CH_4$ and $CO_2$ flux measurements are similar at Gyzmeidan MV with values of 21.61 t/yr and 20.30 t/yr, respectively. These values were measured based on a seepage area of 0.18 km$^2$.

*Table 4-5* *Table over the $CO_2$ and $CH_4$ flux measurements of the Kichik Maraza(M)  Kichik Maraza(LM), Gushchu, Melikchobanly ans Gyzmeidan MV structures.*

| MV structure | Seep type | MV Area (approx. value km$^2$) | fCO$_2$ (t/day) | fCH$_4$ (t/day) | fCO$_2$ (t/yr) | fCH$_4$ (t/yr) |
|---|---|---|---|---|---|---|
| Maraza (M)/ Kichik Maraza (LM) | macro-seepage | 0.53 | 0.004 | 0.101 | 1.374 | 36.732 |
| | mini-seepage (M) | | 0.019 | 0.037 | 6.761 | 13.446 |
| | miniseepage (LM) | | 0.015 | 0.000 | 5.610 | 0.036 |
| | Total emission | | **0.038** | **0.174** | **13.7** | **63.6** |
| Gyzmeidan | macro-seepage | 0.18 | 0.004 | 0.026 | 1.588 | 9.561 |
| | mini-seepage | | 0.051 | 0.033 | 18.708 | 12.047 |
| | Total emission | | **0.056** | **0.059** | **20.3** | **21.6** |
| Gushchu | macro-seepage | 0.32 | 0.001 | 0.002 | 0.197 | 0.651 |
| | mini-seepage | | 0.017 | 0.000 | 6.166 | 0.180 |
| | Total emission | | **0.018** | **0.002** | **0.200** | **0.830** |
| Melikchobanly | macro-seepage | 0.12 | 0.000 | 0.004 | 0.135 | 1.573 |
| | mini-seepage | | 0.014 | 0.003 | 5.008 | 1.275 |
| | Total emission | | **0.014** | **0.008** | **0.135** | **2.85** |

### 4.4.3   Methane and Carbon Dioxide flux maps

Maraza MV and its satellite crater reveal evidence of obvious degassing (Figures 4-19, 4-29). Maraza MV has most degassing in the crater while Kichik Maraza has prominent degassing around the inferred crater, mostly at the rims. This is true for both $CH_4$ and $CO_2$ degassing. A bright spot representing high $CH_4$ flux activity (from 20 to 22 g/m$^2$ day) is observed northwest

from the Maraza crater (Figures 4-19). The high flux zone is bounded on all sides by a wider moderate flux zone (from 17 to 12 $g/m^2$ day). There is a sharp transition from the high $CH_4$ flux zone at the crater to the low flux zone away from the crater. Similar observation is establish for $CO_2$ degassing. A bright, isolated degassing spot is located in the north-western part of the crater indicating high degassing activity (from 12 to 13.5 $g/m^2$ day). The spatial distribution of flux measurements at Maraza MV show that $CH_4$ degassing is more abundant and higher than $CO_2$ degassing.

Southeast from the Maraza, the Kichik Maraza MV reveals prominent degassing on the north-western side of the inferred crater. Two clear spots show sign of significant $CH_4$ degassing (from 20 to 22 $g/m^2$ day) activity on the north-western side of the satellite crater. At the same location, $CO_2$ flux (from 13 to 14 $g/m^2$ day) is indicated by three bright spots. Degassing is most prominent around the bright spots, especially to the west. An elongated pattern around the bright sports representing moderate $CH_4$ and $CO_2$ seepage. One (minor) degassing spot is observed north of the inferred crater on both the $CH_4$ and the $CO_2$ flux maps. This spot is isolated and is brighter on the $CO_2$ flux map than on the $CH_4$ flux map. However, the degassing measurements reveal that $CH_4$ is released in a smaller area but in higher amounts (from 14.8 to 17.2 $g/m^2$ day) than $CO_2$ (from 12 to 12.5 $g/m^2$ day).

Overall, degassing at Maraza is concentrated at the crater, while degassing at Kichik Maraza is dispersed around the crater. The flux maps show that $CH_4$ and $CO_2$ are released in the same areas at different rates and spreading.
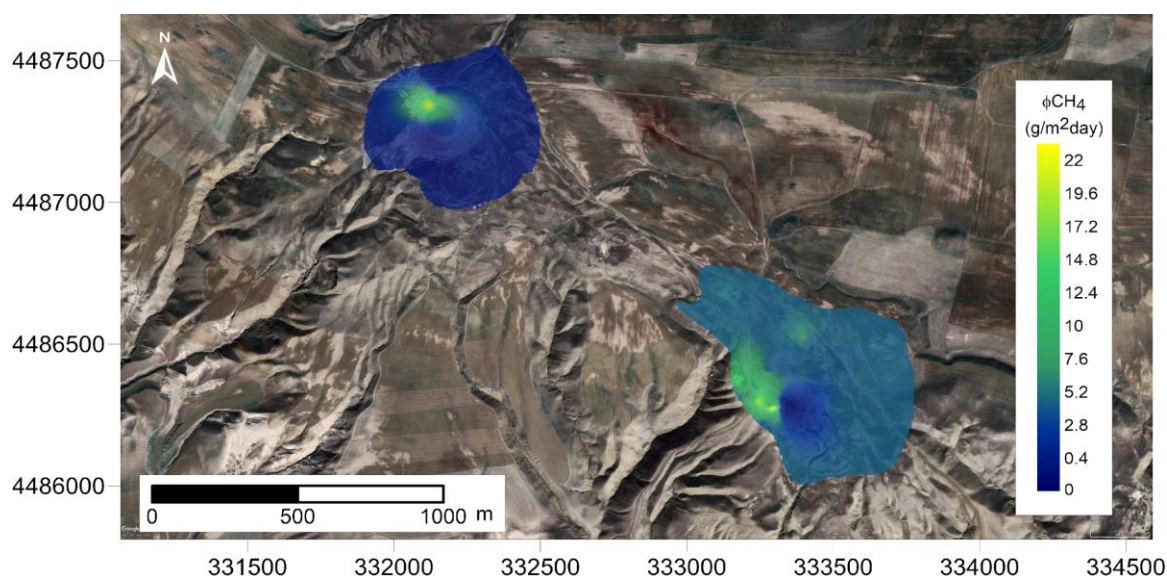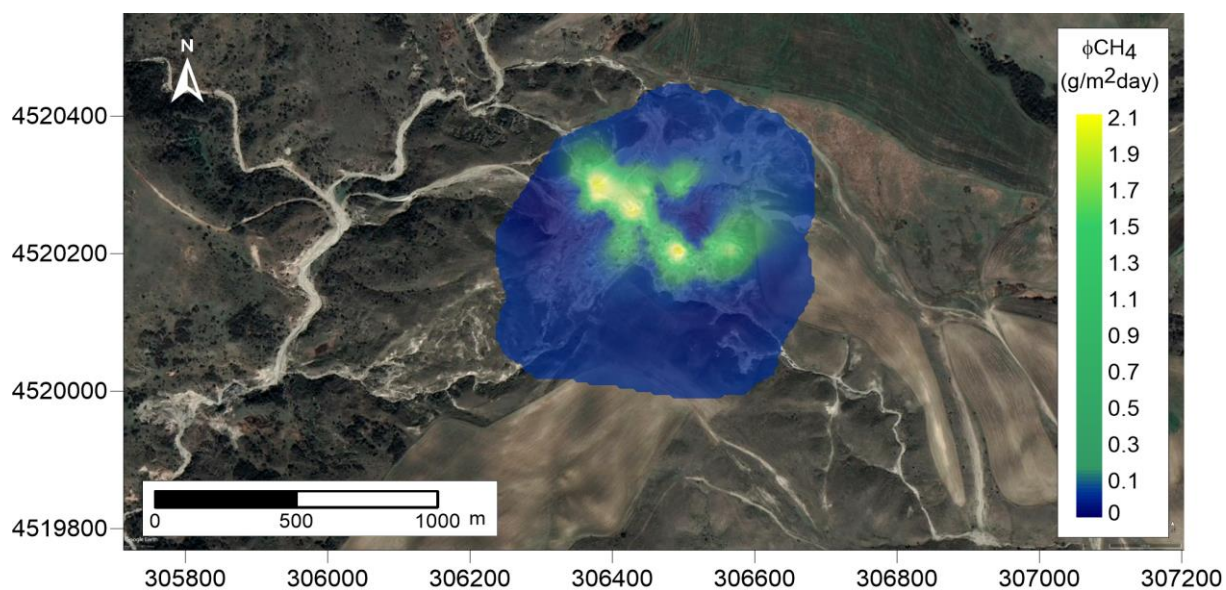


*Figure 4-19* *Satellite picture (Google Earth) of Maraza and Kichik Maraza MV illustrating the spatial distribution of flux measurements for $CH_4$.*
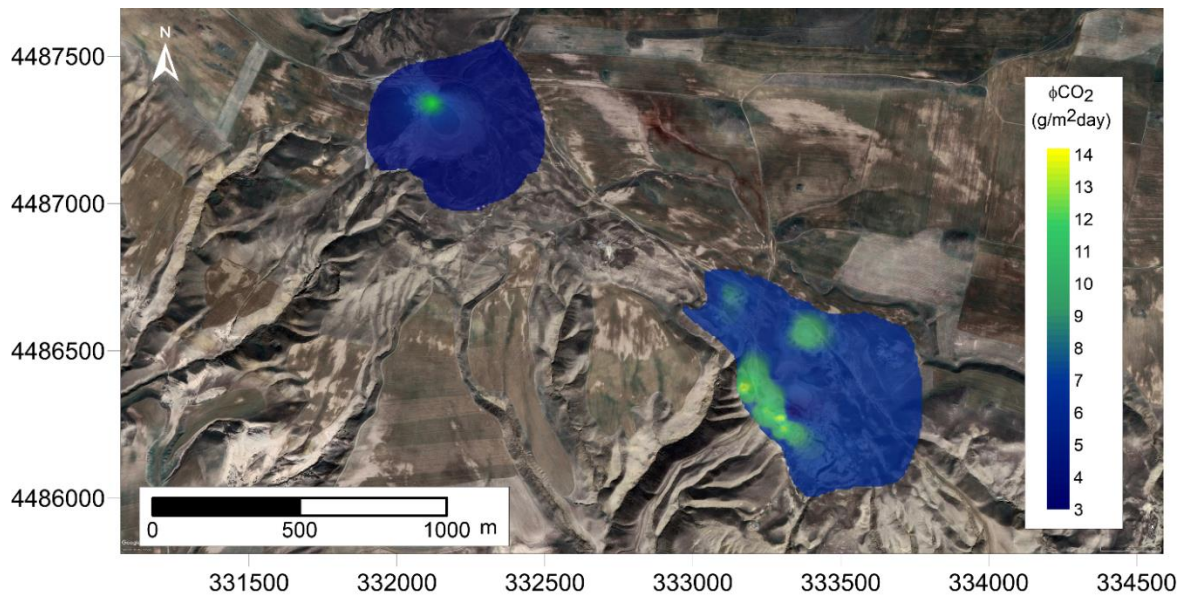
***Figure 4-20*** *Satellite picture (Google Earth) of Maraza and Kichik Maraza MV illustrating the spatial distribution of flux measurements for $CO_2$.*

Significant degassing activity is present at Gyzmeidan MV. Out of all the measured structures, Gyzmeidan has the highest degassing values (table 4-5). The $CH_4$ and $CO_2$ flux maps over Gyzmeidan MV shows high values in the middle of the defined MV area (Figures 4-21, 4-22). Three zones demarked by brighter (yellow) colors, reflect high $CH_4$ flux values (about 2.0 - 2.1 $g/m^2$ day) and high $CO_2$ flux values (from 30 to 36 $g/m^2$ day) where gryphons and pools are located. Around the brighter areas are elongated zones with lower yet substantial $CH_4$ (from 1.6 to 1.9 $g/m^2$ day) and $CO_2$ flux values (from 16 to 20 $g/ m^2$ day). North of the crater are two areas that reflect seepage zones for $CH_4$ (from 1.5 to 1.8 $g/m^2$ day) and $CO_2$ (from 29 to 32 $g/m^2$ day). Generally, flux measurements at Gyzmeidan MV show high degassing activity, especially in the center of the MV area where most degassing features reside.

86

***Figure 4-21*** *Satellite picture (Google Earth) of Gyzmeidan MV illustrating the spatial distribution of flux measurements for $CH_4$.*
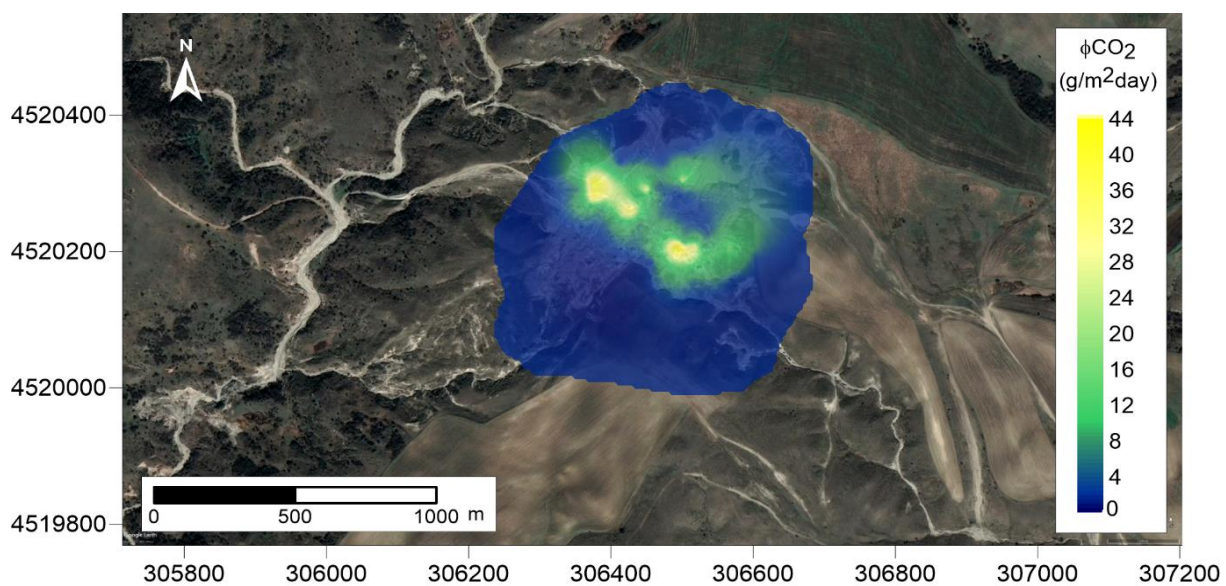


***Figure 4-22*** *Satellite picture (Google Earth) of Gyzmeidan MV illustrating the spatial distribution of flux measurements for $CO_2$*

Gushchu MV reveals generally low degassing in and around the crater. The $CH_4$ and $CO_2$ flux maps display degassing activity only at the center of the crater and inactive seepage around the crater. More specifically, at the center of the crater, the $CH_4$ flux ranges from 3 to 6 g/m$^2$ day while $CO_2$ flux ranges from 8 to 12 g/m$^2$ day (Figures 4-22, 4-23). The degassing of $CO_2$ is expands to the western side of the crater indicating an area of more moderate seepage (1.0- 2.5

87

g/m$^2$ day) on the western side of the crater with two minor zones of high flux (from 5.5 to 6 g/m$^2$ day) at the center. On the other hand, the CH$_4$ degassing expands (slightly) towards the southeast indicating an different area of more moderate seepage (from 8 to 10 g/m$^2$ day). Overall, the majority of the Gushchu MV area is inactive, with the exception of the crater area.



**Figure 4-23** *Satellite picture (Google Earth) of Gushchu MV illustrating the spatial distribution of flux measurements for CH$_4$*
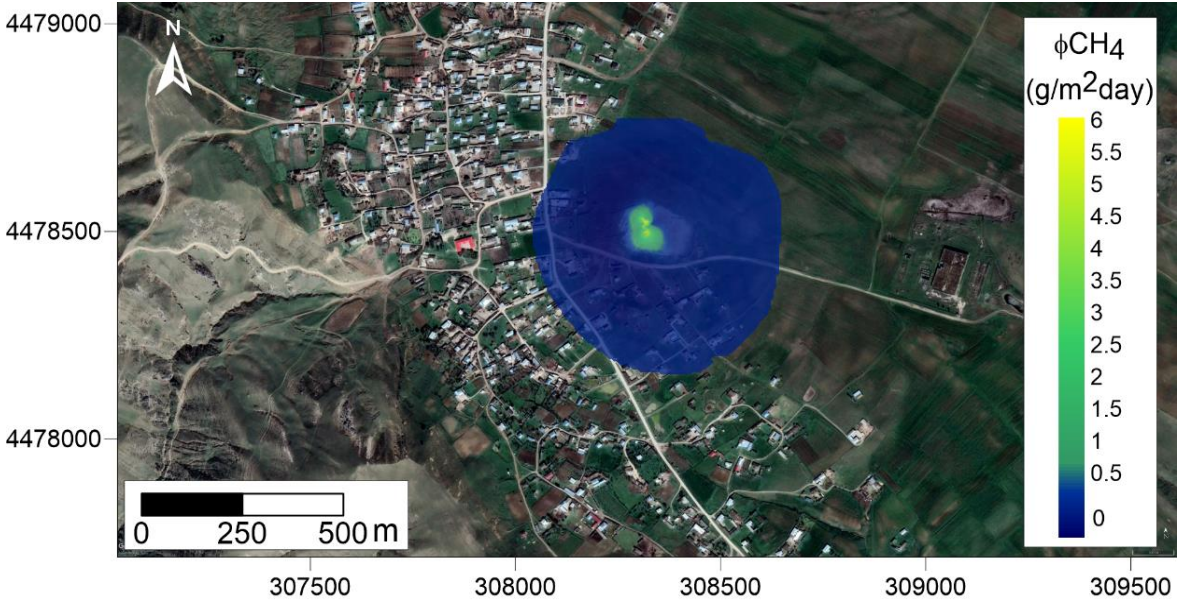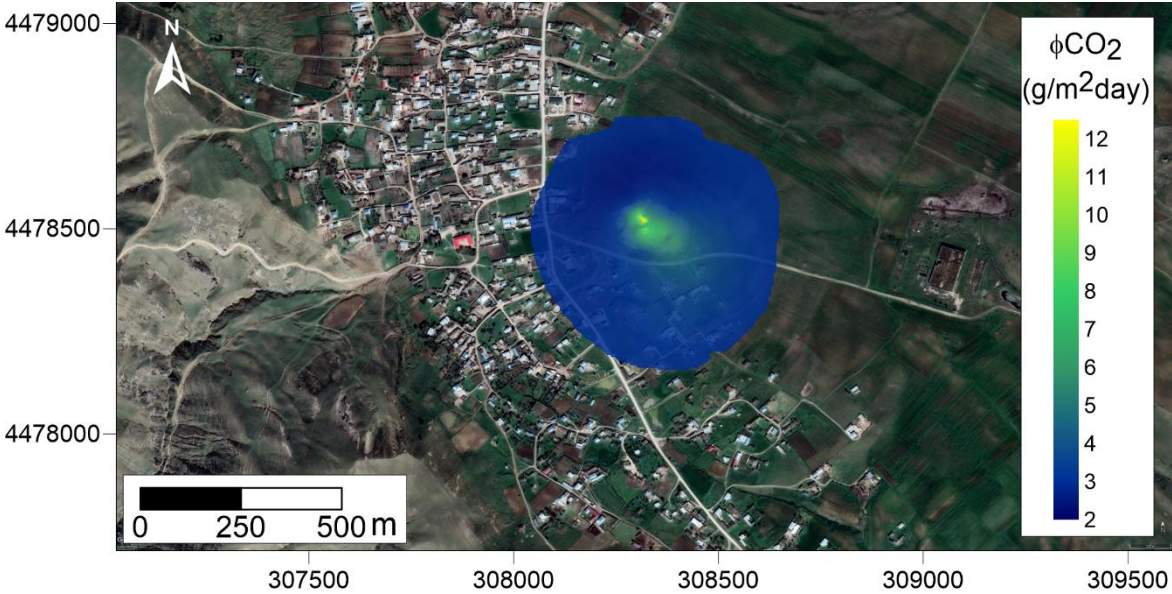


**Figure 4-24** *Satellite picture (Google Earth) of Gushchu MV illustrating the spatial distribution of flux measurements for CO$_2$*

Finally, Melikchobanly MV displays little degassing activity. The $CH_4$ and $CO_2$ map shows a very small area of high flux in the northern part of the crater (Figures 4-25, 4-26). More specifically, the $CH_4$ flux (from 1.7 to 1.8 $g/m^2$ day) is weaker than the $CO_2$ flux (from 5.6 to 6.0 $g/m^2$ day). Additionally, the $CH_4$ degassing are propagates west from the bright spot and gradually faints, to eventually reveal no degassing activity. On the other hand, $CO_2$ flux reveals degassing south of the crater, characterized by small zone of high flux (from 6.1 to 6.2 $g/m^2$ day). Overall, there is little degassing activity at Melikchobanly, where the crater area is the only zone of seepage activity.



***Figure 4-25*** *Satellite picture (Google Earth) of Melikchobanly MV illustrating the spatial distribution of flux measurements for $CH_4$*

***Figure 4-26*** *Satellite picture (Google Earth) of Melikchobanly MV illustrating the spatial distribution of flux measurements for CO₂*
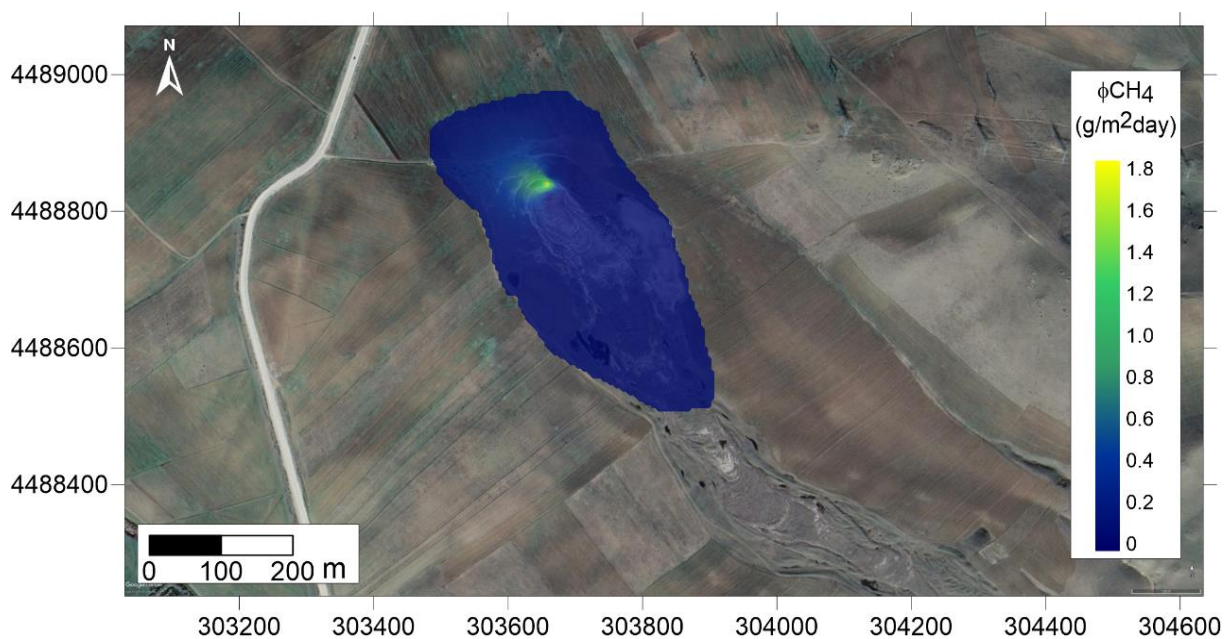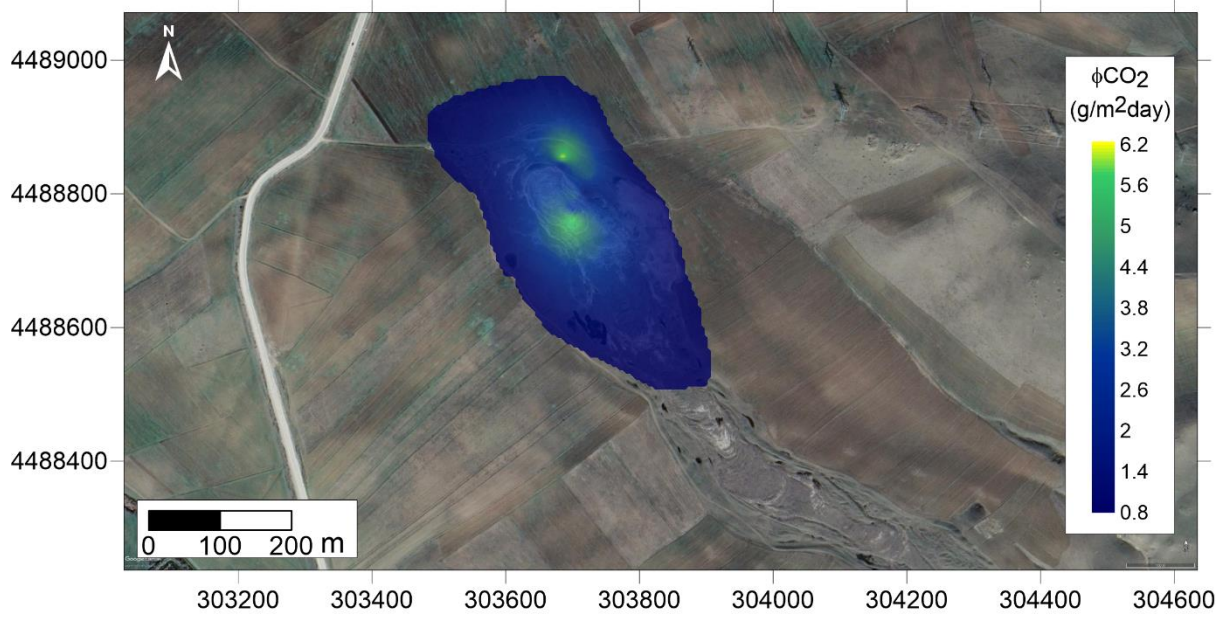
# 5 Discussion

The previous chapter presents the morphology, geochemical composition, and flux measurements of each target MVs. The morphological reviews are based on satellite images and field observations. They include interpretations of past eruption evens, the distribution, and types of degassing features at each MV and establish the shape of each MV. Novel geochemical data was presented in the form of tables and graphs. Finally, $CH_4$ and $CO_2$ flux measurements are reported in table 4-5 and are visually represented on maps.

This chapter uses these results to discuss the origin of the gas and the distribution of the morphological features at each mud volcano of this study (section 5.1, 5.2). $CO_2$ and $CH_4$ flux results are used to evaluate the plausible impacts of the $CH_4$ and $CO_2$ emissions of the targeted MV on the atmosphere (section 5.3). Furthermore, the limitations and uncertainties of this study are discussed in section 5.5. Finally, suggestions for further research are presented in section 5.6.

## 5.1 Gas composition and origin

In context with the results in table 4-4, it is clear that the gas collected at the targeted MV is mostly methane-dominated. As previously mentioned, geological $CH_4$ can either have an abiotic (magmatic and gas-water-rock reactions) or biotic origin (from sedimentary organic matter). Knowing that hydrothermal processes do not drive mud volcanoes, they must seep biotic methane gas. Biotic gas can either have a thermogenic or microbial origin, two subgroups with different processes accountable for their formations (Brooks et al., 1979).

Already in 1977, Bernard et al. implied that the characterisation of hydrocarbon gas sources could be done using geochemical models (Bernard et al., 1977). They also concluded that the interpretation of gas sources should involve more than one geochemical parameter due to potential alternation in the thermogenic and microbial natural gas. The original molecular and isotopic composition of gas may be altered after its formation and accumulation in a reservoir and its migration from the reservoir to the surface (Etiope, 2009). Therefore, post-genetic processes must be considered when assessing gas origin in MVs. Mud volcano systems may

(not always) be affected by the following post-genetic processes: (a) aerobic and anaerobic microbial oxidation of methane, (b) abiotic oxidation, (c) isotopic fractionation by diffusion, (d) molecular fractionation by advection, (e) gas mixing, (f) anaerobic biodegradation of petroleum and secondary methanogenesis (Etiope, 2017).

Some of the possible processes that can affect the molecular and isotopic composition of the gas are illustrated in figure 5-1a, b, and c. Hence, the assessment of gas origin in mud volcanoes requires a thorough analysis of the individual genetic diagrams along with $\delta^{13}C$-CH$_4$, $\delta^2H$-CH$_4$, $\delta^{13}C$-CO$_2$ and C$_1$/(C$_2$+C$_3$) values.
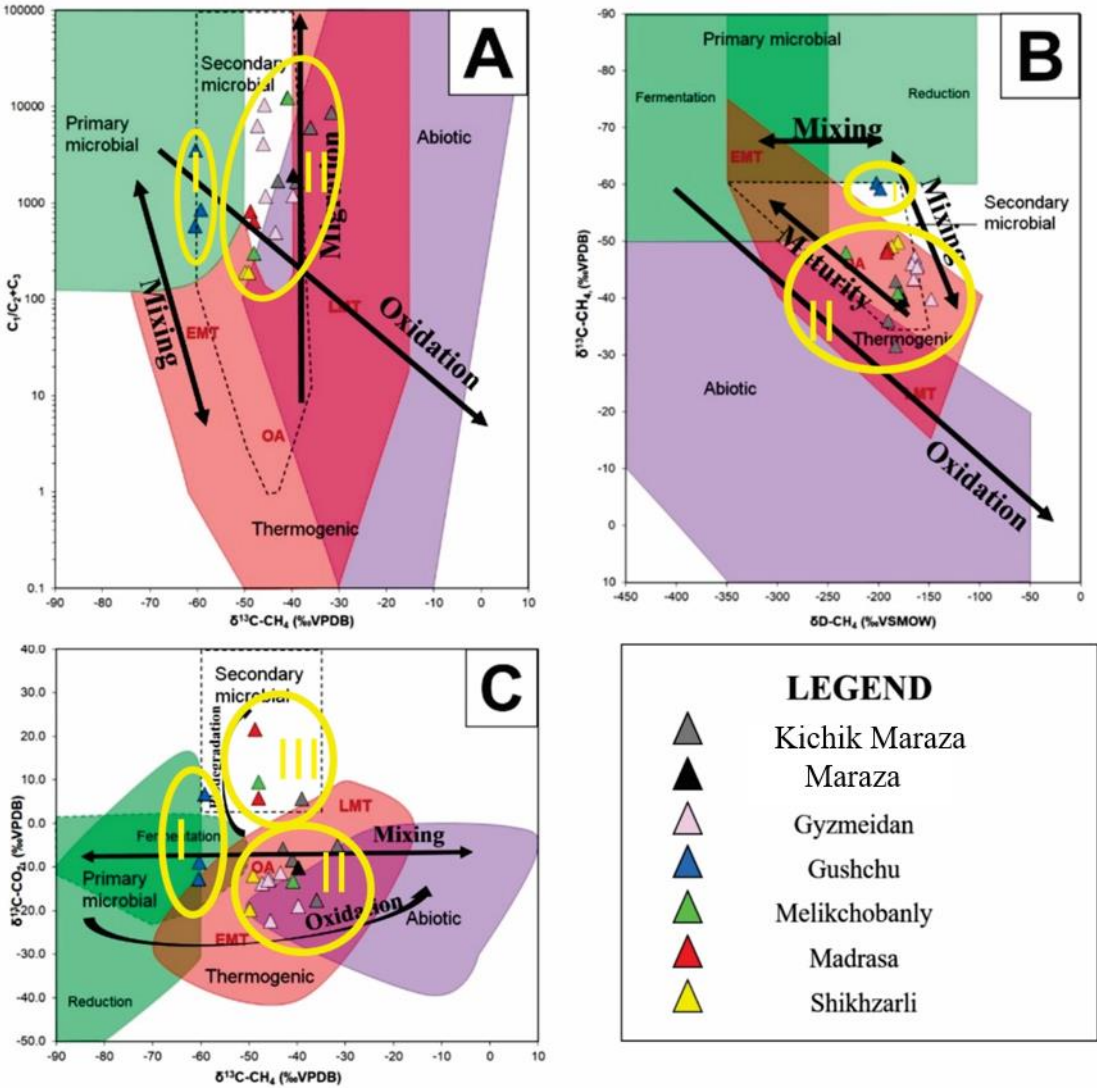


***Figure 5-1*** *Genetic diagrams of $\delta^{13}C$-CH$_4$ versus C$_1$/(C$_2$+C$_3$) (A), $\delta^{13}C$-CO$_2$ versus $\delta D$-CH$_4$ (B), and $\delta^{13}C$-CH$_4$ versus $\delta^{13}C$-CO$_2$ (C) with arrows indicating processes that can affect the molecular and isotopic composition of the gas from Milkov and Etiope (2018).*

The distribution of the gas data in the genetic diagrams can be categorized in two or three distinct groups: **I**, **II** and **III** (Figure 5-1a, b, c).

**Group I** plots in the primary microbial genetic field and is observed in all three diagrams. It comprises only of data from Gushchu MV. Whether the Gushchu gas originates from fermentation or reduction ($CO_2$) processes in not clear looking at the genetic diagrams (Figure 5-1b, c). The generation of microbial gas is an anerobic process (Liu & Whitman, 2008; Zeikus, 1977). Methanogenesis is the last stage of biochemical decomposition and generally occurs through either $CO_2$ reduction or as acetate fermentation (Whiticar et al., 1986). Such reaction can be described as follows:

$$CO_2 + 4H_2 \rightarrow CH_4 + 2H_2O \text{ (CO}_2 \text{ reduction)}$$

$$CH_3COOH \rightarrow CH_4 + CO_2 \text{ (acetate fermentation)}$$
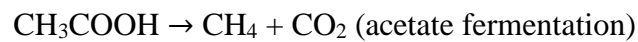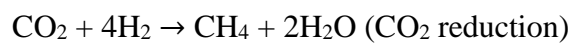
Accoding to Katz (2011), an examination of deuterium can determine which pathway (reduction or fermentation) methanogenesis occurred (Katz, 2011). Acetate fermentation results in greater Hydrogen isotope fractionation because of the transfer of a (deuterium depleted) methyl group.(Whiticar et al., 1986). As a result, gas produced through acetate fermentation $\delta D$ values ranging from -450 to -250‰. On the other hand, gas that originate from $CO_2$ reduction displays $\delta D$ values ranging from -250 to -150‰ (Michael J Whiticar, 1999). With dry gas ($C_1/(C_2+C_3) > 1000$) and depleted $\delta^{13}C$-$CH_4$ values (between -60.4‰ to -59.2‰), $CH_4$ gas seepage from Gushchu MV has typical values for gas with primary microbial origins from $CO_2$ reduction. Given that only 4% of MVs have primary microbial origins, Gushchu MV displays unusual geochemical data (Etiope, 2009). This might be because the substrates for methanogenesis is be generated where OM is enriched (inside mudstones), whereas mathanogenesis actually occurs within its related sands and silts where pore space is high (McMahon et al., 1992). Hence, there is little chance for a MVs to purely originate from primary microbial gas with no secondary alternations.

**Group II** plots in two different genetic fields: the secondary microbial (Figure 5-1a,b) and the oil associated (OA) thermogenic (Figure 5-1b, c) and includes of data from Maraza, Kichik Maraza, Melikchobanly, Gizmeydan, and Shikhzagirli. The $C_1/(C_2+C_3)$ vs. $\delta^{13}C$-$CH_4$ diagram (Figure 5-1a) indicates that group II gases have strictly secondary microbial origins while the

and $\delta^{13}C$-$CH_4$ versus $\delta^{13}C$-$CO_2$ diagram (Figure 5-1c) indicates that group II gases indicates that group II gases have strictly OA thermogenic origin.

Thermogenic gases generally have $C_1/(C_2+C_3)$ values less than 100 for $\delta^{13}C$-$CH_4$ values between -70‰ to -35‰. Most of the gas sampled at the targeted MVs is dry ($C_1/(C_2+C_3)$ average of 3538), implying that the gas has microbial origins. However, oil-associated thermogenic gases may have unusually higher $C_1/(C_2+C_3)$ values due to enrichment in $C_1$ due to a molecular fractionation by advection induced during migration (Bernard et al., 1977). Molecular fractionating by advection is the differential segregation of light hydrocarbon molecules associated with absorption (e.g., on solid grains of mud) and solubility properties when ascending gas migrates from the subsurface to the surface. Uprising gas interacts with water and sediments in particularly "less active" (dormant) mud volcano systems. Reports show that Azerbaijani MVs are typically affected by molecular fractioning due to migration (Deville et al., 2003; Mazzini, 2009; Milkov & Etiope, 2005). According to Etiope et al. (2009), molecular fractionation during migration may increase the $C_1/(C_2+C_3)$ ratio but does not affect the isotopic composition of $\delta^{13}C$-$CH_4$. The majority of the geochemical results also have low $\delta^{13}C$-$CH_4$ values (from -60.3‰ to -31.6‰, average -45.8‰). Previous geochemical reports defined thermogenic gases as $C_1$ with $\delta^{13}C$ > -50‰. However, recent studies show that $\delta^{13}C$-$CH_4$ values for thermogenic methane can range from -75‰ to -15‰ when considering early mature and very late mature thermogenic gases (Etiope, 2009; Milkov & Dzou, 2007). Finally, samples with $C_1$ with $\delta^{13}C$-$CH_4$ between -60‰ and -40‰ and $\delta D$-$CH_4$ between 250‰ and 150‰ may also have mixed origins (Etiope, 2009). More specifically, thermogenic gas mixed with secondary microbial gas may have carbon isotopes between -55‰ to -35‰. Generally, thermogenic gases are distinguished by a positive relationship between methane, ethane, lower $C_1/C_{2+}$, heavier $\delta^{13}C$-$CH_4$, and more radiogenic noble gases (e.g., He, Ne) (Etiope, 2009). With an average $C_2$ composition of only 0.10%, it can be speculated that group II gases have an mixed origin with both oil-associated thermogenic gas and low alkane secondary microbial gas

Thermogenic and secondary microbial gas is defined to have $\delta^2H$-$CH_4$ values ranging from -350‰ to -100‰ and -350‰ to 150‰, accordingly. More specifically, the oil-associated thermogenic gas is defined by $\delta^2H$-$CH_4$ values ranging from about -250‰ to -175‰. Looking at the $\delta^2H$-$CH_4$ values (from -232‰ to -148‰, average -181‰) from geochemical data, it can be speculated (yet again) that overall, the methane gas collected at the targeted MVs have oil associate thermogenic origins. As group II gases follow the expected path for gas affected by migration processes and have $\delta^{13}C$-$CH_4$ values between -55‰ to -35‰.

**Group III** plots in the secondary microbial genetic field and is only observed one genetic diagram (Figure 5-1c). This group includes Kichik Maraza, Melikchobanly, and Madrasa MV. Enriched $CO_2$ is highly indicative of secondary microbial methane formed during petroleum biodegradation (Boreham et al., 2001; Jeffrey, 1991; R. Pallasser, 2000). Typically, $\delta^{13}C$-$CO_2$ values for secondary microbial methane gas are positive ($^{13}C$ enriched), ranging between 0.1 ‰ to 40.0‰. However, table 4-3 shows that only five samples (AZ19-18, AZ19-29, AZ19-33, AZ19-34, and AZ19-35) out of 23 (22%) have positive $\delta^{13}C$-$CO_2$ values. Among the MV gases collected in the South Caspian region, few indicate secondary anaerobic biodegradation processes characterized by positive $\delta^{13}C$-$CO_2$ values (Etiope et al., 2009; Etiope et al., 2007). Hence, it is unlikely that gas collected in eastern Azerbaijan has such an origin. Knowing that shale gas is prevalent in Azerbaijan, the samples with positive $\delta^{13}C$-$CO_2$ value are possibly affected by late-generated shale gas. The measured carbon isotope of $CH_4$ ($\delta^{13}C$-$CH_4$) for secondary microbial methane range between -55‰ and -35‰ (Etiope, 2009; Milkov, 2010; Milkov & Etiope, 2018). The gas data retrieved from the sampling stations at the different MVs significantly vary in the measured carbon isotope of $CO_2$ ($\delta^{13}C$-$CO_2$) with values ranging from -22.5‰ to 21.6‰. All data points from Madrasa MV plot in the secondary microbial gas field, with $\delta^{13}C$-$CO_2$ values from 5.9‰ to 21.6‰ and $\delta^{13}C$-$CH4$ values from -48.7‰ to -48‰. Two data points, one from Melikchobanly and another from Kichik Maraza, also plot in the secondary microbial gas field with $\delta^{13}C$-$CO_2$ values of 6.8‰ and 5.6‰ accordingly. The secondary microbial gas field in the $\delta^{13}C$-$CH_4$ versus $\delta^{13}C$-$CO_2$ diagram is associated with biodegradation. Subsurface anaerobic biodegradation processes are known to affect oil and gas composition and properties (Connan, 1984; Head et al., 2003; Philippi, 1977; Wenger & Isaksen, 2002). $C_{2+}$ gas concentrations can give information on the biodegradation stages in reservoirs. High $CO_2$ content and high $C_{2+}$ concentrations may indicate the initial stage of biodegradation. On the other hand, if $CO_2$ content is low and most $C_{2+}$ components are removed by microbes that rely on the $CO_2$ reduction or acetate fermentation pathways (e.g., archea), biodegradation may be advanced. If biodegradation is advanced, gases are dry due to the conversion of $CO_2$ to methane during secondary methanogenesis after anaerobic biodegradation (Dimitrakopoulos & Muehlenbachs, 1987; Jenden et al., 1993; R. J. Pallasser, 2000). Such reaction can be described as follows:

$$CO_2 + 4H_2 \rightarrow CH_4 + 2H_2O$$
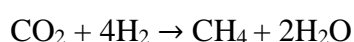
Residual $CO_2$ can have high (+15‰ to +20‰) $\delta^{13}C$-$CO_2$ due to fractionation between $CO_2$ and methane during $H_2$/ $CO_2$ methanogenesis.,

With this, the origin of the gas sampled at the targeted MVs is the following: Mixed (Maraza, Kichik Maraza, Melikchobanly, Gizmeydan, and Shikhzagirli), secondary microbial (Madrasa, Kichik Maraza, Melikchobanly, and Shikhzagirli) and primary microbial (Gushchu). Hence, some MVs ( Kichik Maraza, Melikchobanly and Shikhzagirli) have multiple/mixed origins.

Previous studies have anaylsed samples of natural gas seepages from some of structures presented in this thesis. The molecular and isotopic geochemistry data by Valyaev et al. (1985) and Feyzullayev (2003) is presented in table 5-1

*Table 5-1* *Geochemical data collected at the studied structures in 1985 and 2003.*

| MV structure | $CH_4$% | $CO_2$ % | $\delta^{13}CH_4$‰ | $\delta^{13}CO_2$‰ | $C_1/(C_2+C_3)$ | References |
|---|---|---|---|---|---|---|
| Kichik Maraza | 98.11 | 1.85 | -40.3 | 8.9 | 2453 | Valyaev et al. (1985) |
| Shikhzagirli | 99.06 | 0.99 | -42.5 | 0.1 | 3302 | Valyaev et al. (1985) |
| Melikchobanly | 84.1 | 12.1 | -45.2 | 20.9 | 140 | Feyzullayev (2003) |
| Melikchobanly | 72.3 | 7.3 | -44.7 | -14 | | Feyzullayev (2003) |
| Gushchu (Gushchi) | 97.55 | 1.42 | -56 | -6.8 | | Valyaev et al. (1985) |

These values coincide with the findings of this thesis: The MVs are methane-dominant with $\delta^{13}$C-$CH_4$ values corresponding to thermogenic origin. The data shows variations in $\delta^{13}$C-$CO_2$ values, indicating that gas from Kichik Maraza, Melikchobanly, and Shikhzagirli likely have mixed origins. The $\delta^{13}$C-$CH_4$ values for gas emission at Gushchu MV indicate primary microbial origin. Plotting geochemical data from Valyaev et al. (1985) and Feyzullayev (2003) against the data from chapter 4 shows consistency (Figure 5-2 a,b,c). Both genetic plots ($\delta^{13}$C-$CH_4$ versus $C_1/(C_2+C_3)$ and $\delta^{13}$C-$CH_4$ versus $\delta^{13}$C -$CO_2$) show the same trends in the data: oil-associated thermogenic gas with high molecular fractioning and some anaerobic biodegradation due to gas migration. It is essential to underline that these findings are based partly on the plots interpretations but these should be integrated with additional information such as the geological setting, the sampling location relative to the MV crater, the type of degassing feature from which the gas was sampled, and the presence of oil or microbial mats.
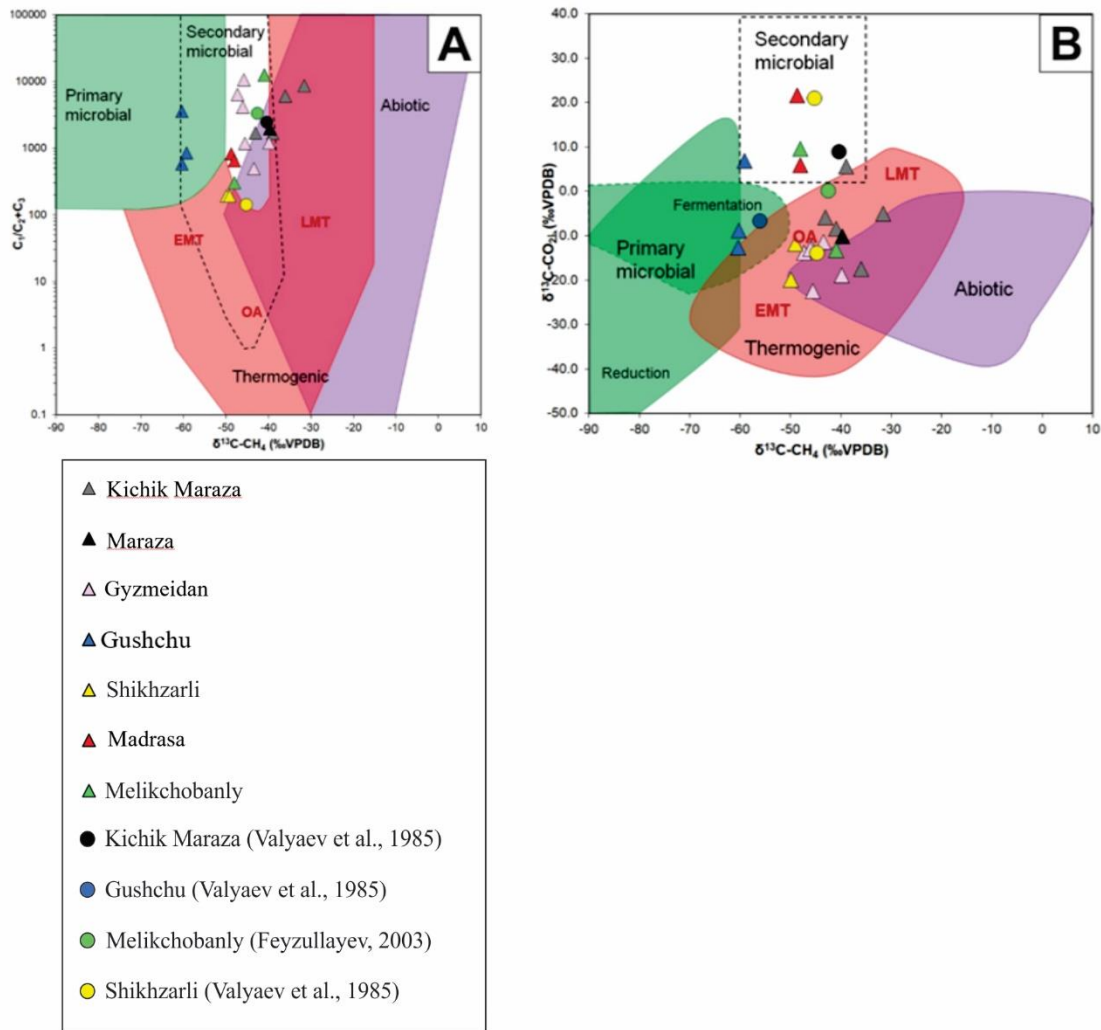
***Figure 5-2*** *Novel and past (Valyaev et al.,1985 and Feyzullayev, 2003) geochemistry gas data from Kichik Maraza, Melikchobanly, and Shikhzagirli mud volcanoes plotted in the genetic diagrams from Milkov and Etipoe (2018) (A) $\delta^{13}C$-CH$_4$ versus C$_1$/(C$_2$+C$_3$) and (B) $\delta_{13}$C-CH$_4$ versus $\delta^{13}C$ -CO$_2$.*

Overall, there majority of the targeted MVs seep thermogenic methane which the expected gas composition and origin of MVs from Azerbaijan. The volcanoes are mostly pie-shaped, which is the most reported MV shape worldwide (Mazzini and Etiope, 2017). Geochamical data from this thesis can be compared to MVs from the Southern Gobustan and Absheron regions of Azerbaijan (Table 5-2). Given that they are related to similar geodynamic setting it is anticipated that the data from the eastern Azerbaijan MVs show similar $\delta^{13}$C-CH$_4$values and C$_1$/(C$_{2+}$) ratios.

**Table 5-2** *Published geochemical data collected at Azerbaijani MVs of the S Gobustan and Absheron regions in 2017.*

| MV structure | Sampling station | CH$_4$ (%) | C$_2$H$_6$ (%) | C$_1$/C$_2$+C$_3$ | δ$^{13}$CH$_4$ | δ$^{13}$CO$_2$ | References |
|---|---|---|---|---|---|---|---|
| Pirekeshkyul | AZ-05A-21 | 97.8 | 0.02 | 4890 | -38.9 | -17.4 | Mazzini and Etiope (2017) |
| Pirekeshkyul | AZ-05A-24 | 96.07 | 0.08 | 1200.88 | -43.1 | 7.1 | Mazzini and Etiope (2017) |
| Pirekeshkyul | AZ-05A-23 | 97.29 | 0.15 | 648.6 | -42 | 11.8 | Mazzini and Etiope (2017) |
| Dashgil | AZ-05A-32 | 98.41 | 0.25 | 393.64 | -41.6 | -12.1 | Mazzini and Etiope (2017) |
| Dashgil | AZ-05A-33 | 98.69 | 0.24 | 411.21 | -40.8 | 3.2 | Mazzini and Etiope (2017) |
| Dashgil | AZ-05A-46 | 99.58 | 0.01 | 9958 | -41.1 | -17.2 | Mazzini and Etiope (2017) |
| Dashgil | AZ-05A-47 | 99.63 | 0.01 | 9963 | -40.9 | -19.4 | Mazzini and Etiope (2017) |
| Dashgil | AZ-06A-05 | 99.02 | 0.18 | 550.11 | -41.8 | 2 | Mazzini and Etiope (2017) |
| Dashgil | AZ-06A-07 | 99.19 | 0.37 | 268.08 | -42.1 | 1.9 | Mazzini and Etiope (2017) |
| Dashgil | AZ-06A-08 | 98.96 | 0.15 | 659.73 | -43.9 | -8.2 | Mazzini and Etiope (2017) |
| Dashgil | AZ-05A-30 | 99.61 | 0.11 | 905.55 | -40.4 | -13.1 | Mazzini and Etiope (2017) |
| Dashgil | AZ-06A-15 | 99.35 | 0.07 | 1419.29 | -43.2 | -12.2 | Mazzini and Etiope (2017) |
| Dashgil | AZ-06A-16 | 94.87 | 0.04 | 2371.75 | -35.2 | -17.9 | Mazzini and Etiope (2017) |
| Dashgil | AZ-05A-31 | 99.33 | 0.12 | 827.75 | -42.3 | -6.8 | Mazzini and Etiope (2017) |
| Dashgil | AZ-05A-29 | 99.65 | 0.01 | 9965 | -41.6 | -23.5 | Mazzini and Etiope (2017) |
| Bakhar | AZ-06A-09 | 98.17 | 0.07 | 1402.43 | -48.6 | 2.5 | Mazzini and Etiope (2017) |
| Bakhar | AZ-06A-10 | 98.73 | 0.09 | 1097 | -48.7 | 7.5 | Mazzini and Etiope (2017) |
| Bakhar | AZ-06A-12 | 99.74 | 0 | 99.74 | -46.8 | -16.9 | Mazzini and Etiope (2017) |
| Bakhar | AZ-06A-21 | 99.55 | 0.01 | 9955 | -45.6 | -9.4 | Mazzini and Etiope (2017) |
| Little Bakhar | AZ-06A-19 | 99.29 | 0.01 | 9929 | -46.6 | -6.3 | Mazzini and Etiope (2017) |
| Koturdag | AZ-06A-25 | 99.31 | 0.34 | 292.09 | -50.9 | 12.7 | Mazzini and Etiope (2017) |
| Koturdag | AZ-06A-27 | 90.52 | 2.48 | 36.5 | -50.4 | 7.5 | Mazzini and Etiope (2017) |

In fact, when plotting the geochemical data from Mazzini and Etiope (2017), it is clear that the mud volcanoes from this study share similar chemical processes of those from the Southern Gobustan and Absheron regions (Figure 5-11). The data shows that the gas is affected by molecular fractionation (($C_1$/($C_2$+$C_3$) ratio (from 36 to 2371), and mainly has oil associated thermogenic origins. Similarly to Kichik Madrasa MV, Koturdag and Pirekeshkyul MV gas plot in the secondary microbial field with mostly positive δ$^{13}$C-CO$_2$ values and low ethane concentrations. Similarly to Kichik Maraza, Melikchobanly, and Shikhzagirli MV, Little Bakhar emit gas with both oil-associated thermogenic and secondary microbial origins. Interestingly, little Bahar and Pirekeshkyul MVs are located in the southern Gobustan region. Both some degassing features with secondary microbial origins. This suggests that the Gobustan region is prone to secondary microbial gas production. Remarking that the Shamakhy and Gobustan regions are rich in shale gas, the samples with positive δ13C-CO$_2$ values may possibly be affected by late-generated shale gas as post-mature shale gas, result in a richer $^{12}$C latter.
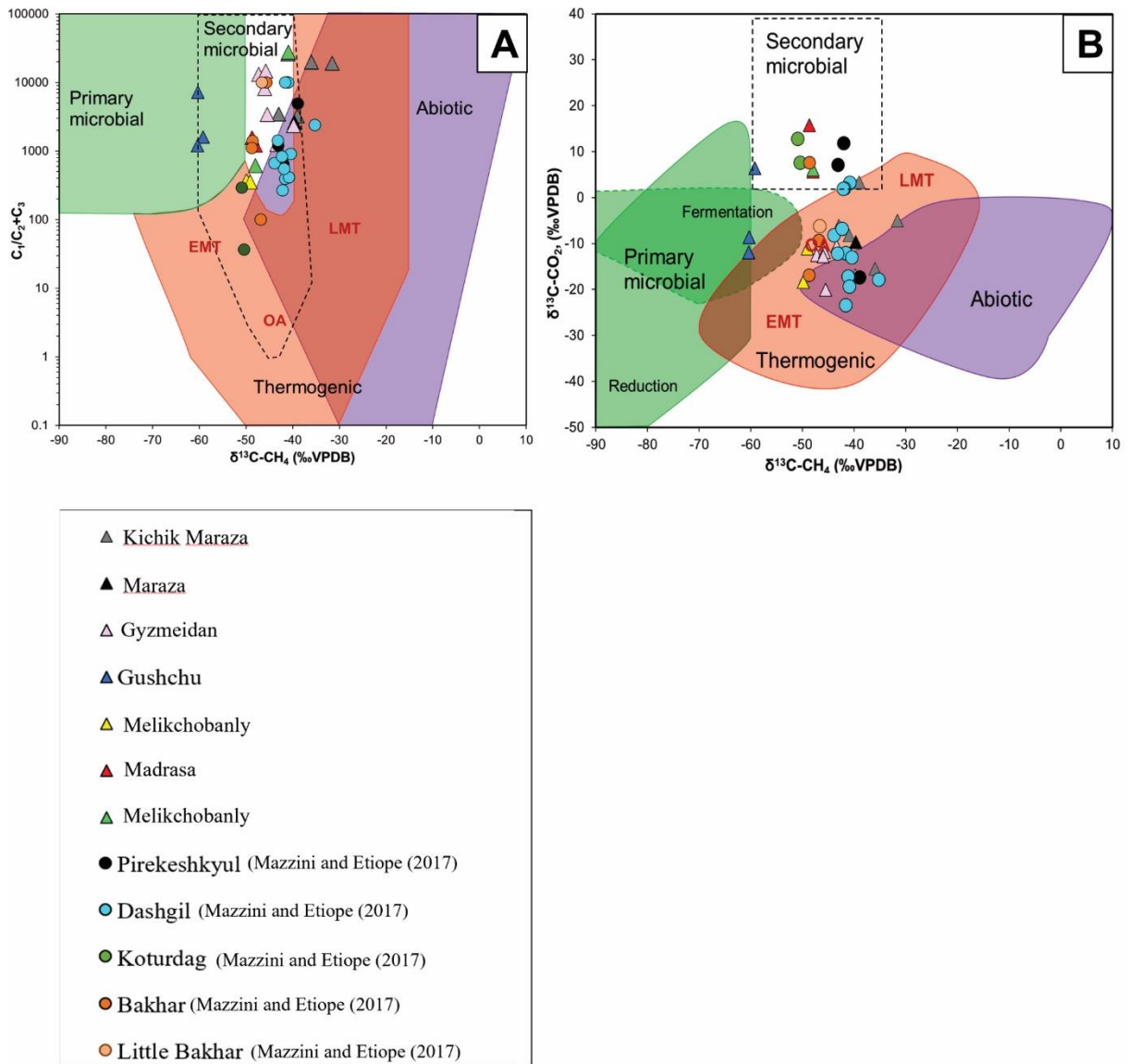
**Figure 5-3** *Published geochemical data (Mazzini and Etiope., 2017) plotted in genetic diagrams from Milkov and Etipoe (2018) with data from chapter 4.*

# 5.2 Shamakhy-Gobustan MVs

To better understand chemical processes in the sub surface, the interpretation of gas sources using empirical graphs should be convoyed with geological investigations (Bernard et al., 1977; Gutsalo & Plotnikov, 1981; Mazzini & Etiope, 2017; M. Schoell, 1983; Whiticar et al., 1986). The relationship between fluid origin and mud volcano formation mechinams has been established by several strudies (Dimitrov, 2002b; Mazzini, 2009). Thereby, the geochemistry characteristics and origin (section 5.2) along with morphological reviews (section 4.2) can provide better understanding of the subsurface processes occurring at MV sites. In section 5.1 it is anticipated that the six targeter MV can be cathegorised into three groups: Group I, Group II and Group III.

In the following section, the gas origins and potential subsurface architecture of the targeted MV is discussed.

## 5.2.1   Group I

Geochemical analysis of the gas collected at Gushchu MV implies that the gas has a primary microbial origin. Hence, the methane-dominated gas seeping from Gushchu MV is possibly produced in shallow and cool sediments (diagenesis) by microbes that rely on the $CO_2$ reduction pathways. However, according to Abbasov (2016), Gushchu MV has very high organic content of oil shale (Paleogene-Miocene reserves), of 42.55% (Abbasov, 2016). With this, Gushchu MV would be expected to seep thermogenic methane, produced in deep sediments by the thermal degradation of organic matter or oil cracking (catagenesis). Such genesis would be more suitable for an Azerbaijani MV, given that hydrocarbon production in the south Caspian Basin is known to be uncommonly deep (Feyzullayev et al., 2001). According to Milkov and Dzou (2007), gas with $^{13}$C-depleted composition may also have early mature thermogenic origins with $\delta^{13}$C-CH$_4$ values as low as −70‰ VPDB (Milkov & Dzou, 2007). Given that all MVs in the Shamakhy-Gobustan region as associated with petroleum systems, and that only 4% of MVs have microbial origin, it is likely that the depleted $^{13}$C-CH$_4$ values are due to the early maturation stage of thermogenic gas. The microbial gas origin hypothesis, however, cannot be ruled out due to the very favourable $\delta^{13}$C-CH$_4$ values. According to some studies, shallow gas can trigger mud extrusions but cannot be its driving force (Croker & O'Loughlin, 1998; Heggland, 1997; Wallmann et al., 1997).

It is noteworthy to mention that all the gas sampled at Gushchu MV were collected at gryphons located in the center of the main crater due limited degassing activity outside the crater. These are pristine because the MV conduit (located below) is vertical resulting in fast-moving fluids. This is reflected in the studied $CH_4$ and $CO_2$ gas flux which are more concentrated in the central part of the structure. One sample (AZ19-28) however is affected by molecular fractionation indicating slower seepage. Out of three sampling stations, two of the gryphons contained oil. It is therefore clearly evident that the seeping gas of Gushchu does not have primary microbial origins. In fact, early mature stages of thermogenic gas can be generation of along the molecules that produce oil (Ferrer & Thurman, 2013; Sherwood et al., 2013).

Located in the Southwestern Gobustan region, Gushchu is associated with anticlines that are strongly broken by longitudinal and transverse faults (Aliyev et al., 2015). With this, segregation processes are likely to affect the gas composition. According to Aliyev et al., 2015, Gushchu MV was formed with local overthrust anticline genesis. Such geological environment is likely to result in local weaknesses and a branched architecture. Based on satellite images, Gushchu MV may have multicrater structure. At least one satellite crater is anticipated based on the profile of the MV. The aligned of the main crater and the potential second crater matches perfectly with the E-W directed local anticline (Figure 2-5). The morphology of Gushchu MV has a smooth dome structure which is likely to have formed from a faulted anticline. Gushchu MV likely has a branched plumbing system with one main crater. The number of satellite craters present at the volcano is unknown but there are at least two. Both the main crater and its satellite craters are align with a fault. With this, it can be assumed that the main feeder channel lies below the main crater, and branches off to the NE, along the fault. Figure 5-4 represents a cartoon, which displays the location of the main degassing features and satellite craters of Gushchu MV. It also speculates the subsurface architecture of the volcano.

The original gas composition of Gushchu MV could be thermogenic with secondary alternation through abiotic oxidation and further mixed at the surface with microbial methane. This could be due to slightly abated seismic activity resulting in Gushchu MV being in a late-stage development phase.
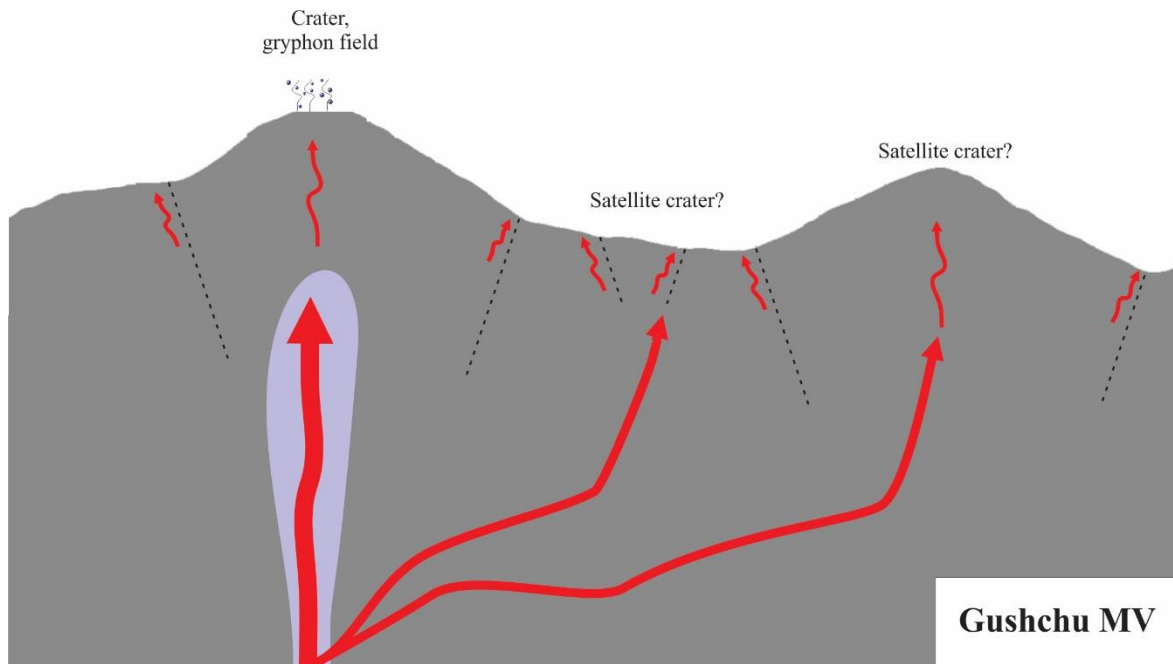
*Figure 5-4 Cartoon illustrating Gushchu MV, with location of gryphon field from which gas samples were collected. The location of the proposed satellite craters are indicated. Red arrows indicate rising fluids.*

### 5.2.2 Group II

Gas seeping from Maraza MV is different than gas from Kichik Maraza. More specifically, gas from Maraza MV is nitrogen-dominated (from 82 vol.% to 84.2 vol.%) with little methane (from 15.4 vol.% to 16.2 vol.%) and even less carbon dioxide (from 0.27 vol.% to 1.62 vol.%). $N_2$ enrichment in natural gases are not typical for petroleum gas seeps and are normally associated to high He concentrations (Etiope, Nakada, et al., 2011). Maraza MV, like every other MV in the Shamkhy-Gobustan region, is associated with a petroleum system and has a relatively low He content (from 0.0035 vol.% to 0.0389 vol.%). The revised empirical graphs proposed by Milkov and Etiope (2018) suggests that the Maraza gas is derived from organic matter and unaffected by post-genetic secondary processes. However, as the gas samples have been normalized to account for air-contamination, high $N_2$ values must originate from the subsurface. $N_2$-rich gas seepage from MVs have been reported in Romania, at the Homorod mud volcano. The unusually $N_2$-dominated (90 vol.%.) seepage at Homorod MV is supposedly due to the metamorphism of ammonium-containing sedimentary rocks. In this process, ammonia ($NH_3$) is absorbed by clay minerals (e.g., illites) during diagenesis of sedimentary rocks, producing $NH_{4+}$ which replaces $K^+$ in K-bearing minerals. It has been suggested that $N_2$ gases are released when the formation of $CH_4$ has stopped. Hence, $N_2$ gases are generated during the final stages of gas generation (Krooss et al., 1995). The generation of $N_2$-rich gas at Maraza

MV is likely due to frequent eruptions which extinguishes the locally presence of $CH_4$. Note that all the samples at Maraza MV are collected in the northern part of the crater. Hence, only minor changes in the original gas composition is expected. It is therefore suitable to assume that Maraza was in its final stages of gas generation at the time of gas sampling.

On the other hand, gas from Kichik Maraza is methane-dominated (from 93.5 vol.% to 98.8 vol.%) with minor $CO_2$ concentrations (from 1.16 vol.% to 2.05 vol.%). Only one degassing structure contains $N_2$ (4.6 vol.%). The isotopic data ($\delta^{13}$C-CH4, $\delta^2$H-CH$_4$ and $\delta^{13}$C-CO$_2$) indicates that the Kichik Maraza gas is affected by secondary methanogenesis related to subsurface biodegradation of petroleum. With different geochemical composition, Maraza and Kichik Maraza MV must have different subsurface processes.

On its own, the main Maraza MV has an elongated structure with a crater that hosts only small gryphons. On the other hand, Kichik Maraza MV is pie-shaped and features a salsa lake and several gryphons with associated pools. From a small (local) point of view, Maraza MV has a focused seepage style, while Kichik Maraza has a diffused seepage style. This indicates that the seeping mechanisms of the two craters are different. Mudflow observation are in harmony with this assumption. The mudflow interpretation from satellite images in chapter 4 (section 4.2.1) shows that Maraza and Kichik Maraza MVs have erupted similar degassing activity but different eruption styles. Around Maraza MV, mudflow extends radially around the crater while the mudflow of Kichik Maraza MV is propagated unevenly. This mirrors the distribution and types of the degassing features present around the two craters, controlled by the volcano's subsurface architecture. This is reflected in the flux measurements, where the $CH_4$ and $CO_2$ maps show high degassing at both Maraza and Kichik Maraza. This is also reflected in the distribution of degassing features at both craters, further suggesting differences in their local subsurface architecture and eruption mechanisms.

Two gas samples (AZ19-16 and AZ19-17) from Kichik Maraza show higher $\delta^{13}$C-CH$_4$ values (-36.0‰ and -31.6‰), plotting in the late mature thermogenic gas field. These two samples were collected on the northwest rim of the Kichik Maraza crater. Additionally, microbial mats were observed in the pool of station AZ19-17. Hence, the development of microbial mats on northwest rim of Kichik Maraza may cause the gas of these two samples to be slightly different than the rest of the samples.

Figure 5-5 represents a cartoon of Maraza and Kichik Maraza MV, which includes the location of their craters and their main degassing features. Maraza MV is most prominent, with higher

elevation and a more defined crater. Therefore, it can be assumed that the main feeder channel is located below the crater.
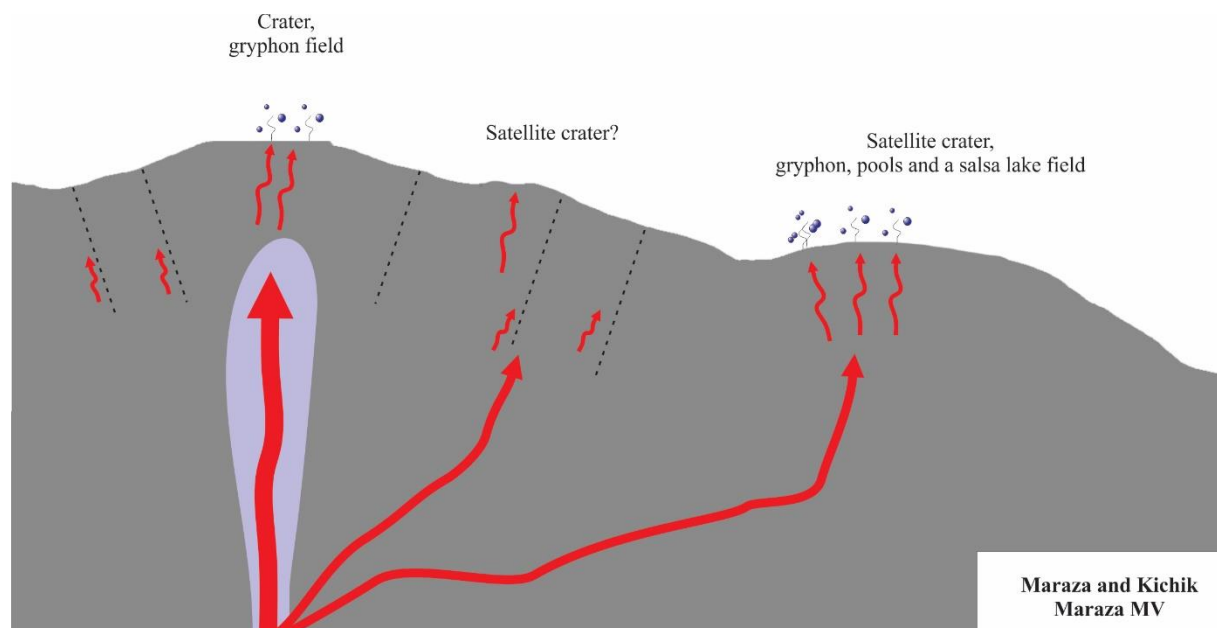


*Figure 5-5* *Cartoon illustrating Maraza and Kichik Maraza MV, with location of gryphon and pool fields from which gas samples were collected. The location of the proposed satellite craters are indicated. Red arrows indicate rising fluids.*

This feeder channel is most likely branched in the subsurface, resulting in the formation of a satellite crater (Kichik Maraza MV). Understanding how and why the channel is branched would require more geophysical investigations (e.g., geoelectric) and will not be discussed here. However, Maraza and Kichik Maraza MV are located at an anticline axis, and several smaller channels along the axis can be expected. Supplementary degassing features and a slight topographic high is observed between Maraza and Kichik Maraza on both satellite images and on profile in figure 4-2 and 4-3. Hence, the channelized hypothesis stands, and Maraza MV could potentially have three different craters. Overall, the architecture of Maraza and Kichik Maraza MV can be looked at in two ways: joint or individually. They are both parts of the same subsurface system, controlled by the longitudinal tectonic ruptures in the Central Gobustan zone. On the other hand, branched conduits with their own degassing styles possibly separate them. The conduit of Kichik Maraza probably penetrates sediments or meteoric water resulting in anaerobic secondary microbial gas production during the gas migration to the surface.

All but one sample (AZ19-25) from Gyzmeidan MV are methane-dominated with oil-associated thermogenic origins. AZ19-25 sample is $N_2$-dominated. (69.9 vol.%) with little methane (28.8 vol.%) and minimal carbon dioxide concentration (1.54 vol.%). As discusses in 5.2.2, the generation of $N_2$-rich gas is likely due due to frequent eruptions leading to the extinguished locally presence of $CH_4$. Interestingly, the $N_2$-rich sample is collected at the center of the MV structure, where most degassing is expected. Sample AZ19-21 is also sampled in the center of Gyzmeidan but has no $N_2$ in its gas. Microbial mats were observed in AZ19-21. The remainder gas samples are collected throughout the MV area. Overall, the gas samples from Gyzmeidan MV disclose little variance in molecular and isotopic composition (with the exception of sample AZ19-25).

All the gas samples are taken from pools located in different areas of Gyzmeidan MV. This implies that there is little interaction between the gas seeping in the feeder channel and subsurface sediments or waters. This is most likely due to little or no branching in the subsurface. The studied $CH_4$ and $CO_2$ gas flux at Gyzmeidan reveal significant degassing throught the MV area with exception of the western part. This is reflected in the large variations in the ($C_1/(C_2+C_3)$) ratio (from 496 to 10530). The sample (AZ19-22) collected in the western part has a $C_1/(C_2+C_3)$ ration of 10530, because reduced seepage in the area is most affected by molecular fractionation as the gas seeps slowly.

Gyzmeidan MV is a pie-shaped MV located perpendicular to a fault plane. The number of craters at this structure is not established as no crater rims are observed. Figure 5-6 represents a cartoon which displays the location of the main degassing features of Gyzmeidan MV. With the majority of the degassing features located SW and SE of the MV structure, it can be assumed that the main crater is located at the centre of the dome structure, at the fault, and seeps along the WE oriented fault to the south due to weaknesses in the local subsurface
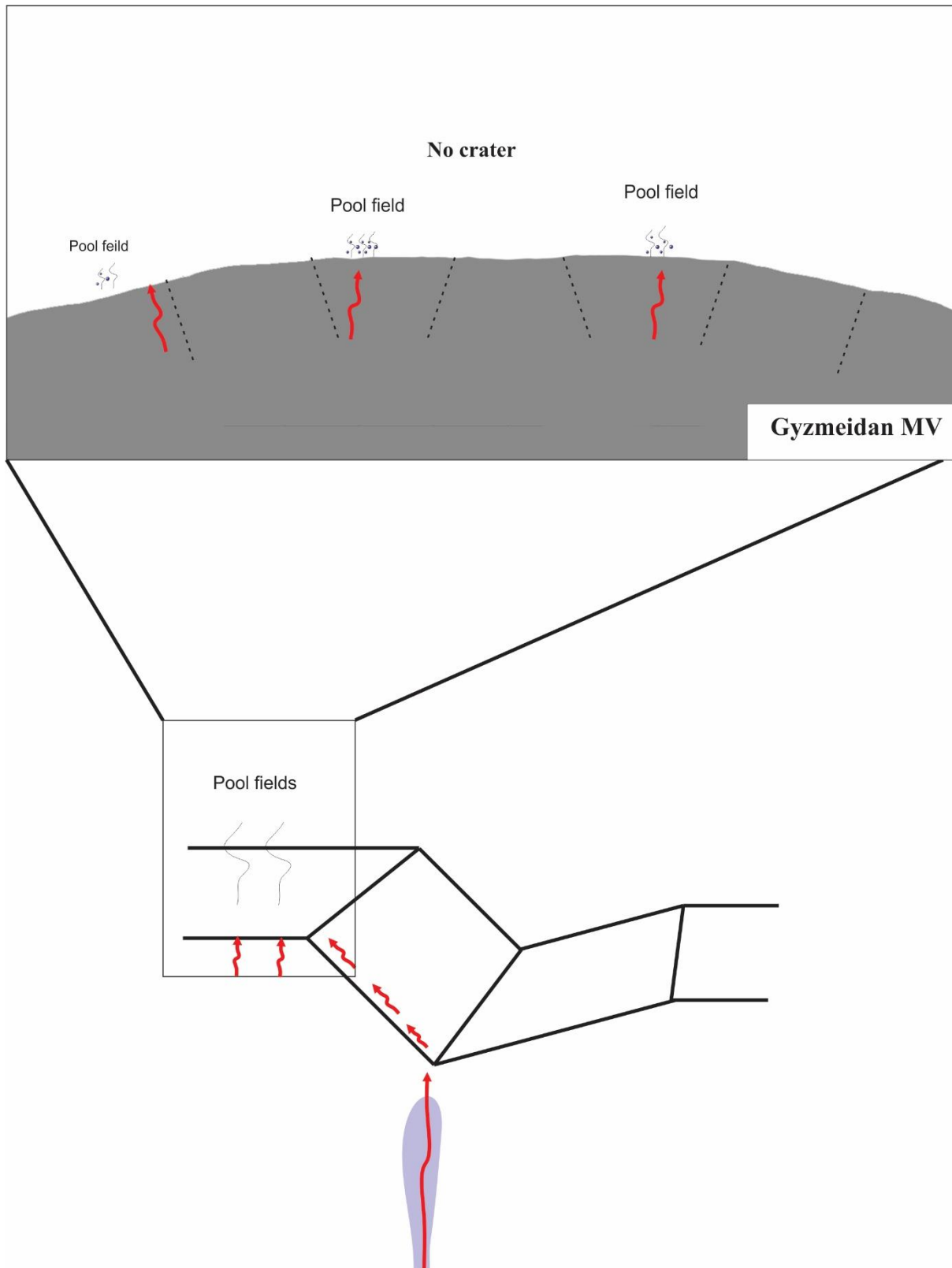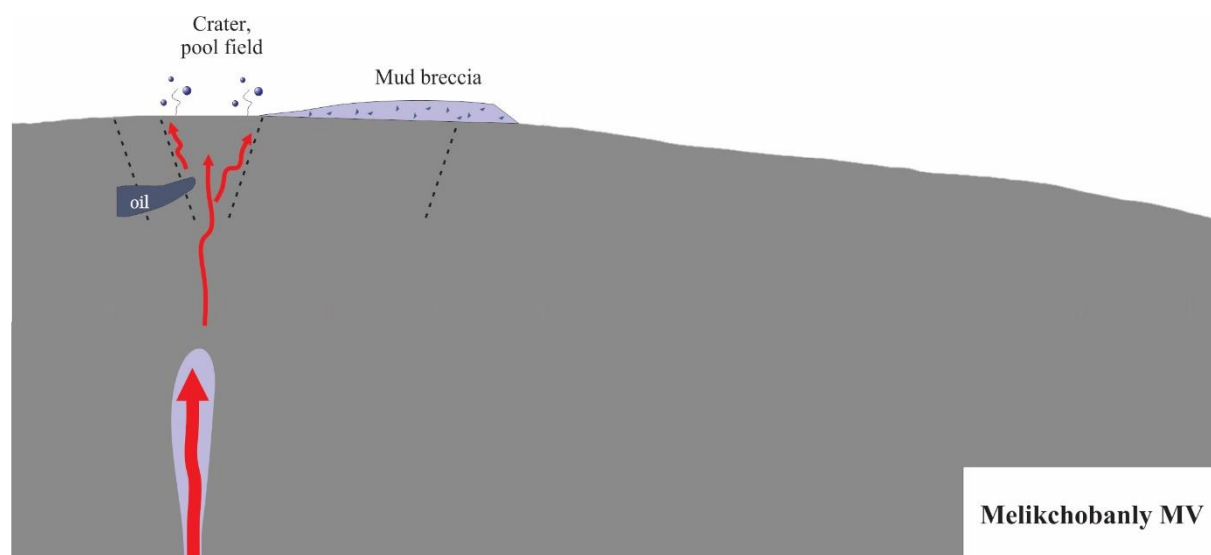
*Figure 5-6* Cartoon illustrating the hypothetical setting at Gyzmeidan MV, seepage mechanism, and location of pool fields from which gas samples were collected. Red arrows indicate rising fluids.

The two gas samples from Melikchobanly MV are methane-dominated. Both samples (AZ19-31 and AZ19-32) are taken at pools located in the north of the crater. However, the geochemical analysis of the two samples reveal that they have different gas origins: oil associated thermogenic and secondary microbial. It can be assumed that gas from sample AZ19-32 originates from a shallow reservoir below the crater where a biodegraded oil pool seeps gas through a local fracture.

Both gas samples from Melikchobanly MV show sign of weak molecular fractionation with a $(C_1/(C_2+C_3))$ ratio of 190. Hence, the gas is released slowly. In fact, the $CH_4$ and $CO_2$ flux measurements reflect relatively low seepage activity at Melikchobanly MV. There is no substantial sign of degassing features outside the crater which confirms that the MV is not very active. Even within the crater area, only two samples could be collected due to the lack of degassing structures.

Melikchobanly is located on a gently dipping slope which results in an elongated mudflow. It is likely that the flowing mud breccia along the slope have a ploughing effect, resulting in the destruction of most degassing structures. According to Mazzini et al., (2021), this erosional effect is prominent in the area closer to the crater. where the erupted mud is more confined, and becomes less effective moving downslope along the flanks. A hypothetical cartoon illustration the gas seepage and the bulldozing effects of mud breccia flow is illustrated in figure 5-7.



***Figure 5-7** Cartoon illustrating Melikchobanly MV, with location of pool fields from which gas samples were collected and the erosional mud breccia. The location of the proposed oil pool is indicated. Red arrows indicate rising fluids.*

The gas characterisation of Shikhzarli MV shows that seepage is methane-dominated with sign of molecular fractionation due to large variations in the $(C_1/(C_2+C_3))$ ratio. The origin of the

methane gas seeping at Shikhzarli MV has oil-associated thermogenic origins. The two sampling locations at Shikhzarli MV are located far from one another: one is in the main crater while the other is at the satellite crater (0.73 km away). The smooth dome structure of Shikhzarli MV and its satellite crater are aligned with a SW orientation and are most likely connected in the subsurface via branching of the degassing channel. Based on field observations, there is prominent seepage at the main Shikhzarli MV, and significantly less seepage at little Shikhzarli.

Located in the central Gobustan, Shikhzarli MV is affected by longitudinal tectonic ruptures. According to Kokh et al. (2017), Shikhzarli MV is one of the most active mud volcanoes in the Shamakhy–Gobustan region (Kokh et al., 2017). More explicitly, the volcano has erupted twenty-three times between 1810 and 2015 (in 1844, 1848, 1868, 1872, 1902, 1927, 1929, 1939, 1944, 1946, 1949, 1955, 1969, 1974, 1980, 1986, 1987, 1991, 1992, 1997, 2004, 2011, 2013, 2014, 2021). In 1902, Shikhzarli MV erupted for 2 day, as a result of an earthquake in the town of Shamakhy. It has been estimated that the erupting emitted 48,000 $m^3$ of mud, and a 100 m high gas-ignited flare (Kokh et al., 2017). Shikhzarli MV eruptions seem to follow a trend: Shamkhi earthquakes result in the release and ignition of gas gushers, and significant eruption of mud. These events are followed by deformation in the subsurface which produces large fractures (Aliyev et al., 2009). Recent eruptions have most likely destroyed previously existing degassing features such as gryphons and pools, resulting in few structures to samples gas from. Additionally, the frequent and intense eruptions at Shikhzarli MV probably release pristine gas that has little alternation from subsurface reservoirs. Hence why the gas collected at this volcano is purely thermogenic with no secondary alternations. Figure 5-8 represents a cartoon of the Shikhzarli. Little Shikhzarli MV is not included in this illustration as it is located
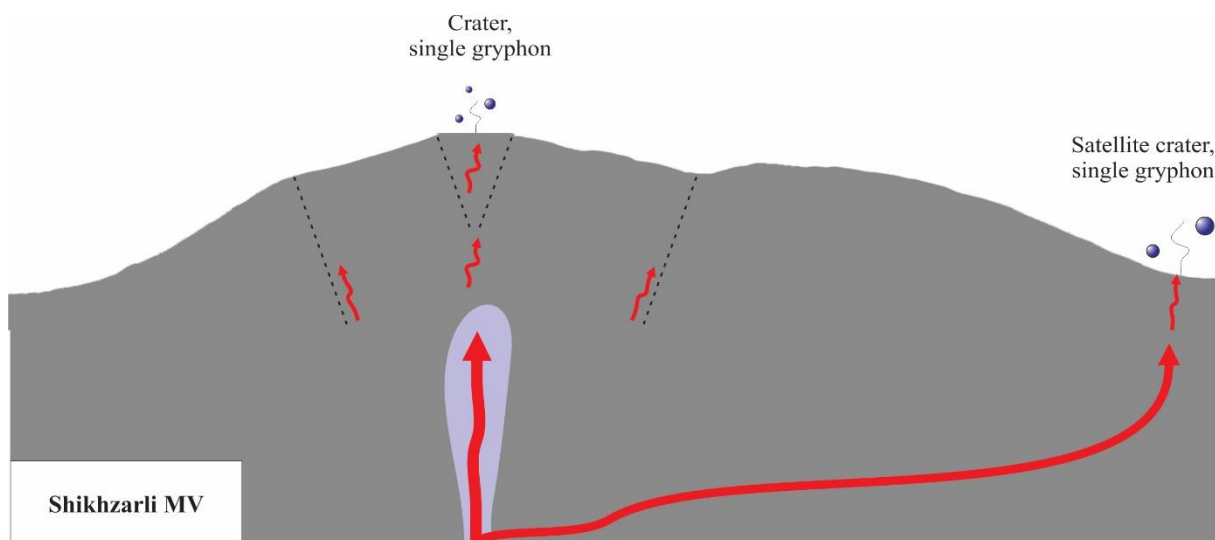
*Figure 5-8* *Cartoon illustrating Shikhzarli MV, with location of gryphons from which gas samples were collected. Red arrows indicate rising fluids.*

### 5.2.3 Group III

Geochemical analysis of the gas collected at Madrasa MV implies that the gas has a strictly secondary microbial origin. With this, Madrasa MV stands out from all the structures of this thesis. Secondary microbial methane is generated by anaerobic biodegradation process. In order for Secondary microbial gas to form, the presence of an oil pool susceptible to biodegradation must be present. According to Bernard (1992), biodegradation occur in reservoirs which are the following: i) relatively cool (<70–90 °C), ii) mostly clastic, iii) considered to have high porosity and permeability, iv) linked to nearby aquifer, v) not significantly compartmentalized and overpressured and vi) comprise of water with low salinity (<150 g/l NaCl) (Bernard et al., 1992).

The South Caspian Basin is one of six sedimentary basins where the production of secondary microbial methane is possible (Milkov, 2011). In Azerbaijan specifically, the secondary microbial methane is produced as free accumulations (above oil legs) then dissolved in biodegraded oils in Miocene–Pliocene clastic reservoirs at temperatures 25–93 °C.

A prominent fault oriented E-W hosts Madrasa MV. In both field and satellite images, Madrasa MV shows no edifice, only degassing features with oil, mud and gas expulsions. All gas samples were collected from oil-rich gryphons located in the northern part of the MV area, on a fault plane. Hence, the gas is probably generated by a biodegraded oil pool away from the volcano, and seeps along the fault This steep tectonic structure facilitates the migration of fluids that

109

reach the surface along the fault via gryphon structures. Note that the gas samples are not taken from or by the MV crater. Morphologically, it is not possible to classify Madrasa MV as it has no structure. Unfortunately, no flux measurements are taken at Madrasa limiting the interpretation of its degassing activity. Figure 5-9 represents a cartoon inspired by figure 4.10B which displays the location of the main Madrasa MV degassing features.
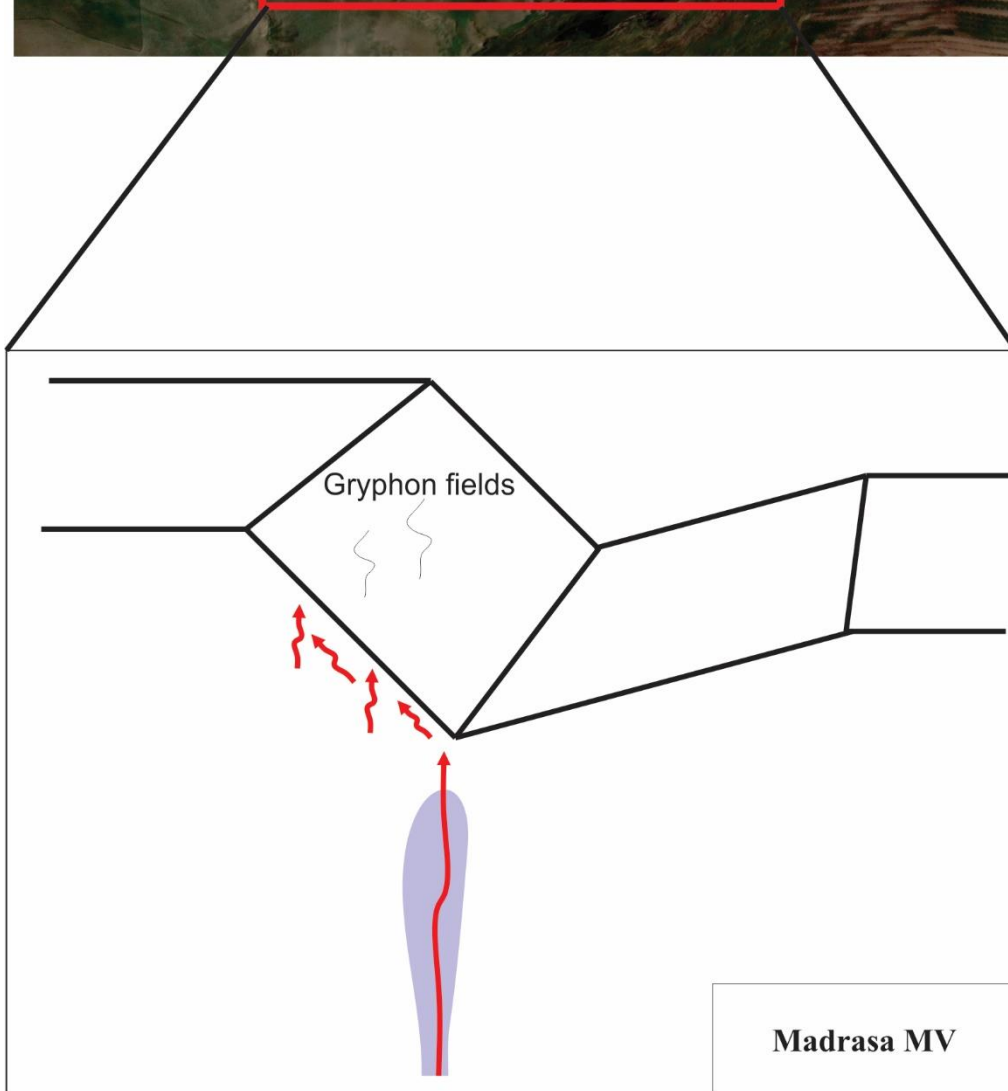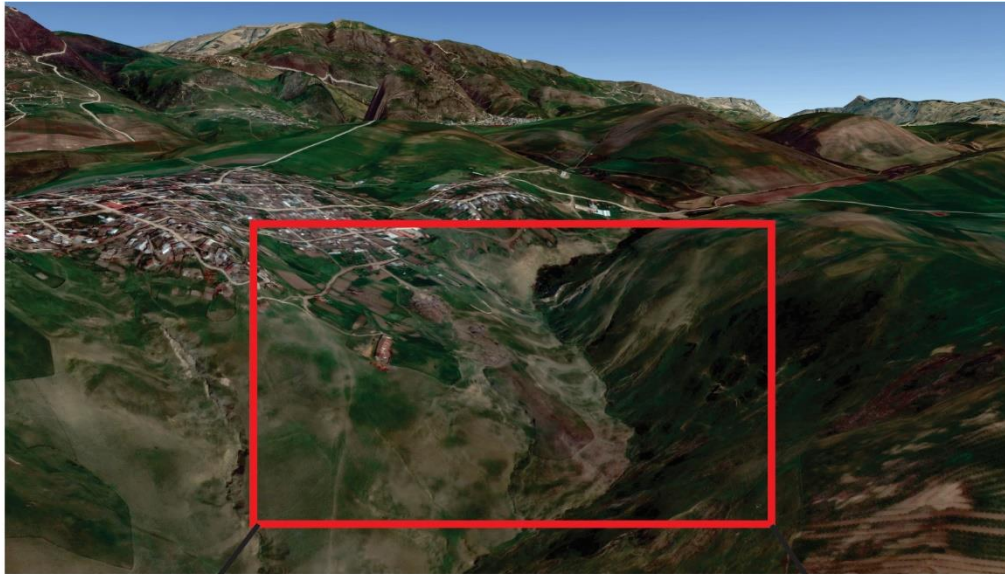
*Figure 5-9* *Satellite image (Google Earth) of Madrasa and a corresponding cartoon illustrating Madrasa MV, with location of gryphon fields from which gas samples were collected. The proposed seepage pathway is indicated. Red arrows indicate rising fluids.*

# 5.3 $CH_4$ and $CO_2$ emission budget of mud volcanoes

Since 1974, the enormous amounts of methane released to the atmosphere by onshore MVs have been established (Higgins & Saunders, 1974). According to survey on Azerbaijani MVs, $CH_4$ flux from MVs is $10^2$ and $10^3$ tonnes km$^{-2}$ yr$^{-1}$ (Etiope et al., 2004). Etiope and Milkov (2004) have suggested that the global $CH_4$ flux from both onshore and shallow offshore dormant MVs is about 2.8–4 Mt·yr$^{-1}$. Hence, Azerbaijani MVs contribute to about 20% of this yearly $CH_4$ flux. $CO_2$ flux measurements at MVs is not usually considered. However, this study shows that MVs realse a significant amount of $CO_2$. $CO_2$ flux from Gyzmeidan MV are estimated to be 20.3 tonnes yr$^{-1}$. Maraza (along with its satellite crater) also reveal a massive $CO_2$ flux of 13.7 tonnes yr$^{-1}$. To set things into perspective, an average car releases about 4.6 tonne $CO_2$ per year (EPA, 2018). With this, the $CO_2$ released from Gyzmeidan is equivalent to 4 cars while Maraza MV's $CO_2$ emissions is equivalent to 3 cars per year.

Two of the investigates MVs yielded low methane flux detection ($<5$ mg m$^{-2}$ day$^{-1}$) while other two generate medium methane flux values (5-50 mg m$^{-2}$ day$^{-1}$). Ideally, many more measurements would have been collected at each MV structure for a more robust statistical evaluation. However, with a limited number of measurements, the data shows the existence of significant gas seepage at two sites. Flux measurements show that Maraza and Kichik Maraza releases a whopping 63.7 ton $CH_4$ and 13.7 tonnes $CO_2$ per year. Note that all $CH_4$ flux values measured at the studied MV are, however, relatively high: Gyzmeidan MV (21.6 ton/yr), Gushchu MV (0.83 ton/yr) and Melikchobanly MV (2.9 ton/yr). This is emphasized when looking at previous studies, from MVs in Italy, Japan and Taiwan (Table 5-3).

Methane emission released by geological sources to the atmosphere is 60 Tg/yr (Etiope, 2015). Specifically, the emission of $CH_4$ from Mud volcanoes averages at 10–20 Tg/yr (Etiope et al., 2019). Hence about 16.7% of the geological sources of $CH_4$ to the atmosphere are from MVs. With this, MVs have been classified as "Big emitters" (Etiope et al., 2019).
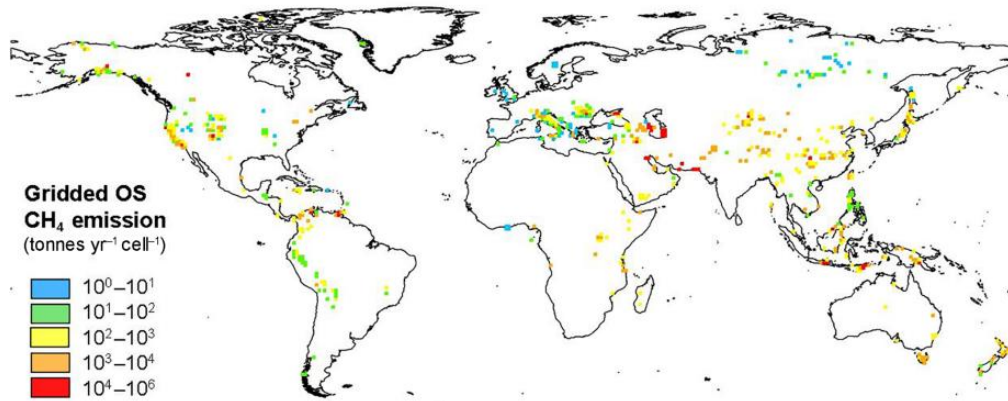
***Figure 5-10*** *Gridded world map over the distribution and quantification of onshore sheeps (OS) CH4 emission (Etiope et al., 2019)*

The Intergovernmental Panel on Climate Change (IPCC) reports typically include a chapter focused on the emission of methane to the atmosphere. However, the first three reports in 1990 (AR1), 1995 (AR2), and 2001 (AR3), did not include data from geological seepage (IPCC, 1990 and 1992, 1995, 2001, 2013). It was not before the AR4 report in 2007 that geological sources were mentioned, with 4 - 14Tg/yr (IPCC, 2007). Note that this report only referred to marine seeps. The 2013 IPCC report, AR5, included geological emission estimates of 54 Tg/year, close to the accepted value of 60 Tg/yr. This value integrated MVs. To set things in perspective, $CH_4$ emissions from fossil fuels were reported at 89 Tg/yr. Despite their enormous contribution to the global $CH_4$ emissions, MVs remain unpopular. Compared to fossil fuels, MVs emit about 11% as much $CH_4$. Unlike the anthropogenic fossil $CH_4$, the geological MV $CH_4$ emissions cannot be regulated by laws and innovation. More statistical data is needed to further examine their behaviours and accurately report the impact of MV to the atmosphere.

It is clear that MVs have a significant contribution to the release of greenhouse gases to the atmosphere, which has environmental consequences. The fact that geological activities can contribute to meteorological changes (e.g. rise in temperatures) exposes fascinating interactions of our dynamic planet.

*Table 5-3* *Published methane flux (tonnes/year) data collected at MVs in different countries (Azerbaijan, Italy, Japan and Taiwan)(Etiope & Milkov, 2004; Etiope, Oehler, et al., 2011; Yang et al., 2004) .*

| Country | MV structure | CH$_4$ flux | References |
|---|---|---|---|
| Azerbajian | Lokbatan | 342.0 | Etiope et al. (2004) |
| | Dashgil | 843.0 | Etiope et al. (2004) |
| | Bahar | 45.0 | Etiope et al. (2004) |
| | Kechaldag | 94.0 | Etiope et al. (2004) |
| | | | |
| Italy | Nirano | 12.0 | Etiope et al. (2007) |
| | Regnano | 34.0 | Etiope et al. (2007) |
| | Nirano | 32.4 | Etiope et al. (2007) |
| | Ospitaletto | 1.4 | Etiope et al. (2007) |
| | Dragone | 0.3 | Etiope et al. (2007) |
| | | | |
| Japan | Murono Tokamachi | >20 | Etiope et al. (2011) |
| | Kamou (Gamo) Tokamach | 3.7 | Etiope et al. (2011) |
| | | | |
| Taiwan | Luo-shan | 0.1 | Yang et al. (2004) |
| | Kuan-tze-ling | 0.1 | Yang et al. (2004) |
| | Yan-chao | 0.7 | Yang et al. (2004) |
| | Gung-shuei-ping | 1.1 | Yang et al. (2004) |
| | Diang-kuang | 0.7 | Yang et al. (2004) |

# 5.4 Limitations and Uncertainties

The main uncertainties and limitations of this study lies in the complexity of mud volcanism. In this section, limitations, and uncertainties related to the data sampling (sub-section 5.4.1) and quantification of CH$_4$ and CO$_2$ emission (sub-section 5.4.2) are presented.

### 5.4.1 Data sampling

Geochemical data from MVs cannot simply be interpreted without understanding the dynamics, activity and the sampling locations of the targeted MV. In principle, samples taken in the central part of the MV crater are the most pristine because the conduit (located below) is vertical resulting in fast-moving fluids. This is why samples collected at the center of the crater have less molecular fractionation. However, gas samples that are affected by molecular fractionation are not undesirable as they tell a story about the reactions and the fluids. Hence, samples with

secondary alternations reflect different reactions and interactions with the surrounding rocks. They also give information about the speed of the migrated fluids.

Fluids travel differently, hence, from a big scale, (in the crater, crater rims, outside) to the small scale (inside a gryphon or a pool), gas composition can be very different depending from where you sample despite them being from close source (few meters apart).This is well illustrated in figure 5-11, which demonstrates the complexity of rising fluids and the sub-surface architecture of MVs. Samples that are collected close to one another may miss the complexity of the MV strcucture. In order to get a full overview of the subsurface mechanisms and related reactions samples should be collected both inside and outside the crater area at different degassing features. Depending on the amounts of samples, some conclusions may be inaccurate simply because only one part of the plumbing system is analysed. The geochemical analysis of gas sampled at MVs can therefore give very different results depending on the sampling site.

Samples in this study are fairly clusters with some exceptions. The outliers in the study strengthen the overall understanding of the structures. The interpretation of the results is done using field mapping, and analysing satellite images to understand the framework of the volcanoes. However, the true behaviours of MVs cannot be known for sure. The proposed speculations of the fluid origin considers the sample location on the MV structure and the activity of the targeted MVs. However, more samples with broader distribution are likely to give a more reliable analysis of the sub-surface processes of MVs.
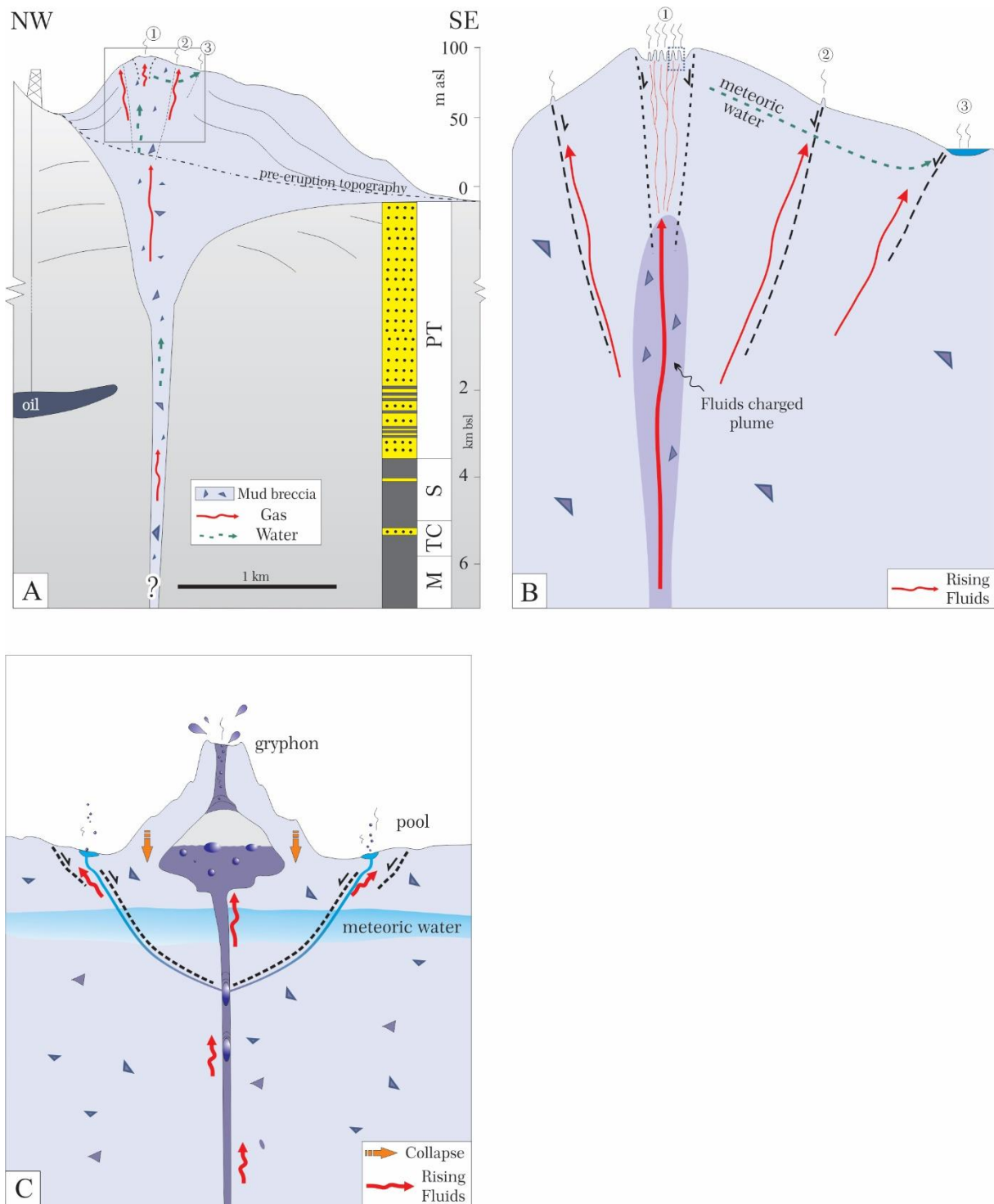
**Figure 5-11** *Cartoons illustrating the complexity of fluid degassing pathways. (A) Dashgil MV with marked locations in and around the crater representing (1) The gryphon field inside the crater; (2) diffuse seepage along the outer fault margin; and (3) salsa lakes. (B) Insight to seepage controlled by faults that act as preferential pathways for deeper fluids seepage.(C) The complexity of a gryphon-pool plumbing system (Mazzini, Svensen, et al., 2009).*

### 5.4.2  Quantification of $CH_4$ and $CO_2$ gas

The quantification of $CO_2$ and $CH_4$ budget released at selected MV is done computing statistical elaboration of the measurements collected on the field over a region through which the structure extends. The size, and more specifically the area of a given structure is calculated using Google Earth (GE) pro. satellite images. The uncertainties and limitations related to this process are two. The first is related to the user that defines arbitrarily the surface of a MV. Although some structures have well defined boundaries, others, especially when affected by erosion or extensive deformations, can be partially debated. The second uncertainty is related to the accuracy of GE itself. GE Pro is based on the World Geodetic System (WGS). The digital images of GE are obtained combining photos collected from different satellites and therefore from different altitudes and angles. These images are further processed and placed on the WGS84 globe and the algorithm behind this process may not always be accurate (Lopes, 2012). Additionally, the variance in the precision of the "measure distance and area" tool provided by the software should be considered. The accuracy of this tool has 1.5% error. However, when calculating a surface with GE it is essential to consider that the higher is the magnification used, the more inaccurate the tool may be. Hence, the estimation of MV areas from satellite images may be off by some meters.

# 5.5 Suggestions for further research

This study provides an improved understanding of the morphologies and gas emissions from Shamakhy-Gobustan mud volcanoes. However, additional research is necessary to better understand the subsurface of the targeted MVs and further reduce uncertainties related to gathering and quantify MV gas emissions. This includes:

- Perform a detailed petrography study on the erupted clasts at each targeted MV to reconstruct the stratigraphy intersected by the feeder channel and define the roots of the conduits. Typical mud volcano deposits consists of erupted mud breccia which are fine grained matrix incorporating clast of the different lithologies brecciated throughout the MV conduit and expelled at the surface. Petrography of the erupted clasts can provide important information about the petrophysical properties of the rocks (e.g. specific parameters such as cementation type, pore space geometry and porosity of a sandstone can be established)(Giresse et al., 2010). Dating of the clasts and the matrix conducted through palynological, micro paleontological studies will reveal the age of the erupted sediments from different parts of the subsurface, providing free stratigraphy of the MV plumbing system.

- Conduct a Interferometric Synthetic Aperture Radar (InSAR) survey at each targeted MVs to monitor inflation of the structures and ideally predict imminent eruptions or to monitor the rate of the collapsed area after eruptions. Such survey could measure with high precision deformation changes associated with MV activity, as well as strain resulting from changes in the distribution of gas in the plumbing system and volcano-tectonic deformation signals.

- Deploy networks of seismometers at selected MVs to monitor their activity and observe potential changes in behavior prior to or after seismic events (Somoza et al., 2003). This will be useful to further evaluate the geohazard implication of MVs in Shamakhy-Gobustan region.

- Assessing the geochemical characteristics and origin of the water at degassing features of the targeted MVs (Mazzini, Svensen, et al., 2009).

# 6 Conclusions

The main objectives of this study were to i) establish the morphologies and activity of the targeted MVs by considering recent eruptive events and the distribution and types of degassing features observed on the field, ii) present novel geochemical data on the targeted MVs and determine the origin of fluids released at the surface and iii) quantify flux measurements of the targeted MVs to evaluate the local methane and carbon dioxide budgets released to the atmosphere from marco- and mini-seepage.

Objective i) was met by creating a detailed morphological descriptions of the targeted MVs using satellite images and field observations. Furthermore, objective ii) was achieved by assessing and discussing geochemical data of fluid degassing manifestations. Lastly, objective iii) was accomplished through $CH_4$ and $CO_2$ flux measurements taken above and around seeps with prominent signs of degassing activity on four MVs: Maraza, Gyzmeidan, Gushchu, Malikchobanli.

The key observations and results from objectives i), ii) and iii) are:

- Majority of the mud volcanoes in the Shamakhy-Gobustan region are pie-shaped. They indicate faulted or branched plumbing systems that are likely affected by regional large scale tectonic structures. Fluid seepage along these anticline and fault structures result in wide distribution in degassing features at and around the MV craters.

- The geochemical data of the Shamakhy-Gobustan MV structures of this study reflect typical characteristics and origin from the western Caspian basin. Like the other Azerbaijan gases, those from Shamakhy-Gobustan region are methane-dominated with thermogenic origins. Fluid collected away from the crater center are more affected by secondary alternations and molecular fractionation. There is therefore a trend in the observed distribution of marco- and mini-seepage and gas affected with secondary alternations.

- Degassing structures with prevalent $N_2$ concentration are likely located at active MVs where $CH_4$ seepage is extinguished or at sites that are in their final stage of gas generation. Observations from this study reveal that $N_2$ dominated gas is only present at the center of the MV structures (Maraza and Gyzmeidan MVs).

- The quantification of $CH_4$ and $CO_2$ gas reveal significant degassing (reaching values up to 20.3 and 63.6 tonnes $yr^{-1}$, accordingly), especially at Gyzmeidan and Maraza MVs. The emission budget of the investigated MVs is comparable to other structures investigated worldwide. The measurements confirm that MVs represent one of the major natural methane emitters on Earth.

- It is well documented that MVs are geological geohazards and in several instances were observed settlements and constructions neighboring the actively seeping craters. A more accurate managements of the territory surrounding MVs is imperative to avoid potential fatalities.

# Reference list

Abbasov. (2016). Geological and geochemical properties of oil shale in Azerbaijan and petroleum potential of deep-seated Eocene-Miocene deposits. *European journal of natural history*(2), 31-40.

Abbasov, O. (2016). Distribution regularities of oil shale in Azerbaijan. *Theoretical & Applied Science*(3), 165-171.

Abdullayev, E., Baldermann, A., Warr, L. N., Grathoff, G., & Taghiyeva, Y. (2021). New constraints on the palaeo-environmental conditions of the Eastern Paratethys: Implications from the Miocene Diatom Suite (Azerbaijan). *Sedimentary Geology*, *411*, 105794.

Abdullayev, N., Kadirov, F., & Guliyev, I. (2017). Subsidence history and basin-fill evolution in the South Caspian Basin from geophysical mapping, flexural backstripping, forward lithospheric modelling and gravity modelling. *Geological Society, London, Special Publications*, *427*(1), 175-196.

Abikh, G. (1863). New Islands on the Caspian Sea and the cognition of mud volcanoes of the Caspian Region. *Mem Acad Sci Peterbourg Ser*, *8*(6), 5.

Abrams, M. A. (2005). Significance of hydrocarbon seepage relative to petroleum generation and entrapment. *Marine and Petroleum Geology*, *22*(4), 457-477. https://doi.org/http://dx.doi.org/10.1016/j.marpetgeo.2004.08.003

Abrams, M. A., & Narimanov, A. A. (1997). Geochemical evaluation of hydrocarbons and their potential sources in the western South Caspian depression, Republic of Azerbaijan. *Marine and Petroleum Geology*, *14*(4), 451-468.

Abrams, M. A., & Narimanov, A. A. (1997). Geochemical evaluation of hydrocarbons and their potential sources in the western South Caspian depression, Republic of Azerbaijan. *Marine & Petroleum Geology*, *14*, 451-468.

Adamia, S., Zakariadze, G., Chkhotua, T., Sadradze, N., Tsereteli, N., Chabukiani, A., & Gventsadze, A. (2011). Geology of the Caucasus: a review. *Turkish journal of earth sciences*, *20*(5), 489-544.

Adamia, S. A., Chkhotua, T., Kekelia, M., Lordkipanidze, M., Shavishvili, I., & Zakariadze, G. (1981). Tectonics of the Caucasus and adjoining regions: implications for the evolution of the Tethys ocean. *Journal of Structural Geology*, *3*(4), 437-447.

Adamia, S. A., Lordkipanidze, M., & Zakariadze, G. (1977). Evolution of an active continental margin as exemplified by the Alpine history of the Caucasus. *Tectonophysics*, *40*(3-4), 183-199.

Afandiyeva, M. A. Reconstruction of sedimentation in Maikop paleobasin in Azerbaijan. AAPG Europe Regional Conference, Global Analogues of the Atlantic Margin,

Akhmetzhanov, A. M., Kenyon, N. H., Ivanov, M. K., Westbrook, G., & Mazzini, A. (Eds.). (2008). *Deep-water depositional systems and cold seeps of the Western Mediterranean, Gulf of Cadiz and Norwegian continental margins*. IOC Technical Series No. 76, UNESCO.

Aliev, H. (1960). On the vertical zonality of the soils of the Great Caucasus eastern part (Azerbaijan SSR. *Transactions 7th int. Congr. Soil Sci.*, *4*, 325-328.

Aliyev, A., Guliyev, F., Dadashev, F. G., & Rahmannov, R. R. (2015). Atlas of the world mud volcanoes. *Nafta-Press, ISBN 978-9952-437-60-7*.

Aliyev, A. A. (2004). Mud volcanism of the South-Caspian oil-gas basin, in South-Caspian Basin. *Geology, Geophysics, Oil and Gas Content, Nafta, Baku, Azerbaijan*, 186-212.

Aliyev, A. A., Guliyev, I. S., & Rakhmanov, R. R. (2009). *Catalogue of Mud Volcanoes Eruptions of Azerbaijan: 1810-2007*. Nafta-Press.

Alizadeh, A. A., ogly Guliyev, I. S., Kadirov, F. A., & Eppelbaum, L. V. (2016). *Geosciences of Azerbaijan* (Vol. 1). Springer.

Allen, M. B., & Armstrong, H. A. (2008). Arabia–Eurasia collision and the forcing of mid-Cenozoic global cooling. *Palaeogeography, Palaeoclimatology, Palaeoecology*, *265*(1-2), 52-58.

Allen, M. B., Vincent, S. J., Alsop, G. I., Ismail-zadeh, A., & Flecker, R. (2003). Late Cenozoic deformation in the South Caspian region: effects of a rigid basement block within a collision zone. *Tectonophysics*, *366*(3-4), 223-239.

Avantor. (2022). *Multi-parameter meter (pH/conductivity/DO), handheld, pHenomenal® MU 6100 H, VWR®*. Retrieved 07/06/222 from https://si.vwr.com/store/product/12125328/multi-parameter-meter-ph-conductivity-do-handheld-phenomenal-mu-nbsp-6100-nbsp-h

Axen, G. J., Lam, P. S., Grove, M., Stockli, D. F., & Hassanzadeh, J. (2001). Exhumation of the west-central Alborz Mountains, Iran, Caspian subsidence, and collision-related tectonics. *Geology*, *29*(6), 559-562.

Babadi, M., Mehrabi, B., Tassi, F., Cabassi, J., Pecchioni, E., Shakeri, A., & Vaselli, O. (2021). Geochemistry of fluids discharged from mud volcanoes in SE Caspian Sea (Gorgan Plain, Iran). *International Geology Review*, *63*(4), 437-452.

Babayev, G., Tibaldi, A., Bonali, F., & Kadirov, F. (2014). Evaluation of earthquake-induced strain in promoting mud eruptions: the case of Shamakhi–Gobustan–Absheron areas, Azerbaijan. *Natural hazards*, *72*(2), 789-808.

Barber, A. J., Tjokosapoetro, S., & Charlton, T. R. (1986). Mud volcanoes, shale diapirs, wrench faults and melanges in accretionary complexes, eastern Indonesia. *American Association of Petroleum Geologists Bulletin*, *70*, 1729-1741.

Bean, C. J., De Barros, L., Lokmer, I., Metaxian, J.-P., O/' Brien, G., & Murphy, S. (2014). Long-period seismicity in the shallow volcanic edifice formed from slow-rupture earthquakes [Article]. *Nature Geosci*, *7*(1), 71-75. http://dx.doi.org/10.1038/ngeo2027

Berberian, M. (1983). The southern Caspian: a compressional depression floored by a trapped, modified oceanic crust. *Canadian Journal of Earth Sciences*, *20*(2), 163-183.

Bergamaschi, P., Krol, M., Meirink, J. F., Dentener, F., Segers, A., van Aardenne, J., Monni, S., Vermeulen, A., Schmidt, M., & Ramonet, M. (2010). Inverse modeling of European CH4 emissions 2001–2006. *Journal of Geophysical Research: Atmospheres*, *115*(D22).

Bernard, B., Brooks, J. M., & Sackett, W. M. (1977). A geochemical model for characterization of hydrocarbon gas sources in marine sediments. Offshore Technology Conference,

Bernard, F., Connan, J., & Magot, M. (1992). Indigenous microorganisms in connate water of many oil fields: a new tool in exploration and production techniques. SPE Annual Technical Conference and Exhibition,

Bjorlykke, K. (2010). *Petroleum Geoscience: From Sedimentary Environments to Rock Physics*. Berlin, Heidelberg: Springer Berlin / Heidelberg. https://doi.org/10.1007/978-3-642-02332-3

Bonini, M. (2012). Mud volcanoes: indicators of stress orientation and tectonic controls. *Earth-Sci Rev*, *115*. https://doi.org/10.1016/j.earscirev.2012.09.002

Bonini, M., Tassi, F., Feyzullayev, A. A., Aliyev, C. S., Capecchiacci, F., & Minissale, A. (2013). Deep gases discharged from mud volcanoes of Azerbaijan: New geochemical evidence. *Marine and Petroleum Geology*, *43*(0), 450-463. https://doi.org/http://dx.doi.org/10.1016/j.marpetgeo.2012.12.003

Boote, D., Sachsenhofer, R., Tari, G., & Arbouille, D. (2018). Petroleum provinces of the Paratethyan region. *Journal of Petroleum Geology*, *41*(3), 247-297.

Boreham, C., Hope, J., & Hartung-Kagi, B. (2001). Understanding source, distribution and preservation of Australian natural gas: a geochemical perspective. *The APPEA Journal*, *41*(1), 523-547.

Brooks, J. M., Bernard, B. B., Sackett, W. M., & Schwarz, J. (1979). Natural gas seepage on the south Texas shelf. Offshore Technology Conference,

Brown, K. M. (1990). The nature and hydrogeologic significance of mud diapirs and diatremes for accretionary systems. *Journal of Geophysical Research*, *95*(B6), 8969-8982. http://www.sciencedirect.com/science/article/B6WPY-3V4PKDS-4TC/1/2de9260c0272feac01c740aa53155127

Brunet, M.-F., & Cloetingh, S. (2003). Integrated peri-Tethyan basins studies (peri-Tethys programme). *Sedimentary Geology*, *156*(1-4), 1-10.

Canadell, J. G., Monteiro, P. M., Costa, M. H., Cotrim da Cunha, L., Cox, P. M., Eliseev, A., Henson, S., Ishii, M., Jaccard, S., & Koven, C. (2021). Global carbon and other biogeochemical cycles and feedbacks. *Climate change*.

Chiodini, G., & Frondini, F. (2001). Carbon dioxide degassing from the Albani Hills volcanic region, Central Italy. *Chem. Geol.*, *177*, 67–83.

Ciais, P., Sabine, C., Bala, G., Bopp, L., Brovkin, V., Canadell, J., Chhabra, A., DeFries, R., Galloway, J., Heimann, M., Jones, C., Le Quéré, C., Myneni, R. B., Piao, S., & Thornton, P. (2013). Carbon and other biogeochemical cycles.

. In T. F. Stocker, D. Qin, G.-K. Plattner, M. Tignor, S. K. Allen, J. Boschung, A. Nauels, Y. Xia, V. Bex, & P. M. Midgley (Eds.), *Climate change 2013: the physical science basis. Contribution of working group I to the fifth assessment report of IPCC* (pp. 465-570). Cambridge University Press, Cambridge, United Kingdom and New York, NY, USA.

Ciotoli, G., Procesi, M., Etiope, G., Fracassi, U., & Ventura, G. (2020). Influence of tectonics on global scale distribution of geological methane emissions. *Nature Communications*, *11*(1), 1-8.

Connan, J. (1984). Biodegradation of crude oil in reservoirs. In J. Brooks & D. Welte (Eds.), *Advances in Petroleum Geochemistry, vol. 1* (Vol. 1, pp. 299-335). Academic Press, London.

Croker, P., & O'Loughlin, O. (1998). A catalogue of Irish offshore carbonate mud mounds. Proceedings of Carbonate Mud Mounds and Cold Water Reefs Conference,

Deville, E., Battani, A., Griboulard, R., Guerlais, S. H., Herbin, J. P., Houzay, J. P., Muller, C., & Prinzhofer, A. (2003). Mud volcanism origin and processes. New insights from Trinidad and the Barbados Prism. In P. Van Rensbergen, R. R. Hillis, A. J. Maltman, & C. Morley (Eds.), *Surface Sediment Mobilization* (Vol. 216, pp. 475–490). Special publication of the Geological Society (London)

Deville, E., & Guerlais, S. H. (2009). Cyclic activity of mud volcanoes: Evidences from Trinidad (SE Caribbean). *Marine and Petroleum Geology*, *26*(9), 1681-1691. https://doi.org/DOI 10.1016/j.marpetgeo.2009.03.002

Devlin, B., & Roeder, K. (1999). Genomic control for association studies. *Biometrics*, *55*(4), 997-1004.

Dewey, J., Hempton, M., Kidd, W., Saroglu, F., & Şengör, A. (1986). Shortening of continental lithosphere: the neotectonics of Eastern Anatolia—a young collision zone. *Geological Society, London, Special Publications*, *19*(1), 1-36.

Dewey, J. F., PITMAN III, W. C., Ryan, W. B., & Bonnin, J. (1973). Plate tectonics and the evolution of the Alpine system. *Geological Society of America Bulletin*, *84*(10), 3137-3180.

Dia, A. N., Castrec-Rouelle, M., Boulegue, J., & Comeau, P. (1999). Trinidad mud volcanoes: where do the expelled fluids come from? *Geochimica et Cosmochimica Acta*, *63*(7-8), 1023-1038. http://www.sciencedirect.com/science/article/B6V66-3WX20FM-5/2/1f87a389edcdaa79eceb2e3b90b4db53

Dimitrakopoulos, R., & Muehlenbachs, K. (1987). Biodegradation of petroleum as a source of 13C-enriched carbon dioxide in the formation of carbonate cement. *Chemical Geology: Isotope Geoscience section 65.3-4* 283-291.

Dimitrov. (2002a). Contribution to atmospheric methane by natural seepages on the Bulgarian continental shelf. *Continental Shelf Research*, *22*(16), 2429-2442.

Dimitrov. (2002b). Mud volcanoes--the most important pathway for degassing deeply buried sediments. *Earth-Science Reviews*, *59*(1-4), 49-76. http://www.sciencedirect.com/science/article/B6V62-451S9DG-2/2/861a27f366b4781f3c775efb5441b582

EPA. (2018). *Greenhouse Gas Emissions from a Typical Passenger Vehicle* (EPA-420-F-18-008). U. S. E. P. Agency. https://nepis.epa.gov/Exe/ZyPDF.cgi?Dockey=P100U8YT.pdf

Ershov, A. V., Brunet, M.-F., Nikishin, A. M., Bolotov, S. N., Nazarevich, B. P., & Korotaev, M. V. (2003). Northern Caucasus basin: thermal history and synthesis of subsidence models. *Sedimentary Geology*, *156*(1-4), 95-118.

Etiope, G. (2009). Natural emissions of methane from geological seepage in Europe. *Atmospheric Environment*, *43*(7), 1430-1443. https://doi.org/DOI: 10.1016/j.atmosenv.2008.03.014

Etiope, G. (2015). Natural Gas Seepage. The Earth's hydrocarbon degassing. *Springer International Publishing Switzerland, ISBN 978-3-319-14601-0 (eBook), DOI 10.1007/978-3-319-14601-0.*, 199.

Etiope, G. (2017). Natural Gas. In *Encyclopedia of Geochemistry*. Springer.

Etiope, G., Baciu, C., Caracausi, A., Italiano, F., & Cosma, C. (2004). Gas flux to the atmosphere from mud volcanoes in eastern Romania. *Terra Nova*, *16*(4), 179-184. https://doi.org/DOI 10.1111/j.1365-3121.2004.00542.x

Etiope, G., Ciotoli, G., Schwietzke, S., & Schoell, M. (2019). Gridded maps of geological methane emissions and their isotopic signature. *Earth System Science Data*, *11*(1), 1-22. https://doi.org/10.5194/essd-11-1-2019

Etiope, G., Drobniak, A., & Schimmelmann, A. (2013). Natural seepage of shale gas and the origin of "eternal flames" in the Northern Appalachian Basin, USA. *Marine and Petroleum Geology*, *43*, 178-186. https://doi.org/10.1016/j.marpetgeo.2013.02.009

Etiope, G., Feyzullayev, A., Milkov, A. V., Waseda, A., Mizobe, K., & Sun, C. H. (2009). Evidence of subsurface anaerobic biodegradation of hydrocarbons and potential secondary methanogenesis in terrestrial mud volcanoes. *Marine and Petroleum Geology*, *26*(9), 1692-1703. http://www.sciencedirect.com/science/article/B6V9Y-4V75YX5-2/2/ce7a44ee2696cf9217065d700f4c00c7

Etiope, G., & Ionescu, A. (2015). Low-temperature catalytic $CO_2$ hydrogenation with geological quantities of ruthenium: a possible abiotic $CH_4$ source in chromitite-rich serpentinized rocks. *Geofluids*, *15*(3). https://doi.org/10.1111/gfl.12106

Etiope, G., & Klusman, R. W. (2002). Geologic emissions of methane to the atmosphere. *Chemosphere*, *49*(8), 777-789. https://doi.org/Pii S0045-6535(02)00380-6

Etiope, G., Lassey, K. R., Klusman, R. W., & Boschi, E. (2008). Reappraisal of the fossil methane budget and related emission from geologic sources. *Geophys Res Lett*, *35*. https://doi.org/10.1029/2008gl033623

Etiope, G., & Martinelli, G. (2009). "Pieve Santo Stefano" is not a mud volcano: Comment on "Structural controls on a carbon dioxide-driven mud volcano field in the Northern Apennines" (by Bonini, 2009). *Journal of Structural Geology*, *31*(10), 1270-1271. https://doi.org/DOI 10.1016/j.jsg.2009.06.009

Etiope, G., Martinelli, G., Caracausi, A., & Italiano, F. (2007). Methane seeps and mud volcanoes in Italy: gas origin, fractionation and emission to the atmosphere. *Geophysical Research Letters*, *34, L14303, doi: 10.1029/2007GL030341*.

Etiope, G., & Milkov, A. (2004). A new estimate of global methane flux from onshore and shallow submarine mud volcanoes to the atmosphere. *International Journal of Geosciences*, *46*(8), 997-1002. https://doi.org/10.1007/s00254-004-1085-1

Etiope, G., Nakada, R., Tanaka, K., & Yoshida, N. (2011). Gas seepage from Tokamachi mud volcanoes, onshore Niigata Basin (Japan): origin, post-genetic alterations and $CH_4$-$CO_2$ fluxes. *Applied Geochemistry*, *26*, 348-359.

Etiope, G., Oehler, D. Z., & Allen, C. C. (2011). Methane emissions from Earth's degassing: Implications for Mars. *Planetary and Space Science*, *59*(2-3), 182-195. https://doi.org/DOI 10.1016/j.pss.2010.06.003

Etiope, G., & Schoell, M. (2014). Abiotic gas: atypical, but not rare. *Elements*, *10*(4), 291-296.

Etiope, G., & Schwietzke, S. (2019). Global geological methane emissions: an update of top-down and bottom-up estimates. *Elem Sci Anth.*, *7*(1), 47, http://doi.org/10.1525/elementa.1383

Ferrer, I., & Thurman, M. E. (2013). *Advanced techniques in gas chromatography-mass spectrometry (GC-MS-MS and GC-TOF-MS) for environmental chemistry*. Newnes.

Feseker, T., Dahlmann, A., Foucher, J. P., & Harmegnies, F. (2009). In-situ sediment temperature measurements and geochemical porewater data suggest highly dynamic fluid flow at Isis

mud volcano, eastern Mediterranean Sea. *Marine Geology*, *261*(1-4), 128-137. https://doi.org/DOI 10.1016/j.margeo.2008.09.003

Feyzullayev, A. (2003). Geological conditions and precularities of mud volcanoes formation. AAPG Annual Meeting, Salt Lake City, Utah,

Feyzullayev, A. (2012). Mud volcanoes in the South Caspian basin: nature and estimated depth of its products. *Natural Science*, *2012*.

Feyzullayev, A. A., Guliyev, I. S., & Tagiyev, M. F. (2001). Source potential of the Mesozoic–Cenozoic rocks in the South Caspian Basin and their role in forming the oil accumulations in the Lower Pliocene reservoirs. *Petroleum Geoscience*, *7*(4), 409-417.

GDI-BGR. (2020). *GeoViewer*. BGR. Retrieved 02/04 from https://geoviewer.bgr.de/mapapps4/resources/apps/geoviewer/index.html?lang=en&tab=geologie&cover=geologie_europa&layers=+:geologie_europa,geologie_iqe_2500_wms&center=5314948.512835046,4927505.8167972695,3857&lod=8

Giresse, P., Loncke, L., Huguen, C., Muller, C., & Mascle, J. (2010). Nature and origin of sedimentary clasts associated with mud volcanoes in the Nile deep-sea fan. Relationships with fluid venting. *Sedimentary Geology*, *228*(3-4), 229-245.

Gontharet, S., Pierre, C., Blanc-Valleron, M.-M., Rouchy, J.-M., Fouquet, Y., Bayon, G., Foucher, J.-P., Woodside, J., Mascle, J., & Party, T. N. S. (2007). Nature and origin of diagenetic carbonate crusts and concretions from mud volcanoes and pockmarks of the Nile deep-sea fan (eastern Mediterranean Sea). *Deep Sea Research Part II: Topical Studies in Oceanography*, *54*(11-13), 1292-1311.

Goodwin, N., Abdullayev, N., Javadova, A., Volk, H., & Riley, G. (2020). Diamondoids and basin modelling reveal one of the world's deepest petroleum systems, South Caspian Basin, Azerbaijan. *Journal of Petroleum Geology*, *43*(2), 133-149.

Granath, J., Soofi, K., Baganz, O., & Baghirov, E. (2000). Gravity modeling and its implications to the tectonics of the South Caspian Basin: AAPG Inaugural Regional Conference Istanbul. Extended Abstracts,

Greinert, J., Bohrmann, G., & Suess, E. (2001). Gas hydrate-associated carbonates and methane-venting at Hydrate Ridge classification, distribution, and origin of authigenic lithologies. In C. K. Paull & W. K. Dillon (Eds.), *Natural Gas Hydrates: Occurrence, Distribution and Detection* (pp. 99-113). Geophysical Monograph 124, American Geophysical Union.

Greinert, J., Lewis, K. B., Bialas, J., Pecher, I. A., Rowden, A., Bowden, D. A., De Batist, M., & Linke, P. (2010). Methane seepage along the Hikurangi Margin, New Zealand: Overview of studies in 2006 and 2007 and new evidence from visual, bathymetric and hydroacoustic investigations. *Marine Geology*, *272*(1–4), 6-25. https://doi.org/http://dx.doi.org/10.1016/j.margeo.2010.01.017

Guliev, I., & Feizullayev, A. (1996). Geochemistry of hydrocarbon seepages in Azerbaijan.

Guliyev, I., & Feizullayev, A. (1997). All about mud volcanoes. Baku Pub. House. *Nafta-Press*, *120*.

Guliyev, I. S. (2006). Mud volcanism in Azerbaijan. AIP Conference Proceedings,

Gurevich, A. E., & Chilingar, G. V. (1995). Abnormal Pressures in Azerbaijan: A Brief Critical Review and Recommendations. *Journal of Petroleum Science and Engineering*, *13*(2), 125-135.

Gutsalo, L., & Plotnikov, A. (1981). The origin identification of methane and carbon dioxide by the carbon isotope system of CH4 and CO2 in the earth. *Bull Soviet Acad Sci*, *259*, 470-473.

Head, I. M., Jones, D. M., & Larter, S. R. (2003). Biological activity in the deep subsurface and the origin of heavy oil. *Nature*, *426(6964)*, 344-352.

Heggland, R. (1997). Detection of gas migration from a deep source by the use of exploration 3D seismic data. *Marine Geology*, *137*(1-2), 41-47. http://www.sciencedirect.com/science/article/B6V6M-3SVY6JP-5/1/f848213d4bd8375978787bf133e1a5e6

Hempton, M. R. (1987). Constraints on Arabian plate motion and extensional history of the Red Sea. *Tectonics*, *6*(6), 687-705.

Higgins, G. E., & Saunders, J. B. (1974). Mud volcanoes - Their nature and origin. *Verh. Naturforsch. Ges. Basel*, *84*, 101-152.

Hmiel, B., Petrenko, V., Dyonisius, M., Buizert, C., Smith, A., Place, P., Harth, C., Beaudette, R., Hua, Q., & Yang, B. (2020). Preindustrial 14CH4 indicates greater anthropogenic fossil CH4 emissions. *Nature*, *578*(7795), 409-412.

Hong, W.-L., Etiope, G., Yang, T. F., & Chang, P.-Y. (2013). Methane flux from miniseepage in mud volcanoes of SW Taiwan: Comparison with the data from Italy, Romania, and Azerbaijan. *Journal of Asian Earth Sciences*, *65*(C), 3-12. https://doi.org/10.1016/j.jseaes.2012.02.005

Hovland, M., Nygaard, E., & Thorbjørnsen, S. (1998). Piercement shale diapirism in the deep-water Vema Dome area, Vøring Basin, offshore Norway. *Marine and Petroleum Geology*, *15*(3), 191-201.

Hovland, M., Talbot, M. R., Qvale, H., Olaussen, S., & Aasberg, L. (1987). Methane-related carbonate cements in pockmarks of the North Sea. *Journal of Sedimentary Petrology*, *57*(5), 881-892. http://www.sciencedirect.com/science/article/B6WPY-3V4SVBM-43G/1/1780e97924686524247a9fd7ef6b04ac

Hunt, J. M. (1996). *Petroleum Geochemistry and Geology* Freeman (2nd ed.).

Inan, S., Yalçin, M. N., Guliev, I. S., Kuliev, K., & Feizullayev, A. A. (1997). Deep petroleum occurrences in the Lower Kura Depression, South Caspian Basin, Azerbaijan: an organic geochemical and basin modeling study. *Marine and Petroleum Geology*, *14*(7-8), 731-762.

IPCC. (1990 and 1992). *Climate Change: The IPCC 1990 and 1992 Assessments* (Intergovernmental Panel on Climate Change, Issue. C. Cambridge University Press.

IPCC. (1995). *Climate Change 1995: The Science of Climate Change: Contribution of Working Group I to the Second Assessment Report of the Intergovernmental Panel on Climate Change* C. Cambridge University Press.

IPCC. (2001). *Climate change 2001: synthesis report* (Intergovernmental Panel on Climate Change (IPCC), Geneva, Switzerland, Issue. C. Cambridge University Press.

IPCC. (2007). *Climate change 2007: synthesis report*. C. Cambridge University Press.

IPCC. (2013). *Climate Change 2013: The Physical Science Basis. Contribution of Working Group I to the Fifth Assessment Report of the Intergovernmental Panel on Climate Change*. C. Cambridge University Press.

Isaksen, G. H., Aliyev, A., Barboza, S. A., Plus, D., & Guliev, I. S. (2007). Regional evaluation of source rock in Azerbaijan from the geochemistry of organic-rich rocks in mud-volcano ejecta. In P. O. Yilmaz & G. H. Isaksen (Eds.), *Oil and gas of the Greater Caspian area* (pp. 51-64). AAPG Studies in Geology, 55.

Ivanov, M. K., Limonov, A. F., & van Weering, T. C. E. (1996). Comparative characteristics of the Black Sea and Mediterranean Ridge mud volcanoes. *Marine Geology*, *132*(1-4), 253-271. http://www.sciencedirect.com/science/article/B6V6M-3VW11G7-K/1/f4446106cac8f6ad159ae2e88ba72951

Jakubov, A. A., AliZade, A. A., & Zeinalov, M. M. (1971). Mud volcanoes of the Azerbaijan SSR. *atlas (in Russian), Azerbaijan Academy of Sciences, Baku*.

Javadova, A., & Hauck, M. (2000). The Stratigraphy and Hydrocarbon Potential of the Lower Kura Area.

Jeffrey, A. W. A., Alimi, H.M., Jenden, P.D., . . (1991). Geochemistry of the Los Angelesc Basin oil and gas systems. In: Biddle, K.T. (Ed.), Active Margin Basins. *American Association of Petroleum Geologists Memoir*, *52*, 197-219.

Jenden, P. D., Hilton, D. R., Kaplan, I. R., & Craig, H. (1993). Abiogenic hydrocarbons and mantle helium in oil and gas fields. In D. G. Howell (Ed.), *The Future of Energy Gases* (pp. 31–56). (US Geological Survey Professional Paper 1570), United States Government Printing Office, Washington.

Joannin, S., Cornée, J.-J., Münch, P., Fornari, M., Vasiliev, I., Krijgsman, W., Nahapetyan, S., Gabrielyan, I., Ollivier, V., & Roiron, P. (2010). Early Pleistocene climate cycles in continental

deposits of the Lesser Caucasus of Armenia inferred from palynology, magnetostratigraphy, and 40Ar/39Ar dating. *Earth and Planetary Science Letters*, *291*(1-4), 149-158.

Kadirov, F., Floyd, M., Alizadeh, A., Guliev, I., Reilinger, R., Kuleli, S., King, R., & Toksoz, M. N. (2012). Kinematics of the eastern Caucasus near Baku, Azerbaijan. *Natural Hazards*, *63*(2), 997-1006.

Katz, B. J. (2011). Microbial processes and natural gas accumulations. *The Open Geology Journal*, *5*(1).

Kaz'min, V. G., & Tikhonova, N. F. (2006). Late Cretaceous Eocene marginal seas in the black sea-Caspian region: paleotectonic reconstructions. *Geotectonics*, *40*, 169-182.

Kholodov, V. N. (2002). Mud Volcanoes, Their Distribution Regularities and Genesis: Communication 1. Mud Volcanic Provinces and Morphology of Mud Volcanoes. *Lithology and Mineral Resources*, *37*(3), 197-209.

Kioka, A., & Ashi, J. (2015). Episodic massive mud eruptions from submarine mud volcanoes examined through topographical signatures. *Geophysical Research Letters*, *42*(20), 8406-8414. https://doi.org/10.1002/2015GL065713

Kocherla, M., Teichert, B. M. A., Pillai, S., Satyanarayanan, M., Ramamurty, P. B., Patil, D. J., & Rao, A. (2015). Formation of methane-related authigenic carbonates in a highly dynamic biogeochemical system in the Krishna–Godavari Basin, Bay of Bengal. *Marine and Petroleum Geology*, *64*, 324-333. https://doi.org/http://dx.doi.org/10.1016/j.marpetgeo.2015.02.034

Kokh, S., Sokol, E., Dekterev, A., Kokh, K., Rashidov, T., Tomilenko, A., Bul'Bak, T., Khasaeva, A., & Guseinov, A. (2017). The 2011 strong fire eruption of Shikhzarli mud volcano, Azerbaijan: a case study with implications for methane flux estimation. *Environmental Earth Sciences*, *76*(20), 1-20.

Kopf, A., & Deyhle, A. (2002). Back to the roots: boron geochemistry of mud volcanoes and its implications for mobilization depth and global B cycling. *Chemical Geology*, *192*, 195-210.

Kopf, A. J. (2002). Significance of mud volcanism. *Review of Geophysics*, *40*(2), 1-52.

Kroonenberg, S., Badyukova, E., Storms, J., Ignatov, E., & Kasimov, N. (2000). A full sea-level cycle in 65 years: barrier dynamics along Caspian shores. *Sedimentary Geology*, *134*(3-4), 257-274.

Krooss, B., Littke, R., Müller, B., Frielingsdorf, J., Schwochau, K., & Idiz, E. (1995). Generation of nitrogen and methane from sedimentary organic matter: implications on the dynamics of natural gas accumulations. *Chemical Geology*, *126*(3-4), 291-318.

Link, W. K. (1952). Significance of oil and gas seeps in world oil exploration. *Am. Assoc. Pet. Geol. Bull.*, *36*, 1505-1540.

Link, W. K. (1952). Significance of oil and gas seeps in world oil exploration. *Aapg Bulletin*, *36*(8), 1505-1540.

Liu, Y., & Whitman, W. B. (2008). Metabolic, phylogenetic, and ecological diversity of the methanogenic archaea. *Annals of the New York Academy of Sciences*, *1125*(1), 171-189.

Lopes, E. E. (2012). Proposta metodológica para validação de imagens de alta resolução do Google Earth para a produção de mapas.

Maestrelli, D., Bonini, M., Delle Donne, D., Manga, M., Piccardi, L., & Sani, F. (2017). Dynamic triggering of mud volcano eruptions during the 2016–2017 Central Italy seismic sequence. *Journal of Geophysical Research: Solid Earth*, *122*(11), 9149-9165.

Magoon, L. B., & Schmoker, J. W. (2000). *The Total Petroleum System - the natural fluid network that constraints the assessment units*. World Energy Assessment Team.

Manga, M., Brumm, M., & Rudolph, M. L. (2009). Earthquake triggering of mud volcanoes. *Marine and Petroleum Geology*, *26*(9), 1785-1798. https://doi.org/10.1016/j.marpetgeo.2009.01.019

Mascle, J., Mary, F., Praeg, D., Brosolo, L., Camera, L., Ceramicola, S., & Dupré, S. (2014). Distribution and geological control of mud volcanoes and other fluid/free gas seepage features in the Mediterranean Sea and nearby Gulf of Cadiz. *Geo-Marine Letters*, *34*(2-3), 89-110. https://doi.org/10.1007/s00367-014-0356-4

Mazzini, A. (2009). Mud volcanism: Processes and implications. *Marine and Petroleum Geology*, *26*(9), 1677-1680. https://doi.org/10.1016/j.marpetgeo.2009.05.003

Mazzini, A., Akhmanov, G., Manga, M., Sciarra, A., Huseynova, A., Huseynov, A., & Guliyev, I. (2021). Explosive mud volcano eruptions and rafting of mud breccia blocks. *Earth and Planetary Science Letters*, *555*, 116699. https://doi.org/https://doi.org/10.1016/j.epsl.2020.116699

Mazzini, A., & Etiope, G. (2017). Mud volcanism: An updated review. *Earth-Science Reviews*, *168*, 81–112. https://doi.org/http://dx.doi.org/10.1016/j.earscirev.2017.03.001

Mazzini, A., Nermoen, A., Krotkiewski, M., Podladchikov, Y., Planke, S., & Svensen, H. (2009). Strike-slip faulting as a trigger mechanism for overpressure release through piercement structures. Implications for the Lusi mud volcano, Indonesia. *Marine and Petroleum Geology*, *26*(9), 1751-1765. https://doi.org/https://doi.org/10.1016/j.marpetgeo.2009.03.001

Mazzini, A., Svensen, H., Planke, S., Guliyev, I., Akhmanov, G. G., Fallik, T., & Banks, D. (2009). When mud volcanoes sleep: Insight from seep geochemistry at the Dashgil mud volcano, Azerbaijan. *Marine and Petroleum Geology*, *26*(9), 1704-1715. https://doi.org/10.1016/j.marpetgeo.2008.11.003

McMahon, P. B., Chapelle, F. H., Falls, W. F., & Bradley, P. M. (1992). Role of microbial processes in linking sandstone diagenesis with organic-rich clays. *Journal of Sedimentary Research*, *62*(1), 1-10.

Medialdea, T., Somoza, L., Pinheiro, L. M., Fernández-Puga, M., Vázquez, J. T., León, R., Ivanov, M., Magalhaes, V., Díaz-del-Río, V., & Vegas, R. (2009). Tectonics and mud volcano development in the Gulf of Cádiz. *Marine Geology*, *261*(1-4), 48-63.

Mellors, R., Kilb, D., Aliyev, A., Gasanov, A., & Yetirmishli, G. (2007). Correlations between earthquakes and large mud volcano eruptions. *Journal of Geophysical Research*, *112*, B04304.

Milkov, A. V. (2000). Worldwide distribution of submarine mud volcanoes and associated gas hydrates. *Marine Geology*, *167*(1-2), 29-42. http://www.sciencedirect.com/science/article/B6V6M-40J1G0K-2/2/28d5cbe8054cae844f38fec43bed5ad5

Milkov, A. V. (2005). Global distribution of mud volcanoes and their significance in petroleum exploration as a source of methane in the atmosphere and hydrosphere and as a geohazard. *Mud Volcanoes, Geodynamics and Seismicity*, 29-34.

Milkov, A. V. (2010). Methanogenic biodegradation of petroleum in the West Siberian Basin (Russia): Significance for formation of giant Cenomanian gas pools. *Aapg Bulletin*, *94*(10), 1485-1541.

Milkov, A. V. (2011). Worldwide distribution and significance of secondary microbial methane formed during petroleum biodegradation in conventional reservoirs. *Organic Geochemistry*, *42*(2), 184-207. https://doi.org/DOI 10.1016/j.orggeochem.2010.12.003

Milkov, A. V., Claypool, G. E., Lee, Y. J., Xu, W., Dickens, G. R., Borowski, W. S., & Party, O. D. P. L. S. (2003). In situ methane concentrations at Hydrate Ridge, offshore Oregon: New constraints on the global gas hydrate inventory from an active margin. *Geology*, *31*(10), 833-836.

Milkov, A. V., & Dzou, L. (2007). Geochemical evidence of secondary microbial methane from very slight biodegradation of undersaturated oils in a deep hot reservoir. *Geology*, *35*(5), 455-458. https://doi.org/10.1130/g23557a.1

Milkov, A. V., & Etiope, G. (2005). Global methane emission through mud volcanoes and its past and present impact on the Earth's climate—a comment. *International Journal of Earth Sciences*, *94*(3), 490-492. http://springerlink.metapress.com/openurl.asp?genre=article&id=doi:10.1007/s00531-005-0480-5

Milkov, A. V., & Etiope, G. (2018). Revised genetic diagrams for natural gases based on a global dataset of> 20,000 samples. *Organic Geochemistry*, *125*, 109-120.

Mitchell, J., & Westaway, R. (1999). Chronology of Neogene and Quaternary uplift and magmatism in the Caucasus: constraints from K–Ar dating of volcanism in Armenia. *Tectonophysics*, *304*(3), 157-186.

Muskat, M., & Wyckoff, R. D. (1946). The flow of homogeneous fluids through porous media.

Nadirov, R., Bagirov, E., Tagiyev, M., & Lerche, I. (1997). Flexural plate subsidence, sedimentation rates, and structural development of the super-deep South Caspian Basin. *Marine and Petroleum Geology*, *14*(4), 383-400.

Nadirov, R. S., Bagirov, E., & Tagiyev, M. (1997). Flexural plate subsidence, sedimentation rates, and structural development of the super-deep South Caspian Basin. *Marine & Petroleum Geology*, *14*, 383-400.

Naehr, T. H., Rodriguez, N. M., Bohrmann, G., Paull, C. K., & Botz, R. (2000). Methane-derived authigenic carbonates associated with gas hydrate decomposition and fluid venting above the Blake Ridge Diapir. In C. K. Paull, R. Matsumoto, P. J. Wallace, & W. P. Dillon (Eds.), *Proc. ODP Scientific Results* (Vol. 164, pp. 286-300). College Station, TX (Ocean Drilling Program).

Narimanov, A., & Dore, A. (1993). The petroleum systems of the South Caspian Basin. *Basin Modeling Advances and Applications. Norwegian Petroleum Society, Special Publications*, *3*, 599-608.

Oppo, D., De Siena, L., & Kemp, D. (2020). A record of seafloor methane seepage across the last 150 million years. *Scientific Reports*, *10*(1), 1-12.

Pallasser, R. (2000). Recognising biodegradation in gas/oil accumulations through the δ13C compositions of gas components. *Organic Geochemistry*, *31*(12), 1363-1373.

Pallasser, R. J. (2000). Recognising biodegradation in gas/oil accumulations through the d13C compositions of gas components. *Organic Geochemistry*, *31*, 1363-1373.

Panahi, B. M. (2006). Seismicity in Azerbaijan and adjacent Caspian Sea. AIP Conference Proceedings,

Perez-Garcia, C., Feseker, T., Mienert, J., & Berndt, C. (2009). The Håkon Mosby mud volcano: 330 000 years of focused fluid flow activity at the SW Barents Sea slope. *Marine Geology*, *262*(1-4), 105-115. http://www.sciencedirect.com/science/article/B6V6M-4W0R0S6-1/2/0c27c2033ec4fc3ba9b3078ce8439144

Philip, H., Cisternas, A., Gvishiani, A., & Gorshkov, A. (1989). The Caucasus: an actual example of the initial stages of continental collision. *Tectonophysics*, *161*(1-2), 1-21.

Philippi, G. (1977). On the depth, time and mechanism of origin of the heavy to medium-gravity naphthenic crude oils. *Geochimica et Cosmochimica Acta*, *41*(1), 33-52.

Planke, S., Svensen, H., Hovland, M., Banks, D., & Jamtveit, B. (2003). Mud and fluid migration in active mud volcanoes in Azerbaijan. *Geo-Marine Letters*, *23*, 258-268.

Priestley, K., Baker, C., & Jackson, J. (1994). Implications of earthquake focal mechanism data for the active tectonics of the South Caspian Basin and surrounding regions. *Geophysical Journal International*, *118*(1), 111-141.

Reilinger, R., McClusky, S., Vernant, P., Lawrence, S., Ergintav, S., Cakmak, R., Ozener, H., Kadirov, F., Guliev, I., & Stepanyan, R. (2006). GPS constraints on continental deformation in the Africa-Arabia-Eurasia continental collision zone and implications for the dynamics of plate interactions. *Journal of Geophysical Research: Solid Earth*, *111*(B5).

Revil, A. (2002). Genesis of mud volcanoes in sedimentary basins: A solitary wave-based mechanism. *Geophys. Res. Lett.*, *29 (12), doi:10.1029/2001GL014465, 2002.*

Rudolph, M. L., & Manga, M. (2010). Mud volcano response to the 4 April 2010 El Mayor–Cucapah earthquake. *J Geophys Res*, *115*. https://doi.org/10.1029/2010jb007737

Saint-Germes, M., Bazhenova, O., Baudin, F., Zaporozhets, N., & Fadeeva, N. (2000). Organic matter in Oligocene Maikop sequence of the North Caucasus. *Lithology and Mineral Resources*, *35*(1), 47-62.

Saintot, A., Brunet, M.-F., Yakovlev, F., Sébrier, M., Stephenson, R., Ershov, A., Chalot-Prat, F., & McCann, T. (2006). The Mesozoic-Cenozoic tectonic evolution of the Greater Caucasus. *Geological Society, London, Memoirs*, *32*(1), 277-289.

Saroni, A., Sciarra, A., Grassa, F., Eich, A., Weber, M., Lott, C., Ferretti, G., Ivaldi, R., & Coltorti, M. (2020). Shallow submarine mud volcano in the Northern Tyrrhenian sea, Italy. *Applied Geochemistry*, 104722. https://doi.org/10.1016/j.apgeochem.2020.104722

Saunois, M., Bousquet, P., Poulter, B., Peregon, A., Ciais, P., Canadell, J. G., Dlugokencky, E. J., Etiope, G., Bastviken, D., Houweling, S., Janssens-Maenhout, G., Tubiello, F. N., Castaldi, S., Jackson, R. B., Alexe, M., Arora, V. K., Beerling, D. J., Bergamaschi, P., Blake, D. R., . . . Zhu, Q. (2016).

The global methane budget 2000-2012. *Earth System Science Data*, *8*(2), 697-751. https://doi.org/10.5194/essd-8-697-2016

Schoell, M. (1983). Genetic-Characterization of Natural Gases. *Aapg Bulletin-American Association of Petroleum Geologists*, *67*(3), 2225-2238. <Go to ISI>://A1983QK01400393

Schoell, M. (1983). Genetic characterization of natural gases. *Aapg Bulletin*, *67*(12), 2225-2238.

Schwietzke, S., Sherwood, O. A., Bruhwiler, L. M., Miller, J. B., Etiope, G., Dlugokencky, E. J., Michel, S. E., Arling, V. A., Vaughn, B. H., & White, J. W. (2016). Upward revision of global fossil fuel methane emissions based on isotope database. *Nature*, *538*(7623), 88-91.

Sciarra, A., Cantucci, B., Sapia, V., De Ritis, R., Ricci, T., Civico, R., Galli, G., Cinti, D., & Coltorti, M. (2020). Geochemical and geoelectrical characterization of the Terre Calde di Medolla (Emilia-Romagna, northern Italy) and relations with 2012 seismic sequence. *Journal of Geochemical Exploration*, 106678. https://doi.org/https://doi.org/10.1016/j.gexplo.2020.106678

Sciarra, A., Cantucci, B., Sapia, V., De Ritis, R., Ricci, T., Civico, R., Galli, G., Cinti, D., & Coltorti, M. (2021). Geochemical and geoelectrical characterization of the Terre Calde di Medolla (Emilia-Romagna, northern Italy) and relations with 2012 seismic sequence. *Journal of Geochemical Exploration*, *221*, 106678.

Senese, F. (2010). General chemistry online.

Şengör, A. C. l. (1990). Plate tectonics and orogenic research after 25 years: A Tethyan perspective. *Earth-Science Reviews*, *27*(1-2), 1-201.

Sherwood, O. A., Travers, P. D., & Dolan, M. P. (2013). Hydrocarbon maturity and migration analysis using production gas stable isotopic signatures in the Wattenberg Field, Denver Basin, Colorado, USA. SPE/AAPG/SEG Unconventional Resources Technology Conference,

Shikhalibeyli, E. S., Abdullayev, R., & Ali-Zade, A. A. (1988). Geological results from the Saatly superdeep drillhole. *International Geology Review*, *30*(12), 1272-1277.

Skinner, J. A., & Mazzini, A. (2009). Martian mud volcanism: Terrestrial analogs and implications for formational scenarios. *Marine and Petroleum Geology*, *26*(9), 1866-1878. https://doi.org/10.1016/j.marpetgeo.2009.02.006

Somoza, L., Dıaz-del-Rıo, V., León, R., Ivanov, M., Fernández-Puga, M., Gardner, J., Hernández-Molina, F., Pinheiro, L., Rodero, J., & Lobato, A. (2003). Seabed morphology and hydrocarbon seepage in the Gulf of Cadiz mud volcano area: Acoustic imagery, multibeam and ultra-high resolution seismic data. *Marine Geology*, *195*(1-4), 153-176.

Spulber, L., Etiope, G., Baciu, C., Malos, C., & Vlad, S. N. (2010). Methane emission from natural gas seeps and mud volcanoes in Transylvania (Romania). *Geofluids*, *10*(4), 463-475. https://doi.org/DOI 10.1111/j.1468-8123.2010.00301.x

Tari, G., Blackbourn, G., Boote, D., Sachsenhofer, R., & Yukler, A. (2021). Exploration plays in the Caucasus region. *Journal of Petroleum Geology*, *44*(3), 213-236.

Tassi, F., Feyzullayev, A. A., Bonini, M., Sani, F., Aliyev, C. S., Darrah, T. H., Vaselli, O., & Baghirli, R. J. (2020). Mantle vs. crustal fluid sources in the gas discharges from Lesser Caucasus and Talysh Mountains (Azerbaijan) in relation to the regional geotectonic setting. *Applied Geochemistry*, *118*, 104643.

Telesca, L., Kadirov, F., Yetirmishli, G., Safarov, R., Babayev, G., & Ismaylova, S. (2017). Statistical analysis of the 2003–2016 seismicity of Azerbaijan and surrounding areas. *Journal of Seismology*, *21*(6), 1467-1485.

Tsereteli, N., Tibaldi, A., Alania, V., Gventsadse, A., Enukidze, O., Varazanashvili, O., & Müller, B. (2016). Active tectonics of central-western Caucasus, Georgia. *Tectonophysics*, *691*, 328-344.

Turner, A., Jacob, D. J., Wecht, K. J., Maasakkers, J. D., Lundgren, E., Andrews, A. E., Biraud, S. C., Boesch, H., Bowman, K. W., & Deutscher, N. M. (2015). Estimating global and North American methane emissions with high spatial resolution using GOSAT satellite data. *Atmospheric Chemistry and Physics*, *15*(12), 7049-7069.

Valyaev, B. M., Grinchenko, Y. I., Erokhin, V. E., Prokhorov, V. S., & Titkov, G. A. (1985). Isotopic composition of gases from mud volcanoes. *Lithology and Mineral Resources*, *20*, 62-75.

Wallmann, K., Linke, P., Suess, E., Bohrmann, G., Sahling, H., Schluter, M., Dahlmann, A., Lammers, S., Greinert, J., & von Mirbach, N. (1997). Quantifying fluid flow, solute mixing, and biogeochemical turnover at cold vents of the eastern Aleutian subduction zone. *Geochimica et Cosmochimica Acta*, *61*(24 SU -), 5209-5219. http://www.sciencedirect.com/science/article/B6V66-3SWR3M1-4/2/ed2cdc814c34ea85c8811effd424816b

Wenger, L. M., & Isaksen, G. H. (2002). Control of hydrocarbon seepage intensity on level of biodegradation in sea bottom sediments. *Organic Geochemistry*, *33*(12), 1277-1292.

WestSystems. (2020). *West Systems Portable Fluxmeter*. Retrieved 07/06 from

White, W. M. (2015). *Isotope geochemistry*. John Wiley & Sons.

Whiticar, M. J. (1999). Carbon and hydrogen isotope systematics of bacterial formation and oxidation of methane. *Chemical Geology*, *161*(1-3), 291-314.

Whiticar, M. J. (1999). Carbon and hydrogen isotope systematics of bacterial formation and oxidation of methane. *Chemical Geology*, *161*, 291-314.

Whiticar, M. J., & Faber, E. (1986). Methane oxidation in sediment and water column environments—isotope evidence. *Organic Geochemistry*, *10*(4-6), 759-768.

Whiticar, M. J., Faber, E., & Schoell, M. (1986). Biogenic methane formation in marine and freshwater environments: CO2 reduction vs. acetate fermentation—isotope evidence. *Geochimica et Cosmochimica Acta*, *50*(5), 693-709.

Yang, T. F., Yeh, G. H., Fu, C. C., Wang, C. C., Lan, T. F., Lee, H. F., Chen, C. H., Walia, V., & Sung, Q. C. (2004). Composition and exhalation flux of gases from mud volcanoes in Taiwan. *Environmental Geology*, *46*(8), 1003-1011. https://doi.org/DOI 10.1007/s00254-004-1086-0

Zaputlyaeva, A., Mazzini, A., Blumenberg, M., Scheeder, G., Kürschner, W. M., Kus, J., Jones, M. T., & Frieling, J. (2020). Recent magmatism drives hydrocarbon generation in north-east Java, Indonesia. *Scientific Reports*, *10*(1), 1786. https://doi.org/10.1038/s41598-020-58567-6

Zeikus, J. (1977). The biology of methanogenic bacteria. *Bacteriological reviews*, *41*(2), 514-541.

Zonenshain, L. P., & Pichon, X. (1986). Deep basins of the Black Sea and Caspian Sea as remnants of Mesozoic back-arc basins. *Tectonophysics*, *123*(1-4), 181-211.

# Appendices

## Appendix 1

**Table Appendix 1** Table of abbreviations used in the study and their meaning.

| Abbreviations | Meaning |
|---|---|
| asl | Above mean Sea Level |
| EMT | Early Mature Thermogenic |
| HC | Hydrocarbon |
| INGV | Istituto Nazionale Geofisica e Vulcanologia |
| LMT | Late Mature Thermogenic |
| MV | Mud Volcano |
| OA | Oil Associated |
| OM | Organic Matter |
| SCB | South Caspian Basin |
| SM | Secondary Microbial |
| SM | Secondary Microbial |
| TC | Thermal Couple |
| TOC | Total Organic Matter |

# Appendix 2
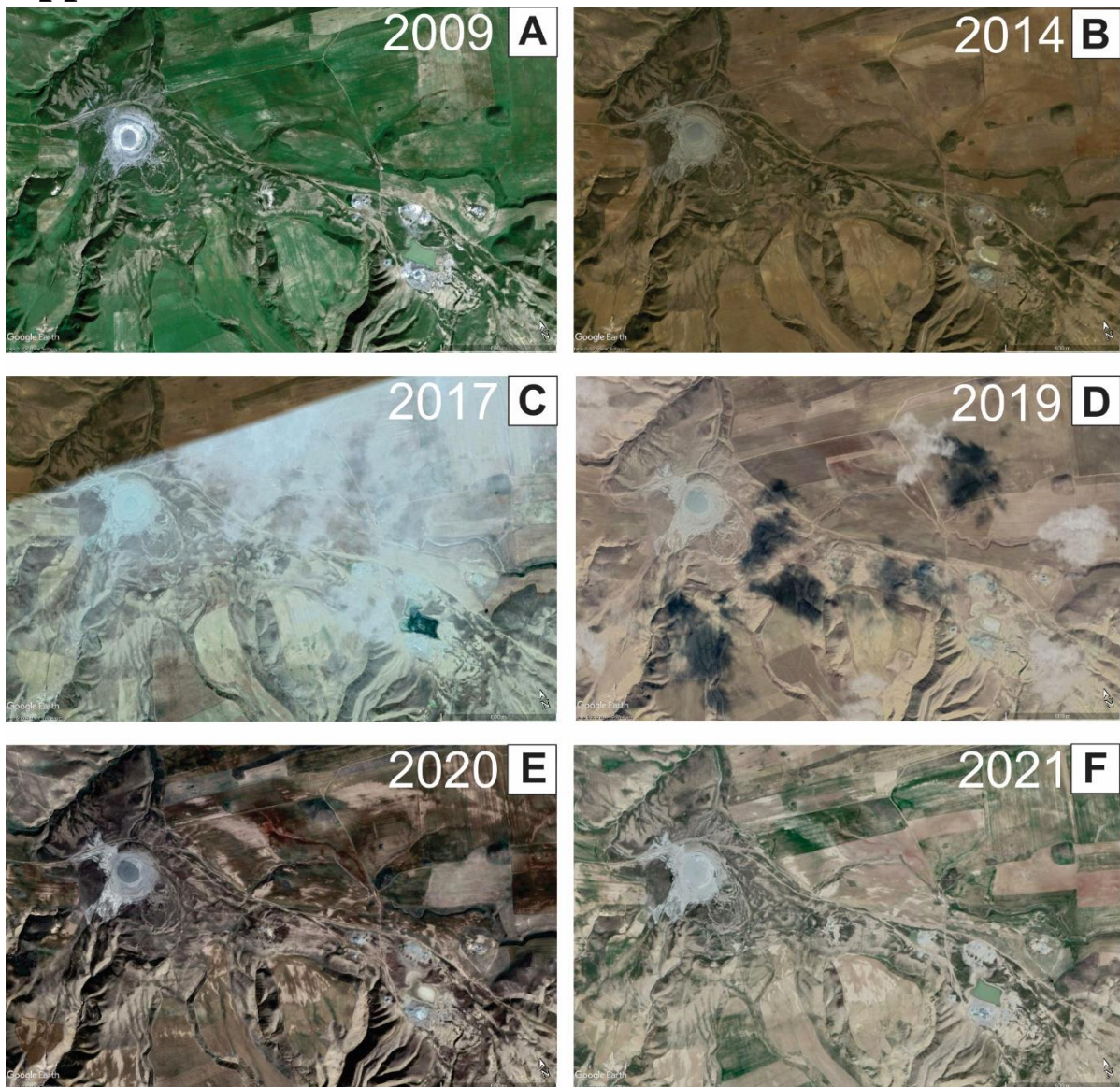


***Figure Appendix 2*** *Assemblage of satellite images of Kichik Maraza (on the left) and Kichik Maraza MV (on the right) illustrating changes in image quality, and mudflow and for the years 2009 (A), 2014 (B), 2017(C), 2019 (D), 2020 (E) and 2021 (F).*

# Appendix 3



***Figure Appendix 3*** *Assemblage of satellite images of Gyzmeidan MV illustrating some changes in image quality, and mudflow and over the years 2019 (A), 2020 (B) and 2021 (C).*

# Appendix 4



*Figure Appendix 4* *Assemblage of satellite images of Gushchu MV illustrating some changes in image quality, and mudflow and over the years 2012 (A) and 2021 (B).*
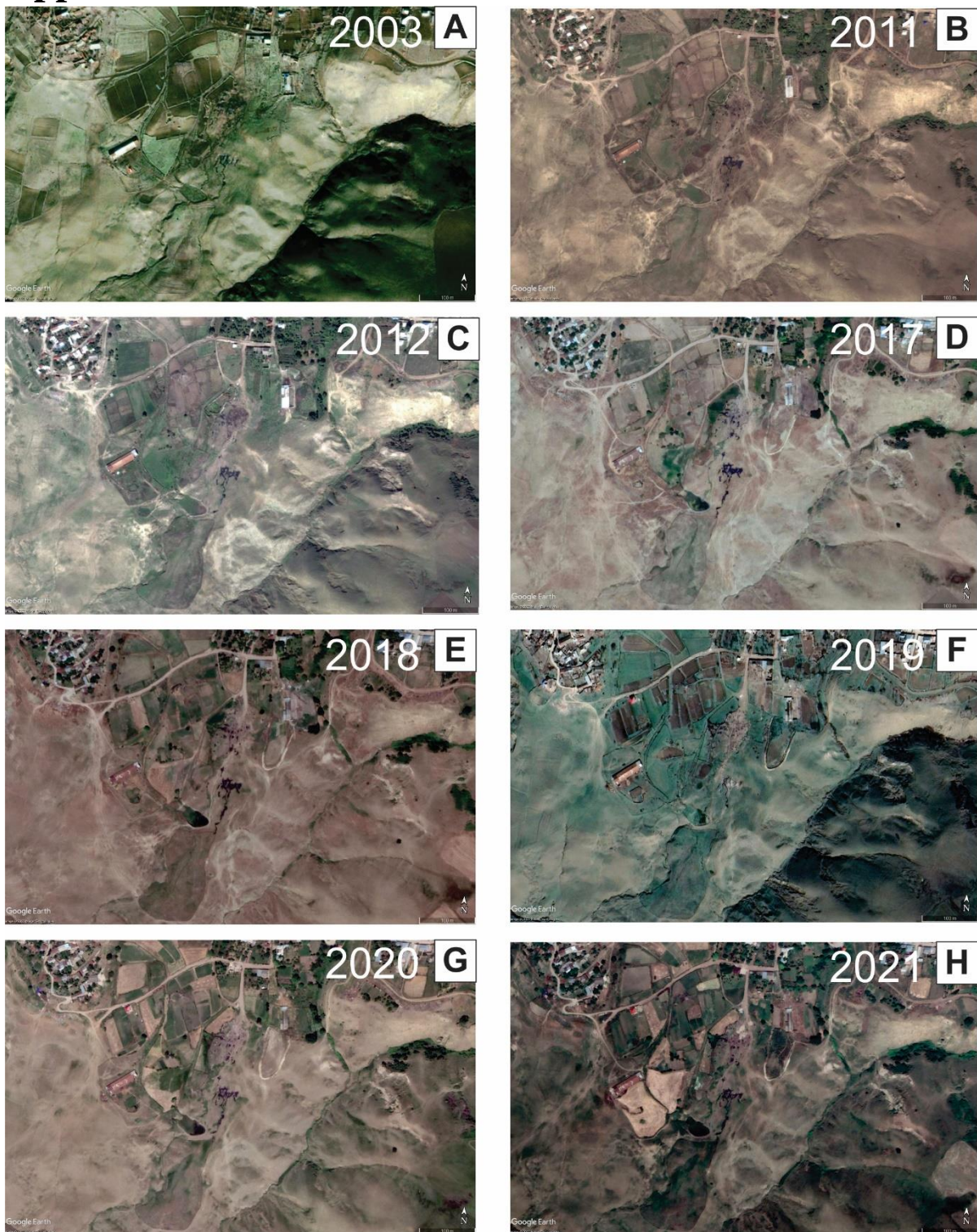
# Appendix 5



***Figure Appendix 5*** *Assemblage of satellite images of Melikchbanly MV illustrating some changes in image quality, colours and mudflow and over the years 2001 (A), 2019 (B) and 2021 (C).*
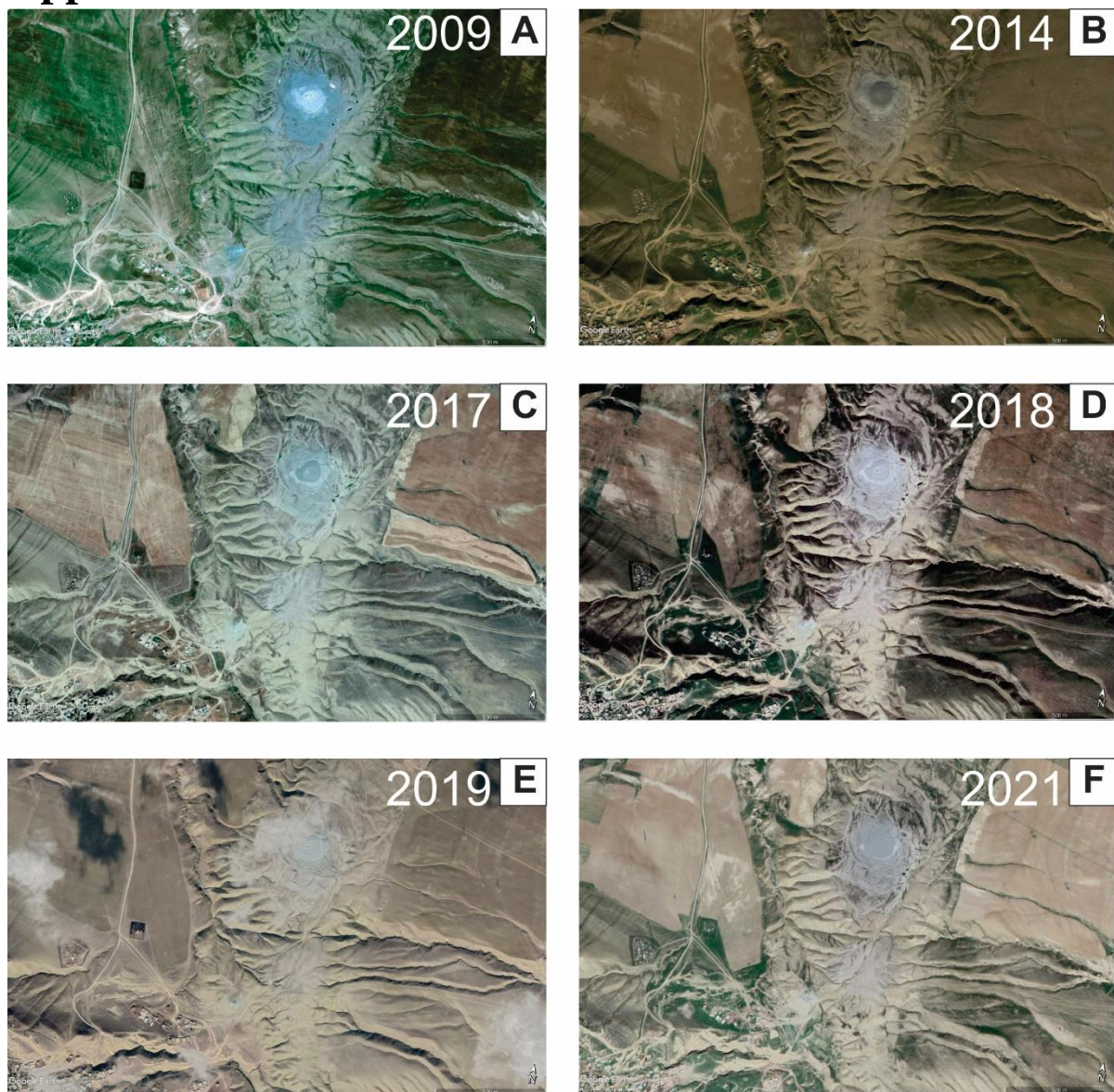
# Appendix 6



**Figure Appendix 6** Assemblage of satellite images of Madrasa *MV illustrating some changes in image quality, colors and mudflow and over the years 2003 (A), 2011 (B), 2012 (C), 2017 (D), 2018 (E), 2019 (F), 2020 (G), 2021 (H).*

# Appendix 7



***Figure Appendix 7*** *Assemblage of satellite images of Shikhzarli MV illustrating some changes in image quality, and mudflow and over the years 2009 (A), 2014 (B), 2017 (C), 2018 (D), 2019 (E), 2021 (F).*